

Fault Diagnosis and Estimation of Dynamical Systems with Application to Gas Turbines

Esmaeil Naderi

A Thesis
in
The Department
of
Electrical and Computer Engineering

Presented in Partial Fulfillment of the Requirements
for the Degree of Doctor of Philosophy at
Concordia University
Montréal, Québec, Canada

October 2016

© Esmaeil Naderi, 2016

CONCORDIA UNIVERSITY
School of Graduate Studies

This is to certify that the thesis proposal prepared

By: **Esmail Naderi**

Entitled: **Fault Diagnosis and Estimation of Dynamical Systems with
Application to Gas Turbines**

and submitted in partial fulfilment of the requirements for the degree of

Doctor of Philosophy

complies with the regulations of this University and meets the accepted standards
with respect to originality and quality.

Signed by the final examining committee:

_____ Dr. Jiayuan Yu, Chair
_____ Dr. Farid Golnaraghi, External examiner
_____ Dr. Fariborz Haghighat, External examiner
_____ Dr. Shahin Hashtrudi Zad, Examiner
_____ Dr. Wei Ping Zhu, Examiner
_____ Dr. Khashayar Khorasani, Supervisor

Approved by _____
Chair of the ECE Department

Dean of Engineering

ABSTRACT

Fault Diagnosis and Estimation of Dynamical Systems with Application to Gas Turbines

Esmail Naderi, Ph.D.

Concordia University, 2016

This thesis contributes and provides solutions to the problem of fault diagnosis and estimation from three different perspectives which are i) fault diagnosis of nonlinear systems using nonlinear multiple model approach, ii) inversion-based fault estimation in linear systems, and iii) data-driven fault diagnosis and estimation in linear systems. The above contributions have been demonstrated to the gas turbines as one of the most important engineering systems in the power and aerospace industries.

The proposed multiple model approach is essentially a hierarchy of nonlinear Kalman filters utilized as detection filters. A nonlinear mathematical model for a gas turbines is developed and verified. The fault vector is defined using the Gas Path Analysis approach. The nonlinear Kalman filters that correspond to the defined single or concurrent fault modes provide the conditional probabilities associated with each fault mode using the Bayes' law. The current fault mode is then determined based on the maximum probability criteria. The performance of both Extended Kalman Filters (EKF) and Unscented Kalman Filters (UKF) are investigated and compared which demonstrates that the UKF outperforms the EKF for this particular application.

The problem of fault estimation is increasingly receiving more attention due to its practical importance. Fault estimation is closely related to the problem of linear systems inversion. This thesis includes two contributions for the stable inversion of non-minimum phase systems. First, a novel methodology is proposed for direct estimation of unknown inputs by using only measurements of either minimum or non-minimum phase systems as well as systems with transmission zeros on the unit circle. A dynamic filter is then identified whose poles coincide with the transmission zeros of the system. A feedback is then introduced to stabilize the above filter dynamics as well as provide an unbiased estimation of the unknown input. The methodology is then applied to

the problem of fault estimation and has been shown that the proposed inversion filter is unbiased for certain categories of faults. Second, a solution for unbiased reconstruction of general inputs is proposed. It is based on designing an unknown input observer (UIO) that provides unbiased estimation of the minimum phase states of the system. The reconstructed minimum phase states serve then as inputs for reconstruction of the non-minimum phase states. The reconstruction error for non-minimum phase states exponentially decrease as the estimation delay is increased. Therefore, an almost perfect reconstruction can be achieved by selecting the delay to be sufficiently large. The proposed inversion scheme is then applied to the output-tracking control problem.

An important practical challenge is the fact that engineers rarely have a detailed and accurate mathematical model of complex engineering systems such as gas turbines. Consequently, one can find a trend towards data-driven approaches in many disciplines, including fault diagnosis. In this thesis, explicit state-space based fault detection, isolation and estimation filters are proposed that are directly identified from only the system input-output (I/O) measurements and through the system Markov parameters. The proposed procedures do not involve a reduction step and do not require identification of the system extended observability matrix or its left null space. Therefore, the performance of the proposed filters is directly connected to and linearly dependent on the errors in the Markov parameters estimation process. The estimation error dynamics is then derived in terms of the Markov parameters identification errors and directly synthesized from the healthy system I/O data. Consequently, the estimation errors have been effectively compensated for. The proposed data-driven scheme requires the persistently exciting condition for healthy input data which is not practical for certain real life applications and in particular to gas turbine engines. To address this issue, a robust methodology for Markov parameters estimation using frequency response data is developed. Finally, the performance of the proposed data-driven approach is comprehensively evaluated for the fault diagnosis and estimation problems in the gas turbine engines.

ACKNOWLEDGEMENTS

I would like to greatly thank my supervisor, Prof. Khorasani, for the patient guidance, encouragement and advice he has provided throughout my time as his student. I have been extremely lucky to have a supervisor who cared so much about my work, and who devotes astonishing effort to improve his students works.

TABLE OF CONTENTS

List of Figures	x
List of Tables	xvi
Nomenclature	xx
1 Introduction	1
1.1 Introduction	1
1.2 Multiple Model Based Fault Detection and Isolation	7
1.3 Inversion-Based Fault Estimation	9
1.4 Inversion-Based Reconstruction of System States and General Un- known Input	11
1.5 Data Driven Fault Detection, Isolation and Estimation	13
1.6 Fault Diagnosis of Gas Turbines	17
1.7 Contributions of the Thesis	20
1.8 Structure of the Thesis	24
2 Background	25
2.1 Physics of the Gas Turbines	25
2.2 The Gas Turbine Mathematical Model	27
2.3 Inversion-Based Fault Estimation for Minimum Phase Systems	33
2.3.1 General Form of the Sain & Massey Algorithm	34
2.3.2 Application to Gas Turbine	39
3 Nonlinear Multiple Model Based FDI of Gas Turbines	46
3.1 MM-Based FDI Algorithm	47
3.2 Multiple Model-Based Fault Diagnosis Design	51
3.2.1 Fault Modeling and Detection Filter Design	52

3.3	Simulation Results	54
3.3.1	Single Fault Scenarios	55
3.3.2	Concurrent Fault Scenarios	58
3.3.3	Operational Condition Variations	61
3.3.4	A Comparison Between the Performance of the UKF and the EKF Detection Filters	64
3.4	Conclusions	67
4	Inversion-Based Fault Estimation	69
4.1	Problem Statement	70
4.1.1	Problem 1: Inversion-Based Input Estimation of Discrete- Time Linear Systems	70
4.1.2	Problem 2: Inversion-Based Fault Estimation of Discrete-Time Linear Systems	71
4.2	Notations	72
4.3	The Proposed Inversion-Based Input Estimation of Linear Systems .	73
4.3.1	Linear Systems With No Invariant Zeros	74
4.3.2	Minimum Phase Linear Systems	77
4.3.3	Non-Minimum Phase Systems	82
4.4	The Proposed Inversion-Based Fault Estimation for Non-Minimum Phase Fault to Output Systems	91
4.5	Four Case Studies	93
4.6	Conclusion	99
5	Reconstruction of System States and General Unknown Inputs and Faults	100
5.1	Problem Statement	101
5.2	State and Unknown Input Reconstruction	103

5.2.1	Partial Or Full Estimation of the System States	103
5.2.2	Partitioning of the States	108
5.2.3	Dynamics of the MP and NMP States	110
5.2.4	Estimation of the NMP States	115
5.3	Inversion-Based Output Tracking	120
5.4	Extension to Fault Estimation	123
5.5	Numerical Case Study Simulations	127
5.6	Conclusion	132
6	Data Driven Fault Detection, Isolation and Estimation	135
6.1	Preliminaries	136
6.2	Proposed Fault Estimation Scheme Using Exact Markov Parameters and Observability Matrix	140
6.3	Data-Driven Fault Detection and Isolation (FDI) Scheme	144
6.3.1	Data-Driven Estimation of the Filter Parameters	145
6.3.2	Fault Detection and Isolation Filters	149
6.3.3	Residual Dynamics In Presence of A Fault	152
6.4	The Proposed Fault Estimation Scheme	153
6.4.1	Sensor Fault Estimation Filters	154
6.4.2	Actuator Fault Estimation Filters	158
6.4.3	A Methodology for Solving the Minimization Problems	159
6.5	Simulation Results	160
6.6	Conclusion	170
7	Implementation and Application of the FDI&E Methodologies to Gas Turbines	171
7.1	Preliminaries	172
7.2	Identification of the Aircraft Gas Turbine Engine Markov Parameters	173

7.3	Simulation Case Studies	177
7.4	Conclusion	185
8	Summary	196
9	Conclusions and Future Work	200
9.1	Conclusion	200
9.2	Future Work	203
	References	205
A		223
A.1	Validity of the Estimated Markov Parameters	223
A.2	Markov Parameter Estimation Error for Different PLA	224
A.3	Confusion Matrix Analysis for PLA= 55%	226
A.4	Analysis On the Selection of the Parameter E	230

List of Figures

1.1	A schematic representation of the inverse-based fault estimation scheme	5
1.2	Historical development of FDI schemes	5
2.1	A schematic of gas turbine	26
2.2	Information flow diagram in a modular modeling of the gas turbine dynamics.	28
2.3	Steady state series at PLAs ranging from 0.4 to 1	32
2.4	A schematic representation of the gas turbine inverse-based fault estimation scheme. The inherent delay of the gas turbine model is 1 (i.e., $L = 1$). For a description of notations, refer to Figure 1.1.	42
2.5	Residuals that are generated by the fault estimation scheme under four distinct simulation scenarios.	44
2.6	Residuals generated by the fault estimation scheme in presence of concurrent faults.	45
3.1	General architecture of our proposed MM-based FDI scheme.	51
3.2	The mode probabilities corresponding to the injected 2% decrease in the compressor efficiency that is applied at $t = 5$ seconds (Mode #3) (a) the UKF is used in the MM-based FDI scheme, and (b) the EKF is used in the MM-based FDI scheme.	56
3.3	The output measurements corresponding to the injected 2% decrease in the compressor efficiency that is applied at $t = 5$ seconds (Mode #3).	56

3.4	The mode probabilities corresponding to the injected 3% decrease in the turbine efficiency that is applied at $t = 5$ seconds (Mode #5) (a) the UKF is used in the MM-based FDI scheme, and (b) the EKF is used in the MM-based FDI scheme.	57
3.5	The detection time for each mode of fault that is applied at $t = 5$ seconds as a function of the fault severity (a) the UKF is used in the MM-based FDI scheme, and (b) the EKF is used in the MM-based FDI scheme.	58
3.6	The mode probabilities corresponding to the injected 2%	59
3.7	The output measurements corresponding to the injected 2%	59
3.8	The mode probabilities corresponding to the injected 2% decrease in the turbine mass flow rate that is applied at $t = 5$ seconds (Mode #4) while the ambient temperature is varying (a) the UKF is used in the MM-based FDI scheme, and (b) the EKF is used in the MM-based FDI scheme.	62
3.9	The output measurements corresponding to the injected 2% decrease in the turbine mass flow rate that is applied at $t = 5$ seconds (Mode #4) while the ambient temperature is varying.	62
3.10	The mode probabilities corresponding to the injected 2% decrease in the turbine mass flow rate that is applied at $t = 5$ seconds (Mode #4) while the PLA is varying (a) the UKF is used in the MM-based FDI scheme, and (b) the EKF is used in the MM-based FDI scheme.	63
3.11	The output measurements corresponding to the injected 2% decrease in the turbine mass flow rate that is applied at $t = 5$ seconds (Mode #4) while the PLA is varying.	63

3.12	The detection time for each mode of fault that is applied at $t = 5$ seconds as a function of the noise power factor. The empty places indicates the unsuccessful detection or isolation of the corresponding fault. (a) the UKF is used in the MM-based FDI scheme, and (b) the EKF is used in the MM-based FDI scheme.	66
3.13	The detection time for each mode of fault that is applied at $t = 5$ seconds as a function of the number of the measurements or sensors that are employed. (a) the UKF is used in the MM-based FDI scheme, and (b) the EKF is used in the MM-based FDI scheme.	66
4.1	A graphical illustration of the \mathbf{C}_{2M} and \mathbf{H}_{2M} spaces. Note that projections of \mathbf{Y}_{2M} , $\mathbf{D}_{2M}\mathbf{U}_{2M}$ and $\mathbf{D}_{2M}\mathbf{U}_{2M}^{aux}$ onto the row space of \mathbf{H}_{2M} are identical.	77
4.2	Input estimation for the system (4.67) using two different rotation matrices: (a) $\theta = \frac{5\pi}{180}$, and (b) $\theta = \frac{45\pi}{180}$	96
4.3	The LOE fault input estimation of the MIMO non-minimum phase system (4.70).	97
4.4	The LOE fault estimation for the system (4.71).	98
4.5	Input estimation for system (4.72)	99
5.1	Upper bound of the NMP state estimation error versus n_d	128
5.2	The estimation of the MP state by utilizing the filter (5.18).	129
5.3	The estimation of the NMP state (the graphs are shifted by $n_d - n$ time steps to the left for the purpose of comparison) by utilizing the filter (5.39).	129
5.4	The estimation of the unknown input (the graphs are shifted by $n_d - n$ time steps to the left for the purpose of comparison) by utilizing equation (5.42).	130

5.5	The output tracking performance corresponding to different values of n_d by utilizing equations (5.45), (5.46) and (5.48).	130
5.6	The output tracking performance by utilizing equations (5.45), (5.46) and (5.48) corresponding to a smooth trajectory.	131
5.7	Simulation results for the MIMO system (5.62), (a) The NMP state estimation error versus n_d , (b) The MP state estimates, (c) The NMP state estimates, and (d) The unknown input estimates.	133
6.1	A fault is injected in the actuator 1 of the system (6.71) at $k = 150$. (a) The output of the residual generator filter for achieving the fault detection task, (b) The output of the residual generator filter insensitive to the fault in the actuator 2, and (c) The output of the residual generator filter that is insensitive to the fault in the actuator	1.162
6.2	A fault having a severity of 2 is injected in the sensor 2 of the system (6.72) at $k = 150$. (a) The output of the original sensor fault estimation filter, and (b) The output of the tuned sensor fault estimation filter.	165
6.3	Faults having severities of 1 and -1 are injected in the actuators or sensors of the system (6.72)	167
6.4	(a) The first actuator fault estimation error versus the second actuator fault estimation error for the system (6.74) using 500 Monte Carlo simulation runs, and (b) The first sensor fault estimation error versus the second sensor fault estimation error for the system (6.74) using 400 Monte Carlo simulation runs.	169
7.1	The frequency response \tilde{G}_i^p (from the input channel to the shaft rotational speed (N) output channel) ($i = 0, 1, \dots, 50$ and $p = 3$) computed at three PLAs equal to 50, 75 and 100%.	186

7.2	The relative errors between the estimated and the actual Markov parameters of the input channel to the shaft rotational speed output channel at the PLA=75% for three different values of Q	186
7.3	The relative errors between the estimated and the actual Markov parameters of the input channel to the compressor pressure output channel at the PLA=75% for three different values of Q	187
7.4	Fault detection filter residuals designed with the data obtained at PLA=75% but stimulated at PLA=80% while a 10% actuator fault is injected at the time step 150.	188
7.5	Fault detection filter residuals designed with the data obtained at PLA=75% but stimulated at PLA=80% while a 1% sensor fault in shaft rotational speed sensor is injected at the time step 150.	188
7.6	Residuals generated by a bank of two filters for the sensor fault isolation. The filters are designed with the data obtained at PLA=75% but stimulated at PLA=80% while a 1% fault is injected in the sensor measuring T_C at the time step 150.	190
7.7	Residuals generated by a bank of three filters for the sensor fault isolation. The filters are designed with the data obtained at PLA=75% but stimulated at PLA=80% while a 1% fault is injected in the sensor measuring T_C and N at the time steps 150 and 200, respectively. . . .	193
7.8	Actuator fault estimation filter residuals fed by measurements P_C and P_T for a 10% fault in the actuator. The filter is designed with the data obtained at PLA=75%. Note that the average of $\hat{f}(k)$ approach to 0.1 after the injection of the fault at the time step 150.	193

7.9	Actuator fault estimation filter residuals fed by the measurements P_C and N for a 10% fault in the actuator. The filter is designed with the data obtained at PLA=75%. Note that the average of $\hat{f}(k)$ approach to 0.1 after the injection of the fault at the time step 150.	194
7.10	Sensor estimation filter residuals fed by the measurements P_C and P_T for 1% and -1% concurrent sensor faults in P_C and P_T injected at the time steps 100 and 200, respectively. The filter is designed with the data obtained at PLA=75%.	194
A.1	The relative errors between the estimated and the actual Markov parameters of the input channel to the shaft rotational speed output channel at the PLA=50% for three different values of Q	224
A.2	The relative errors between the estimated and the actual Markov parameters of the input channel to the compressor pressure output channel at the PLA=50% for three different values of Q	225
A.3	The relative errors between the estimated and the actual Markov parameters of the input channel to the shaft rotational speed output channel at the PLA=100% for three different values of Q	225
A.4	The relative errors between the estimated and the actual Markov parameters of the input channel to the compressor pressure output channel at the PLA=100% for three different values of Q	226

List of Tables

2.1	The definition and description of the considered component faults. . .	40
2.2	The noise standard deviation (as % of the nominal noise at cruising condition).	43
3.1	The Extended Kalman Filter Algorithm	48
3.2	The Unscented Kalman Filter Algorithm	49
3.3	The definition and description of the considered component faults. . .	52
3.4	The operating modes corresponding to various possible two concurrent faults scenarios.	53
3.5	The average detection times for all the fault modes (P2 to P6) that are applied at $t = 5$ seconds as a function of the fault severity levels. .	58
3.6	The average detection times for all the modes of faults (P2 to P6) that are applied at $t = 5$ seconds as a function of the noise power factor.	65
3.7	The average detection times for all the fault modes (P2 to P6) that are applied at $t = 5$ seconds as a function of the number of the measurements or sensors that are employed.	65
5.1	Inversion-based output tracking algorithm.	124
5.2	Definition of parameters that are used for NMP state reconstruction using FIR filter (5.55)	126
6.1	The Monte Carlo simulation results for estimation of the faults	165
7.1	The average estimation relative errors for the first ten Markov parameters for all channels over 100 Monte Carlo simulation runs. . . .	187

7.2	Confusion matrix for the actuator fault detection performance. The fault severity and the PLA are 1% and 80%, respectively.	189
7.3	Confusion matrix for the actuator fault detection performance. The fault severity and the PLA are 5% and 80%, respectively.	189
7.4	Confusion matrix for the actuator fault detection performance. The fault severity and the PLA are 10% and 80%, respectively.	189
7.5	Confusion matrix for the sensor fault detection performance. The fault severity and the PLA are 1% and 80%, respectively.	189
7.6	The confusion matrix and definition of the parameters in equation (7.9). TP (true positive) denotes the number of healthy cases that are identified as healthy, FN (false negative) denotes the number of healthy cases that are identified as faulty, FP (false positive) denotes the number of faulty cases that are identified as healthy, and TN (true negative) denotes the number of cases that are faulty and identified as faulty.	190
7.7	The fault definitions for the confusion matrix analysis.	191
7.8	Confusion matrix of the sensor fault isolation performance for $Q = 25$, PLA=80% and the fault severity of 1%. The filters are designed with the data obtained at PLA=75%.	191
7.9	Confusion matrix of the sensor fault isolation performance for $Q = 50$, PLA=80% and the fault severity of 1%. The filters are designed with the data obtained at PLA=75%.	192
7.10	Confusion matrix of the sensor fault isolation performance for $Q = 100$, PLA=80% and the fault severity of 1%. The filters are designed with the data obtained at PLA=75%.	192

7.11	Average actuator fault estimation errors for 100 Monte Carlo simulation runs at PLA=80%. The filters are designed with the data obtained at PLA=75%.	195
7.12	Average sensor fault estimation errors for 100 Monte Carlo simulation runs at PLA=80%. The filters are designed with the data obtained at PLA=75%.	195
7.13	Average sensor fault estimation errors for different methods based on Markov parameter estimation and set of measurements (100 Monte Carlo simulation runs at PLA=80%). The filters are designed with the data obtained at PLA=75%.	195
A.1	Confusion matrix of the actuator fault detection performance. The fault severity and Q are 5% and 100, respectively.	223
A.2	Confusion matrix of the actuator fault detection performance. The fault severity and Q are 5% and 100, respectively.	224
A.3	Confusion matrix for the actuator fault detection performance. The fault severity and PLA are 1% and 55%, respectively.	226
A.4	Confusion matrix for the actuator fault detection performance. The fault severity and PLA are 5% and 55%, respectively.	227
A.5	Confusion matrix for the actuator fault detection performance. The fault severity and PLA are 10% and 55%, respectively.	227
A.6	Confusion matrix for the sensor fault detection performance. The fault severity and PLA are 1% and 55%, respectively.	227
A.7	Confusion matrix of the sensor fault isolation performance for $Q = 25$, PLA=55% and the fault severity of 1%. The filters are designed with the data obtained at PLA=50%.	228

A.8	Confusion matrix of the sensor fault isolation performance for $Q = 50$, PLA=80% and the fault severity of 1%. The filters are designed with the data obtained at PLA=75%.	228
A.9	Confusion matrix of the sensor fault isolation performance for $Q = 100$, PLA=55% and the fault severity of 1%. The filters are designed with the data obtained at PLA=50%.	229
A.10	Average actuator fault estimation error for 100 Monte Carlo simulations at PLA=55%. The filters are designed with the data obtained at PLA=50%.	229
A.11	Average sensor fault estimation error for 100 Monte Carlo simulations at PLA=55%. The filters are designed with the data obtained at PLA=50%.	230
A.12	Confusion matrix for the sensor fault detection performance with different values of E . The fault severity, PLA and Q are 1%, 80% and 100, respectively.	231
A.13	Confusion matrix for the actuator fault detection performance with different values of E . The fault severity, PLA and Q are 5%, 80% and 100, respectively.	231

Nomenclature

Abbreviations

FDI Fault Detection and Isolation

FDI&E Fault Detection, Isolation and Estimation

GPA Gas Path Analysis

MM Multiple Model

MP Minimum Phase

NMP Non-Minimum Phase

PE Persistently Exciting

PLA Power Lever Angle

SIM Subspace Identification Method

Subscripts

amb Ambient

C Compressor

CC Combustion chamber

f Fuel

mech Mechanical

n Nozzle

o Intake

T Turbine

Variables

β Bypass ratio

\dot{m} Mass flow rate, $\frac{Kg}{s}$

η Efficiency

γ Heat capacity ratio

c_p Specific heat at constant pressure, $\frac{J}{Kg.K}$

c_v Specific heat at constant volume, $\frac{J}{Kg.K}$

H_u Fuel specific heat, $\frac{J}{Kg}$

J Rotor moment of inertia, $Kg.m^2$

M Mach

N Rotational Speed, RPM

P Pressure, Pascal

P_0 Pressure at sea level at Standard Day

R Gas Constant, $\frac{J}{Kg.K}$

T Temperature, K

T_0 Temperature at sea level at Standard Day

V Volume, m^3

W Power, Watt

Chapter 1

Introduction

1.1 Introduction

There is an increasing demand for automation of fault diagnosis of systems since it will promote safety and reduce maintenance costs. There are some faults which are not identifiable manually at their commencement while their evolution may cause serious damages to the system. An autonomous fault diagnosis scheme will detect and isolate such faults and will trigger appropriate recovery automatic or manual actions; which makes the whole maintenance process cheaper and more reliable. Also, the benefits of autonomous fault diagnosis is better disclosed if it can be successfully implemented in fleet management of a product. The current fleet management of products imposes significant costs on customers since, in absence of an autonomous health status monitoring, a rigid schedule for product inspection in order to detect possible faults is used. Hence, beside costly unnecessary inspections for some vehicles, the delayed inspection of some others in which a fault has been maturely evolved entails additional costs which are avertable. An autonomous fault diagnosis may fully or partially replace such time-regulated maintenance policies, thus providing a more efficient fleet management strategy.

The term ‘autonomous fault diagnosis’ may refer to three tasks which are **i)** fault detection, **ii)** fault isolation, and **iii)** fault estimation. The task of fault detection is concerned with alarming the presence of a fault (or concurrent faults) in the system. In many cases, only detection of the fault does not suffice. One should isolate the detected fault among possible faults which is generally known as fault isolation problem. Typically, fault detection and fault isolation are simultaneously addressed in the literature and is well-known as Fault Detection and Isolation (FDI). The objective of fault estimation is to provide an estimate of the present faults in the system. One can immediately conclude that fault estimation under some special circumstances and scenarios can include the tasks of fault detection and isolation. In other words, if faults are successfully estimated, then it implies faults are also successfully detected and isolated. However, the task of fault estimation is significantly more complex and involved. Therefore, fault detection and isolation is generally considered in the literature.

The basic idea in autonomous fault detection and isolation- as well as in fault estimation- is construction of a dynamical filter (or a bank of dynamic filters) that receives the system I/O data and generates the so-called residuals. The residuals are processed through a logic - mostly known as FDI logic - to detect and isolate faults. The above idea is initially introduced by Beard [1].

Since the concept of autonomous FDI schemes was introduced by Beard [1], it has received enormous attraction in the literature. Some excellent surveys have been published that summarize the extensive literature on FDI [2–6]. The two main categories of FDI schemes are model-based and data-driven approaches. The available model-based approaches can be roughly categorized as follows [7,8], **i)** full state observer-based methods [9–12], **ii)** unknown input observer methods [10,13–16], **iii)**

parity relation approach [17–19], **iv**) Kalman filter based approaches [20–22], **v**) stochastic approaches [23,24], **vi**) system identification approaches [25], **vii**) nonlinear system approaches [26–28], and **viii**) discrete event system approaches [29–32]. The term ‘data-driven’ covers a wide range of techniques in the literature. Some of the most important categories are, **i**) Subspace based methods reviewed in [33,34], **ii**) neural network [35–39] reviewed in [40], **iii**) fuzzy logic [41,42], and **iv**) hybrid approaches [43–45] reviewed in [46]. The above overview illustrate the extensive literature of FDI.

In this thesis, we have concentrated on three problems which are,

- Nonlinear multiple model based FDI,
- Inversion based fault estimation, and
- Subspace based data-driven FDI and estimation (FDI&E)

The objective of the above problems are to address three main practical issues in FDI&E of real-life applications which are non-linearity of the system, fault estimation for fault tolerant control and strategic planning and lack of mathematical model. We tackle each issue separately by approaches that provide promising solutions. However, our proposed solutions are interconnected and interrelated that could be integrated into a single module as part of our future works. This vision of an integrated solution is the reason we do not select neural networks as a data-driven solution. Our subspace based data-driven approach shares a common ground with our MM-based and inversion-based solutions in terms of falling under the category of observer based methods.

We use multiple model based approach to address the problem of nonlinear

FDI [47–51]. The basic idea is that a bank of Kalman filters each of which is associated with one fault is constructed. For a nonlinear system, a bank of Extended Kalman Filters (EKF) or Unscented Kalman Filters (UKF) is constructed. Then I/O data of the system in operation is fed to these filters and residuals are generated which is in fact conditional probability computed using innovation vectors. These residuals are combined through a Bayesian algorithm which finally determines which fault mode is most probably active. If there is no fault, then the healthy mode will have the highest probability.

We comprehensively discuss the problem of fault estimation due to the fact that it is becoming increasingly important for fault tolerant control and strategic planning. Numerous approaches are proposed in the literature for fault estimation. We selected here to consider inversion based fault estimation which is not arbitrary selection since as we will show it is closely related to our proposed data-driven FDI&E schemes. Figure 1.1 shows a schematic of the inversion-based fault estimation scheme. In inversion-based fault estimation, faults are modeled as unknown inputs, and the fault estimation process deals with the reconstruction of the unknown inputs through the inverse system filter which is fed by the available system measurements and known inputs. The linearization of the nonlinear mathematical model that is developed in this thesis yields a minimum phase system at all operating points. Therefore, the present faults in our model can be estimated using the conventional inversion-based approaches that are available in the literature. Yet, we propose a general framework for fault estimation in both minimum phase and non-minimum phase systems due to the fact that it cannot be guaranteed that the corresponding linear model to all types of gas turbines at all operating points is minimum phase.

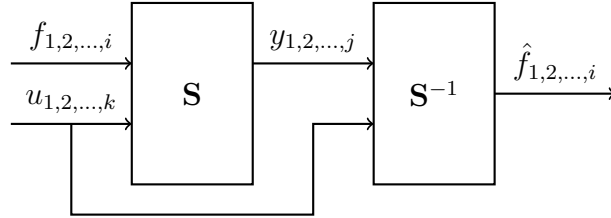


Figure 1.1: A schematic representation of the inverse-based fault estimation scheme, where \mathbf{S} represents the plant, \mathbf{S}^{-1} represents the fault estimation filter which is the inverse of the system \mathbf{S} , $f_{i,2,\dots,i}$ is the fault vector which is modeled as unknown input, $u_{1,2,\dots,k}$ is the known input vector, $y_{1,2,\dots,j}$ is the measurement vector, and $\hat{f}_{1,2,\dots,i}$ is the estimated fault vector using the FDI filter \mathbf{S}^{-1} .

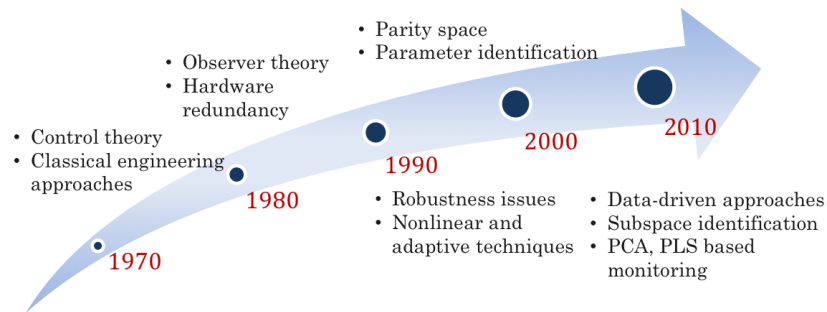


Figure 1.2: Historical development of FDI schemes (taken from [52])

Finally, we addressed the problem of data-driven FDI&E. Figure 1.2 shows a time-line of FDI historical development. As it can be seen, state-of-art FDI research are data-driven approaches for one obvious reason. As engineering systems evolve to be more complex from design and operation perspectives, it is less likely to have a well-defined and accurate mathematical model for such systems. Numerous data-driven approaches are proposed in the literature for instance Artificial Intelligence-based, statistical approaches, and subspace-based identification methods. In this thesis, we utilized subspace-based FDI&E methods [34] due to its numerous advantages such as non-iterative design procedure, analytic conditions of existence and stability and low required computational power. We will demonstrate that one can actually construct an FDI&E scheme for gas turbines only using the system I/O data.

In this thesis, we considered gas turbines - as one of the most important engineering systems in energy and aerospace - as our application. Safety of the aviation is directly linked with the safety and reliability of the aerial engines. Restrict policies are implemented in all phases of aerial engines life cycle in order to ensure safety standards and requirements are met, however, these policies are imposing increasing maintenance costs which are avertable if better maintenance solution, without compromising safety, is proposed. The fleet management of aerial engines is overwhelmingly difficult task which requires a complex coordination and management of human resource, hardware and software. Currently time-based and condition-based solutions are utilized for fleet management of aerial engines. As it is reported in some researches, these methods are suffering from large number of false alarms. One possible solution to deal with these issues is to design and implement autonomous FDI schemes. Compared to the time-based and condition-based solutions, the cost benefit of the autonomous FDI schemes have made them an attractive alternative

solution for gas turbines fleet management as well as other industrial applications.

In the following, we discuss the above subjects in more details. Specifically, we provide literature review for each subject and elaborate on our contributions in the context of the available literature.

1.2 Multiple Model Based Fault Detection and Isolation

The term "multiple model" covers a wide range of approaches in which the common goal is to propose an architecture (or hierarchy) for a bank of estimators for isolation and identification of faults. The differences arise due to application domain, configurations used, fault isolation logic implemented and the estimator types invoked. A possible choice is implementing linear and nonlinear Kalman Filters as estimators in bank of filters which has become a popular technique in gas turbine fault diagnosis as reported in [53]. For instance, a multiple model approach that has utilized Linear Kalman Filters (LKF) as estimators is comprehensively investigated by Kobayashi et al [54, 55] and Meskin and his colleagues [56]. The disadvantage of the FDI schemes based on LKF is that they are not robust to the variations of operation conditions while this situation occurs often during a flight, i.e. during takeoff and landing, and should be addressed. One can deal with this issue by implementing nonlinear Kalman filters which have become popular in nowadays applications. In gas turbine FDI applications, Simon [57] has systematically compared the performance of LKF, Extended Kalman Filter (EKF), and Unscented Kalman Filter (UKF) from computational effort and estimation performance perspectives; however, the FDI scheme used is not MM-based.

In this thesis, a multiple model (MM)-based scheme that employs nonlinear

Kalman filters as state estimators (detection filters) is developed and implemented for the first time in the literature for fault diagnosis of gas turbines. This is a natural extension of our previous work [56] in which we have proposed a MM-based approach that employed LKF as state estimators (detection filters). This is partially motivated by the limitations of the MM-based approach that uses LKF in its structure that makes it incapable of fully coping with the variations in the ambient conditions and power settings.

Our proposed MM-based fault diagnosis approach assumes that the dynamics of the engine is adequately represented by a nonlinear model that is parameterized by a fault vector. It is further assumed that the fault vector can take an only M discrete values corresponding to the normal and various failure modes in the engine. The nonlinear model corresponding to each fault vector is obtained from the fully nonlinear model of the system, and a bank of nonlinear Kalman filters is then designed where each nonlinear Kalman filter corresponds to and is associated with a specific value of the fault vector. The conditional probabilities of each discrete parameter value being the correct one, given the measurement history, are calculated iteratively by using the Bayes' law. The current operating mode of the engine is then determined based on the maximum probability criteria. This approach has an advantage over the approaches that residuals are compared with specified thresholds [54] that is no need to evaluate and verify thresholds in advance. A hierarchical approach is proposed where multiple levels of the detection filters are designed that according to the current engine status and operating mode (that is healthy or faulty), only an appropriate set of the bank of filters becomes and is active at any given time. This hierarchical architecture enables the detection and isolation of the engine concurrent faults without imposing any additional computational load on the FDI scheme as compared to the single fault detection and isolation case.

We have investigated the performance of both the Extended Kalman Filter

(EKF) and the Unscented Kalman Filter (UKF) as state estimators (detection filters) in our proposed MM-based architecture. Simulation results presented for a single spool gas turbine demonstrate the effectiveness and capabilities of our proposed fault diagnosis framework and algorithm. Also, simulation results convincingly verify that indeed considerable improvements are obtained in the performance of the UKF over that of the EKF schemes in terms of the fault detection time, robustness to sensor noises and functionality with different sets of measurements.

1.3 Inversion-Based Fault Estimation

The problem of estimating system faults that could occur in actuators and sensors has been recently receiving extensive attention due to advances in the field of fault tolerant control and growth in demand for higher levels of reliability and autonomy in safety critical systems. Numerous approaches have been proposed for fault estimation of dynamical systems, such as unknown input observers (UIO) [13,14,58,59] and sliding mode observers [60]. An important category of available solutions are known as inversion-based approaches that are addressed in the works such as [61–65]. However, these results have one major drawback in common. Specifically, they will fail for non-minimum phase systems. In fact, stable inversion of non-minimum phase systems is an outstanding challenge in any given context associated with the problem of input reconstruction.

Inversion of linear systems was first systematically treated by Brockett and Mesarovic in [66]. The classic references are *structure algorithm* [67], Sain & the Massey algorithm [68], and the Moylan algorithm [69]. Gillijns [70] has also proposed a general form of the Sain & Massey algorithm in which some free parameters

are available that can be adjusted under certain circumstances for obtaining a stable inverse system provided that the original system does not have any unstable transmission zeros (that is, minimum phase systems). The inversion problem has been tackled by more sophisticated methods. Palanthandalam-Madapusi and his colleagues have considered the problem of input reconstruction in several works, however the solutions provided all apply to only minimum-phase systems [71–73]. Flouquet and his colleagues proposed a sliding mode observer for the input reconstruction that is only valid for minimum phase systems [74]. Marro and Zattoni have proposed a geometric approach [75] for state reconstruction of both minimum and non-minimum phase systems given the system does not have any transmission zeros on the unit circle. Wahls and his colleague developed an stable inversion for both minimum and non-minimum phase systems while assuming that the throughput matrix is full column rank [76].

We propose a novel inversion-based approach for fault estimation of linear discrete-time dynamical systems. Faults can be modeled in various forms in the literature as either additive faults or multiplicative faults. The proper choice depends on the actual characteristics of a fault. Typically, sensor bias, actuator bias and actuator loss of effectiveness (LOE) are considered as additive faults. Multiplicative fault models are more suitable for representing changes in the system dynamic parameters such as gains and time constants [77]. Moreover, additive faults are typically considered as LOE step-wise or linearly varying (ramp-wise) inputs that are injected to the system. In this work, we consider estimation of step-wise or ramp-wise additive faults that cover a wide range of faults in real life applications.

Our novel inversion-based unknown input reconstruction scheme has several advantages over the available methods in the literature. The most important one is the fact that it can handle systems with transmission zeros on the unit circle. Moreover, we introduce a feedback control signal that not only stabilizes the unstable

inverse dynamics, but also it provides an unbiased estimation for certain categories of faults. We will highlight the contributions of our solution in more details in Section 1.7.

1.4 Inversion-Based Reconstruction of System States and General Unknown Input

We discussed the problem of inversion-based fault estimation. In order to augment our contribution, we then consider the general problem of system state and unknown input reconstruction. The inversion-based state and unknown input reconstruction has several important applications in control theory such as fault estimation and output tracking. We specifically discuss the problem of Output tracking since it can be considered as dual problem of unknown input reconstruction.

It is well-known that unbiased inversion-based output tracking is essentially non-causal since it requires the information on the entire trajectory in future that is not a reasonable assumption for many applications. Zou and Devasia [78–80] have introduced preview-based stable-inversion method for continuous-time systems. Basically, this method requires access to a finite window of future data instead of having the entire future trajectory, although the approach results in a degraded output tracking error performance. This technique has been significantly improved by the recent work [81, 82], however, these works are also developed for continuous-time LTI systems. Moreover, the method is constrained under restrictive assumptions, such as the smoothness of the desired trajectories. Several other work using different approaches are available in the literature that are mostly application of a particular method known as the Q-learning [83] or by using filtered basis functions [84] to this problem.

In this study, we first address the inversion-based unknown state and input reconstruction problem. A general unknown input observer is proposed that accurately and independently reconstructs the minimum phase states of the system by using only the available system measurements. The minimum phase states here refers to $n - p$ states of the overall system, where n denotes the order of the system and p denotes the number of unstable transmission zeros. Next, the estimated minimum phase states are considered as inputs to an FIR filter to reconstruct the p non-minimum phase states of the system. The FIR filter estimates the non-minimum phase system states with a time delay of $n + n_d$ steps. It also yields an estimation error which is a function of the to be selected parameter n_d . We have explicitly derived subsequently the relationship between the reconstruction error and n_d .

Specifically, we have shown that the estimation error is proportional to inverse of the smallest non-minimum phase zero to the power of n_d . Hence, if the system does not have any transmission zeros on the unit circle, the estimation error asymptotically decays to zero as n_d is increased. This can therefore ensure that an unbiased input and states estimation can be obtained. For most cases, an n_d equal to four or five times n would yield an almost perfect estimation results for any smooth or non-smooth unknown input. For a smooth input, an n_d as small as 2 may suffice.

We comprehensively address and discuss the dynamics of the non-minimum phase states and have derived the relationships among the system matrices. Finally, by invoking a minor modification, our proposed methodology is extended to solve the inversion-based output tracking control problem. As opposed to a delayed reconstruction, our method now requires data corresponding to $n + n_d$ time steps ahead of the desired trajectory. As in the previous problem, we have quantified the tracking error characteristics and have shown that an almost perfect tracking is achievable by properly selecting n_d that yields an unbiased state reconstruction

that can be achieved as in the first problem.

Finally, we extend the proposed methodology of system state and unknown input reconstruction for the case fault estimation. The difference is due to the fact that known inputs are involved in the case of fault estimation that should be incorporated in the solution. We will demonstrate the performance of our proposed methodology through comprehensive simulations and comparative studies.

1.5 Data Driven Fault Detection, Isolation and Estimation

As engineering systems evolve, it is less likely that engineers have a detailed and accurate mathematical description of the dynamical systems they work with. On the other hand, advances in sensing and data acquisition systems can provide a large volume of raw data for most engineering applications. Consequently, one can find a trend towards data-driven based approaches in many disciplines and problems, including fault diagnosis.

The term ‘data-driven’ covers a wide range of techniques in the literature. Some of the most important strategies are neural networks [35], fuzzy logic [41], and hybrid approaches [43]. In addition to artificial intelligence based methods, some efforts have been made that are aimed at extending the rich model-based fault diagnosis techniques to data-driven based approaches.

A trivial solution will be the one where one can first identify a mathematical dynamical model of the system from the available data, and then by using the resulting explicit model one then implements and designs conventional model-based

schemes. However, this approach suffers from the subsequent errors that are introduced in the system identification process and that may ultimately aggravate the FDI scheme design process errors which can result in a totally unreliable fault diagnosis scheme.

In recent years, a new paradigm has emerged in the literature that aims at direct and explicit construction of the FDI schemes from the available system input-output (I/O) data [85–87]. Subspace-based data-driven fault detection and isolation methods [25, 88] represent as one of the main approaches that have been reviewed in [25]. These methods are developed based on identifying the left null space of the system extended observability matrix using the I/O data. An estimate of the system order and an orthogonal basis for the system extended observability matrix - or its left null space - are obtained via the SVD decomposition of a particular data matrix that is constructed from the system I/O data. This process is known as the reduction step.

Essentially, in the reduction step it is assumed that the number of the first set of significantly nonzero singular values and the associated directions provide an estimate of the system order and a basis for the extended observability matrix. However, in most cases, this process leads to erroneous results due to the fact that the truncation point for neglecting small singular values, as being insignificant, is not obvious a trivial and is subjective and problem dependent.

Consequently, an erroneous system order and basis for the extended observability matrix - or its left null space - can be obtained. This error manifests itself in the fault diagnosis scheme performance in a nonlinear manner. In other words, the performance representation of the FDI scheme is not a linear function of the gap between the estimated system order and the system extended observability matrix

and the actual ones. Due to these drawbacks, other works that have appeared in the literature are mainly concerned with only the fault estimation problem in which the main objective is to eliminate and remove the above reduction step.

Dong and his colleagues [89] have developed a fault detection scheme that can be directly synthesized from the system I/O data without involving the reduction step. The detection filter is in fact a high order FIR filter parameterized by the system Markov parameters. The extension of this work to the fault isolation task is not trivial and straightforward. It can be performed by obtaining a projection vector that is computed through the SVD decomposition of a transfer matrix parameterized by the Markov parameters estimation errors [90]. However, the Markov parameters estimation errors are not generally available. Therefore, the authors in [90] have managed to synthesize this matrix from the I/O data. The order of the isolation filters can be as large as 30. Dong and Verhaegen [91] used the same strategy for direct construction of the fault estimation filter. The underlying assumption is that the system should have a stable inverse. It will be asymptotically unbiased if the FIR filter order tends to infinity.

Wan and his colleagues [92] have reasoned in their recent work that the method of [91] cannot be applied to certain open-loop systems. Moreover, it does not compensate for the estimation errors. Consequently, Wan and his colleagues have proposed offline and online algorithms for compensating for the estimation errors. Yet, it suffers from two major drawbacks. First, the estimation is asymptotically unbiased if the filter order tends to infinity. Second, the computational time per sample for the online optimization algorithm - which is the one that yields an almost unbiased results among the others proposed - is significantly high as compared to the offline methods in [92].

In this work, to overcome the above drawbacks and limitations, we have proposed fault detection, isolation and estimation filters that are constructed directly in the state-space representation form from and using only the available system I/O data. Our proposed schemes only require identification of the system Markov parameters that are achieved by using conventional methods, such as correlation analysis [93] or subspace methods [94–97] from the healthy I/O data.

Our method does not involve the reduction step or equivalent forms of the extended observability matrix. Therefore, the estimation error is linearly dependent on the Markov parameter estimation errors. This step is already addressed in the literature as reviewed above. However, it turns out that our state-space based approach can address several important difficulties that are associated with the currently available works in the literature. First, our proposed identification and isolation filters are conveniently configured for the isolation task of both single as well as concurrent faults through constructing filter banks.

An important feature of our proposed state-space based method is that estimation will be achieved asymptotically unbiased by a filter order as low as the maximum of the system relative degree and the system observability index. Both of these parameters are bounded by the system order. Moreover, it does not necessarily require the condition of having an entire stable inverse system. The flexibility of our proposed scheme allows arbitrary selection of the subsystems for achieving the fault isolation or for performing the fault estimation tasks.

In other words, one can select a different subsystem if an actuator fault estimation is blocked due to unstable inversion of a specific subsystem. Finally, the

state-space based approach allows one to implement a simple and yet effective procedure for compensating for the estimation errors. Towards this end, in this work we derive the estimation error dynamics and show that it can be directly identified from the healthy system I/O data.

We provide several illustrative simulations to demonstrate merits of our proposed data-driven approach. More importantly, we apply our proposed data-driven FDI&E scheme to the case of gas turbine. However, it requires several adjustments as discussed in the next Section.

1.6 Fault Diagnosis of Gas Turbines

Research on aircraft gas turbine engine fault detection and isolation (FDI) has been and continues to be at the core of an extensive body of literature [36, 98–100]. Several excellent surveys and reviews have addressed this vast literature from different perspectives [101–104]. The main theme of research in gas turbine FDI is based on Gas Path Analysis (GPA) in which by measurement and estimation of lumped parameters of the system such as temperature and pressure at each stage, one attempts to isolate and identify actuator, sensor, or component faults [101]. This approach has mainly been developed by Urban [105] and Volponi [106].

Model-based approaches constitute a major part of the aircraft gas turbine engine FDI literature [20, 107–109]. The major drawback of model-based approaches is the need for a reasonably accurate mathematical model of the system, which is rarely available. This fact has motivated researches to consider data-driven approaches as an alternative and a more practical solution [98, 110–112]. Consequently, numerous

data-driven solutions based on neural networks [35, 36, 113, 114], statistical and feature extraction methods [115], and fuzzy logic [116], among others have appeared in the literature. Certainly, neural network and fuzzy logic are powerful tools for nonlinear fault diagnosis and estimation in complex nonlinear systems. However, gas turbines can be accurately represented by linear systems in most phases of their operation such as cruise in aircraft or steady state operation in power plants. On the other hand, two challenges are outstanding in the implementation of these methods for linear phases of operation. First, these data-driven methods require a large amount of actual data that are difficult to process and can be as challenging as high fidelity mathematical models. Secondly, they have complicated structures with numerous tuning parameters that have to be determined through computationally involved procedures.

We extend and apply our proposed data-driven FDI&E scheme described above to the application of aircraft gas turbine engine. The design procedure is as follows. The healthy aircraft gas turbine engine is stimulated by a harmonic input containing a limited number of frequencies at a given operating point. In other words, the identification input is the sum of simple harmonic signals each of which has a different frequency. The frequency response of the system is then obtained by computing the FFT of the input and measurement signals. Conventionally, one may invoke the correlation analysis to estimate the system impulse response coefficients (Markov parameters) from the frequency response data, however, our simulations have shown that this procedure is not robust when one is dealing with a low number of frequencies. Consequently, we utilize a method that is devised in [117] and which is robust for estimation of the Markov parameters. Once the Markov parameters are estimated, then we will be able to construct our proposed FDI&E filters as described in our work.

Our proposed approach does not require any *a priori* knowledge of the system mathematical model. This is an important advantage over the model-based techniques. Yet, it enjoys the advantages of the model-based techniques in terms of its simplicity and the guaranteed stability. It also has several advantages over the currently available data-driven solutions in the literature. First, our approach does not require availability of a large amount of data. The frequency response of the system at only a limited number of frequencies will suffice. Second, the FDI&E filters are directly and conveniently designed and constructed from the estimated Markov parameters. Consequently, one will avoid the complicated trade-off studies, tuning techniques and iterative optimization procedures that are typically required in other data-driven methods such as statistical or neural network-based approaches that are developed in the literature.

It should also be pointed out that some studies aim to identify the system dynamics or tune the thermodynamic model of the gas turbine engine by fitting a transfer function to the frequency response data [118]. One may suggest to utilize these models to first identify a model and then use model-based techniques for constructing the FDI&E filters. This solution is not reliable due to several reasons. First, *a priori* knowledge of the system number of poles and zeros is required for these methods. Different selection of the number of poles and zeros may lead to solutions that may not correspond to an accurate representation of the system actual dynamics. There is no formal and rigorous methodology for *a priori* optimally selecting the number of poles and zeros of the system model. Moreover, the system identification errors will stack up and compound with other errors resulting in an unreliable FDI&E scheme. Our approach, on the other hand, has several advantages as follows,

- It allows a direct design and construction of the FDI&E filters from only the available system I/O data that indeed significantly reduces the overall resulting errors.
- It eliminates the intermediate step of system identification which is often challenging and may not lead to a conclusive result.
- Finally, no *a priori* knowledge about the linearized model of the system as well as its number of poles and zeros are required.

This completes our detailed literature review and elaboration on our contributions. In the next section, we highlight the main contributions of the thesis.

1.7 Contributions of the Thesis

We consider three problems in this thesis which are **i)** nonlinear MM-based FDI, **ii)** Inversion-based fault estimation, and **iii)** data-driven FDI&E. All the proposed solutions are applied and demonstrated to the application problem of gas turbine. In fact, our proposed solutions address three important practical issues in gas turbines FDI&E which are non-linearity, estimation of present faults and lack of mathematical model. In the following, we specify and highlight the most important contributions of our proposed solutions.

The objective of our proposed MM-based FDI approach is to design a nonlinear FDI scheme such that a bank of filters covers all the operational envelop. The main contributions of our proposed nonlinear MM-based FDI are,

1. Proposed a nonlinear MM-based FDI using bank of EKF and UKF for the first time in the literature.
2. Comprehensively compared the performance of the EKF and UKF for detection and isolation of gas turbine faults.

3. The robustness of the proposed scheme to noise and outlier is established through comprehensive simulations. In fact, our proposed nonlinear MM-based FDI has a game-theoretic nature that makes it significantly robust to noise and parameter variations.

We earlier mentioned that the demand for fault estimation schemes is increasing as the fault tolerant controllers and autonomous strategic and maintenance planning tools are evolving. An important category of observe based methods for fault estimation is the inversion-based approaches. We propose two independent inversion-based fault estimation schemes. In the first proposed scheme, we introduce a dynamic filter that provides an unbiased estimation for certain categories of faults. The contribution of the first solution can be summarized as follows,

1. Our proposed scheme can handle both minimum phase and non-minimum phases systems as well as systems having transmission zeros on the unit circle under a single framework. To the best of our knowledge, the available solutions in the literature cannot cope with the problem of unknown input reconstruction for systems having transmission zeros on the unit circle.
2. Our solution yields an estimate of the unknown inputs (i.e., faults) by only using the system measurements directly (that is, in one single operation) as it eliminates the conventional intermediary step of state estimation process. This is a significant improvement and extension from the current practices in the literature for linear systems inversion.
3. Finally, our scheme allows relaxation of several restrictive assumptions such as the controllability condition or certain rank conditions that are imposed on the system matrices. It also provides further degrees of freedom for addressing other design challenges such as robustness if one is interested in considering these additional requirements.

We further investigated the problem of inversion-based approach for reconstruction of states, inputs and faults. In contrast to the first solution, it can reconstruct any unknown input or fault. The contributions of the thesis in this part are as follows,

1. A methodology for estimation of unknown states and unknown inputs (or faults) of both minimum and non-minimum phase linear discrete-time systems is proposed and developed,
2. In our proposed methodology, the minimum phase states are decoupled and estimated by using the system measurements that are then used as inputs to an FIR filter for estimation of the non-minimum phase states,
3. Several important theorems and lemmas are stated that specify, determine, and quantify the interrelations between the system matrices and the system transmission zeros,
4. An algorithm and a simple constructive procedure for designing an inversion-based output tracking control scheme is proposed, and finally
5. The accuracy of our proposed input and state estimation scheme as well as the output tracking control performance as a function of the delay parameter are quantified and investigated.

Our proposed data-driven approach constitutes a major contribution of this thesis. Our solution renders direct construction of FDI&E filters from system I/O data. Therefore, it resolves one of the most important issues frequently present in real-life applications which is lack of mathematical model. Our contributions in this part of the thesis can be summarized as follows,

1. A general fault detection and isolation filter for both actuator and sensor faults is developed and directly constructed from only the available system I/O data

in the state-space form in a manner that does not involve a reduction step. Moreover, our approach does not require an *a priori* knowledge of the system order. The proposed fault detection and isolation filters can be conveniently configured for both single and concurrent fault detection and isolation tasks by using a subset of the I/O data.

2. A fault estimation scheme for both actuator and sensor faults (single and concurrent) is developed and directly constructed from the available system I/O data in the state-space form in a manner that does not involve a reduction step. The proposed estimation filter is asymptotically unbiased having an order as small as the maximum of the observability index and the system relative degree.
3. A new offline procedure for tuning the estimation filters are proposed to compensate for errors that are caused by the Markov parameters estimation uncertainties.

Our proposed data-driven FDI&E scheme cannot be directly applied to the case of gas turbine since it is less likely that a gas turbine is stimulated by a wide-band inputs. Instead, we use frequency-domain data for applying our proposed data-driven methodology. In other words, the main contribution of this part of the thesis can be stated as follows:

1. Development of a data-driven methodology for direct design of fault detection filters, fault isolation filters, as well as fault estimation filters by using only the gas turbine engine frequency response data that are collected at limited number of frequencies.

The contributions of this thesis are established using rigorous derivation of lemmas and theorems. Moreover, they are illustrated and demonstrated through comprehensive simulations as well as comparative studies.

1.8 Structure of the Thesis

The remainder of the thesis is organized as follows. The mathematical model of the gas turbine used throughout this thesis is presented in Chapter 2. It turns out that our model is minimum phase at all operating points. Therefore, we also included conventional inversion-based fault estimation method for minimum phase systems and applied it to the gas turbines. These results presented should provide a benchmark and point of reference for the subsequent methods that are developed in this thesis. Chapter 3 is devoted to the nonlinear multiple model based fault diagnosis of gas turbines. The inversion-based fault estimation for both minimum phase and non-minimum phase systems is presented in Chapter 4. A general solution to the problem of system state and unknown input reconstruction and its dual problem of output tracking is provided in Chapter 5. The data driven fault diagnosis and estimation of the linear systems is proposed in Chapter 6. Chapter 7 includes the application of the proposed data driven scheme to the application of gas turbines. Finally, the thesis is concluded in Chapter 9.

Chapter 2

Background

In this chapter, we present our developed mathematical model for gas turbines. This model serve as basis for our simulations and case studies through this thesis. Moreover, we provide a description of well-established inversion methods for minimum phase systems and its application to the gas turbine.

2.1 Physics of the Gas Turbines

Gas turbines have unique features that have made them an essential part of aviation and power industries. They are light, reliable and efficient. Figure 2.1 shows a schematic of a gas turbine structure. Typically, it has a duct, compressor, combustion chamber, turbine and nozzle. Duct is designed to conduct a smooth air flow from outside to the compressor. The pressure of the air is slightly increased at each stage of the compressor until it reaches the final stage to be injected into the combustion chamber. The typical pressure ratio is 10 to 20 times depending on the number of stages. The process of air compression consumes energy which is provided by turbine. For this reason, the compressor and turbine are installed on a single shaft. An assembly of compressor and turbine on a single shaft is called ‘spool’.

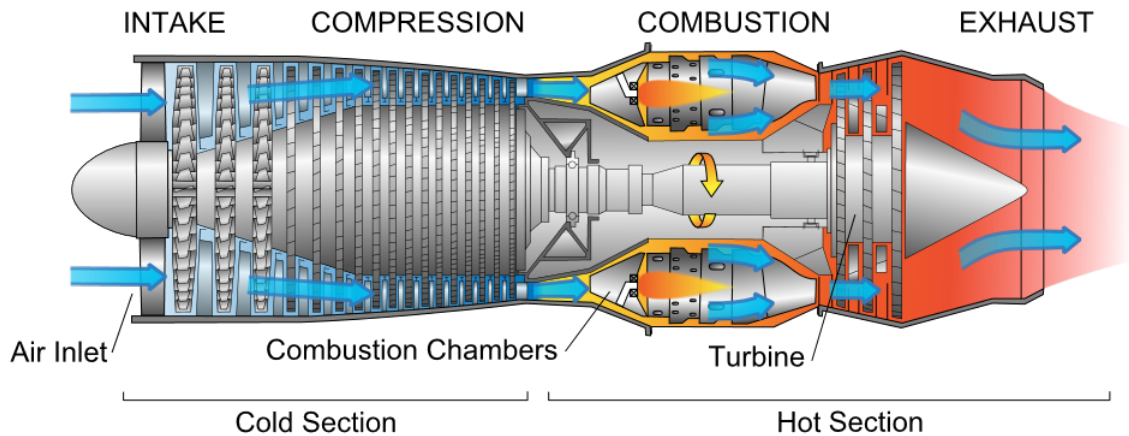


Figure 2.1: A schematic of gas turbine (Taken from [119]).

The high pressure air is mixed with fuel and burnt in the combustion chamber. In contrast to the auto engines, the gas turbine combustion chamber has a constant and stable flame. The hot pressurized air flow passes through turbine and partially losses its energy which in fact is converted to the kinetic energy of the spool. Then, the hot pressurized air is accelerated through nozzle which creates jet stream and pushes the aircraft forward. In turboshafts, turbine has many stages, therefore all the energy of hot pressurized air is converted to the kinetic energy for rotating a generator or helicopter blades in addition to compressors.

Gas turbines are complex engineering systems. Moreover, they operate under extremely harsh conditions of high temperature combined with the extremely high centrifugal stresses and vibrations. Therefore, gas turbines are subjected to enormous physical faults that may lead to total failures. Some faults are easily detected and isolated such as compressor surge or fire. However, most of the faults have smaller scales so they cannot be immediately detected, for instance, cell stall, crack and erosion. One cannot deal with a wide range of gas turbine faults by devising a single FDI scheme since each fault has a different nature and signature. Every interrelated set of faults should be separately investigated.

We used Gas Path Analysis to define the faults considered in this thesis [105, 106]. In this approach, the decreases in efficiency or deviation from normal mass flow rate in compressor and turbine are considered as parameters that represent a wide range of physical faults. Therefore, once a fault (or concurrent fault) is alarmed using this approach, then it assures the presence of a physical fault that should be investigated by more advanced inspection methods. In addition, we considered actuator and sensor faults which point to physical malfunctions in these subsystems.

2.2 The Gas Turbine Mathematical Model

Based on the available literature on modeling a nonlinear dynamics of a gas turbine [120, 121], a SIMULINK model for a single spool engine is first developed. In order to obtain this nonlinear dynamics, rotor and volume dynamics are both considered. Heat transfer dynamics also contributes to this nonlinear behavior particularly when there exist considerable differences between the temperatures of the air stream and the components due to a large power excursion, e.g. during the startup or rapid maneuvers of an agile aircraft [122]. Nevertheless, the above effect has been neglected since in this paper we are concerned with a commercial single spool gas turbine at normal operating conditions. We have used the commercial software GSP 10 [123] for the purposes of conducting model validation studies. A more detailed description of the model can be found in [37, 120, 121].

In the following, detailed mathematical expressions corresponding to each specific component of the gas turbine are presented. Next, these equations are combined to construct a nonlinear Simulink model for gas turbine. Figure 2.2 shows the information flow process in our Simulink model.

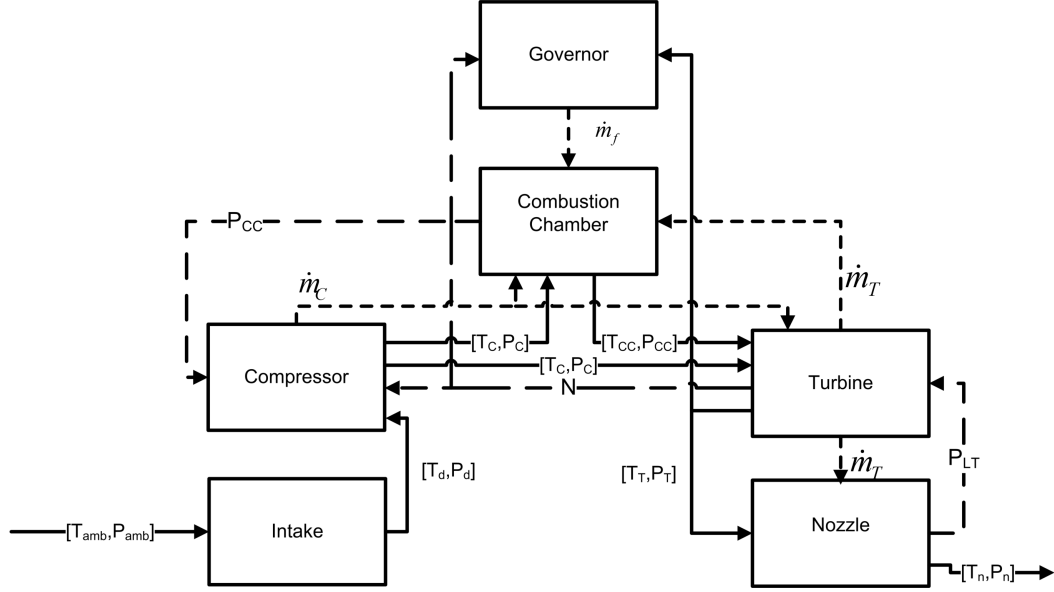


Figure 2.2: Information flow diagram in a modular modeling of the gas turbine dynamics.

Rotor Dynamics

The Energy balance between turbine and compressor is described by,

$$\frac{dE}{dt} = \eta_{mech} W_T - W_C \quad (2.1)$$

where $E = \frac{J(\frac{N \cdot 2\pi}{60})^2}{2}$, and W_C and W_T are the power consumed by compressor and generated by turbine as given by equations (2.6) and (2.8), respectively. Basically, the above equation implies that the rotational speed of the spool depends on the energy generated by turbine and energy consumed by compressor.

Volume Dynamic

The volume dynamics describes the pressure dynamics inside a volume. Assume that the gas has zero speed and has homogenous properties over the volumes, then this dynamics is described by,

$$\dot{P} = \frac{RT}{V} (\sum \dot{m}_{in} - \sum \dot{m}_{out}) \quad (2.2)$$

where \dot{m}_{in} and \dot{m}_{out} denote incoming and exiting mass flow rate from the considered volume.

Compressor

The compressor behavior, as a quasi-steady component, is determined by using the compressor performance map. Given the pressure ratio (π_C) and the corrected rotational speed ($N/\sqrt{\theta}$), one can obtain the corrected mass flow rate ($\dot{m}_C\sqrt{\theta}/\delta$) and efficiency (η_C) from the performance map by using a proper interpolation technique, where $\theta = T_C/T_0$ and $\delta = P_C/P_0$, i.e. $\dot{m}_C\sqrt{\theta}/\delta = f_{\dot{m}_C}(N/\sqrt{\theta}, \pi_C)$ and $\eta_C = f_{\eta_C}(N/\sqrt{\theta}, \pi_C)$. Once these parameters are obtained, the compressor temperature rise and the mechanical power are obtained as follows:

$$\frac{P_o}{P_{amb}} = \left[1 + \eta_d \frac{\gamma - 1}{2} M^2 \right]^{\frac{\gamma}{\gamma - 1}} \quad (2.3)$$

$$\frac{T_o}{T_{amb}} = 1 + \frac{\gamma - 1}{2} M^2 \quad (2.4)$$

$$T_C = T_o \left[1 + \frac{1}{\eta_C} (\pi_C^{\frac{\gamma - 1}{\gamma}} - 1) \right] \quad (2.5)$$

$$W_C = \dot{m}_C c_p (T_o - T_C) \quad (2.6)$$

Turbine

Similar to the compressor, the turbine behavior is also determined by using the turbine performance map. Given the pressure ratio (π_T) and the corrected rotational speed ($N/\sqrt{\theta}$), the corrected mass flow rate ($\dot{m}_T\sqrt{\theta}/\delta$) and the efficiency (η_T) are obtained from the performance map, i.e. $\dot{m}_T\sqrt{\theta}/\delta = f_{\dot{m}_T}(N/\sqrt{\theta}, \pi_T)$ and $\eta_T = f_{\eta_T}(N/\sqrt{\theta}, \pi_T)$. The temperature drop and the turbine mechanical power are

obtained as follows:

$$T_T = T_{CC} \left[1 - \eta_T (1 - \pi_T^{\frac{\gamma-1}{\gamma}}) \right] \quad (2.7)$$

$$W_T = \dot{m}_T c_p (T_{CC} - T_T) \quad (2.8)$$

Combustion Chamber

The pressure and temprature dynamics inside the combustion chamber is governed by equations (2.9) and (2.10).

$$\dot{P}_{CC} = \frac{P_{CC}}{T_{CC}} \dot{T}_{CC} + \frac{\gamma R T_{CC}}{V_{CC}} (\dot{m}_C + \dot{m}_f - \dot{m}_T) \quad (2.9)$$

$$\begin{aligned} \dot{T}_{CC} = & \frac{1}{c_v m_{CC}} [(c_p T_C \dot{m}_C + \eta_{CC} H_u \dot{m}_f - c_p T_{CC} \dot{m}_T) - \\ & c_v T_{CC} (\dot{m}_C + \dot{m}_f - \dot{m}_T)] \end{aligned} \quad (2.10)$$

In fact, these are volume dynamics between compressor and turbine and energy balance of combustion process.

Nozzle

If condition (2.11) holds, the nozzle mass flow rate is obtained using equation (2.12), otherwise using equation (2.13). Note that $P_n = P_T$ and $T_n = T_T$.

$$\frac{P_{amb}}{P_n} < \left[1 + \frac{1 - \gamma}{\eta_n (1 + \gamma)} \right]^{\frac{\gamma}{\gamma-1}} \quad (2.11)$$

$$\frac{\dot{m}_n \sqrt{T_n}}{P_n} = \frac{u}{\sqrt{T_n}} \frac{A_n}{R} \frac{P_{amb}}{P_n} \frac{T_n}{T_{no}} \quad (2.12)$$

where $\frac{u}{\sqrt{T_n}} = \sqrt{2c_p \eta_n (1 - (\frac{P_{amb}}{P_n})^{\frac{\gamma-1}{\gamma}})}$, $\frac{T_{no}}{T_n} = 1 - \eta_n (1 - (\frac{P_{amb}}{P_n})^{\frac{\gamma-1}{\gamma}})$, and

$$\frac{\dot{m}_n \sqrt{T_n}}{P_n} = \frac{u}{\sqrt{T_n}} \frac{A_n}{R} \frac{P_{crit}}{P_n} \frac{T_n}{T_{crit}} \quad (2.13)$$

and where $\frac{P_{crit}}{P_n} = (1 - \frac{1}{\eta_n} (\frac{\gamma-1}{\gamma+1}))^{\frac{\gamma}{\gamma-1}}$, $\frac{u}{\sqrt{T_n}} = \frac{2\gamma R}{\gamma+1}$, and $\frac{T_{crit}}{T_n} = \frac{2}{\gamma+1}$.

Set of nonlinear equations

The ambient conditions (T_{amb} , P_{amb} and M) are usually measured. Therefore, the parameters P_o and T_o are easily computed using equations (2.3) and (2.4), respectively. If we have π_c and η_c , then we can calculate T_C and W_c using equations (2.5) and (2.6), respectively. The compressor pressure ratio is given by P_{CC}/P_o , and P_{CC} is obtained by integrating equation (2.9). In order to do this, we need compressor, turbine and fuel mass flow rates. The fuel mass flow rate (\dot{m}_f) is known. Having rotational speed (N) and (π_c), we read the compressor mass flow rate (\dot{m}_c) and efficiency (η_c) from the ‘compressor map’. The rotational speed (N) is given by differential equation (2.1) which needs the calculation of W_T as given by equation (2.8). The parameters T_T and T_{CC} in equation (2.8) are calculated using equations (2.7) and (2.10), respectively. In order to calculate T_T using equation (2.7), we need turbine pressure ratio (π_T) and efficiency (η_T). The turbine pressure ratio is given by P_T/P_{CC} . The pressure after turbine is governed by the following volume dynamics,

$$\dot{P}_T = \frac{RT_M}{V_M}(\dot{m}_T + \frac{\beta}{1+\beta}\dot{m}_C - \dot{m}_n)$$

Having P_T and N , it is straightforward to read \dot{m}_T and η_T from ‘turbine map’. Putting all together, the set of nonlinear equations corresponding to a single spool gas turbine is given in equation (2.14).

$$\begin{aligned} \dot{T}_{CC} &= \frac{1}{c_v m_{CC}} [(c_p T_C \dot{m}_C + \eta_{CC} H_u \dot{m}_f - c_p T_{CC} \dot{m}_T) - \\ &\quad c_v T_{CC} (\dot{m}_C + \dot{m}_f - \dot{m}_T)] \\ \dot{N} &= \frac{\eta_{mech} \dot{m}_T c_p (T_{CC} - T_T) - \dot{m}_C c_p (T_C - T_o)}{JN(\frac{\pi}{30})^2} \\ \dot{P}_T &= \frac{RT_M}{V_M} (\dot{m}_T + \frac{\beta}{1+\beta} \dot{m}_C - \dot{m}_n) \\ \dot{P}_{CC} &= \frac{P_{CC}}{T_{CC}} \dot{T}_{CC} + \frac{\gamma RT_{CC}}{V_{CC}} (\dot{m}_C + \dot{m}_f - \dot{m}_T) \end{aligned} \tag{2.14}$$

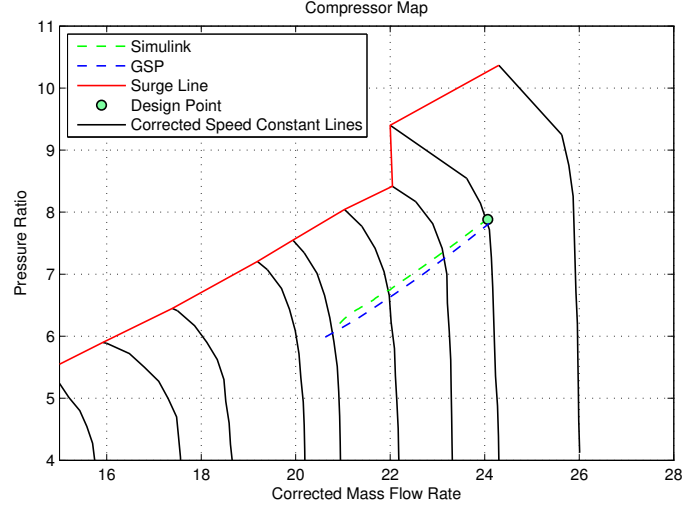


Figure 2.3: Steady state series at PLAs ranging from 0.4 to 1 on the compressor performance map. The initial condition is initially set equal to PLA=30%, and then followed by a transient to reach to the desired PLA. Each point corresponds to the final state of the engine at the end of the transient response.

Furthermore, using [120] the following dynamics for the fuel mass flow rate are considered

$$\tau \frac{d\dot{m}_f}{dt} + \dot{m}_f = G u_{fd} \quad (2.15)$$

where τ is the time constant of the governor, G is the gain associated with fuel valve and u_{fd} denotes the fuel demand which is computed by using a feedback from the rotational speed as described in [120]. A modular Simulink model is developed to simulate the above gas turbine nonlinear dynamics as described by equations (2.14) and (2.15).

Figure 2.3 shows the series of steady states that are obtained from our non-linear model and the commercial software GSP [123] at PLAs ranging from 0.4 to 1. At each point, the initial condition of the PLA equal is set to 0.3 followed by a transient to reach to the steady state corresponding to the desired PLA. Since the steady state corresponding to each PLA is independent of the path taken during the transient (unless the compressor surges), it provides a suitable basis for comparison. As can be observed from Figure 2.3 the responses corresponding to our model and

the GSP match each other within an acceptable error tolerance (below 5%). The difference between the two representations is manifested in terms of the complexity of the mathematical model used where our form is simpler as compared to the more complicated representation of the GSP ([123]).

2.3 Inversion-Based Fault Estimation for Minimum Phase Systems

Consider an LTI discrete-time system as follows,

$$\mathbf{S} : \begin{cases} x(k+1) = Ax(k) + Bf(k) + Ev(k) \\ y(k) = Cx(k) + Df(k) \end{cases} \quad (2.16)$$

where $x \in \mathbb{R}^n$, the known input $v \in \mathbb{R}^r$, the unknown fault signal $f \in \mathbb{R}^m$, and the measurement $y \in \mathbb{R}^l$. All the matrices are known. Moreover, the subsystem from unknown fault signal to outputs are minimum phase. The objective is to estimate the unknown signal fault $f(k)$ using the known inputs $v(k)$ and known outputs $y(k)$ through system inversion.

Essentially the inversion of the system \mathbf{S} is itself another system \mathbf{S}^{-1} whose inputs are the outputs and known inputs of the system \mathbf{S} and its output is an estimate of the unknown inputs f that are applied to the system \mathbf{S} . Consider the case when D is full column rank so that one can easily compute the *instantaneous inverse* of the system as follows,

$$\mathbf{S}^{-1} : \begin{cases} \eta(k+1) = (A - BD^\dagger C)\eta(k) + Ev(k) + BD^\dagger y(k) \\ f(k) = -D^\dagger Cz\eta(k) + D^\dagger y(k). \end{cases} \quad (2.17)$$

where D^\dagger denotes the Moore–Penrose pseudo inverse of the matrix D . Note that in case when the matrix D is not full column rank, then it is not possible to compute

an *instantaneous inverse*. The solution in this case is to consecutively differentiate or delay the measurement equation of the system \mathbf{S} , and eliminate the derivatives or the delays of the unknown inputs at each step by a proper transformation, until the matrix D becomes full rank. This is the basics of standard approaches that are proposed in the literature for computation of an inverse system as in the *structure algorithm* [67], Sain & the Massey algorithm [68] and the Moylan algorithm [69].

The major drawback of the *structure algorithm* [67] and the Sain & Massey algorithm [68] is that in certain cases both yield an unstable inverse system. On the other hand, the Moylan algorithm always produces a stable inverse system provided that the original system is not non-minimum phase. Gillijns [70] has proposed a general form of the Sain & Massey algorithm in which there exists some free parameters which can be adjusted under certain circumstances for obtaining a stable inverse system. Since the *structure algorithm* is also a special case of this general form, we only consider here the general form of the Sain & Massey algorithm.

2.3.1 General Form of the Sain & Massey Algorithm

We define $\mathbf{Y}(k-L)$, $\mathbf{V}(k-L)$ and $\mathbf{F}(k-L)$ as

$$\mathbf{Y}(k-L) = \begin{bmatrix} y(k-L) \\ y(k-L+1) \\ \vdots \\ y(k) \end{bmatrix}, \mathbf{V}(k-L) = \begin{bmatrix} v(k-L) \\ v(k-L+1) \\ \vdots \\ v(k) \end{bmatrix}, \mathbf{F}(k-L) = \begin{bmatrix} f(k-L) \\ f(k-L+1) \\ \vdots \\ f(k) \end{bmatrix} \quad (2.18)$$

so that one can easily verify from the measurement equation of the system \mathbf{S} the following:

$$\mathbf{Y}(k-L) = \mathbf{C}x(k-L) + \mathbf{E}\mathbf{V}(k-L) + \mathbf{D}\mathbf{F}(k-L) \quad (2.19)$$

where,

$$\mathbf{C} = \begin{bmatrix} C \\ CA \\ \vdots \\ CA^L \end{bmatrix}; \mathbf{C}_- = \begin{bmatrix} C \\ CA \\ \vdots \\ CA^{L-1} \end{bmatrix} \quad (2.20)$$

$$\mathbf{E} = \begin{bmatrix} 0 & 0 & \dots & 0 \\ CE & 0 & \dots & 0 \\ \vdots & \vdots & \ddots & \vdots \\ CA^{L-1}E & CA^{L-2}E & \dots & 0 \end{bmatrix} \quad (2.21)$$

$$\mathbf{D} = \begin{bmatrix} D & 0 & \dots & 0 \\ CB & D & \dots & 0 \\ \vdots & \vdots & \ddots & \vdots \\ CA^{L-1}B & CA^{L-2}B & \dots & D \end{bmatrix}; \mathbf{D}_- = \begin{bmatrix} D & 0 & \dots & 0 \\ CB & D & \dots & 0 \\ \vdots & \vdots & \ddots & \vdots \\ CA^{L-2}B & CA^{L-3}B & \dots & D \end{bmatrix} \quad (2.22)$$

Let us assume that there exist a matrix \mathcal{M}_L of size $m \times l(L+1)$ such that

$$\mathcal{M}_L \mathbf{D} = \mathcal{M}_L \left[\begin{array}{c|ccc} D & 0 & \dots & 0 \\ CB & D & \dots & 0 \\ \vdots & \vdots & \ddots & \vdots \\ CA^{L-1}B & CA^{L-2}B & \dots & D \end{array} \right] = \left[\mathbf{I} \mid \mathbf{0} \right] \quad (2.23)$$

It is then obvious from equation (2.19) that the unknown input is given by:

$$f(k-L) = -\mathcal{M}_L \mathbf{C}x(k-L) - \mathcal{M}_L \mathbf{E}\mathbf{V}(k-L) + \mathcal{M}_L \mathbf{Y}(k-L) \quad (2.24)$$

The general condition under which the matrix \mathcal{M}_L exists is given by the following theorem.

Theorem 2.1. *Assume $Y \in \mathbb{R}^{k \times p}$ and $Z \in \mathbb{R}^{q \times p}$ are known. Then there exists a matrix $X \in \mathbb{R}^{q \times k}$ that satisfies $XY = Z$ if and only if*

$$\text{rank} \left(\begin{bmatrix} Z \\ Y \end{bmatrix} \right) = \text{rank}(Y) \quad (2.25)$$

and the general solution is given by

$$X = ZY^\dagger + U(\mathbf{I} - YY^\dagger) \quad (2.26)$$

where $U \in \mathbb{R}^{q \times k}$ is an arbitrary matrix [124].

Note that Y^\dagger is the Moore-Penrose pseudo inverse of the matrix Y i.e. it is any matrix that satisfies $YY^\dagger Y = Y$. If one defines $\mathfrak{J} = \begin{bmatrix} \mathbf{I} & \mathbf{0} \end{bmatrix}$, given that $\mathcal{M}_L \mathbf{D} = \mathfrak{J}$ it follows immediately from Theorem 2.1 that \mathcal{M}_L exists if and only if

$$\text{rank} \left(\begin{bmatrix} \mathfrak{J} \\ \mathbf{D} \end{bmatrix} \right) = \text{rank}(\mathbf{D})$$

On the other hand,

$$\mathbf{D} = \begin{bmatrix} D & 0 \\ \mathbf{C}_- B & \mathbf{D}_- \end{bmatrix}$$

Therefore,

$$\text{rank} \left(\begin{bmatrix} \mathfrak{J} \\ \mathbf{D} \end{bmatrix} \right) = \text{rank}(\mathbf{D}_-) + m$$

Thus, we have the following proposition:

Proposition 2.1. *A matrix \mathcal{M}_L that satisfies equation (2.23) exists if and only if*

$$\text{rank}(\mathbf{D}) - \text{rank}(\mathbf{D}_-) = m. \quad (2.27)$$

where $\text{rank}(\mathcal{D}_{-1}) = 0$, and the general solution is given by

$$\mathcal{M}_L = \begin{bmatrix} \mathbf{I} & \mathbf{0} \end{bmatrix} \mathbf{D}^\dagger + \mathbf{g}_L (\mathbf{I} - \mathbf{D} \mathbf{D}^\dagger) \quad (2.28)$$

where \mathbf{g}_L of size $m \times l(L+1)$ is an arbitrary matrix [70].

In order to compute an inverse of the system \mathbf{S} , one should increase L until an L is found for which the condition 2.27 holds. This parameter L is known as the *inherent delay* of the system [68]. The value of the *inherent delay* is bounded according to the following theorem [125].

Theorem 2.2. *If system \mathbf{S} is invertible, then the inherent delay of \mathbf{S} can not exceed $n - q + 1$, where q is the dimension of the nullspace of D [125].*

It follows from equation (2.24) that one also needs to estimate the system states x in order to reconstruct the unknown input. An estimator that estimates both the states and the unknown inputs is called the *joint input-state estimator* [70]. Since the inputs of the inverse system \mathbf{S}^{-1} are $\mathbf{Y}(k - L)$ and $\mathbf{V}(k - L)$, one can assume the following state estimator of the form,

$$\eta(k + 1) = (A - \mathcal{B}_L \mathbf{C})\eta(k) + \mathcal{B}_L \mathbf{Y}(k - L) - \mathcal{B}_L \mathbf{E} \mathbf{V}(k - L) + E v(k - L) \quad (2.29)$$

where \mathcal{B}_L should be determined such that the state estimation error asymptotically converges to zero. If one substitutes $\mathbf{Y}(k - L)$ from equation (2.19) into equation (2.29), one obtains

$$\begin{aligned} \eta(k + 1) &= (A - \mathcal{B}_L \mathbf{C})(\eta(k) - x(k - L)) \\ &+ Ax(k - L) + \mathcal{B}_L \mathbf{D} \mathbf{F}(k - L) \\ &+ Ev(k - L) \end{aligned} \quad (2.30)$$

In order to obtain equation (2.30), we have added and subtracted $Ax(k - L)$ from equation (2.29). On the other hand, from the state equation of system \mathbf{S} , we have

$$x(k - L + 1) = Ax(k - L) + Bf(k - L) + Ev(k - L) \quad (2.31)$$

Hence, the state estimation error dynamics is obtained by subtracting equation (2.30) from equation (2.31) as follows,

$$\begin{aligned} \eta(k + 1) - x(k - L + 1) &= (A - \mathcal{B}_L \mathbf{C})(\eta(k) - x(k - L)) \\ &+ \mathcal{B}_L \mathbf{D} \mathbf{F}(k - L) - Bf(k - L) \end{aligned} \quad (2.32)$$

If one chooses \mathcal{B}_L such that,

$$\mathcal{B}_L \mathbf{D} = \begin{bmatrix} B & \mathbf{0} \end{bmatrix} \quad (2.33)$$

and assumes $e_x(k) = \eta(k) - x(k - L)$, then it follows from equations (2.32) and (2.33) that the state estimation error dynamics is given by,

$$e_x(k + 1) = (A - \mathcal{B}_L \mathbf{C})e_x(k) \quad (2.34)$$

Once again we invoke Theorem 2.1 for solving equation (2.33). Therefore, the following proposition is immediate.

Proposition 2.2. *A matrix \mathcal{B}_L that satisfies equation (2.33) exists if and only if*

$$\text{rank}(\mathbf{D}) = \text{rank}(\mathbf{D}_-) + \text{rank} \left(\begin{bmatrix} B \\ D \end{bmatrix} \right) \quad (2.35)$$

and the general solution is given by

$$\mathcal{B}_L = \begin{bmatrix} B & \mathbf{0} \end{bmatrix} \mathbf{D}^\dagger + \mathbf{k}_L (I - \mathbf{D}\mathbf{D}^\dagger) \quad (2.36)$$

where \mathbf{k}_L of size $n \times l(L + 1)$ is an arbitrary matrix [70].

If one combines equations (2.24) and (2.29), the general form of the inverse system \mathbf{S}^{-1} is given by,

$$\mathbf{S}^{-1} : \begin{cases} \eta(k + 1) = (A - \mathcal{B}_L \mathbf{C})\eta(k) - \mathcal{B}_L \mathbf{E}\mathbf{V}(k - L) + Ev(k - L) + \mathcal{B}_L \mathbf{Y}(k - L) \\ \hat{f}(k - L) = -\mathcal{M}_L \mathbf{C}\eta(k) - \mathcal{M}_L \mathbf{E}\mathbf{V}(k - L) + \mathcal{M}_L \mathbf{Y}(k - L) \end{cases} \quad (2.37)$$

Provided that the parameters \mathbf{g}_L and \mathbf{k}_L are set to zero, then a special form is obtained which is well-known as the Sain & Massey inverse system [68] as follows:

$$\mathbf{S}_{SM}^{-1} : \begin{cases} \eta(k + 1) = (A - B\mathcal{M}_L \mathbf{C})\eta(k) - B\mathcal{M}_L \mathbf{E}\mathbf{V}(k - L) + Ev(k - L) + B\mathcal{M}_L \mathbf{Y}(k - L) \\ \hat{f}(k - L) = -\mathcal{M}_L \mathbf{C}\eta(k) - \mathcal{M}_L \mathbf{E}\mathbf{V}(k - L) + \mathcal{M}_L \mathbf{Y}(k - L) \end{cases} \quad (2.38)$$

The most important disadvantage of the Sain & Massey algorithm is that in certain cases it produces an unstable inverse system although the original system is not non-minimum phase. It can clearly be seen in equation (2.38) that there are

no free parameters for adjusting the poles of the unstable inverse. This issue can be resolved in the general form (2.37) by adjusting the free parameters \mathbf{g}_L and \mathbf{k}_L , however, one derive the conditions under which this can be accomplished. It follows from equations (2.24) and (2.37) that the estimation error of the unknown input is given by

$$e_u(k) = \hat{f}(k-L) - f(k-L) = -\mathcal{M}_L \mathbf{C} e_x(k)$$

Therefore, the state estimation error should converge asymptotically to zero for successful recovering of the unknown input especially when the system \mathbf{S}^{-1} is initialized to an arbitrary initial conditions. If one combines equations (2.34) and (2.36), then we have

$$\begin{aligned} e_x(k+1) &= \left(A - \begin{bmatrix} B & \mathbf{0} \end{bmatrix} \mathbf{D}^\dagger \mathbf{C} \right) e_x(k) \\ &\quad - \mathbf{k}_L \left((I - \mathbf{D} \mathbf{D}^\dagger) \mathbf{C} \right) e_x(k) \\ &= (\mathcal{A} - \mathbf{k}_L \mathcal{F}) e_x(k) \end{aligned}$$

It is well-known from the control theory that \mathbf{k}_L can be chosen such that the poles of $(\mathcal{A} - \mathbf{k}_L \mathcal{F})$ are placed at any desired locations if and only if the pair $(\mathcal{A}, \mathcal{F})$ is observable which is in fact equivalent to the condition that system should be minimum phase [126].

2.3.2 Application to Gas Turbine

We linearize the nonlinear dynamic model (2.14) using a sampling period of 0.01 seconds corresponding to a given operating point to obtain an LTI system of the form (2.16). In our model the states are $x = [T_{CC}, N, P_T, P_{CC}]^T$, the known inputs are $v = PLA$, the measurements are $y = [T_C, P_C, N, T_T, P_T]^T$, and the unknown fault inputs are $[f_{mC}, f_{eC}, f_{mT}, f_{eT}]^T$. Table 2.1 defines the faults that are considered. As an example, the numerical values of the matrices of the system (2.16), which are obtained from the linearization of the nonlinear system (2.14) with sampling time

Table 2.1: The definition and description of the considered component faults.

Component Fault	Description
f_{mC}	Decrease in the compressor flow capacity
f_{eC}	Decrease in the compressor efficiency
f_{mT}	Decrease in the turbine flow capacity
f_{eT}	Decrease in the turbine efficiency

equal to 0.01 seconds at $PLA = 80\%$, $T = 0^\circ C$, $P = 0.9$ bar and $M = 0.3$, are as follows. One can easily verify the system from faults to output is minimum phase.

$$A = \begin{bmatrix} 0.553 & 0.001 & 0.000 & -0.006 \\ 7.847 & 0.971 & 0.025 & -14.860 \\ 3.746 & -0.031 & 0.924 & 0.325 \\ 0.095 & 0.000 & 0.000 & 0.694 \end{bmatrix}$$

$$B = \begin{bmatrix} 2.028 & -0.040 & -2.269 & 0.044 \\ -51.790 & 62.950 & 40.920 & 64.700 \\ -49.300 & -20.690 & -7.511 & -1.101 \\ 0.153 & -0.004 & 0.741 & -0.113 \end{bmatrix}$$

$$C = \begin{bmatrix} 28.130 & -0.011 & 0.000 & 0.000 \\ 1.000 & 0.000 & 0.000 & 0.000 \\ 0.000 & 1.000 & 0.000 & 0.000 \\ -22.680 & -0.003 & 0.811 & 70.020 \\ 0.000 & 0.000 & 0.000 & 1.000 \end{bmatrix}; E = \begin{bmatrix} 0.856 \\ 7.208 \\ 195.100 \\ 0.064 \end{bmatrix}; D = 0$$

It should be noted that the main methodology in gas turbines engine fault estimation is based on the Gas Path Analysis (GPA) in which by measurement and estimation of lumped parameters of the system, such as temperature and pressure at each stage, one attempts to isolate and identify actuator, sensor, or component faults [101]. This approach has mainly been developed by Urban [105] and Volponi [106]. More specifically, in the GPA analysis component faults are modeled

as deficiencies in the component efficiency and/or mass flow rate. This is a reasonable approach since although faults have roots in a physical change in the components nevertheless their effects are manifested through deficiencies in the component efficiency and/or mass flow rate.

In order to estimate faults, one needs to set up an architecture in which the fault estimation filter is concatenated in a specific configuration with the original system. The proposed fault estimation scheme is graphically illustrated in Figure 2.4. The system does not have an instantaneous inverse, which implies that delays should be allowed in order to compute the inverse system. Simple calculations show that the inherent delay of the gas turbine model is 1 (that is, $L = 1$). Consequently, one delay is needed to construct the signals $\mathbf{Y}(k - L)$ and $\mathbf{V}(k - L)$ as defined in equation (2.18). Finally, one should characterize the inverse system \mathbf{S}^{-1} . The original Sain & Massey algorithm (equation (2.38)) gives an unstable inverse system. For instance, for the system that is given above, the eigenvalues of the inverse system are $[1.00, 0.73, 0.00, 0.00]^T$, which implies that the inverse is not stable. Therefore, we use the general form of the Sain & Massey algorithm (equation (2.37)) and adjust the free parameter \mathbf{k}_L to place the poles at desired locations.

The numerical values for the inverse of the above system are as follows. The poles of the system are placed at $[0.5, -0.5, 0.25, -0.25]^T$ (see equation(2.37)). Note that $A(a : b, c : d)$ refers to the elements in rows a to b of columns c to d of matrix A . Also $A(:, c : d)$ refers to elements in all rows of columns c to d of matrix A .

$$(A - \mathcal{B}_L \mathbf{C}) = \text{diag}(0.5, -0.5, 0.25, -0.25)$$

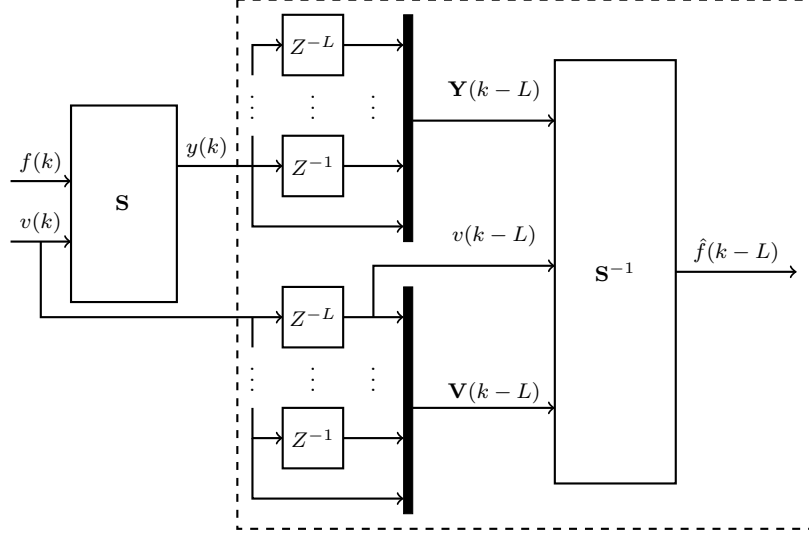


Figure 2.4: A schematic representation of the gas turbine inverse-based fault estimation scheme. The inherent delay of the gas turbine model is 1 (i.e., $L = 1$). For a description of notations, refer to Figure 1.1.

$$\mathcal{B}_L(:, 1 : 5) = \begin{bmatrix} 0.000 & 0.500 & 0.000 & 0.000 & 0.000 \\ 0.000 & 0.000 & -0.500 & 0.000 & 0.000 \\ 1.256 & -97.910 & -4.850 & 1.231 & -29.516 \\ 0.000 & 0.000 & 0.000 & 0.000 & -0.250 \end{bmatrix}$$

$$\mathcal{B}_L(:, 6 : 10) = \begin{bmatrix} 0.000 & 1.000 & 0.000 & 0.000 & 0.000 \\ 0.000 & 0.000 & 1.000 & 0.000 & 0.000 \\ 0.000 & 97.911 & 4.849 & 0.000 & 21.701 \\ 0.000 & 0.000 & 0.000 & 0.000 & 1.000 \end{bmatrix}$$

$$\mathcal{M}_L(:, 1 : 5) = \begin{bmatrix} -0.0041 & 0 & 0 & -0.0046 & 0 \\ -0.0039 & 0 & 0 & 0.0000 & 0 \\ 0.0008 & 0 & 0 & 0.0003 & 0 \\ 0.000 & 0 & 0 & -0.0039 & 0 \end{bmatrix}; \mathcal{M}_L(:, 6 : 10) = \begin{bmatrix} 0 & 0 & -0.0166 & 0 & 0.9111 \\ 0 & 0 & 0.0000 & 0 & 0.0000 \\ 0 & 0 & 0.0034 & 0 & 1.1532 \\ 0 & 0 & 0.0000 & 0 & 0.0000 \end{bmatrix}$$

Assume that in the cruise condition where the fuel flow rate and the ambient conditions are constant, a 5% single fault occurs in one component of the gas turbine. Since the inverse system is driven by the noisy measurement vector in practice,

Table 2.2: The noise standard deviation (as % of the nominal noise at cruising condition).

N	P_C	T_C	P_T	T_T
0.051	0.164	0.230	0.164	0.097

we have also applied noise to the measurement signals in order to examine the performance of the system to noise. The noise power that are applied are shown in Table 2.2. These numerical values are taken from [127]. Figure 2.5 shows the residuals that are generated by the fault estimation scheme with and without noise. As it can be seen, the proposed fault estimation scheme successfully estimates the faults.

Figure 2.6 shows the fault estimation scheme performance in presence of concurrent faults. Faults are consecutively injected at the time steps 1000, 1500, 2000 and 2500. It follows that the fault estimation scheme is successful in detecting and isolating faults as they occur consequentially in this simulation scenario. Note that as each fault occurs, the estimated fault severities of the previously occurred faults are slightly changed. This is due to the fact that as each fault occurs, it slightly changes the dynamics of the model, and thus it induces certain linearization errors that result in a slightly induced errors in the estimated severities of the faults. This explains the “ladder” shape of the signals shown in Figure 2.6. In fact, one can conclude that the fault estimation scheme is not reasonably robust to the linearization errors that are induced due to the fault occurrences, specially when the number of concurrent faults increases.

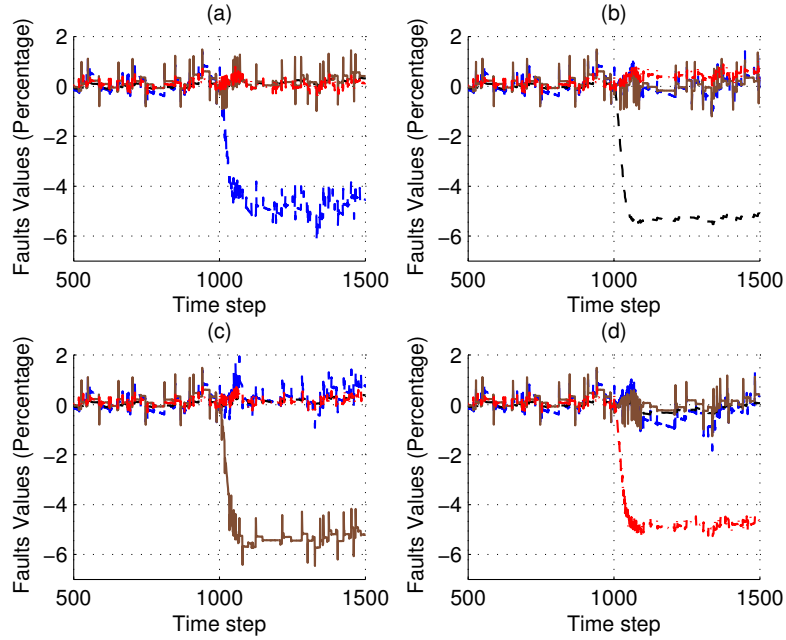


Figure 2.5: Residuals that are generated by the fault estimation scheme under four distinct simulation scenarios . (a) A 5% single fault is injected at the time step $k = 1000$ in the compressor mass flow rate while the other components are healthy. Blue signal represents the residual corresponding to the fault f_{mC} . The estimation error is 7%. Other signals represent the residuals corresponding to other faults. Similarly, we have for (b) a 5% single fault in the compressor efficiency (black signal) (estimation error: 7%) (c) a 5% single fault in the turbine mass flow rate (brown signal) (estimation error: 2.5%), and (d) a 5% single fault in the turbine efficiency (red signal) (estimation error: 4%). For all cases, the PLA setting, ambient temperature, pressure and Mach number are 80%, 0°C, 0.9 bar and 0.3 respectively. The poles of the filter are placed at $[0.5, -0.5, 0.25, -0.25]^T$.

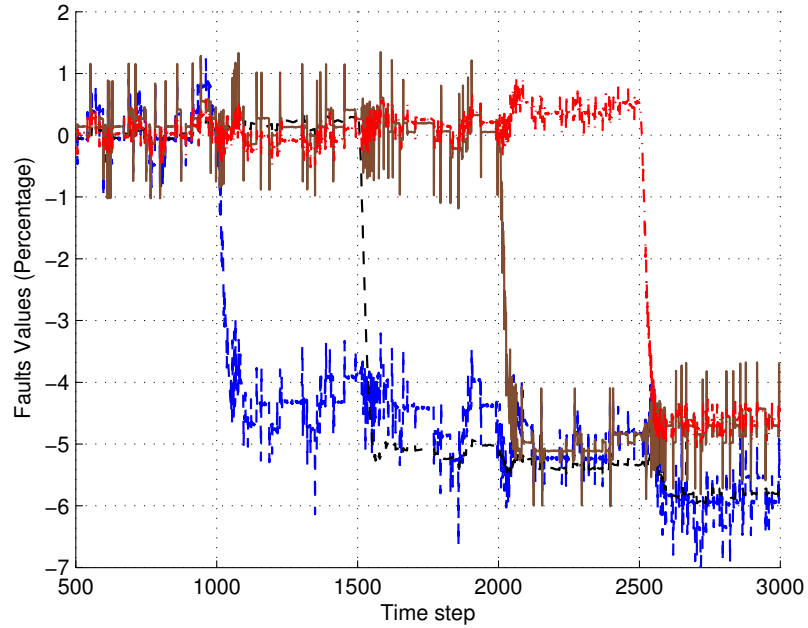


Figure 2.6: Residuals generated by the fault estimation scheme in presence of concurrent faults. The PLA setting, the ambient temperature, the pressures and the Mach number are 80%, 0°C, 0.9 bar, and 0.3, respectively. The poles of the filter are placed at $[0.5, -0.5, 0.25, -0.25]^T$. First a 5% fault is injected in the compressor mass flow rate at the time step $k = 1000$ (blue line). Then a 5% fault is injected in the compressor efficiency at the time step $k = 1500$ (black line). Another 5% fault is injected in the turbine mass flow rate at the time step $k = 2000$ (brown line). Finally, a 5% fault is injected in the turbine efficiency at the time step $k = 2500$ (red line). The final estimation error for blue, black, brown and red signals are 17%, 16%, 5% and 5% respectively.

Chapter 3

Nonlinear Multiple Model Based FDI of Gas Turbines

In this chapter, a nonlinear fault detection and isolation (FDI) scheme that is based on the concept of multiple model (MM) approach is proposed for gas turbines. A modular and a hierarchical architecture is proposed which enables the detection and isolation of both single as well as concurrent permanent faults in the engine. A set of nonlinear models of the gas turbine in which compressor and turbine maps are used for performance calculations corresponding to various operating modes of the engine (namely, healthy and different fault modes) is obtained. Using the multiple model approach the probabilities corresponding to the engine modes of operation are first generated. The current operating mode of the system is then detected based on evaluating the maximum probability criteria. The performance of our proposed multiple model FDI scheme is evaluated by implementing both the Extended Kalman Filter (EKF) and the Unscented Kalman Filter (UKF). Simulation results presented demonstrate the effectiveness of our proposed multiple model FDI algorithm for both structural and actuator faults in the gas turbine.

The remainder of this chapter is organized as follows. In Section 3.1, a brief overview of the multiple model (MM) approach is presented. In Section 3.2, the MM-based FDI algorithm is formally proposed and developed for a gas turbine. In Section 3.3, simulation results corresponding to different fault scenarios in the gas turbine are presented, and comparisons between the EKF and the UKF schemes in terms of their sensitivity to external noise levels and availability of the measurements are conducted. Conclusions and future work are presented in Section 3.4. *The materials of this chapter has been developed in collaboration with Dr. Nader Meskin.*

3.1 MM-Based FDI Algorithm

In this section, a brief overview of the multiple model (MM)-based fault detection and isolation (FDI) scheme is presented [47]. Let \mathbf{a} denote the vector of fault parameters in a given dynamical system where it can take on only one of the M representative values $\mathbf{a}_i, i = 1, \dots, M$ (\mathbf{a}_i is a vector and has the same dimension as that of \mathbf{a}). The model corresponding to \mathbf{a}_i is described by the following nonlinear discrete-time system

$$\begin{aligned} x(k+1) &= f_i(x(k), u(k)) + \xi_i(k) \\ z(k) &= h_i(x(k)) + \eta_i(k) \end{aligned} \tag{3.1}$$

where $x(k)$ is the state of the system, $z(k)$ is the measurement vector, and $u(k)$ is the control input vector. The fault parameter \mathbf{a}_i may correspond to the actuator, the sensor or the structural faults in the system. For instance, in the single-spool gas turbine model that is considered in this chapter we have the following specific definitions, namely $x = [P_{CC}, N, T_{CC}, P_T]^T$, $z = [T_C, P_C, N, T_T, P_T]^T$, and u is the power level angle (PLA) (refer to the nomenclature section for the physical meaning and definitions of these variables). The process and the measurement noise vectors ξ_i and η_i are mutually independent white Gaussian noise of zero mean and covariance

Table 3.1: The Extended Kalman Filter Algorithm

The Prediction Step
$\hat{x}_i^-(k) = f_i(\hat{x}_i(k-1), u_i(k-1))$ $P_i^-(k) = A_i(k)P_i(k-1)A_i^T(k) + Q_i$
The Update Step
$v_i(k) = z_i(k) - h_i(\hat{x}_i^-(k))$ $S_i(k) = C_i(k)P_i^-(k)C_i^T(k) + R_i$ $K_i(k) = P_i^-(k)C_i^T(k)S_i^{-1}(k)$ $\hat{x}_i(k) = \hat{x}_i^-(k) + K_i(k)[y_i(k) - h_i(\hat{x}_i^-(k))]$ $P_i(k) = (I - K_i(k)C_i(k))P_i^-(k)$
Notation
$A_i(k) = \left. \frac{\partial f_i}{\partial x} \right _{\hat{x}_i(k-1), u_i(k-1)}$ $C_i(k) = \left. \frac{\partial h_i}{\partial x} \right _{\hat{x}_i^-(k)}$

Q_i and R_i , respectively.

Remark 3.1. *For sake of illustration and as shown subsequently in Section 3.2, for the gas turbine considered in this work we take $M = 6$, where the parameter a_1 corresponds to the healthy mode of the engine, the parameters a_2, \dots, a_5 correspond to the common gas turbine component faults, and the parameter a_6 denotes the fuel flow valve fault.*

Let the hypothesis conditional probability $p_i(k)$ be defined as the probability that \mathbf{a} assumes the value \mathbf{a}_i (for $i = 1, \dots, M$), conditioned on the observed measurement history up to time k , that is

$$p_i(k) = Pr[\mathbf{a} = \mathbf{a}_i | \mathcal{Z}(k) = \mathcal{Z}_k] \quad (3.2)$$

where the measurement history random vector $\mathcal{Z}(k)$ is made up of the partitions $z(1), \dots, z(k)$ that represent the available measurements up to the k th sample time and similarly, the realization \mathcal{Z}_k of the measurement history vector has partitions z_1, \dots, z_k [47]. It can be shown that $p_i(k)$ can be evaluated recursively for all i via the iteration

$$p_i(k) = \frac{F_{z(k)|\mathbf{a}, \mathcal{Z}(k-1)}(z_i | \mathbf{a}_i, \mathcal{Z}_{k-1})p_i(k-1)}{\sum_{j=1}^M F_{z(k)|\mathbf{a}, \mathcal{Z}(k-1)}(z_i | \mathbf{a}_j, \mathcal{Z}_{k-1})p_j(k-1)} \quad (3.3)$$

Table 3.2: The Unscented Kalman Filter Algorithm

<p>The Prediction Step</p> <p>Augmentation</p> $x_i^a(k-1) = \begin{bmatrix} \hat{x}_i^T(k-1) & E[\xi_i^T(k)] \end{bmatrix}^T$ $P_i^a(k-1) = \begin{bmatrix} P_i(k-1) & 0 \\ 0 & Q_i \end{bmatrix}$ <p>Sigma Points</p> $\chi_i^0(k-1) = x_i^a(k-1)$ $\chi_i^j(k-1) = x_i^a(k-1) + (\sqrt{(L+\lambda)P_i^a(k-1)})_j \quad j = 1 \dots L$ $\chi_i^j(k-1) = x_i^a(k-1) - (\sqrt{(L+\lambda)P_i^a(k-1)})_j \quad j = L+1 \dots 2L$ <p>Time Update</p> $\chi_i^j(k) = f(\chi_i^j(k-1), u_i(k-1))$ $\hat{x}_i^-(k) = \sum_{j=0}^{2L} W_m^j \chi_i^j(k)$ $P_i^-(k) = \sum_{j=0}^{2L} W_c^j [\chi_i^j(k) - \hat{x}_i^-(k)] [\chi_i^j(k) - \hat{x}_i^-(k)]^T$
<p>The Update Step</p> <p>Augmentation</p> $x_i^{-a}(k) = \begin{bmatrix} \hat{x}_i^{-T}(k) & E[\eta_i^T(k)] \end{bmatrix}^T$ $P_i^{-a}(k) = \begin{bmatrix} P_i^-(k) & 0 \\ 0 & R_i \end{bmatrix}$ <p>Sigma Points</p> $\chi_i^0(k) = x_i^{-a}(k)$ $\chi_i^j(k) = x_i^{-a}(k) + (\sqrt{(L+\lambda)P_i^-(k)})_j \quad j = 1 \dots L$ $\chi_i^j(k) = x_i^{-a}(k) - (\sqrt{(L+\lambda)P_i^-(k)})_j \quad j = L+1 \dots 2L$ <p>Measurement Update</p> $\mathcal{Y}_i^j(k) = h(\chi_i^j(k)) \quad j = 1 \dots 2L$ $\hat{y}_i(k) = \sum_{j=0}^{2L} W_m^j \mathcal{Y}_i^j(k)$ $v_i(k) = z_i(k) - \hat{y}_i(k)$ $S_i(k) \equiv P_{\hat{y}_i}(k) = \sum_{j=0}^{2L} W_c^j [\mathcal{Y}_i^j(k) - \hat{y}_i(k)] [\mathcal{Y}_i^j(k) - \hat{y}_i(k)]^T$ $P_{\hat{x}\hat{y}_i}(k) = \sum_{j=0}^{2L} W_c^j [\chi_i^j(k) - \hat{x}_i^-(k)] [\mathcal{Y}_i^j(k) - \hat{y}_i(k)]^T$ $K_i(k) = P_{\hat{x}\hat{y}_i}(k) P_{\hat{y}_i}^{-1}(k)$ $\hat{x}_i(k) = \hat{x}_i^-(k) + K_i(k) [y_i(k) - \hat{y}_i(k)]$ $P_i(k) = P_i^-(k) - K_i(k) P_{\hat{y}_i}(k) K_i^T(k)$
<p>Notation and Parametrization</p> <p>$(\sqrt{A})_j$ denotes the jth row of \sqrt{A}</p> <p>L is the dimension of the augmented state</p> $W_m^0 = \frac{\lambda}{L+\lambda}$ $W_c^0 = \frac{\lambda}{L+\lambda} + (1 - \alpha^2 + \beta)$ $W_m^j = W_c^j = \frac{1}{2(L+\lambda)}$ $\lambda = \alpha^2(L + \kappa) - L$ $\alpha = 0.001; \kappa = 0; \beta = 2$

in terms of the previous values of $p_1(k-1), \dots, p_M(k-1)$, and conditional probability densities for the current measurement $z(k)$ (denoted by $F_{z(k)|\mathbf{a}, \mathcal{Z}(k-1)}(z_i|\mathbf{a}_i, \mathcal{Z}_{k-1})$).

The MM-based FDI scheme is now composed of a bank of M individual and separate nonlinear Kalman filters, each based on a particular value of \mathbf{a}_i , $i = 1, \dots, M$. The innovation vector $v_i(k)$ is used to compute $p_1(k), \dots, p_M(k)$ via equation (3.3) with a Gaussian density function that is given by

$$F_{z(k)|m, \mathcal{Z}(k-1)}(z_i|\mathbf{a}_i, \mathcal{Z}_{k-1}) = \zeta_i(k) e^{-(1/2)v_i'(k)S_i^{-1}(k)v_i(k)} \quad (3.4)$$

where $\zeta_i(k) = \frac{1}{(2\pi)^{m/2}|S_i(k)|^{1/2}}$ and m is the measurement dimension. The innovation $v_i(k)$ and the innovation covariance matrix $S_i(k)$ are computed by using the standard equations of the Extended Kalman Filter (EKF) and the Unscented Kalman Filter (UKF) as given in Tables 3.1 and 3.2 ([57], [128]), respectively.

Let us assume that the actual value of the fault parameter \mathbf{a} is given by \mathbf{a}_i . Then, it is expected that a mean squared value of the residual generated by the nonlinear Kalman filter based on \mathbf{a}_i is in consonance with the residual covariance matrix $S_i(k)$ over time, while mismatched filters generate larger residuals than those predicted by their own residual covariance matrices. Hence, the MM-based algorithm will most heavily weight the nonlinear Kalman filter that corresponds to \mathbf{a}_i . The problem of fault detection and isolation (FDI), or equivalently the status of the current operating mode of the system at the time instant k can therefore be stated as and simplified to that of evaluating the quantity $\arg \max_i p_i(k)$ for the desired solution. Figure 3.1 shows the schematic of the general architecture of our proposed MM-based FDI approach.

Remark 3.2. *It follows from equation (3.3) that if any p_i is ever computed to be zero at any given time k , this probability will be locked to zero for all time thereafter. In order to prevent this lock out [47], an artificially small lower bound was considered for all p_i 's. Moreover, it was shown in [129] that the leading coefficient*

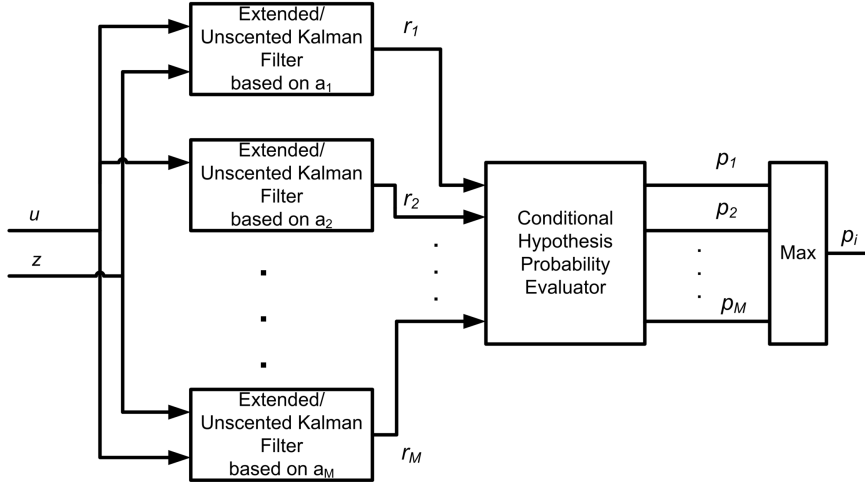


Figure 3.1: General architecture of our proposed MM-based FDI scheme.

$\zeta_i(k)$ in (3.4) does not provide any useful information for fault identification and even may cause incorrect fault identification. Therefore, the term $\zeta_i(k)$ is usually removed from the equation (3.4). It should be noted that since the denominator of (3.3) is the summation of all the numerators, even by removing the term $\zeta_i(k)$, the sum of the computed probabilities remains one.

3.2 Multiple Model-Based Fault Diagnosis Design

In this section, a fault detection and isolation (FDI) strategy for a single spool gas turbine that is based on the MM-based approach is developed. Towards this end, first the nonlinear Kalman filters corresponding to each operating mode (healthy and faulty) is derived. The MM-based nonlinear filters are then designed according to the procedure that is described in Section 3.1. As pointed out after equation (3.1), the output measurements, z , or the available sensors are taken as the pressure and the temperature after the compressor (P_C and T_C), the pressure and the temperature after the turbine (P_T and T_T), and the rotational speed (N).

Table 3.3: The definition and description of the considered component faults.

Component Fault	Description	Mode Label
ΔFC_C	Decrease in the compressor flow capacity	P2
$\Delta \eta_C$	Decrease in the compressor efficiency	P3
ΔFC_T	Decrease in the turbine flow capacity	P4
$\Delta \eta_T$	Decrease in the turbine efficiency	P5

3.2.1 Fault Modeling and Detection Filter Design

In this chapter, both component anomalies as well as an actuator anomaly are considered as sources of gas turbine faults. Common component faults [106] are modeled as changes in the component efficiency and flow capacity. Four component faults are investigated in this work as shown in Table 3.3. Moreover, a fault in the fuel valve is considered as an actuator fault. Hence, the total number of operating modes is **six** (as stated in Remark 1) where mode #1 (P1) corresponds to the healthy gas turbine, modes #2 to #5 (P2 to P5) correspond to the component faults as specified in Table 3.3, and mode #6 (P6) corresponds to the loss of effectiveness fault in the fuel valve actuator (equation(2.15)). Faults that are considered here are multiplicative e.g. the fault compressor efficiency is defined as $\Delta \eta_C \times \eta_C$.

Faulty models corresponding to the component faults in Table 3.3 are obtained by considering a 2% decrease in the efficiency or the flow capacity with respect to the normal (healthy) mode. For instance, for obtaining the nonlinear model associated with the operating mode #2, the compressor efficiency is decreased by 2% [127,130]. Moreover, the nonlinear model associated with the operating mode #6 (actuator fault mode) is obtained by considering a 5% loss of effectiveness or gain fault in the fuel actuator valve.

In our proposed hierarchical approach, it is assumed that the engine starts from the healthy condition when the “first level” of filters are active and the proposed algorithm observes the engine for occurrence of one of the five faults that are

Table 3.4: The operating modes corresponding to various possible two concurrent faults scenarios.

Levels	Operating Modes					
	# 1	# 2	# 3	# 4	# 5	# 6
First	Healthy	P2 (2%)	P3 (2%)	P4 (2%)	P5 (2%)	P6 (2%)
Second	P2	P2 (5%)	P2 P3	P2 P4	P2 P5	P2 P6
	P3	P3 P2	P3 (5%)	P3 P4	P3 P5	P3 P6
	P4	P4 P2	P4 P3	P4 (5%)	P4 P5	P4 P6
	P5	P5 P2	P5 P3	P5 P4	P5 (5%)	P5 P6
	P6	P6 P2	P6 P3	P6 P4	P6 P5	P6 (5%)

specified above. Normally, when the engine is operating healthy, the mode probability corresponding to the first mode (#1) is maximum. Once a fault has occurred, the mode probability corresponding to the healthy mode decreases, and the mode probability corresponding to the occurred fault increases until it takes the maximum value among all the modes. The maximum value of the mode probability that is reached by the active mode is 1, and the corresponding probabilities of other modes become 0. Therefore, the fault detection logic is simply a comparison among the mode probabilities by which the corresponding fault is detected and isolated.

For detection and isolation of two concurrent faults in the engine, a hierarchical approach is proposed [47] as illustrated in Table 3.4. Once the first fault is detected and isolated according to the maximum probability criteria, the FDI algorithm will activate the “second level” of filters (as shown in Table 3.4) for detection and isolation of the second concurrent fault in the engine. It should be noted that in our proposed hierarchical architecture, it is assumed that faults do not occur simultaneously and there exists at least a non-zero time interval (dwell time) between the occurrence of faults in the engine. In other words, we are considering and allowing the occurrence of concurrent faults. Table 3.4 depicts details on all the possible configurations for the second bank of filters. For example, if the first fault is detected as a 2% change in the compressor flow capacity (P2), then the first

filter in the second level corresponds to the detected fault scenario (P2) (that is $\Delta FC_C = 2\%$), the second filter corresponds to a further decrease of (3%) in the compressor flow capacity resulting in a total of 5% decrease in the capacity (that is $\Delta FC_C = 5\%$), the third filter corresponds to the concurrent decrease of 2% in the compressor flow capacity and a decrease of 2% in the compressor efficiency (P2 and P3) (that is $\Delta FC_C = 2\%$ and $\Delta \eta_C = 2\%$), etc. Note that this procedure can be similarly extended to the third and higher levels that correspond to the occurrence of multiple (three and higher) concurrent faults.

It should be emphasized again that when the new bank of filters is activated in the second level, there is no need to further operate the first bank of filters and our FDI strategy basically deactivates this bank of filters to save computational resources. In other words, the hierarchical architecture enables one to detect and isolate the occurrence of the second fault without adding any extra computational burden since at any given time, only 6 filters are operating on-line.

Remark 3.3. *Note that in the above hierarchical fault diagnosis architecture, only two levels of fault severities, namely 2% and 5% are considered for the sake of illustration only. It should be emphasized that more fault severities can equally and easily be considered by correspondingly increasing the number of models that are considered in this architecture.*

3.3 Simulation Results

In this section, simulation results and performance evaluations of our proposed diagnostic system corresponding to various fault scenarios are presented. We have implemented both the EKF and the UKF in our MM-based scheme and have provided comparative results. It should be noted that all the faults are actually applied

to and injected in the fully nonlinear model of the gas turbine as governed by equations (2.14) and (2.15). For example, the compressor efficiency (η_c) is replaced by $\Delta\eta_c \times \eta_c$ in equation (2.14) for injection of fault P3. The measurement noise levels that are considered are shown in Table 2.2, where the standard deviations are given as percentage of the nominal values at typical cruise conditions [127]. It is also assumed that the PLA=0.9 and the ambient conditions are set to standard conditions and the Mach number is set to 0.74.

3.3.1 Single Fault Scenarios

Figures 3.2 and 3.3 depict the mode probabilities and the output measurements corresponding to the injected 2% decrease in the compressor efficiency that is applied at $t = 5$ seconds (Mode #3), respectively. In Figure 3.2 (a), for all $t < 10.2$ seconds the quantity $\arg \max_i p_i(k) = p_1$, which corresponds to classifying and identifying the healthy operation of the engine. However, for all $t \geq 10.2$, we have $\arg \max_i p_i(k) = p_3$, which classifies and identifies that the mode P3 is active in the engine. Therefore, the fault in the compressor efficiency is perfectly detected and isolated at $t = 10.2$ seconds. As shown in Figure 3.2, the MM-scheme in which the UKF is used detects the fault at time $t = 10.2$ seconds, whereas the MM-scheme with the EKF detects the fault at time $t = 13.2$ seconds.

Since in real applications there is no guarantee that a fault occurs abruptly or matches exactly the predefined fault severity level, one requires to investigate the performance of the MM-based approach under these realistic circumstances. Figure 3.4 shows the mode probabilities corresponding to the injection of a 3% fault in the turbine efficiency (Mode #5) corresponding to both the EKF and the UKF detection filters in the MM-based scheme. This figure shows that the algorithm is capable of detecting and isolating a fault whose severity lies within the already designed severities of 2% and 5% and does not have to match the mode definition

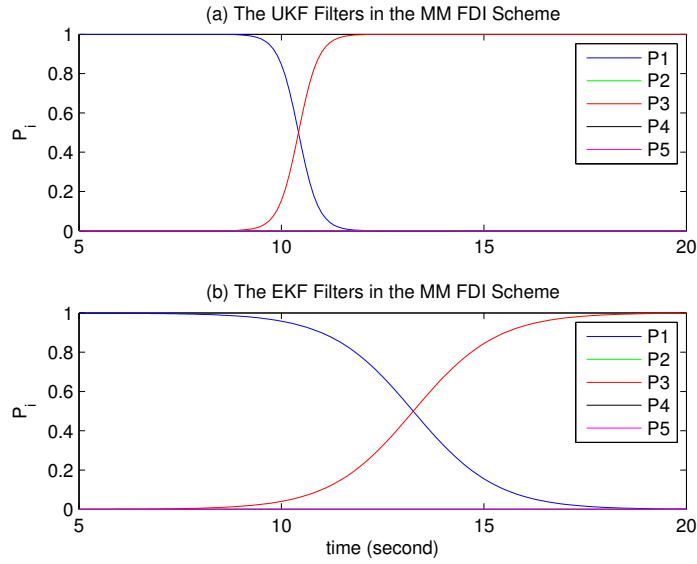


Figure 3.2: The mode probabilities corresponding to the injected 2% decrease in the compressor efficiency that is applied at $t = 5$ seconds (Mode #3) (a) the UKF is used in the MM-based FDI scheme, and (b) the EKF is used in the MM-based FDI scheme.

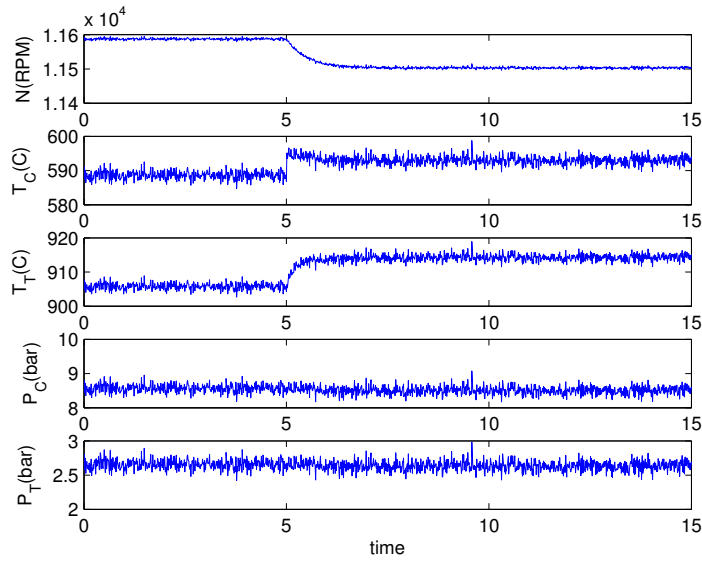


Figure 3.3: The output measurements corresponding to the injected 2% decrease in the compressor efficiency that is applied at $t = 5$ seconds (Mode #3).

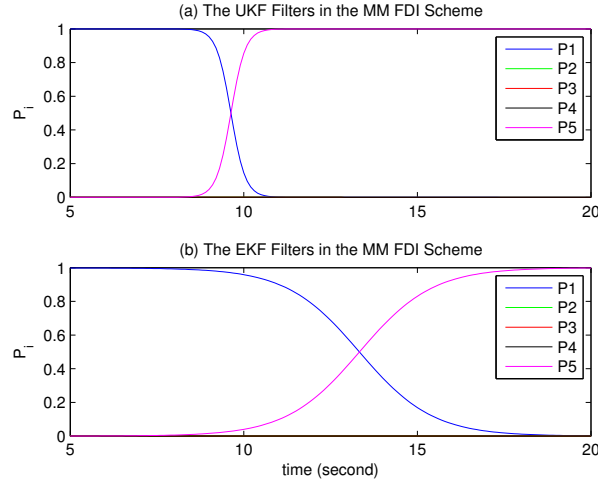


Figure 3.4: The mode probabilities corresponding to the injected 3% decrease in the turbine efficiency that is applied at $t = 5$ seconds (Mode #5) (a) the UKF is used in the MM-based FDI scheme, and (b) the EKF is used in the MM-based FDI scheme.

exactly. The average detection times for all the fault modes (P2 to P6) that are applied at $t = 5$ seconds as a function of the fault severity levels are given in Table 3.5. Figure 3.5 shows the detection time as a function of the fault severity for each mode separately. It can be observed from the Table 3.5 that the higher the fault severity the earlier the detection times specially for faults where the detection filters are specifically designed for.

The superiority of UKF to EKF is well established in the literature ([57] and [131]), however this is not generally guaranteed in the MM-based structure. It is apparent from the equations 3.3 and 3.4 that are used for mode probabilities computation, the convergence of the mode probabilities not only depends on the convergence of the filter that matches the fault mode, but also it depends on the behavior of other filters. In other words, the behavior of UKF and EKF when their dynamics do not match the real active dynamics is also crucial, however, this behavior is not generally known in order to discuss the nature of the generated residuals and their impact on the mode probabilities convergence. Intuitively, since at each time step UKF performs multiple nonlinear simulations while EKF computes

Table 3.5: The average detection times for all the fault modes (P2 to P6) that are applied at $t = 5$ seconds as a function of the fault severity levels.

Fault severity level	2%	3%	4%	5%	6%
UKF Scheme	9.6	10.3	9.5	8.7	9.1
EKF Scheme	11.3	12.9	10.6	10.1	10.4

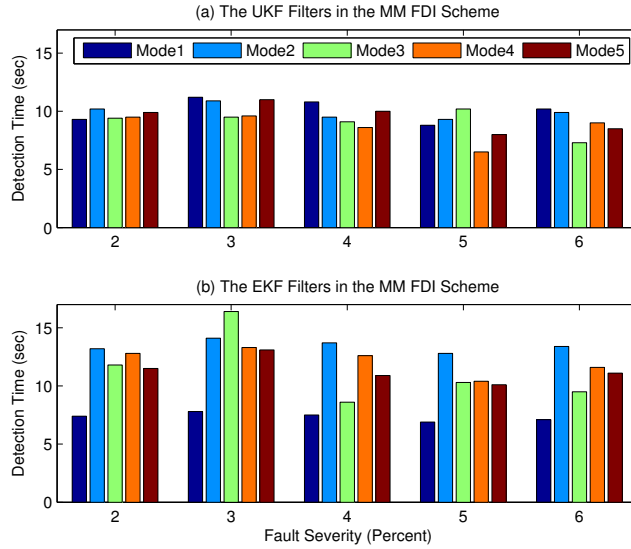


Figure 3.5: The detection time for each mode of fault that is applied at $t = 5$ seconds as a function of the fault severity (a) the UKF is used in the MM-based FDI scheme, and (b) the EKF is used in the MM-based FDI scheme.

Jacobins, and since divergence is less probable in nonlinear simulations of a dynamic model that slightly differs from the real active dynamics in comparison with the computation of jacobins, one can expect that UKF performs better than EKF in MM-based scheme.

3.3.2 Concurrent Fault Scenarios

In this section, we investigate concurrent faults scenarios where a 2% decrease in the compressor efficiency (P3) is injected at $t = 5$ seconds and a 2% decrease in the compressor mass flow rate (P2) is injected at $t = 30$ seconds. Based on the hierarchical multiple model architecture that was described in Section 3.2, our proposed

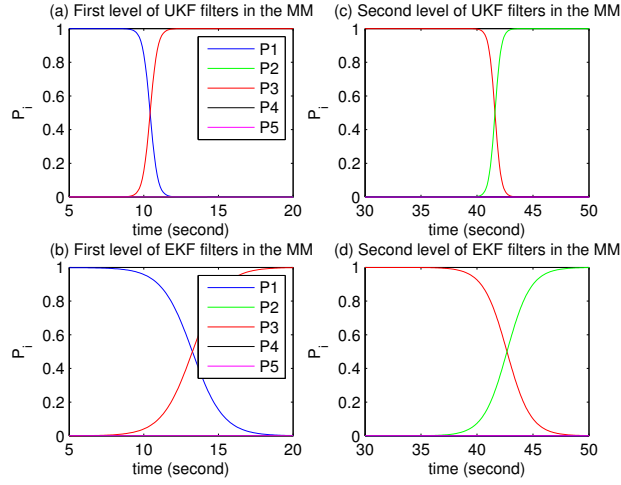


Figure 3.6: The mode probabilities corresponding to the injected 2% decrease in the compressor efficiency that is applied at $t = 5$ seconds (Mode #3) followed by an injection of a 2% decrease in the compressor mass flow rate (Mode #2 in the second level) that is applied at $t = 30$ seconds. (a) The fault detection and isolation by the first level of filters using the UKF in the MM-based scheme, (b) The fault detection and isolation by the first level of filters using the EKF in the MM-based scheme, (c) The fault detection and isolation by the second level of filters using the UKF in the MM-based scheme, and (d) The fault detection and isolation by the second level of filters using the EKF in the MM-based scheme.

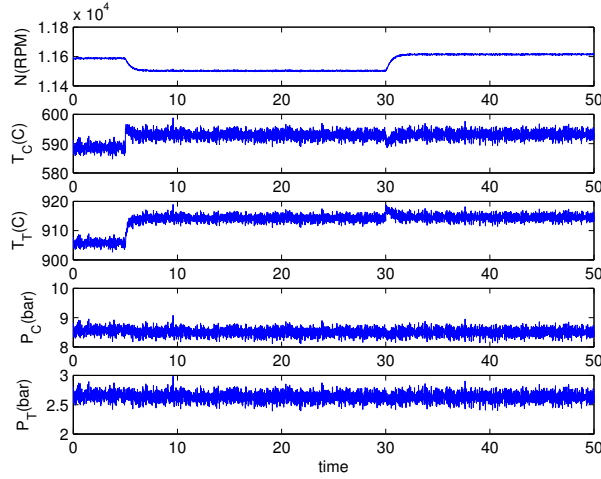


Figure 3.7: The output measurements corresponding to the injected 2% decrease in the compressor efficiency that is applied at $t = 5$ seconds (Mode #3) followed by an injection of a 2% decrease in the compressor mass flow rate (Mode #2 in the second level) that is applied at $t = 30$ seconds.

algorithm first uses the bank of filters that corresponds to the first level (no fault has yet been detected). Figures 3.6 (a) and (b) depict the mode probabilities that are generated by the first level filters. As shown in the figures, the first fault in the compressor efficiency is detected and isolated at $t = 10.0$ seconds corresponding to the UKF detection filters and at $t = 12.1$ seconds corresponding to the EKF detection filters.

Once this fault is detected, the second level bank of filters is initiated to operate where these filters are designed according to Table 3.4. Specifically, the filter #1 in this bank of filters corresponds to the detected fault P3, filter #2 corresponds to the concurrent occurrence of the detected fault P2 and the fault P3, filter #3 corresponds to the further degradation of the compressor efficiency P3 by 3% (resulting in the total decrease of 5%), and similarly for all the other filters they correspond to the concurrent occurrence of the detected fault P2 and the other faults (namely P4 to P6). It should be emphasized again that when a new bank of filters is initiated to run there is no need to further operate the previous level bank of filters so that our proposed FDI algorithm deactivates the previous set of bank of filters. This is done in order to minimize the overall computational resources of the diagnostics system. In other words, at any given time only one set or level of bank of filters is active and running. Figure 3.6 (c) and (d) depict the mode probabilities that are generated by the second level bank of filters. The second fault in the compressor mass flow rate is detected and isolated at $t = 41.4$ seconds corresponding to the UKF detection filters and at $t = 43.4$ seconds corresponding to the EKF detection filters. As in the previous subsection, one can again conclude that the UKF outperforms the EKF in terms of the delay in the fault detection times. Figure 3.7 depicts the output measurements that are observed corresponding to the above concurrent faults scenario.

3.3.3 Operational Condition Variations

When a linear detection filter is used in the MM-based scheme [56], one of the major concerns that arise is due to the validity of the implemented filters subject to the variations of the operating point such as the Mach number, the PLA setting and the ambient conditions. In case of large variations, the diagnostic algorithm may generate false alarms. In order to cope with this drawback, a strategy should be devised to accurately follow the engine operating point variations, and activate the appropriate linear detection filters. However, by implementing our proposed nonlinear detection filters the operating condition variations are automatically taken into account by the nonlinear detection filters. To demonstrate and substantiate this advantage, in the next set of simulations the ambient temperature is linearly varied from from 15° to 5° over an interval of 20 seconds while a 2% fault in the turbine mass flow rate is injected (Mode #4) at time $t = 5$ seconds. Figures 3.8 and 3.9 show the results obtained. It follows that while the ambient temperature is varying, the MM-based FDI scheme is capable of detecting and isolating the fault and indeed the operating variations do not affect the FDI performance. In another set of simulations, in addition to the injection of a fault (i.e. a 2% fault in the turbine mass flow rate (Mode #4) applied at $t = 5$ seconds), the PLA is smoothly varied from 0.9 to 1.1, as shown in Figure 3.11. The results of the simulations that are shown in Figures 3.8 and 3.10 confirm and demonstrate the capability of our proposed approach in dealing with the challenging problem of operating condition variations.

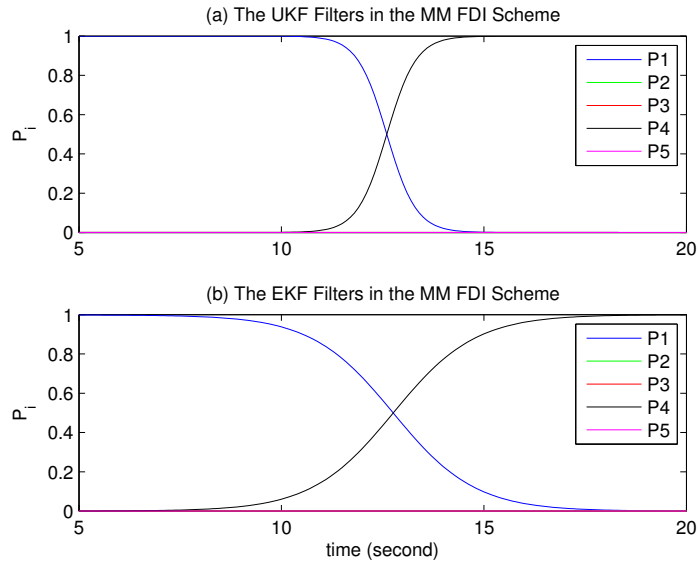


Figure 3.8: The mode probabilities corresponding to the injected 2% decrease in the turbine mass flow rate that is applied at $t = 5$ seconds (Mode #4) while the ambient temperature is varying (a) the UKF is used in the MM-based FDI scheme, and (b) the EKF is used in the MM-based FDI scheme.

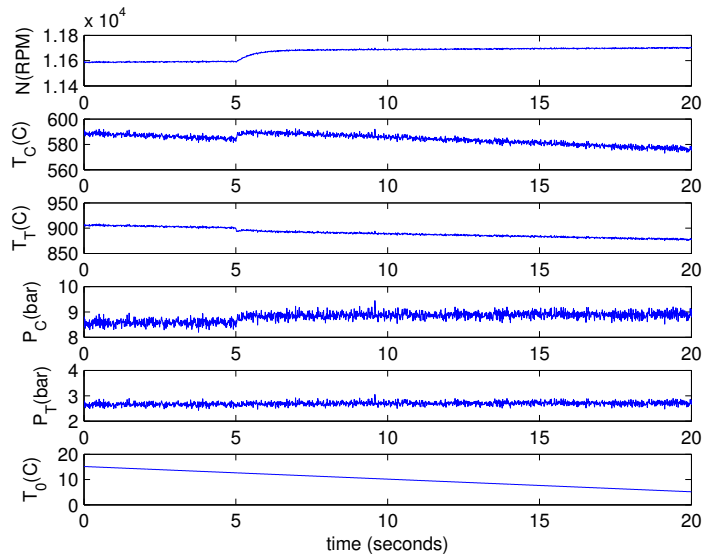


Figure 3.9: The output measurements corresponding to the injected 2% decrease in the turbine mass flow rate that is applied at $t = 5$ seconds (Mode #4) while the ambient temperature is varying.

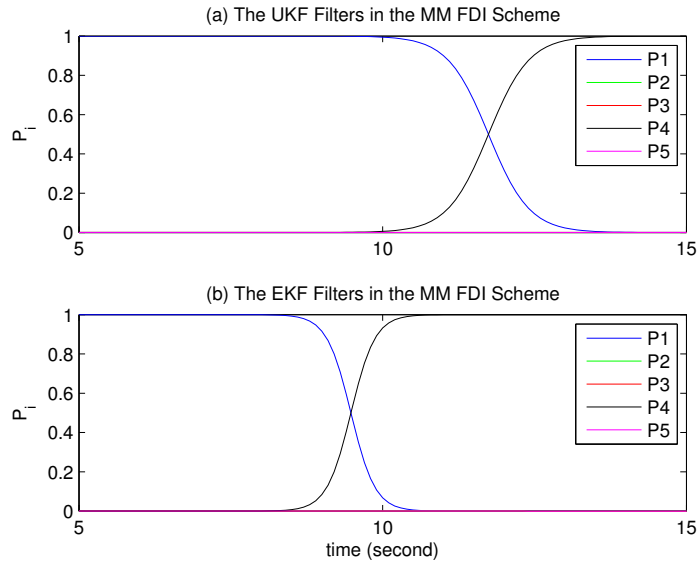


Figure 3.10: The mode probabilities corresponding to the injected 2% decrease in the turbine mass flow rate that is applied at $t = 5$ seconds (Mode #4) while the PLA is varying (a) the UKF is used in the MM-based FDI scheme, and (b) the EKF is used in the MM-based FDI scheme.

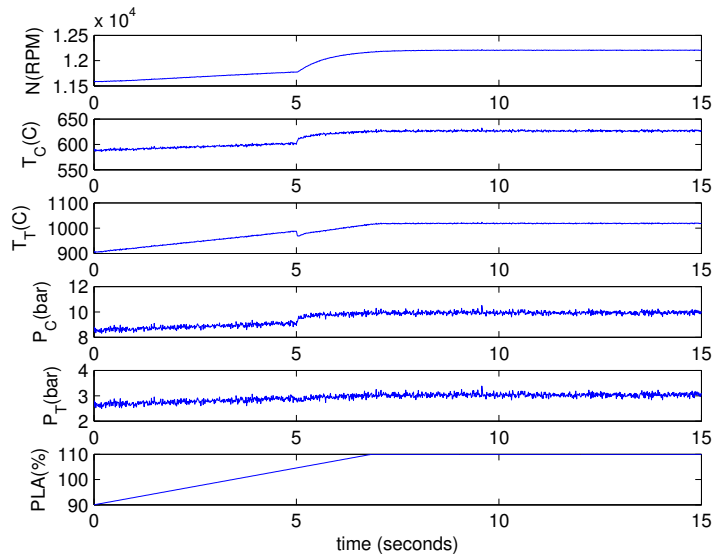


Figure 3.11: The output measurements corresponding to the injected 2% decrease in the turbine mass flow rate that is applied at $t = 5$ seconds (Mode #4) while the PLA is varying.

3.3.4 A Comparison Between the Performance of the UKF and the EKF Detection Filters

While the comparison between single UKF and single EKF is comprehensively studied in the literature, a similar comparison between mentioned filters in a MM-based structure has not been performed yet. However, this task is analytically difficult since one should investigate the behavior of filters and nature of the residuals generated when the filter dynamics does not match the active mode. Typically, it is custom to investigate the filter estimation performance by observing how residuals converges to zero, while in order to have an overall judgment on the performance of filters in the MM-based structure, one also should know the the nature of residuals generated when the residuals of some filters are not supposed to converge to zero.

In this section, we investigate the performance of the the UKF and the EKF detection filters in the MM-based scheme by simulation. An important figure of merit that is of interest in many applications is robustness to sensor and measurement noise. In the previous simulations, we have applied a noise level that is given in Table 2.2 for the measurements. In this subsection, we have increased the noise levels proportionally by a factor (noise power factor), and have examined if the UKF or the EKF detection filters in the MM-based scheme are capable of detecting and isolating all fault modes as described in Table 3.3. The detection time for each fault mode as a function of the noise power factor is shown in Figure 3.12. The results are summarized in Table 3.6 in which numerical values indicate the average fault detection times for all the modes (P2 to P6) when the fault is applied at $t = 5$ seconds. A bullet mark (\bullet) indicates an unsuccessful detection or isolation of at least one fault mode. As expected, the UKF scheme demonstrates a superior performance over the EKF scheme when a higher level of noise is applied.

In another set of simulations, we have investigated the effects of the availability of a certain number of measurements on the performance of the detection filters.

Table 3.6: The average detection times for all the modes of faults (P2 to P6) that are applied at $t = 5$ seconds as a function of the noise power factor.

Noise power factor	1	1.1	1.3	1.5	1.8	2
UKF Scheme	9.6	9.8	10.0	9.9	10.1	10.1
EKF Scheme	11.3	15.6	19.2	•	•	•

Table 3.7: The average detection times for all the fault modes (P2 to P6) that are applied at $t = 5$ seconds as a function of the number of the measurements or sensors that are employed.

Number of measurements/sensors used	5	4	3	2
UKF Scheme	9.6	11.7	12.0	•
EKF Scheme	11.3	13.5	14.1	•

This case is different from the sensor fault scenario since in the presence of a sensor fault the diagnostic or control module will continue to use the faulty sensor data unless a separate strategy for sensor fault detection is employed and considered. In this subsection, we are interested in determining the minimum number of measurements that is required by the detection filters in order to perform the FDI task properly. The detection time for each fault mode as a function of the number of the measurements or sensors is shown in Figure 3.13. Table 3.7 summarizes the results. In this table the average fault detection times numerical values for all the modes (P2 to P6) are provided corresponding to a fault that is applied at $t = 5$ seconds. A bullet mark (•) indicates either an unsuccessful detection or isolation of at least one fault mode. It can be concluded that both the UKF and the EKF detection filters have the same performance capability in terms of functionality with various sets of measurements and sensors, however, the UKF detection filters perform superior over the EKF detection filters in terms of the fault detection times.

Computational requirements is also an important merit of performance which one requires to consider for comparison and evaluation purposes. The UKF scheme

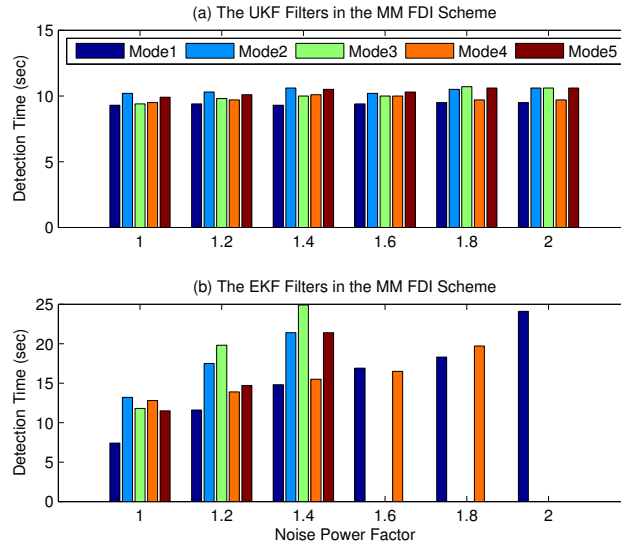


Figure 3.12: The detection time for each mode of fault that is applied at $t = 5$ seconds as a function of the noise power factor. The empty places indicates the unsuccessful detection or isolation of the corresponding fault. (a) the UKF is used in the MM-based FDI scheme, and (b) the EKF is used in the MM-based FDI scheme.

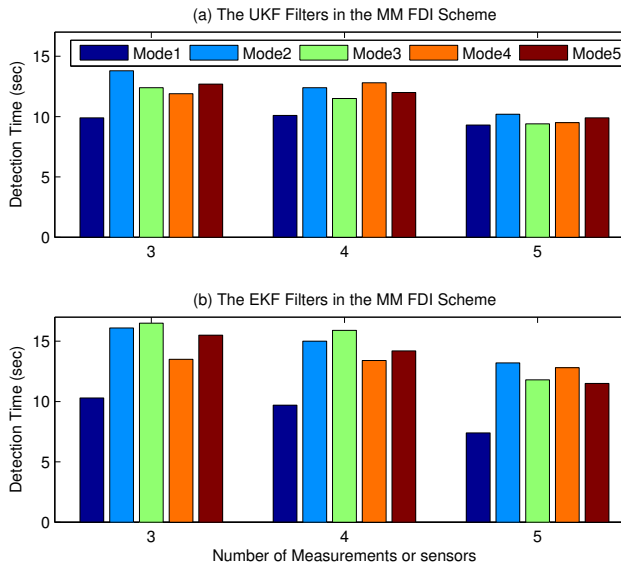


Figure 3.13: The detection time for each mode of fault that is applied at $t = 5$ seconds as a function of the number of the measurements or sensors that are employed. (a) the UKF is used in the MM-based FDI scheme, and (b) the EKF is used in the MM-based FDI scheme.

in general runs slower than the EKF scheme due to the multiple nonlinear computations that are required at each time step. This factor makes the UKF scheme less suitable for real-time applications. On the other hand, one of the advantages of the UKF scheme over the EKF scheme is that it does not require the Jacobian matrix of the system at each time step, which by itself is a computationally costly operation. Especially, when one uses performance maps for modeling the nonlinear dynamics of the gas turbine, the task of computing the Jacobian matrix at each operating point is computationally expensive and complex and can be performed only numerically. However, in our application the linearization approximation performed by the EKF scheme at each time step takes less CPU time than the multiple nonlinear computations that are performed by the UKF scheme.

Based on the above simulations and discussions, one can have this impression in the final analysis that the UKF detection filters do indeed outperform the EKF detection filters in this application.

3.4 Conclusions

In this chapter, a nonlinear multiple model (MM-based) fault detection and isolation scheme for health monitoring of gas turbines is proposed and developed. Starting from the nonlinear dynamics of a gas turbine, a bank of nonlinear detection filters is designed where each filter corresponds to a specific faulty mode of the engine. As earlier mentioned in Section 2.1, fault modes are defined using Gas Path Analysis which covers a wide range of physical faults. A hierarchical fault detection and isolation architecture is proposed corresponding to both single and concurrent faults in the engine. By taking into account the fault occurrence history, only a minimal set of detection and isolation filters is activated so that the same number of filters are always operating at any given point in time. In other words, the complexity of our

proposed fault detection and isolation (FDI) algorithm does not increase as more novel faults are concurrently injected to the engine. We have implemented both the EKF and the UKF detection filters in the MM-based FDI architectures. Simulation results demonstrate that considerable improvements exist on the performance of the UKF scheme over the EKF scheme in terms of the fault detection times and functionality with respect to different number of measurements and sensors. Moreover, the UKF scheme is significantly more robust to the large sensor noise. In this work, we have assumed existence of a set of predefined severity fault levels for construction of the supposed UKF and EKF detection filters from the corresponding nonlinear model of the gas turbine. Therefore, one natural direction for future research will be to develop a robust fault diagnosis scheme in which the fault severity levels are estimated through parameter estimation techniques.

Chapter 4

Inversion-Based Fault Estimation

In the previous chapter, we developed an observer based FDI scheme by utilizing nonlinear Kalman filters. We demonstrated the performance of the proposed MM-based approach through comprehensive simulations. However, in many real-life cases, the system operators need to have an estimation of fault severity to decide on the continuation or abortion of the mission or maintenance strategy. Numerous approaches have been proposed for fault estimation in dynamical systems. An important category of observer based methods for fault estimation is inversion-based approaches which is also closely related to our proposed data-driven FDI&E scheme.

In this chapter, we propose a framework for inversion-based estimation of certain categories of faults in discrete-time linear systems. First, we develop a novel methodology for direct estimation of unknown inputs by using only measurements of either minimum or non-minimum phase systems as well as systems with transmission zeros on the unit circle. The unknown input is reconstructed from its projections onto two subspaces. One projection is achieved through an algebraic operation, whereas the other is given by a dynamic filter whose poles coincide with the transmission zeros of the system. A feedback is then introduced to stabilize the above

filter dynamics as well as provide an unbiased estimation of the unknown input. Next, we have applied our proposed methodology to the problem of fault estimation and have shown that the proposed inversion filter is unbiased for certain categories of faults. Finally, we have illustrated the performance of our proposed methodologies through numerous simulation studies to demonstrate the capabilities and advantages of the developed strategies.

The remainder of the chapter is organized as follows. First, the two problems that are considered in this chapter are formally stated and defined in Section 4.1. The definitions and notations that are used throughout the chapter are provided in Section 4.2. Our proposed solution for a stable inversion of linear systems is presented in Section 4.3. The adoption of the proposed inversion method for solving the fault estimation problem is introduced and developed in Section 4.4. Finally, numerical simulations and case studies are included in Section 4.5.

4.1 Problem Statement

In this chapter, we consider *two* problems as described and formally presented below.

4.1.1 Problem 1: Inversion-Based Input Estimation of Discrete-Time Linear Systems

Consider the dynamics of a given linear time-invariant (LTI) discrete-time system is governed by,

$$\mathbf{S} : \begin{cases} x(k+1) = Ax(k) + Bu(k) \\ y(k) = Cx(k) + Du(k) \end{cases} \quad (4.1)$$

where $x \in \mathbb{R}^n$, $u \in \mathbb{R}^m$ and $y \in \mathbb{R}^l$, where the state $x(t)$ and the input $u(t)$ are assumed to be un-measurable and unavailable. The main objective that is pursued

here is to estimate the unknown sequence $u(k)$ from the generated, and the *only* known and available sequence $y(k)$ under the following general assumption.

Assumption A: It is assumed that,

1. The system \mathbf{S} is stable and observable, and
2. At least one of the matrices B or D is full rank.

In other words, one of the matrices B and D can be rank-deficient or identically zero, but both cannot be simultaneously zero or rank deficient. The other required conditions and assumptions will be given under each result that we will be developing subsequently. We address a solution to this problem in Section 4.3.

4.1.2 Problem 2: Inversion-Based Fault Estimation of Discrete-Time Linear Systems

Consider a faulty LTI discrete-time system that is given by,

$$\mathbf{S}^f : \begin{cases} x(k+1) = Ax(k) + Bu(k) + Lf(k) \\ y(k) = Cx(k) + Du(k) + Ef(k) \end{cases} \quad (4.2)$$

where $x \in \mathbb{R}^n$, $u \in \mathbb{R}^m$, $y \in \mathbb{R}^l$ and the input $f \in \mathbb{R}^p$ denotes the fault signal. The problem that is considered here is to provide an estimate of the fault signal, i.e. $\hat{f}(k)$, by *only* utilizing the available information from the system, namely $y(k)$ and $u(k)$, under the following assumption.

Assumption B: It is assumed that,

1. The system \mathbf{S}^f is observable, and
2. At least one of the matrices L or E is full rank.

The solution to this problem is discussed and provided subsequently in Section 4.4.

4.2 Notations

Let us consider the *Rosenbrock System Matrix* that is given by,

$$M_R(z) = \begin{bmatrix} zI - A & B \\ -C & D \end{bmatrix} \quad (4.3)$$

where if $\text{rank}(M_R(z)) < n + \min(l, m)$, then z is called a *transmission zero* or an *invariant zero* of the system \mathbf{S} . Similarly, if the rank of the following matrix $M_f(z)$ is reduced at a particular value of z , the specific zero is designated as the transmission zero of the *fault-to-output* dynamics, where

$$M_f(z) = \begin{bmatrix} zI - A & L \\ -C & E \end{bmatrix} \quad (4.4)$$

The vectors $\mathbf{U}_{2M}(k - 2M)$, $\mathbf{F}_{2M}(k - 2M)$ and $\mathbf{Y}_{2M}(k - 2M)$ that are directly and specifically constructed from the input $u(k)$, fault $f(k)$ or the output $y(k)$ signals and will be used throughout the chapter are defined as follows

$$\mathbf{U}_{2M}(k - 2M) = \begin{bmatrix} u(k - 2M) \\ u(k - 2M + 1) \\ \vdots \\ u(k - 1) \end{bmatrix} \quad (4.5)$$

where $M \in \mathbb{N}$ and is selected to be equal or greater than n ($M \geq n$), i.e. the order of the system \mathbf{S} . The vectors $\mathbf{F}_{2M}(k - 2M)$ and $\mathbf{Y}_{2M}(k - 2M)$ are similarly constructed by replacing $u(k)$ in (4.5) with $f(k)$ and $y(k)$, respectively.

The above input and output vectors satisfy the following relationship,

$$\mathbf{Y}_{2M}(k - 2M) = \mathbf{C}_{2M}x(k - 2M) + \mathbf{D}_{2M}\mathbf{U}_{2M}(k - 2M) \quad (4.6)$$

where,

$$\mathbf{C}_{2M} = \begin{pmatrix} C \\ CA \\ \vdots \\ CA^{2M-1} \end{pmatrix}; \mathbf{D}_{2M} = \begin{pmatrix} D & 0 & \dots & 0 \\ CB & D & \dots & 0 \\ \vdots & \vdots & \vdots & \vdots \\ CA^{2M-1}B & CA^{2M-2}B & \dots & D \end{pmatrix} \quad (4.7)$$

Give a matrix \mathcal{A} , then \mathcal{A}^\perp , \mathcal{A}^T and $\mathcal{N}(\mathcal{A})$ denotes the orthogonal space, the transpose, and the null space of \mathcal{A} . We extensively use the concept of *Moore Penrose pseudo inverse*. If \mathcal{A} is full row rank, then we denote its *pseudo inverse* by \mathcal{A}^\dagger , and compute it by $\mathcal{A}^T(\mathcal{A}\mathcal{A}^T)^{-1}$. Similarly, if \mathcal{A} is full column rank, then we also denote the *pseudo inverse* by \mathcal{A}^\dagger , and compute it by $(\mathcal{A}^T\mathcal{A})^{-1}\mathcal{A}^T$. If \mathcal{A} is rank deficient, then we denote the pseudo inverse by \mathcal{A}^+ , where \mathcal{A}^+ is a matrix that satisfies the following conditions: 1) $\mathcal{A}\mathcal{A}^+\mathcal{A} = \mathcal{A}$ 2) $\mathcal{A}^+\mathcal{A}\mathcal{A}^+ = \mathcal{A}^+$ 3) $(\mathcal{A}\mathcal{A}^+)^T = \mathcal{A}\mathcal{A}^+$ and 4) $(\mathcal{A}^+\mathcal{A})^T = \mathcal{A}^+\mathcal{A}$. If $U\Sigma V^T$ denotes the SVD decomposition of \mathcal{A} , then \mathcal{A}^+ is given by $V\Sigma^+U^T$, where Σ^+ is obtained by reciprocating each non-zero diagonal element of Σ .

4.3 The Proposed Inversion-Based Input Estimation of Linear Systems

Our main strategy is to construct $\mathbf{D}_{2M}\mathbf{U}_{2M}(k-2M) \in \mathbb{R}^{2Ml}$ by using its projections onto two linearly independent subspaces. First, we identify these subspaces. Next, we will show that the projection of $\mathbf{D}_{2M}\mathbf{U}_{2M}(k-2M)$ onto one of these subspaces is directly and simply given by multiplying $\mathbf{Y}_{2M}(k-2M)$ by a gain. We denote this projection by \mathbf{U}_{2M}^{aux} . Next, we establish an important result that $\mathbf{D}_{2M}(\mathbf{U}_{2M} - \mathbf{U}_{2M}^{aux})$ is zero if the system \mathbf{S} does not have any transmission zeros. Otherwise, computation of the other projection requires that one constructs a dynamical filter. We will identify, specify and characterize this filter and its properties. Specifically, we will show how

the stability condition of this filter is affected by the location of the invariant zeros of the system \mathbf{S} .

4.3.1 Linear Systems With No Invariant Zeros

Let us define the matrix \mathbf{H}_{2M} as follows,

$$\mathbf{H}_{2M}^T = (\mathbf{C}_{2M}^T)^\perp \quad (4.8)$$

Note that since \mathbf{S} is observable as per Assumption A(1), any vector in \mathbb{R}^{2Ml} can be written as a combination of the \mathbf{C}_{2M} columns and the \mathbf{H}_{2M} rows. The dot product of the rows of \mathbf{H}_{2M} with the columns of $\mathbf{D}_{2M}\mathbf{U}_{2M}(k-2M)$ is directly given by

$$\mathbf{H}_{2M}\mathbf{D}_{2M}\mathbf{U}_{2M}(k-2M) = \mathbf{H}_{2M}\mathbf{Y}_{2M}(k-2M) \quad (4.9)$$

Therefore, the projection of $\mathbf{D}_{2M}\mathbf{U}_{2M}(k-2M)$ onto the row space of \mathbf{H}_{2M} is given by $\mathbf{P}_h\mathbf{Y}_{2M}$, where \mathbf{P}_h is the projection operator on the row space of \mathbf{H}_{2M} and is given by,

$$\mathbf{P}_h = \mathbf{H}_{2M}^T(\mathbf{H}_{2M}\mathbf{H}_{2M}^T)^{-1}\mathbf{H}_{2M} \quad (4.10)$$

The matrix $\mathbf{H}_{2M}\mathbf{D}_{2M}$ is not a full rank matrix in general, hence one cannot reconstruct $\mathbf{U}_{2M}(k-2M)$ from equation (4.9). To address this challenge, let us determine another input, namely $\mathbf{U}_{2M}^{aux}(k-2M)$ (designated as the *auxiliary input*), that satisfies equation (4.9) by solving the following optimization problem,

$$\min_{\mathbf{U}_{2M}^{aux}} \|\mathbf{H}_{2M}\mathbf{Y}_{2M}(k-2M) - \mathbf{H}_{2M}\mathbf{D}_{2M}\mathbf{U}_{2M}^{aux}(k-2M)\| \quad (4.11)$$

The solution to the above minimization problem is given by,

$$\mathbf{U}_{2M}^{aux}(k-2M) = \mathbf{K}_1\mathbf{Y}_{2M}(k-2M) \quad (4.12)$$

where,

$$\mathbf{K}_1 = (\mathbf{H}_{2M}\mathbf{D}_{2M})^+\mathbf{H}_{2M} \quad (4.13)$$

In general, it should be noted that $\mathbf{D}_{2M}\mathbf{U}_{2M}^{aux}(k-2M)$ is the construction of $\mathbf{D}_{2M}\mathbf{U}_{2M}(k-2M)$ onto the row space of \mathbf{H}_{2M} . This fact is graphically illustrated in Figure 4.1 for a SISO system with $n = 1$. Moreover, if the system \mathbf{S} does not have any transmission zeros, then the first $2Ml - n$ rows of $\mathbf{U}_{2M}(k-2M)$ and $\mathbf{U}_{2M}^{aux}(k-2M)$ are equal as shown in the following theorem. However, we need to first state the following lemma.

Lemma 4.1. *Let Assumptions A(1) and A(2) hold, $l \geq m$, and $M \geq n$. If the system \mathbf{S} has no transmission zeros, then $\text{rank}(\mathbf{D}_{2M}) \geq 2Mm - n$. The equality holds for square systems, namely when $l = m$.*

Proof. If D is full rank, then $\text{rank}(\mathbf{D}_{2M})$ is obviously greater than $2Mm - n$. If D is zero or rank deficient, since the system has no transmission zeros, then at least $CA^{n-1}B$ is full rank. Note that $CA^{n-1}B$ does not appear in \mathbf{D}_{2M} from the column $2Mm - n + 1$ there after. Hence, it follows that $\text{rank}(\mathbf{D}_{2M}) \geq 2Mm - n$.

For a square system, the equality also holds since one can express the measurement equation in the matrix format as follows,

$$\mathbf{Y}_{2M}(k-2M) = \begin{bmatrix} \mathbf{C}_{2M} & \mathbf{D}_{2M} \end{bmatrix} \begin{bmatrix} x(k-2M) \\ \mathbf{U}_{2M}(k-2M) \end{bmatrix} \quad (4.14)$$

therefore if $\text{rank}(\mathbf{D}_{2M}) > 2Mm - n$, certain columns of \mathbf{C}_{2M} are linearly dependent with the columns of \mathbf{D}_{2M} , which implies that there exist a nonzero initial $x(k-2M)$ and a nonzero input sequence that will yield a zero output. This results in a contradiction, and therefore the rank condition should be satisfied. \square

Lemma 4.1 implies that for square systems, as the number of transmission zeros increases, the rank of \mathbf{D}_{2M} will consequently increase. In other words, \mathbf{C}_{2M} and \mathbf{D}_{2M} will have more linearly dependent columns which allows the injection of a nonzero input for zeroing out the output. This fact is also reflected when the problem of decoupling state estimation process from the unknown input is considered.

Theorem 4.1. *Let Assumptions A(1) and A(2) hold, $l \geq m$, and $M \geq n$. If the system \mathbf{S} has no transmission zeros, then at least the first $2Mm - n$ rows of $\mathbf{U}_{2M}(k - 2M)$ and $\mathbf{U}_{2M}^{aux}(k - 2M)$ are identical.*

Proof. If we subtract equation (4.20) from the measurement equation of the system \mathbf{S}^{aug} and rewrite it in the matrix format, we will obtain,

$$\begin{bmatrix} \mathbf{C}_{2M} & \mathbf{D}_{2M} \end{bmatrix} \begin{bmatrix} x(k - 2M) - z(k - 2M) \\ \mathbf{U}_{2M}(k - 2M) - \mathbf{U}_{2M}^{aux}(k - 2M) \end{bmatrix} = 0 \quad (4.15)$$

Since the system \mathbf{S} does not have any transmission zeros, the columns of \mathbf{C}_{2M} and \mathbf{D}_{2M} are linearly independent. Hence,

$$\mathbf{C}_{2M}(x(k - 2M) - z(k - 2M)) = 0$$

and

$$\mathbf{D}_{2M}(\mathbf{U}_{2M}(k - 2M) - \mathbf{U}_{2M}^{aux}(k - 2M)) = 0 \quad (4.16)$$

On the other hand, from Lemma 4.1, it follows that the first $2Mm - n$ columns of \mathbf{D}_{2M} must be linearly independent. Therefore, one can transform equation (4.16) into the following format using basic operations on the last n columns of \mathbf{D}_{2M} and the last n rows of $\mathbf{U}_{2M}^{aux}(k - 2M) - \mathbf{U}_{2M}(k - 2M)$. Specifically, we have,

$$\begin{bmatrix} \mathcal{D} & 0 \end{bmatrix} \begin{bmatrix} \mathcal{U}_{2M}^{aux}(k - 2M) - \mathcal{U}_{2M}(k - 2M) \\ \mathcal{X} \end{bmatrix} = 0 \quad (4.17)$$

where \mathcal{D} is a nonsingular matrix that has the first $2Mm - n$ columns of \mathbf{D}_{2M} and $\mathcal{U}_{2M}^{aux}(k - 2M) - \mathcal{U}_{2M}(k - 2M)$ is the first $2Mm - n$ rows of $\mathbf{U}_{2M}^{aux}(k - 2M) - \mathbf{U}_{2M}(k - 2M)$. Therefore, the first $2Mm - n$ rows of $\mathbf{U}_{2M}^{aux}(k - 2M)$ and $\mathbf{U}_{2M}(k - 2M)$ are equal as stated. \square

Theorem 4.1 implies that the unknown input for the system \mathbf{S} having no transmission zeros can be algebraically reconstructed from the measurements.

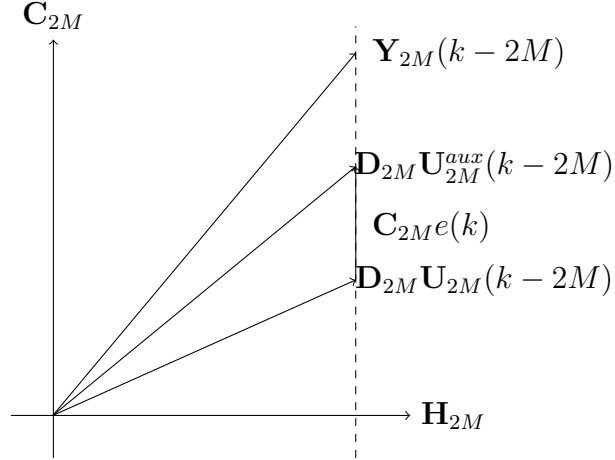


Figure 4.1: A graphical illustration of the \mathbf{C}_{2M} and \mathbf{H}_{2M} spaces. Note that projections of \mathbf{Y}_{2M} , $\mathbf{D}_{2M}\mathbf{U}_{2M}$ and $\mathbf{D}_{2M}\mathbf{U}_{2M}^{aux}$ onto the row space of \mathbf{H}_{2M} are identical.

4.3.2 Minimum Phase Linear Systems

Let us define an *augmented system* \mathbf{S}^{aug} that is governed by,

$$\mathbf{S}^{aug} : \begin{cases} x(k-2M+1) = Ax(k-2M) + B\mathbf{I}_p\mathbf{U}_{2M}(k-2M) \\ \mathbf{Y}_{2M}(k-2M) = \mathbf{C}_{2M}x(k-2M) + \mathbf{D}_{2M}\mathbf{U}_{2M}(k-2M) \end{cases} \quad (4.18)$$

where \mathbf{I}_p is defined according to,

$$\mathbf{I}_p = \begin{bmatrix} \mathbf{I}_{m \times m} & \mathbf{0}_{m \times (2Mm-m)} \end{bmatrix} \quad (4.19)$$

The systems \mathbf{S}^{aug} and \mathbf{S} have the same states, i.e. $x(k)$ subject to $2M$ time delays.

Let us also define a dummy state variable $z(k-2M)$ that satisfies the following relationship,

$$\mathbf{Y}_{2M}(k-2M) = \mathbf{C}_{2M}z(k-2M) + \mathbf{D}_{2M}\mathbf{U}_{2M}^{aux}(k-2M) \quad (4.20)$$

The variable $z(k-2M)$ that satisfies the above equation exists since $\mathbf{Y}_{2M}(k-2M) - \mathbf{D}_{2M}\mathbf{U}_{2M}^{aux}(k-2M)$ belongs to the column space of \mathbf{C}_{2M} , and $\mathbf{Y}_{2M}(k-2M)$ and $\mathbf{U}_{2M}^{aux}(k-2M)$ are known at each time step. Consequently, $z(k-2M)$ is known and is given by,

$$z(k-2M) = \mathbf{C}_{2M}^\dagger (\mathbf{Y}_{2M}(k-2M) - \mathbf{D}_{2M}\mathbf{U}_{2M}^{aux}(k-2M)) \quad (4.21)$$

Note that the variable $z(k)$ is not governed by the dynamics of $x(k)$ except when the system \mathbf{S} does not have any transmission zeros as shown in the proof of Theorem 4.1. In general, $z(k+1) \neq Az(k) + Bu(k)$. In fact the difference between the dynamics of $x(k)$ and $z(k)$ represents the zero dynamics of the system as we will show subsequently.

Let us define the difference between the two variables as a state error according to,

$$e(k) = x(k - 2M) - z(k - 2M) \quad (4.22)$$

We are now in position to state our next result.

Lemma 4.2. *Let Assumptions A(1) and A(2) hold, $l \geq m$, and $M \geq n$. The dynamics associated with the state error (4.22) is now given by,*

$$e(k+1) = (A - B\mathbf{I}_p\mathbf{D}_{2M}^+\mathbf{C}_{2M})e(k) - \begin{bmatrix} \mathbf{I} & -A & -B\mathbf{I}_p \end{bmatrix} \begin{bmatrix} z(k - 2M + 1) \\ z(k - 2M) \\ \mathbf{U}_{2M}^{aux}(k - 2M) \end{bmatrix}. \quad (4.23)$$

Proof. According to the definition of $e(k)$ given by equation (4.22), we have,

$$\begin{aligned} e(k+1) &= x(k - 2M + 1) - z(k - 2M + 1) \\ &= Ax(k - 2M) + B\mathbf{I}_p\mathbf{U}_{2M}(k - 2M) - z(k - 2M + 1) \\ &= Ae(k) + Az(k - 2M) + B\mathbf{I}_p\delta\mathbf{U}_{2M}(k) + B\mathbf{I}_p\mathbf{U}_{2M}^{aux}(k - 2M) - z(k - 2M + 1) \\ &= (A - B\mathbf{I}_p\mathbf{D}_{2M}^+\mathbf{C}_{2M})e(k) - \begin{bmatrix} \mathbf{I} & -A & -B\mathbf{I}_p \end{bmatrix} \begin{bmatrix} z(k - 2M + 1) \\ z(k - 2M) \\ \mathbf{U}_{2M}^{aux}(k - 2M) \end{bmatrix}. \end{aligned} \quad (4.24)$$

This concludes the proof of the lemma. □

It should be noted that the poles associated with the dynamics that is governed by equation (4.23) include the transmission zeros of the system \mathbf{S} for a square system. More specifically, we can state the following result.

Theorem 4.2. *Let Assumptions A(1) and A(2) hold, $l = m$, and $M \geq n$. Let $\mathcal{V} = \{v_i | i = 1, \dots, p\}$ denote the set of the system \mathbf{S} invariant zeros. Let $\mathcal{O} = \{0, \dots, 0\}$, that contains $n - p$ zeros. The eigenvalues of $(A - B\mathbf{I}_p\mathbf{D}_{2M}^+\mathbf{C}_{2M})$ are then given by $\mathcal{V} \cup \mathcal{O}$.*

Proof. Note that the eigenvalues of $A - B\mathbf{I}_p\mathbf{D}_{2M}^+\mathbf{C}_{2M}$ are obtained by solving,

$$|z\mathbf{I} - A + B\mathbf{I}_p\mathbf{D}_{2M}^+\mathbf{C}_{2M}| = 0 \quad (4.25)$$

If the system is square, then \mathbf{D}_{2M}^+ is a nonzero square matrix. Therefore, one can equivalently solve the equation,

$$|\mathbf{D}_{2M}^+| |z\mathbf{I} - A + B\mathbf{I}_p\mathbf{D}_{2M}^+\mathbf{C}_{2M}| = 0 \quad (4.26)$$

On the other hand, using the Schur identity, we have,

$$|\mathbf{D}_{2M}^+| |z\mathbf{I} - A + B\mathbf{I}_p\mathbf{D}_{2M}^+\mathbf{C}_{2M}| = \left| \left[\begin{array}{cc} z\mathbf{I} - A & -B\mathbf{I}_p \\ \mathbf{C}_{2M} & \mathbf{D}_{2M} \end{array} \right] \right| \quad (4.27)$$

Let us partition the terms \mathbf{C}_{2M} and \mathbf{D}_{2M} as follows,

$$\mathbf{C}_{2M} = \left(\begin{array}{c} C \\ C^- \end{array} \right) = \left(\begin{array}{c} C \\ CA \\ \vdots \\ CA^{2M-1} \end{array} \right) \quad (4.28)$$

$$\mathbf{D}_{2M} = \left(\begin{array}{c|c} D & 0 \\ \hline \mathcal{D}_{21}^- & \mathcal{D}_{22}^- \end{array} \right) = \left(\begin{array}{c|ccc} D & 0 & \dots & 0 \\ \hline CB & D & \dots & 0 \\ \vdots & \vdots & \vdots & \vdots \\ CA^{2M-1}B & CA^{2M-2}B & \dots & D \end{array} \right) \quad (4.29)$$

It now follows that the right-hand side of equation (4.27) can be partitioned as,

$$\begin{bmatrix} z\mathbf{I} - A & -B\mathbf{I}_p \\ \mathbf{C}_{2M} & \mathbf{D}_{2M} \end{bmatrix} = \left[\begin{array}{cc|c} z\mathbf{I} - A & -B & 0 \\ C & D & 0 \\ \hline \mathcal{C}^- & \mathcal{D}_{21}^- & \mathcal{D}_{22}^- \end{array} \right] \quad (4.30)$$

Thus, if \mathcal{D}_{22}^- is full row rank, according to the Schur identity, equation (4.25) has only one set of solutions that are given by,

$$\left\| \begin{bmatrix} z\mathbf{I} - A & -B\mathbf{I}_p \\ \mathbf{C}_{2M} & \mathbf{D}_{2M} \end{bmatrix} \right\| = 0 \quad (4.31)$$

and these are exactly the transmission zeros of the system \mathbf{S} . However, if \mathcal{D}_{22}^- is rank deficient, then certain rows of $\begin{bmatrix} \mathcal{C}^- & \mathcal{D}_{21}^- & \mathcal{D}_{22}^- \end{bmatrix}$ are linearly dependent with the rows of $\begin{bmatrix} -A & -B & 0 \end{bmatrix}$. Hence, $z = 0$ is also a solution. On the other hand, since equation (4.25) must have n eigenvalues, therefore if the system \mathbf{S} has p transmission zeros, then $z = 0$ is a solution of multiplicity $n - p$, and this concludes the proof of the theorem. □

Theorem 4.2 links the zero dynamics of the square system \mathbf{S} to the state error dynamics of (4.23). According to this theorem, if a square system \mathbf{S} is minimum phase, then the state error dynamics (4.23) will be stable. This statement is not generally true for non-square systems, since the state error dynamics (4.23) may have unstable pole(s) even for non-square minimum phase systems.

The state error dynamics is associated with the difference between $\mathbf{U}_{2M}(k - 2M)$ and $\mathbf{U}_{2M}^{aux}(k - 2M)$ as follows. If we define,

$$\delta\mathbf{U}_{2M}(k) = \mathbf{U}_{2M}(k - 2M) - \mathbf{U}_{2M}^{aux}(k - 2M)$$

and subtract equation (4.20) from the measurement equation of the system \mathbf{S}^{aug} , one will obtain,

$$\mathbf{D}_{2M}\delta\mathbf{U}_{2M}(k) = -\mathbf{C}_{2M}e(k) \quad (4.32)$$

Figure 4.1 shows a graphical illustration of equation (4.32), i.e., $\mathbf{D}_{2M}\delta\mathbf{U}_{2M}(k)$ (which is equal to $-\mathbf{C}_{2M}e(k)$) that lies in the column space of \mathbf{C}_{2M} . The dynamics (4.23) along with equation (4.32) can be used to construct an inverse filter for a square minimum phase systems as follows. Towards this end, we first provide a definition and present a lemma.

Definition 4.1. Consider a sequence $u(k)$. We let $\hat{u}(k)$ denote an unbiased estimate of $u(k)$ if $\hat{u}(k) \rightarrow z^{-q}u(k)$ as $k \rightarrow \infty$, where $q \in \mathbb{N}$. Otherwise, it will be designated as a biased estimate of $u(k)$.

Lemma 4.3. Let Assumptions A(1) and A(2) hold, $l \geq m$, and $M \geq n$. Then it follows that $\mathbf{I}_P.\mathcal{N}(\mathbf{D}_{2M}) = 0$.

Proof. Note that the first m columns of \mathbf{D}_{2M} are linearly independent. Therefore,

$$\text{rank}\left(\begin{bmatrix} \mathbf{I}_p \\ \mathbf{D}_{2M} \end{bmatrix}\right) = \text{rank}(\mathbf{D}_{2M})$$

which implies that the subspace spanned by the rows of \mathbf{I}_p belongs to the row space that is spanned by the rows of \mathbf{D}_{2M} . Therefore, $\mathbf{I}_P.\mathcal{N}(\mathbf{D}_{2M}) = 0$. \square

We are now in a position to state our next main result.

Theorem 4.3. Let Assumption A(1) and A(2) hold, $l = m$, and $M \geq n$. If the system \mathbf{S} is minimum phase, then the unbiased estimate of the unknown input $u(k - 2M)$ is governed by the filter dynamics,

$$\mathbf{S}^{inv} : \begin{cases} \hat{e}(k+1) = (A - B\mathbf{I}_p\mathbf{D}_{2M}^+\mathbf{C}_{2M})\hat{e}(k) - B_F\mathcal{U}(k-2M) \\ \hat{\mathbf{U}}_{2M}(k) = -\mathbf{D}_{2M}^+\mathbf{C}_{2M}\hat{e}(k) + \mathbf{U}_{2M}^{aux}(k-2M) \\ \hat{u}(k) = \mathbf{I}_p\hat{\mathbf{U}}_{2M}(k) \end{cases} \quad (4.33)$$

where,

$$B_F = \begin{bmatrix} \mathbf{I} & -A & -B\mathbf{I}_p \end{bmatrix} \quad (4.34)$$

$$\mathcal{U}(k-2M) = \begin{bmatrix} z(k-2M+1) \\ z(k-2M) \\ \mathbf{U}_{2M}^{aux}(k-2M) \end{bmatrix}. \quad (4.35)$$

where the state $z(k)$ at each time step is given by equation (4.21).

Proof. First, we show that $(\hat{e}(k) - e(k)) \rightarrow 0$ as $k \rightarrow \infty$. Then we show this will yield $\hat{u}(k) - u(k-2M) \rightarrow 0$ as $k \rightarrow \infty$. Note that the governing dynamics of $e(k)$ is given by Lemma 4.2. Therefore, in view of equations (4.23) and (4.33) we have, $\hat{e}(k+1) - e(k+1) = (A - B\mathbf{I}_p\mathbf{D}_{2M}^+\mathbf{C}_{2M})(\hat{e}(k) - e(k))$. Since the system \mathbf{S} is minimum phase, therefore, according to Theorem 4.2, $(\hat{e}(k) - e(k)) \rightarrow 0$ as $k \rightarrow \infty$ (note that Theorem 4.2 implies that $A - B\mathbf{I}_p\mathbf{D}_{2M}^+\mathbf{C}_{2M}$ is Hurwitz if the system \mathbf{S} is minimum phase). Note that the error in the unknown input reconstruction is given by,

$$\begin{aligned} \hat{\mathbf{U}}_{2M}(k) - \mathbf{U}_{2M}(k-2M) &= -\mathbf{D}_{2M}^+\mathbf{C}_{2M}\hat{e}(k) + \mathbf{U}_{2M}^{aux}(k-2M) - \mathbf{U}_{2M}(k-2M) \\ &\rightarrow -\mathbf{D}_{2M}^+\mathbf{C}_{2M}e(k) - \delta\mathbf{U}_{2M}(k) \\ &= \mathbf{D}_{2M}^+\mathbf{D}_{2M}\delta\mathbf{U}_{2M}(k) - \delta\mathbf{U}_{2M}(k) \end{aligned} \quad (4.36)$$

Consequently, we have,

$$\hat{u}(k) - u(k-2M) \rightarrow \mathbf{I}_p(\mathbf{D}_{2M}^+\mathbf{D}_{2M} - \mathbf{I})\delta\mathbf{U}_{2M}(k) \quad (4.37)$$

where $(\mathbf{D}_{2M}^+\mathbf{D}_{2M} - \mathbf{I})$ is the projector onto the null space of \mathbf{D}_{2M} . Since $\mathbf{I}_p.\mathcal{N}(\mathbf{D}_{2M}) = 0$, according to Lemma 4.3, the right-hand side of equation (4.37) is zero. Therefore, it follows that $\hat{u}(k) \rightarrow u(k-2M)$ as $k \rightarrow \infty$. \square

4.3.3 Non-Minimum Phase Systems

It should be noted that one cannot use Theorem 4.3 for non-minimum phase and/or non-square systems as well as systems with transmission zeros on the unit circle.

Consequently, below we will derive the dynamics associated with $\delta\mathbf{U}_{2M}(k)$ and attempt to stabilize it to ensure a zero tracking error. Let us define,

$$\eta(k) = \mathbf{D}_{2M}\delta\mathbf{U}_{2M}(k) \quad (4.38)$$

It now follows that the dynamics of $\eta(k)$ is governed by,

$$\eta(k+1) = \tilde{A}\eta(k) + \mathbf{C}_{2M}B_F\mathcal{U}(k-2M) \quad (4.39)$$

where

$$\tilde{A} = \mathbf{C}_{2M}(A - \mathbf{B}\mathbf{I}_P\mathbf{D}_{2M}^+\mathbf{C}_{2M})\mathbf{C}_{2M}^\dagger. \quad (4.40)$$

This follows by multiplying both sides of equation (4.23) by \mathbf{C}_{2M} and then replacing $\mathbf{C}_{2M}e(k)$ by equation (4.32), to yield the result.

In order to obtain a stable filter for non-minimum phase systems that is applicable to both square and non-square systems, we rotate both \mathbf{C}_{2M} and \mathbf{H}_{2M} through a rotation matrix $\mathbf{R} \in \mathbb{R}^{2M \times 2M}$ about an *arbitrary axis* as follows,

$$\mathbf{C}_{2M}^{new} = \mathbf{R}\mathbf{C}_{2M} \quad (4.41)$$

$$\mathbf{H}_{2M}^{new} = (\mathbf{R}\mathbf{H}_{2M}^T)^T \quad (4.42)$$

A square matrix is said to be a rotation matrix if $\mathbf{R}\mathbf{R}^T = \mathbf{R}^T\mathbf{R} = \mathbf{I}$ and $\|\mathbf{R}\| = 1$.

This operation represents a *similarity transformation* for the following system ¹,

$$\mathbf{S}^\eta : \begin{cases} \eta(k+1) = \tilde{A}\eta(k) + \mathbf{C}_{2M}B_F\mathcal{U}(k-2M) \\ \mathcal{H}(k) = \mathbf{H}_{2M}\eta(k) \end{cases} \quad (4.43)$$

Note that $\mathcal{H}(k) \equiv 0$ since,

$$\begin{aligned} \mathcal{H}(k) &= \mathbf{H}_{2M}\eta(k) = \mathbf{H}_{2M}\mathbf{D}_{2M}\delta\mathbf{U}_{2M}(k) \\ &= \mathbf{H}_{2M}\mathbf{D}_{2M}(\mathbf{U}_{2M}(k-2M) - \mathbf{U}_{2M}^{aux}(k-2M)) \\ &= \mathbf{H}_{2M}(\mathbf{Y}_{2M}(k-2M) - \mathbf{Y}_{2M}(k-2M)) = 0 \end{aligned} \quad (4.44)$$

¹Note that the system matrices of \mathbf{S}^η , i.e. $(\tilde{A}, \mathbf{C}_{2M}B_F, \mathbf{H}_{2M})$ after applying the similarity transformation by the matrix \mathbf{R} is represented by $(\mathbf{R}\tilde{A}\mathbf{R}^T, \mathbf{C}_{2M}^{new}B_F, \mathbf{H}_{2M}^{new})$.

Therefore, if the system \mathbf{S} has any transmission zeros, then the difference between the real input and the auxiliary input serves as the output-zeroing input of the system (4.43). One may have suggested now to use the feedback from $\mathcal{H}(k)$ to stabilize the system \mathbf{S}^η . However, clearly the system \mathbf{S}^η is neither controllable nor observable.

Therefore, we now instead define $\hat{\eta}(k)$ to be governed as follows,

$$\hat{\eta}(k+1) = (\mathbf{P}_c^{new} \tilde{A} + \mathbf{P}_h^{new} + \mathbf{K}_2 \mathbf{P}_h) \hat{\eta}(k) + \mathbf{P}_c^{new} \mathbf{C}_{2M} B_F \mathcal{U}(k-2M) \quad (4.45)$$

where,

$$\begin{aligned} \mathbf{P}_h^{new} &= \mathbf{H}_{2M}^{newT} (\mathbf{H}_{2M}^{new} \mathbf{H}_{2M}^{newT})^{-1} \mathbf{H}_{2M}^{new} \\ \mathbf{P}_c^{new} &= \mathbf{C}_{2M}^{new} (\mathbf{C}_{2M}^{newT} \mathbf{C}_{2M}^{new})^{-1} \mathbf{C}_{2M}^{newT} \end{aligned}$$

with \mathbf{K}_2 chosen such that all the eigenvalues of $(\mathbf{P}_c^{new} \tilde{A} + \mathbf{P}_h^{new} + \mathbf{K}_2 \mathbf{P}_h)$ lie inside the unit circle.

Note that if the unknown input is a step function, then $\eta(k) - \hat{\eta}(k) \rightarrow 0$ as $k \rightarrow 0^2$.

In order to establish the above claim, first, we discuss the stabilization of the filter (4.45) through selection of \mathbf{K}_2 and then address its tracking error behavior and performance.

It can be easily concluded that the stabilization of the filter (4.45) by the gain \mathbf{K}_2 is possible if and only if the pair $(\mathbf{P}_c^{new} \tilde{A} + \mathbf{P}_h^{new}, -\mathbf{P}_h)$ is observable, which provides an explicit criterion for selection of the rotation matrix \mathbf{R} . However, certain care should be exercised in selection of \mathbf{R} as pointed out in the following two remarks.

Remark 4.1. *If \mathbf{R} is selected such that the column space of \mathbf{C}_{2M}^{new} coincides with the column space of \mathbf{C}_{2M} (or equivalently the row space of \mathbf{H}_{2M}^{new} coincides with the row*

²If one could design a filter in the form of $\hat{\eta}(k+1) = (\mathbf{P}_c^{new} \tilde{A} + \mathbf{P}_h^{new} \tilde{A} + \mathbf{K}_2 \mathbf{P}_h) \hat{\eta}(k) + \mathbf{P}_c^{new} \mathbf{C}_{2M} B_F \mathcal{U}$, then one would have an unbiased estimation of all types of inputs, however, this filter and similar ones would unfortunately be neither controllable nor observable.

space of \mathbf{H}_{2M}), then the pair $(\mathbf{P}_c^{new} \tilde{A} + \mathbf{P}_h^{new}, -\mathbf{P}_h)$ will not be observable since (a) $\mathbf{P}_h^{new} = \mathbf{P}_h$, (b) $\mathbf{P}_h(\mathbf{P}_c^{new} \tilde{A} + \mathbf{P}_h^{new}) = \mathbf{P}_h^{new}$, and (c) \mathbf{P}_h is column rank deficient. Hence, the observability matrix will be rank deficient.

Remark 4.2. If \mathbf{R} is selected such that the column space of \mathbf{C}_{2M}^{new} coincides with the row space of \mathbf{H}_{2M} , then the pair $(\mathbf{P}_c^{new} \tilde{A} + \mathbf{P}_h^{new}, -\mathbf{P}_h)$ will not be observable since $\mathbf{P}_h(\mathbf{P}_c^{new} \tilde{A} + \mathbf{P}_h^{new}) = 0$, and therefore the observability matrix will be rank deficient.

Geometrically speaking, for a SISO system having a single state, Remarks 4.1 and 4.2 imply that \mathbf{R} should not be a matrix resulting in a rotation of $\frac{q\pi}{2}$, $q \in \mathbb{Z}$, about the axis passing through origin and should be perpendicular to both \mathbf{C}_{2M} and \mathbf{H}_{2M} . Otherwise, for example for a rotation angle of $\frac{\pi}{2}$, the column space of \mathbf{C}_{2M}^{new} will coincide with the row space of \mathbf{H}_{2M} . All other \mathbf{R} s except those excluded in Remarks 4.1 and 4.2 will yield an observable $(\mathbf{P}_c^{new} \tilde{A} + \mathbf{P}_h^{new}, -\mathbf{P}_h)$ pair. However, the closer the rotation angle is to $\frac{q\pi}{2}$, a higher gain \mathbf{K}_2 will be required to stabilize the system. This will be numerically illustrated in the simulation case studies in Section 4.5.

Moreover, if a square system has one or more transmission zeros *exactly equal* to 1 (with *no* other transmission zeros on the unit circle), then there will exist no \mathbf{R} such that the pair $(\mathbf{P}_c^{new} \tilde{A} + \mathbf{P}_h^{new}, -\mathbf{P}_h)$ is observable. We can now state the following result.

Lemma 4.4. *If a square system \mathbf{S} has a transmission zero exactly equal to 1 ($z = 1$), then the pair $(\mathbf{P}_c^{new} \tilde{A} + \mathbf{P}_h^{new}, -\mathbf{P}_h)$ will not be observable for any selection of the rotation matrix \mathbf{R} .*

Proof. We use the Hautus test ([132]) to show this lemma. The observability matrix of the pair $(\mathbf{P}_c^{new} \tilde{A} + \mathbf{P}_h^{new}, -\mathbf{P}_h)$ is equivalent to the controllability matrix of the pair $((\tilde{A} + \mathbf{P}_h^{new})^T, -(\mathbf{P}_h)^T)$. The pair $((\mathbf{P}_c^{new} \tilde{A} + \mathbf{P}_h^{new})^T, -(\mathbf{P}_h)^T)$ is controllable if

$$\text{rank} \left(\begin{bmatrix} (\mathbf{P}_c^{new} \tilde{A} + \mathbf{P}_h^{new})^T - \lambda \mathbf{I} & -(\mathbf{P}_h)^T \end{bmatrix} \right) = 2Ml$$

for all $\lambda \in \mathbb{C}$. We now show that when the square system \mathbf{S} has a transmission zero equal to 1, then this condition is not satisfied for $\lambda = 1$. Equivalently, there exists a nonzero w such that $w\Theta = 0$, for $\lambda = 1$, where

$$\Theta = \begin{bmatrix} (\mathbf{P}_c^{new} \tilde{A} + \mathbf{P}_h^{new})^T - \lambda \mathbf{I} & -(\mathbf{P}_h)^T \end{bmatrix}$$

When $\lambda = 1$, it follows that,

$$\begin{aligned} (\mathbf{P}_c^{new} \tilde{A} + \mathbf{P}_h^{new})^T - \lambda \mathbf{I} &= (\mathbf{P}_c^{new} \tilde{A} + \mathbf{P}_h^{new})^T - \mathbf{I} \\ &= (\mathbf{P}_c^{new} \tilde{A} - \mathbf{P}_c^{new})^T \end{aligned} \quad (4.46)$$

Recall from Theorem 4.2 that the transmission zeros of \mathbf{S} are the eigenvalues of $A - B\mathbf{I}_p\mathbf{D}_{2M}^+\mathbf{C}_{2M}$. Hence, if the system \mathbf{S} has a transmission zero equal to 1, there exists a nonzero v such that $\mathbf{P}_c^{new} \tilde{A}v = \mathbf{P}_c^{new}v$. Therefore, by selecting

$$w = \begin{bmatrix} v^T & 0 \end{bmatrix}$$

one can achieve $w\Theta = 0$ independent of the choice of the rotation matrix \mathbf{R} . This completes the proof of the lemma. □

If a square system \mathbf{S} has transmission zeros on the unit circle except at $z = 1$, then every \mathbf{R} except those stated in Remarks 4.1 and 4.2 yield an observable $(\mathbf{P}_c^{new} \tilde{A} + \mathbf{P}_h^{new}, -\mathbf{P}_h)$ pair. Non-square systems rarely have transmission zeros ([133]), therefore it is less likely to have a transmission zero that is equal to 1, or in general on the unit circle. If so then a matrix \mathbf{R} may or may not exist.

Once the observability condition is satisfied, it is straightforward to determine \mathbf{K}_2 by using the Ackerman's method to place the system poles at desired locations. The significance of our proposed solution can be appreciated by the fact that the designed feedback not only stabilizes the system for both minimum and non-minimum phase systems in general, but also it provides an unbiased estimate of the unknown step input as stated in the following theorem.

Theorem 4.4. *Let the Assumptions A(1) and A(2) hold, $l \geq m$, and $M \geq n$. If the unknown input is a step function, and if there exists an \mathbf{R} such that the pair $(\mathbf{P}_c^{new} \tilde{A} + \mathbf{P}_h^{new}, -\mathbf{P}_h)$ is observable, and \mathbf{K}_2 is chosen such that all the eigenvalues of $\mathbf{P}_c^{new} \tilde{A} + \mathbf{P}_h^{new} + \mathbf{K}_2 \mathbf{P}_h$ lie inside the unit circle, then an unbiased estimate of the unknown input $u(k - 2M)$ is given by,*

$$\mathbf{S}_{stp}^{inv} : \begin{cases} \hat{\eta}(k+1) = (\mathbf{P}_c^{new} \tilde{A} + \mathbf{P}_h^{new} + \mathbf{K}_2 \mathbf{P}_h) \hat{\eta}(k) + \mathbf{P}_c^{new} \mathbf{C}_{2M} B_F \mathcal{U}(k - 2M) \\ \hat{\mathbf{U}}_{2M}(k) = \mathbf{D}_{2M}^+ \hat{\eta}(k) + \mathbf{U}_{2M}^{aux}(k - 2M) \\ \hat{u}(k) = \mathbf{I}_p \hat{\mathbf{U}}_{2M}(k) \end{cases} \quad (4.47)$$

Proof. First, it is shown that $\hat{\eta}(k) - \eta(k) \rightarrow 0$ as $k \rightarrow \infty$. Then, we show that it follows that $\hat{u}(k) - u(k - 2M) \rightarrow 0$ as $k \rightarrow \infty$. If one subtracts equation (4.45) from the equation (4.39), one will have,

$$\begin{aligned} \hat{\eta}(k+1) - \eta(k+1) &= (\tilde{A} + \mathbf{P}_h^{new} + \mathbf{K}_2 \mathbf{P}_h)(\hat{\eta}(k) - \eta(k)) \\ &+ (\mathbf{P}_h^{new} \tilde{A} - \mathbf{P}_h^{new})\eta(k) + \mathbf{P}_h^{new} \mathbf{C}_{2M} \mathcal{U}(k) \\ &= (\tilde{A} + \mathbf{P}_h^{new} + \mathbf{K}_2 \mathbf{P}_h)(\hat{\eta}(k) - \eta(k)) + \mathbf{P}_h^{new}(\eta(k+1) - \eta(k)) \end{aligned} \quad (4.48)$$

Let us define $e(k) = \hat{\eta}(k) - \eta(k)$. Also let us take the \mathcal{Z} -transform of both sides of equation (4.48), which after some rearrangements gives us,

$$e(z) = (zI - \tilde{A} - \mathbf{P}_h^{new} - \mathbf{K}_2 \mathbf{P}_h)^{-1} \mathbf{P}_h^{new} (z - 1) \eta(z) \quad (4.49)$$

If the input to the system \mathbf{S} is a step function, then according to the final value theorem, we have

$$\lim_{k \rightarrow \infty} e(k) = \lim_{z \rightarrow 1} (z - 1) e(z) = 0$$

which implies that $\hat{\eta}(k) - \eta(k) \rightarrow 0$ as $k \rightarrow \infty$.

The estimation error in the unknown input reconstruction is given by,

$$\begin{aligned}
\hat{\mathbf{U}}_{2M}(k) - \mathbf{U}_{2M}(k - 2M) &= \mathbf{D}_{2M}^+ \hat{\eta}(k) + \mathbf{U}_{2M}^{aux}(k - 2M) - \mathbf{U}_{2M}(k - 2M) \\
&\rightarrow \mathbf{D}_{2M}^+ \eta(k) - \delta \mathbf{U}_{2M}(k) \\
&= \mathbf{D}_{2M}^+ \mathbf{D}_{2M} \delta \mathbf{U}_{2M}(k) - \delta \mathbf{U}_{2M}(k)
\end{aligned} \tag{4.50}$$

Thus, we have,

$$\hat{u}(k) - u(k - 2M) \rightarrow \mathbf{I}_p (\mathbf{D}_{2M}^+ \mathbf{D}_{2M} - \mathbf{I}) \delta \mathbf{U}_{2M}(k) \tag{4.51}$$

where $(\mathbf{D}_{2M}^+ \mathbf{D}_{2M} - \mathbf{I})$ is the projector onto the null space of \mathbf{D}_{2M} . Since $\mathbf{I}_p \mathcal{N}(\mathbf{D}_{2M}) = 0$, according to Lemma 4.3, the right-hand side of equation (4.37) is zero. Therefore, it can be concluded that $\hat{u}(k) \rightarrow u(k - 2M)$ as $k \rightarrow \infty$. This completes the proof of the theorem. \square

Note that in contrast to the filter (4.33), which is limited to only square and minimum phase systems, the filter (4.47) is a general solution for both minimum and non-minimum phase systems of any size that satisfies $l \geq m$ ³. Moreover, it *can handle* systems that have transmission zeros on the unit circle.

By a close inspection of the proof of Theorem 4.4 it follows that the strategy for constructing a stable and unbiased inversion filter for an *unknown ramp* as well as *step input functions* can be developed. The strategy for the ramp input is to specifically construct a filter that results in increasing the *type* of the error dynamics to diminish the steady state errors. Based on the above observation, the following theorem can now be stated.

Theorem 4.5. *Let Assumptions A(1) and A(2) hold, $l \geq m$, and $M \geq n$. If the unknown input is a ramp function, and if there exists a rotation matrix \mathbf{R} such that the pair $(\mathbf{P}_h^{new} \tilde{A}^2 - 2\mathbf{P}_h^{new} \tilde{A} + \tilde{A} + \mathbf{P}_h^{new}, -\mathbf{P}_h)$ is observable, and \mathbf{K}_2 is chosen such*

³One can obtain similar results with $\hat{\eta}(k+1) = (\mathbf{P}_h^{new} \tilde{A} + \mathbf{P}_c^{new} + \mathbf{K}_2 \mathbf{P}_h) \hat{\eta}(k) + \mathbf{P}_h^{new} \mathbf{C}_{2M} B_F \mathcal{U}$ due to symmetrical properties of the rotation matrix.

that all the eigenvalues of $\mathbf{P}_h^{new} \tilde{A}^2 - 2\mathbf{P}_h^{new} \tilde{A} + \tilde{A} + \mathbf{P}_h^{new} + \mathbf{K}_2\mathbf{P}_h$ lie inside the unit circle, then an unbiased estimate of the unknown input $u(k - 2M)$ is given by,

$$\mathbf{S}_{rmp}^{inv} : \begin{cases} \hat{\eta}(k + 1) = (\mathbf{P}_h^{new} \tilde{A}^2 - 2\mathbf{P}_h^{new} \tilde{A} + \tilde{A} + \mathbf{P}_h^{new} + \mathbf{K}_2\mathbf{P}_h)\hat{\eta}(k) + \Gamma(k - 2M) \\ \hat{\mathbf{U}}_{2M}(k) = \mathbf{D}_{2M}^+ \hat{\eta}(k) + \mathbf{U}_{2M}^{aux}(k - 2M) \\ \hat{u}(k) = \mathbf{I}_p \hat{\mathbf{U}}_{2M}(k) \end{cases} \quad (4.52)$$

where,

$$\begin{aligned} \Gamma(k - 2M) &= \mathbf{P}_h^{new} \mathbf{C}_{2M} B_F \mathcal{U}(k - 2M + 1) \\ &\quad + \left(\mathbf{P}_h^{new} \tilde{A} - 2\mathbf{P}_h^{new} + \mathbf{I} \right) \mathbf{C}_{2M} B_F \mathcal{U}(k - 2M). \end{aligned} \quad (4.53)$$

Proof. First, it is shown that $\hat{\eta}(k) - \eta(k) \rightarrow 0$ as $k \rightarrow \infty$. Then we show that it follows that $\hat{u}(k) - u(k - 2M) \rightarrow 0$ as $k \rightarrow \infty$. Let us define the following dummy variables,

$$\begin{aligned} A_1 &= \mathbf{P}_h^{new} \tilde{A}^2 - 2\mathbf{P}_h^{new} \tilde{A} + \tilde{A} + \mathbf{P}_h^{new} \\ A_2 &= \mathbf{P}_h^{new} \tilde{A}^2 - 2\mathbf{P}_h^{new} \tilde{A} + \tilde{A} + \mathbf{P}_h^{new} + \mathbf{K}_2\mathbf{P}_h \\ B_1 &= \mathbf{P}_h^{new} \mathbf{C}_{2M} B_F \mathcal{U}(k - 2M + 1) + \left(\mathbf{P}_h^{new} \tilde{A} - 2\mathbf{P}_h^{new} + \mathbf{I} \right) \mathbf{C}_{2M} B_F \mathcal{U}(k - 2M) \\ B_2 &= \mathbf{P}_h^{new} \mathbf{C}_{2M} B_F \mathcal{U}(k - 2M + 1) + \left(\mathbf{P}_h^{new} \tilde{A} - 2\mathbf{P}_h^{new} \right) \mathbf{C}_{2M} B_F \mathcal{U}(k - 2M) \end{aligned}$$

If we subtract the state equation of the filter (4.52) from that of equation (4.39), we will have,

$$\begin{aligned} \hat{\eta}(k + 1) - \eta(k + 1) &= \tilde{A}\hat{\eta}(k) + \mathbf{C}_{2M} B_F \mathcal{U}(k) - A_2 \hat{\eta}(k) - B_1 \\ &= A_2(\hat{\eta}(k) - \eta(k)) - A_1 \eta(k) - B_2 \\ &= A_2(\hat{\eta}(k) - \eta(k)) - \mathbf{P}_h^{new}(\eta(k + 2) - 2\eta(k + 1) + \eta(k)) \end{aligned} \quad (4.54)$$

Let us define as before $e(k) = \hat{\eta}(k) - \eta(k)$. Also, let us take the \mathcal{Z} -transform of both sides of equation (4.54), which after some rearrangements gives,

$$e(z) = -(zI - A_2)^{-1} \mathbf{P}_h^{new} (z - 1)^2 \eta(z) \quad (4.55)$$

If the input is a step or a ramp function, then according to the final value theorem it follows that,

$$\lim_{k \rightarrow \infty} e(k) = \lim_{z \rightarrow 1} (z - 1)e(z) = 0$$

which implies that $\hat{\eta}(k) - \eta(k) \rightarrow 0$ as $k \rightarrow \infty$. The remainder of the proof follows along similar lines as those invoked in the proof of Theorem 4.4, and therefore these details are omitted for brevity. \square

It is interesting to note that the filter (4.52) cannot be obtained through standard and basic mathematical operations (such as a similarity transformation) from the filter (4.47) or vice versa. This concludes our proposed general solution to inversion of discrete-time linear systems.

To summarize, the unknown input was reconstructed from its projection onto the column space of \mathbf{C}_{2M} and the row space of \mathbf{H}_{2M} . The projection on the row space of \mathbf{H}_{2M} is simply given by equation (4.9), however, the projection on \mathbf{C}_{2M} is indirectly obtained from the reconstruction of $\mathbf{D}_{2M}\delta\mathbf{U}$. The term $\mathbf{D}_{2M}\delta\mathbf{U}$ has this important property that it is orthogonal to the subspace that is spanned by the rows of \mathbf{H}_{2M} .

Yet, two important issues are associated with this technique. First, the construction of $\mathbf{D}_{2M}\delta\mathbf{U}$ is an unstable process for non-minimum phase systems. Secondly, the calculation of $\delta\mathbf{U}$ requires the inverse of \mathbf{D}_{2M} , which is a non-square and rank-deficient matrix under most circumstances.

To address the first issue, we have proposed a novel technique in which the column space of \mathbf{C}_{2M} and the row space of \mathbf{H}_{2M} are transformed through a rotation matrix about an arbitrary axis, followed by introducing a feedback that not only stabilizes, but also eliminates the steady state error of the inverse filter. To address the second issue, Lemma 4.3 is introduced that is always satisfied for minimal systems with $l \geq m$, even if \mathbf{D}_{2M} is rank deficient.

In the next section, we provide a solution to our Problem 2 introduced in Section II.

4.4 The Proposed Inversion-Based Fault Estimation for Non-Minimum Phase Fault to Output Systems

One of the most important applications of the system inversion is to the problem of fault estimation. A solution to this problem is essential for any successful fault tolerant control scheme and reliable operation of engineering systems. In this section, we show that our proposed system inversion approach can be easily adopted for fault estimation purposes. The advantage of our methodology is that the unknown fault input is directly reconstructed from only the system measurements *without* requiring any *a priori* estimate of the system states. Moreover, it can handle transmission zeros everywhere on the complex plan even on the unit circle.

We follow a similar procedure that was proposed in the previous section with the difference that now in the system \mathbf{S}^f , $u(k)$ is assumed to be known and the unknown input, which is the injected fault signal, is now designated as $f(k)$.

Therefore, let us define the vector \mathbf{F}_{2M}^{aux} as follows,

$$\mathbf{F}_{2M}^{aux}(k - 2M) = \mathbf{K}_1^f(\mathbf{Y}_{2M}(k - 2M) - \mathbf{D}_{2M}\mathbf{U}_{2M}(k - 2M)) \quad (4.56)$$

where \mathbf{K}_1^f is given by,

$$\mathbf{K}_1^f = (\mathbf{H}_{2M}\mathbf{E}_{2M})^+\mathbf{H}_{2M} \quad (4.57)$$

and

$$\mathbf{E}_{2M} = \begin{pmatrix} E & 0 & \dots & 0 \\ CL & E & \dots & 0 \\ \vdots & \vdots & \vdots & \vdots \\ CA^{2M-1}L & CA^{2M-2}L & \dots & L \end{pmatrix} \quad (4.58)$$

According to Theorem 4.1, $\mathbf{F}_{2M}^{aux}(k-2M)$ represents a construction of $\mathbf{F}_{2M}(k-2M)$ if the fault-to-output dynamics has no transmission zeros. For the general case, we define a dummy state variable $z^f(k-2M)$ that satisfies the following relationship,

$$\mathbf{Y}_{2M}(k-2M) = \mathbf{C}_{2M}z^f(k-2M) + \mathbf{D}_{2M}\mathbf{U}_{2M}(k-2M) + \mathbf{E}_{2M}\mathbf{F}_{2M}^{aux}(k-2M) \quad (4.59)$$

Moreover, we define,

$$\eta^f(k) = \mathbf{E}_{2M}\delta\mathbf{F}_{2M}(k) = \mathbf{E}_{2M}(\mathbf{F}_{2M}(k-2M) - \mathbf{F}_{2M}^{aux}(k-2M)) \quad (4.60)$$

Therefore, the dynamics associated with $\eta^f(k)$ is now governed by

$$\eta^f(k+1) = \tilde{A}^f\eta^f(k) + \mathbf{C}_{2M}B_F^f\mathcal{U}^f(k-2M). \quad (4.61)$$

where,

$$\tilde{A}^f = \mathbf{C}_{2M}(A - L\mathbf{I}_p^f\mathbf{E}_{2M}^+\mathbf{C}_{2M})\mathbf{C}_{2M}^\dagger \quad (4.62)$$

$$B_F^f = \begin{bmatrix} \mathbf{I} & -A & -L\mathbf{I}_p^f & -B\mathbf{I}_p \end{bmatrix} \quad (4.63)$$

$$\mathcal{U}^f(k-2M) = \begin{bmatrix} z^f(k-2M+1) \\ z^f(k-2M) \\ \mathbf{F}_{2M}^{aux}(k-2M) \\ \mathbf{U}_{2M}(k-2M) \end{bmatrix} \quad (4.64)$$

and

$$\mathbf{I}_p^f = \begin{bmatrix} \mathbf{I}_{p \times p} & \mathbf{0}_{p \times (2Mp-p)} \end{bmatrix} \quad (4.65)$$

Note that as compared to equation (4.39), the additional known information $\mathbf{U}_{2M}(k-2M)$ appears in $\mathcal{U}^f(k-2M)$. The dynamics of the system (4.61) is unstable

if the fault-to-output dynamics has transmission zeros outside or on the unit circle. On the other hand, a close examination of the dynamics (4.61) reveals that it is quite similar to the dynamics that is described by (4.39). Therefore, the same strategy that was described in the previous section can now be applied here. Specifically, we can conclude the following result.

Theorem 4.6. *Let Assumptions B(1) and B(2) hold, $l \geq p$, and $M \geq n$. If the fault signal is a step loss of effectiveness (LOE) function, and there exists a rotation matrix \mathbf{R} such that the pair $(\mathbf{P}_c^{new} \tilde{A}^f + \mathbf{P}_h^{new}, -\mathbf{P}_h)$ is observable, and \mathbf{K}_2^f is chosen such that all the eigenvalues of $\mathbf{P}_c^{new} \tilde{A}^f + \mathbf{P}_h^{new} + \mathbf{K}_2^f \mathbf{P}_h$ lie inside the unit circle, then an unbiased estimate of the fault vector $f(k - 2M)$ is given by,*

$$\mathbf{S}_{stp}^{inv,f} : \begin{cases} \hat{\eta}^f(k+1) = (\mathbf{P}_c^{new} \tilde{A}^f + \mathbf{P}_h^{new} + \mathbf{K}_2^f \mathbf{P}_h) \hat{\eta}^f(k) + \mathbf{P}_c^{new} \mathbf{C}_{2M} B_F^f \mathcal{U}^f(k-2M) \\ \hat{\mathbf{F}}_{2M}(k) = \mathbf{E}_{2M}^+ \hat{\eta}^f(k) + \mathbf{F}_{2M}^{aux}(k-2M) \\ \hat{f}(k) = \mathbf{I}_p \hat{\mathbf{F}}_{2M}(k) \end{cases} \quad (4.66)$$

Proof. Proof is not included, since it is similar to the proof of Theorem 4.4. \square

One can also establish a result that is similar to Theorem 4.5 for the case when the fault signal is a ramp (drift) loss of effectiveness (LOE) function. The details are not included here for brevity.

This now concludes our proposed methodology for estimation of the loss of effectiveness faults for systems having transmission zeros anywhere on the complex plan. In the next section, we provide illustrative simulations that demonstrate the merits and capabilities of our proposed methodologies.

4.5 Four Case Studies

Consider a first order non-minimum phase SISO system that is governed by ⁴,

⁴For all simulations of this section, we set $M = n$.

$$S : \begin{cases} x(k+1) = 0.5x(k) + u(k) \\ y(k) = -x(k) + u(k) \end{cases} \quad (4.67)$$

The transfer function of this system is given by,

$$G(z) = \frac{z - 1.5}{z - 0.5} \quad (4.68)$$

For the above system, it follows that $\mathbf{C}_{2M} = \begin{bmatrix} -1 \\ -0.5 \end{bmatrix}$, and consequently $\mathbf{H}_{2M} = \begin{bmatrix} -0.45 & 0.90 \end{bmatrix}$. The rotation matrix \mathbf{R} is given by,

$$\mathbf{R}(\theta) = \begin{bmatrix} \cos(\theta) & -\sin(\theta) \\ \sin(\theta) & \cos(\theta) \end{bmatrix}$$

According to Remarks 4.1 and 4.2, the pair $(\mathbf{P}_c^{new} \tilde{\mathbf{A}} + \mathbf{P}_h^{new}, -\mathbf{P}_h)$ is not observable for $\theta = \frac{q\pi}{2}, q \in \mathbb{Z}$, where,

$$\tilde{\mathbf{A}} = \begin{bmatrix} 1.2 & 0.6 \\ 0.6 & 0.3 \end{bmatrix}; \mathbf{P}_h = \begin{bmatrix} 0.2 & -0.4 \\ -0.4 & 0.8 \end{bmatrix}$$

$$\mathbf{P}_c = \begin{bmatrix} 0.8 & 0.4 \\ 0.4 & 0.2 \end{bmatrix}$$

$$\mathbf{P}_h^{new} = \mathbf{R}(\theta)\mathbf{P}_h(\mathbf{R}(\theta))^T; \mathbf{P}_c^{new} = \mathbf{R}(\theta)\mathbf{P}_c(\mathbf{R}(\theta))^T$$

All the other values of θ will yield an \mathbf{R} such that the pair $(\mathbf{P}_c^{new} \tilde{\mathbf{A}} + \mathbf{P}_h^{new}, -\mathbf{P}_h)$ is observable. Hence, one can arbitrarily place the poles of the system. We select the gain \mathbf{K}_2 to place the poles at $z_{1,2} = \pm 0.1$ for two different values of θ that are randomly selected for comparison purposes as follows,

$$\theta = \frac{5\pi}{180} \text{ or } \frac{85\pi}{180} \rightarrow$$

$$\mathbf{P}_c^{new} \tilde{\mathbf{A}} + \mathbf{P}_h^{new} = \begin{bmatrix} 1.41 & 0.12 \\ 0.25 & 1.07 \end{bmatrix}, \mathbf{K}_2 = \begin{bmatrix} 20.09 & -40.18 \\ 11.29 & -22.58 \end{bmatrix}$$

and

$$\theta = \frac{45\pi}{180} \rightarrow$$

$$\mathbf{P}_h^{new} \tilde{A} + \mathbf{P}_h^{new} = \begin{bmatrix} 1.20 & -0.15 \\ 0.60 & 0.55 \end{bmatrix}, \mathbf{K}_2 = \begin{bmatrix} 1.95 & -3.90 \\ 1.85 & -3.7 \end{bmatrix}$$

The closer θ is to $\frac{q\pi}{2}, q \in \mathbb{Z}$ implies that a higher gain is required. This is an important consideration as it may lead to robustness issues when the system is subject to disturbances and noise. Using Theorem 4.4, the inverse filter for the above system when $\theta = \frac{45\pi}{180}$ is given by,

$$S^{inv} : \begin{cases} \hat{\eta}(k+1) = \begin{pmatrix} 3.15 & -4.05 \\ 2.45 & -3.15 \end{pmatrix} \hat{\eta}(k) + \begin{bmatrix} -0.25 & 0.12 & 0.25 & 0 \\ -0.75 & 0.37 & 0.75 & 0 \end{bmatrix} \mathcal{U}(k-2M) \\ \hat{\mathbf{U}}_{2M}(k) = \begin{pmatrix} 1 & 0 \\ 1 & 1 \end{pmatrix} \hat{\eta}(k) + \mathbf{U}_{2M}^{aux}(k-2M) \\ \hat{u}(k) = \mathbf{I}_p \hat{\mathbf{U}}_{2M}(k) \end{cases} \quad (4.69)$$

where $M = n$, $\mathcal{U}(k-2M)$ is defined by equation (4.35) and $\mathbf{U}_{2M}^{aux}(k-2M)$ is given by,

$$\mathbf{U}_{2M}^{aux}(k-2M) = \begin{bmatrix} 0.2308 & -0.4615 \\ -0.1538 & 0.3077 \end{bmatrix} \mathbf{Y}_{2M}(k-2M)$$

Figure 4.2 shows the performance of the input inversion estimation filter corresponding to both values of \mathbf{K}_2 .

For the second simulation case study, we consider a non-minimum phase MIMO

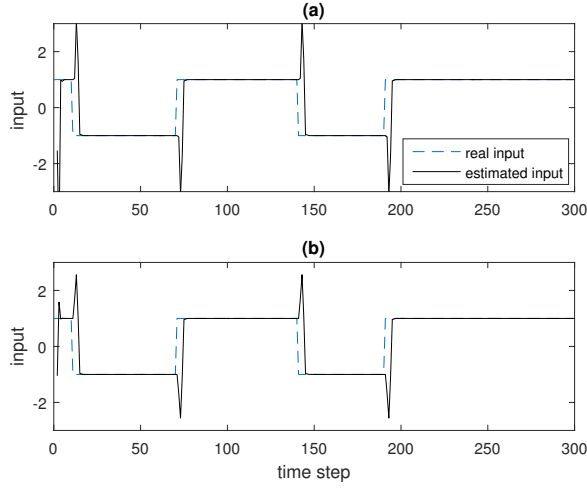


Figure 4.2: Input estimation for the system (4.67) using two different rotation matrices: (a) $\theta = \frac{5\pi}{180}$, and (b) $\theta = \frac{45\pi}{180}$.

system that is governed by,

$$S : \begin{cases} x(k+1) = \begin{pmatrix} 0 & 0 & 0 & 0.10 \\ 1 & 0 & 0 & -0.09 \\ 0 & 1 & 0 & 0.28 \\ 0 & 0 & 1 & 0.07 \end{pmatrix} x(k) + \begin{pmatrix} 1 & -0.80 \\ 0 & -2.05 \\ 0 & 5.13 \\ 0 & 1.78 \end{pmatrix} f(k) \\ y(k) = \begin{pmatrix} -0.46 & -0.35 & -0.1 & 0.14 \\ 0.59 & -0.52 & -0.01 & 0.04 \end{pmatrix} x(k) \end{cases} \quad (4.70)$$

The above system has two transmission zeros at $z_{1,2} = (-1.48, 0.45)$. The system is subjected to *both* a step and a ramp loss of effectiveness (LOE) faults in the channels 1 and 2, respectively. A random rotation matrix ($\mathbf{R} \in \mathbb{R}^{16 \times 16}$)⁵ is generated. The gain matrix $\mathbf{K}_2 \in \mathbb{R}^{16 \times 16}$ is chosen such that 16 poles of the filter (4.52) are placed between -0.1 and 0.1 . The fault estimation results are shown in Figure 4.3, which demonstrates the merits and capabilities of our proposed scheme for fault estimation of non-minimum phase systems. The most important advantage of our proposed solution arises as a result of the fact that it can handle systems with transmission zeros everywhere on the unit circle except at $z = 1$.

⁵ $\mathbf{R} \in \mathbb{R}^{2Ml \times 2Ml}$, $M = n = 4$, and $l = 2$.

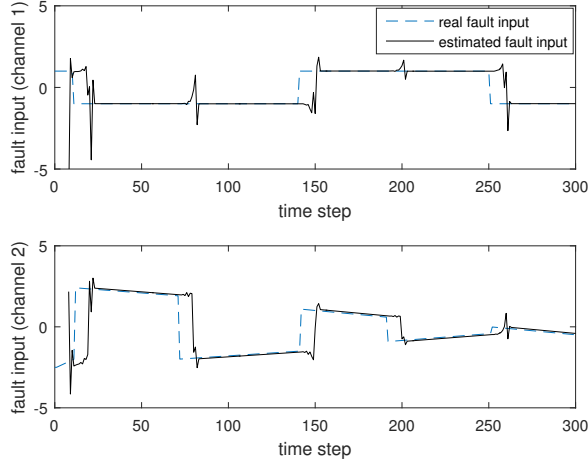


Figure 4.3: The LOE fault input estimation of the MIMO non-minimum phase system (4.70).

In order to demonstrate this point, consider the following *third* case study of the fault-to-output system,

$$\frac{Y(z)}{F(z)} = \frac{(z+1)(z^2+1)}{z^4} \quad (4.71)$$

The simulation results for input estimation of this system are shown in Figure 4.4. The rotation matrix for constructing the filter (4.47) is randomly generated. The gain matrix \mathbf{K}_2 is chosen such that the poles of the filter (4.47) are placed at $z_1, \dots, z_8 = \pm 0.5, \pm 0.3571, \pm 0.2143, \pm 0.0714$. As can be seen from Figure 4.4, our proposed solution can successfully reconstructs the unknown fault even if the system has several transmission zeros on the unit circle.

Finally, for the *fourth* case study and as a comparative study, consider a MIMO system that is taken from the reference [75] with $A \in \mathbb{R}^{4 \times 4}$, $B \in \mathbb{R}^{4 \times 2}$ and $C \in \mathbb{R}^{2 \times 4}$ as follows,

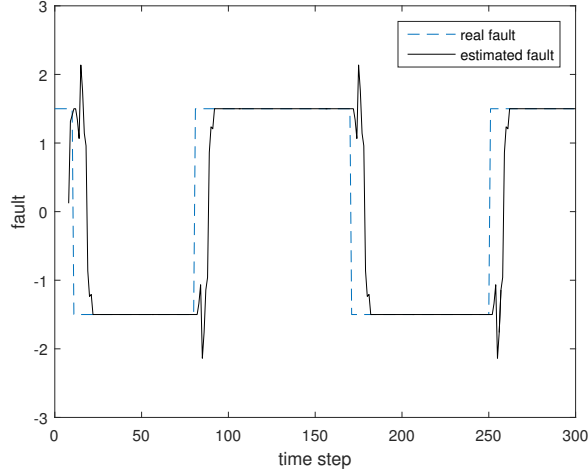


Figure 4.4: The LOE fault estimation for the system (4.71).

$$\left\{ \begin{array}{l} x(k+1) = \begin{bmatrix} 0.6 & -0.3 & 0 & 0 \\ 0.1 & 1 & 0 & 0 \\ -0.4 & -1.5 & 0.4 & -0.3 \\ 0.3 & 1.1 & 0.2 & 0.9 \end{bmatrix} x(k) + \begin{bmatrix} 0 & 0.4 \\ 0 & 0 \\ 0 & -0.1 \\ 0.1 & 0.1 \end{bmatrix} u(k) \\ y(k) = \begin{bmatrix} 1 & 2 & 3 & 4 \\ 2 & 1 & 5 & 6 \end{bmatrix} x(k) \end{array} \right. \quad (4.72)$$

The system (4.72) has two zeros at $z_1 = 0.6072$ and $z_1 = 1.9928$. The authors of [75] proposed a geometric approach and applied it to the system (4.72) to achieve an *almost* perfect estimation of the states and unknown inputs with a delay of 20 time steps ($n_d = 20$). For comparison, our simulation results for the same example is shown in Figure 4.5, which demonstrates that by using our proposed methodology the unknown inputs are almost perfectly reconstructed with only a delay of $n_d = 8$. It should be noted that the approach that is proposed in [75] can handle any type of unknown input, whereas our approach is limited to step and ramp unknown inputs which covers a wide range of faults that occur in physical systems. The main advantage of our proposed methodology over the geometric approach that is

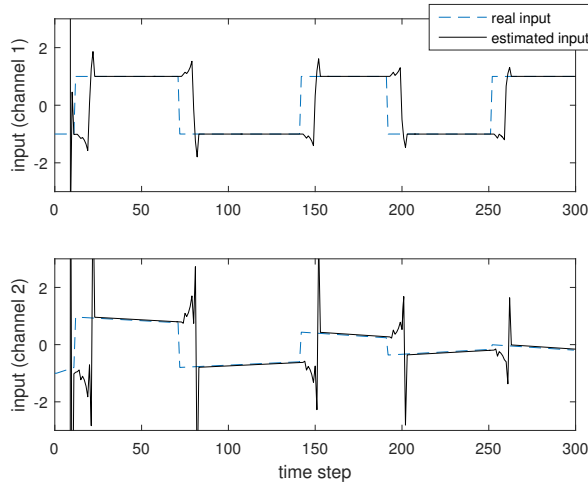


Figure 4.5: Input estimation for system (4.72)

proposed in [75] is the fact that it can handle systems with transmission zeros on the unit circle, whereas the approach in [75] cannot handle this situation.

4.6 Conclusion

We have developed an inversion-based fault estimation scheme for linear discrete-time systems. It was shown that our scheme yields an unbiased estimation of certain types of faults even if the fault-to-output dynamics has transmission zeros outside or on the unit circle (except at $z = 1$). This is achieved by introducing a feedback that not only stabilizes the inverse dynamics (except those having transmission zeros at $z = 1$), but also it provides an unbiased tracking of the unknown input. We have discussed the properties of the proposed inverse filter and conditions that are required for its stabilization design. We have also provided several illustrative simulation case studies that demonstrate the capabilities of our proposed methodologies. Yet, further research are required to generalize our proposed approach to a broader categories of faults.

Chapter 5

Reconstruction of System States and General Unknown Inputs and Faults

In this chapter, we address the problem of unknown state and input reconstruction of both minimum phase (MP) and non-minimum phase (NMP) discrete-time linear systems. An unknown input observer (UIO) is designed that accurately reconstructs the minimum phase states of the system. The reconstructed minimum phase states serve as inputs to an FIR filter for a delayed non-minimum phase state reconstruction. It is shown that a quantified upper bound of the reconstruction error exponentially decreases as the estimation delay is increased. Therefore, an almost perfect reconstruction can be achieved by selecting the delay to be sufficiently large. We extend the proposed approach to the problem of fault estimation. Also, the proposed inversion scheme is applied to the output-tracking control problem. We have also comprehensively addressed and discussed the non-minimum phase dynamics and derived explicit relationships between the system matrices of the above dynamics. Simulation case studies are also presented that demonstrate the merits

and capabilities of our proposed methodology.

The remainder of this chapter is organized as follows. The problem statement and preliminaries are provided in Section 5.1. Section 5.2 is devoted to the problem of developing and designing unknown state and input reconstruction methodologies. The problem of developing inversion-based output tracking strategies is addressed in Section 5.3. The extension to the problem of fault estimation is presented in Section 5.4. Finally, numerical case studies are presented in Section 5.5 to demonstrate and illustrate the capabilities of our proposed methodologies.

5.1 Problem Statement

Consider the following deterministic discrete-time linear time-invariant (LTI) system \mathbf{S} ,

$$\mathbf{S} : \begin{cases} x(k+1) = Ax(k) + Bu(k) \\ y(k) = Cx(k) + Du(k) \end{cases} \quad (5.1)$$

where $x \in \mathbb{R}^n$, $u \in \mathbb{R}^l$ and $y \in \mathbb{R}^l$. The quadruple $\Sigma := (A, B, C, D)$ is assumed to be known *a priori*. The output measurement $y(k)$ is also assumed to be available, however, *both* the system states $x(k)$ and $u(k)$ are assumed to be unmeasurable. In this chapter, we consider the following *two* specific problems.

Problem 1: *The system states and the unknown input reconstruction:* The objective of this problem is to estimate the system state $x(k)$ and the unknown input $u(k)$ from the *only* available system measurement $y(k)$. The main assumption that is imposed to solve this problem is given by Assumption 1 below.

Assumption 1: The system \mathbf{S} is square, has a minimal realization and does not have any zeros on the unit circle.

Other requirements that may be required are provided under each specific statement and result subsequently.

Problem 2: The output tracking: The objective of this problem is to estimate the input signal $u(k)$ such that the output $y(k)$ follows a desired trajectory $y_d(k)$. This problem is in fact another re-statement of the Problem 1 above with the difference that the actual output of the system is now replaced by $y_d(k)$. The main assumption that is also required here is Assumption 1.

We now present the notation that is used throughout the chapter. Given the matrix \mathcal{A} , then \mathcal{A}^\perp , \mathcal{A}^T and $\mathcal{N}(\mathcal{A})$ denote the orthogonal space, the transpose, and the null space of \mathcal{A} , respectively. We use the concept of *pseudo inverse*. If \mathcal{A} is full column rank, then we denote the *pseudo inverse* of \mathcal{A} by \mathcal{A}^\dagger and compute it by $(\mathcal{A}^T \mathcal{A})^{-1} \mathcal{A}^T$. If \mathcal{A} is rank deficient, then we denote its pseudo inverse by \mathcal{A}^+ , where \mathcal{A}^+ is a matrix that satisfies the following four conditions: 1) $\mathcal{A} \mathcal{A}^+ \mathcal{A} = \mathcal{A}$, 2) $\mathcal{A}^+ \mathcal{A} \mathcal{A}^+ = \mathcal{A}^+$, 3) $(\mathcal{A} \mathcal{A}^+)^T = \mathcal{A} \mathcal{A}^+$, and 4) $(\mathcal{A}^+ \mathcal{A})^T = \mathcal{A}^+ \mathcal{A}$. If $U \Sigma V^T$ denotes the SVD decomposition of \mathcal{A} , then \mathcal{A}^+ is given by $V \Sigma^+ U^T$, where Σ^+ is obtained by reciprocating each non-zero diagonal element of Σ . If \mathcal{A} denotes the system matrix, then $\mathcal{A}^{(1)}$ implies transformation of \mathcal{A} under a standard similarity transformation matrix $\mathbf{T}^{(1)}$. If $x(k)$ denotes a vector, then $\hat{x}(k)$ represent an estimate of $x(k)$. Also, $x^{(1)}(k)$ denotes the transformation of $x(k)$ under the similarity matrix $\mathbf{T}^{(1)}$, i.e. $x^{(1)}(k) = \mathbf{T}^{(1)} x(k)$. Finally, $diag(\mathcal{V})$ denotes a diagonal matrix with elements of the vector \mathcal{V} on its diagonal. Consider the *Rosenbrock System Matrix* defined by,

$$M_R(z) = \begin{bmatrix} zI - A & B \\ C & D \end{bmatrix} \quad (5.2)$$

if $rank(M_R(z)) < n + l$, then z is called a *transmission zero* (or simply the zero) of the system \mathbf{S} or the quadruple (A, B, C, D) . The abbreviations MP and NMP stand for minimum phase and non-minimum phase systems, respectively.

5.2 State and Unknown Input Reconstruction

In this section, we consider and develop methodologies for solving the Problem 1. Let us first set up an unknown input observer (UIO) that generates the state $\eta(k)$ as an *estimate* of $\mathbf{M}x(k)$ by using only the system measurements $y(k)$, where $\mathbf{M} \in \mathbb{R}^{q \times n}$ is a full row rank matrix to be specified. If $\text{rank}(\mathbf{M}) = n$, then the system states can be fully reconstructed since $\hat{x}(k) = \mathbf{M}^{-1}\eta(k)$. However, such an \mathbf{M} with rank equal to n does not always exist. In fact, it turns out that the rank of \mathbf{M} is closely related to the transmission zeros of the system \mathbf{S} .

More specifically, we will show that $\text{rank}(\mathbf{M}) = n - \beta$, where α and β are now representing the number of finite MP and NMP transmission zeros of the system \mathbf{S} , respectively. Clearly, $\alpha + \beta$ is not necessarily equal to n . Our strategy is to first construct an \mathbf{M} having the rank $n - \beta$ by using two to be designed matrices \mathbf{M}_0 and $\mathbf{M}_\#$ that are specified subsequently based on the system \mathbf{S} matrices. Given \mathbf{M} , we then introduce a transformation to partition the system states that can be exactly estimated from those where their estimation is obstructed by the NMP transmission zeros of the system. The estimated states will then serve as inputs to a causal scheme that estimates the remaining set of the system states.

5.2.1 Partial Or Full Estimation of the System States

We start by stating our first formal definition.

Definition 5.1. *Assume $\mathbf{M} \in \mathbb{R}^{q \times n}$, where $q \leq n$, is a full row rank matrix. We denote $\eta(k) = \mathbf{M}x(k)$ as a partial or full estimate of the system \mathbf{S} states if $q < n$ or $q = n$, respectively.*

Our goal is to design an unknown input observer (UIO) that estimates $\mathbf{M}x$, where $\mathbf{M} \in \mathbb{R}^{q \times n}$, $q \leq n$, is a full row rank matrix. We consider the governing

dynamics of the unknown input observer (UIO) as follows,

$$\eta(k - n + 1) = \hat{A}\eta(k - n) + F\mathbf{Y}(k - n) \quad (5.3)$$

where,

$$\mathbf{Y}(k - n) = \begin{bmatrix} y(k - n) \\ y(k - n + 1) \\ \vdots \\ y(k) \end{bmatrix} \quad (5.4)$$

with the matrices \hat{A} and F to be specified subsequently. Our objective is to now select the matrices \mathbf{M} , \hat{A} and F such that $\eta(k) - \mathbf{M}x(k) \rightarrow 0$ as $k \rightarrow \infty$. The output measurement equation of the system \mathbf{S} can be alternatively expressed as,

$$\mathbf{Y}(k - n) = \mathbf{C}_n x(k - n) + \mathbf{D}_n \mathbf{U}(k - n) \quad (5.5)$$

where,

$$\mathbf{C}_n = \begin{pmatrix} C \\ CA \\ \vdots \\ CA^{n-1} \end{pmatrix}; \mathbf{D}_n = \begin{pmatrix} D & 0 & \dots & 0 \\ CB & D & \dots & 0 \\ \vdots & \vdots & \vdots & \vdots \\ CA^{n-1}B & CA^{n-2}B & \dots & D \end{pmatrix} \quad (5.6)$$

and $\mathbf{U}(k - n)$ is constructed similar to $\mathbf{Y}(k - n)$ from the input sequence. The state equation of the system \mathbf{S} can be expressed as,

$$x(k - n + 1) = Ax(k - n) + B\mathbf{I}_n \mathbf{U}(k - n) \quad (5.7)$$

where $\mathbf{I}_n = \begin{bmatrix} \mathbf{I}_{m \times m} & \mathbf{0}_{m \times (n-m)} \end{bmatrix}$. Using the equations (5.3), (5.5) and (5.7), the unknown input observer error dynamics is now governed by,

$$\begin{aligned} (\eta - \mathbf{M}x)(k - n + 1) &= \hat{A}(\eta(k - n) - \mathbf{M}x(k - n)) \\ &+ (\hat{A}\mathbf{M} - \mathbf{M}A + F\mathbf{C}_n)\mathbf{Y}(k - n) \\ &+ (F\mathbf{D}_n - \mathbf{M}B\mathbf{I}_n)\mathbf{U}(k - n) \end{aligned} \quad (5.8)$$

It now follows that $\mathbf{M}x$ is accurately estimated if and only if (i) \hat{A} is selected to be a Hurwitz matrix, (ii) $0 = \hat{A}\mathbf{M} - \mathbf{M}A + F\mathbf{C}_n$, and (iii) $0 = F\mathbf{D}_n - \mathbf{M}\mathbf{B}\mathbf{I}_n$. The conditions (i)-(iii) above are the well-known unknown input observer equations that are solvable under certain conditions. We will show that these conditions have a solution if and only if the system \mathbf{S} is MP. However, this will be obtained under the restrictive requirement that \mathbf{M} should be full rank square matrix. We will show subsequently that a solution for NMP systems exists if a lower rank matrix \mathbf{M} is considered.

From the condition (iii) it follows that,

$$F = \mathbf{M}\mathbf{B}\mathbf{I}_n\mathbf{D}_n^+ + \mathbf{K}_n(\mathbf{I} - \mathbf{D}_n\mathbf{D}_n^+) \quad (5.9)$$

where $\mathbf{K}_n \in \mathbb{R}^{nl \times nm}$ is an arbitrary matrix. Let us first denote by \hat{A}_0 and \mathbf{M}_0 as solution to \hat{A} and \mathbf{M} that satisfy the conditions (i)-(iii) corresponding to $\mathbf{K}_n \equiv 0$. Subsequently, we shall return to the general case where \mathbf{K}_n and $(\mathbf{I} - \mathbf{D}_n\mathbf{D}_n^+)$ are nonzero to obtain another solution to \mathbf{M} that we will denote by $\mathbf{M}_\#$. For now for \mathbf{M}_0 , we have,

$$F_0 = \mathbf{M}_0\mathbf{B}\mathbf{I}_n\mathbf{D}_n^+ \quad (5.10)$$

If we substitute F_0 from equation (5.10) into the condition (ii), we obtain,

$$\hat{A}_0\mathbf{M}_0 = \mathbf{M}_0(A - \mathbf{B}\mathbf{I}_n\mathbf{D}_n^+\mathbf{C}_n) \quad (5.11)$$

Equation (5.11) - which is in fact the Sylvester equation - has $\mathbf{M}_0 = 0$ as its trivial solution. The non-trivial solution to (5.11) is obtained if \mathbf{M}_0 is considered as the transpose of the left eigenvectors of $\Gamma = (A - \mathbf{B}\mathbf{I}_n\mathbf{D}_n^+\mathbf{C}_n)$ and \hat{A}_0 as a diagonal matrix of Γ eigenvalues. It now follows that the full estimation of the system states by the UIO observer (5.3) is obstructed by the NMP transmission zeros of the system due to the fact that the eigenvalues of $(A - \mathbf{B}\mathbf{I}_n\mathbf{D}_n^+\mathbf{C}_n)$ contain NMP zeros of the square system \mathbf{S} as formally stated in the Theorem 4.2.

Remark 5.1. *It should be noted that Theorem 4.2 does not hold for non-square systems. The eigenvalues of Γ may or may not coincide with the transmission zeros of \mathbf{S} . Each case needs to be then separately investigated, however, once the eigenvalues of Γ are determined, the remaining procedure for obtaining a solution to the conditions (i)-(iii) is similar to that of a square system.*

If the system \mathbf{S} has at least one MP transmission zero, or it has less than n NMP zeros (therefore, the set \mathcal{Z} in Theorem 4.2 is not empty), then at least one eigenvalue of Γ is less than 1, which is denoted by a . Let us now set $\hat{A}_0 = a$. If \mathbf{M}_0^T is chosen to be the left eigenvector associated with the eigenvalue a , then equation (5.11), and consequently conditions (i)-(iii) are satisfied even if the system \mathbf{S} has nonzero NMP transmission zeros. In general, we can state the following result.

Lemma 5.1. *Let Assumption 1 hold, and $\mathcal{V} = \{v_i | i = 1, \dots, p\}$ denote the set of the system \mathbf{S} invariant zeros, $\mathcal{Z} = \{0, \dots, 0\}$ that contains $n - p$ zeros, and Θ_α the set of MP transmission zeros of \mathbf{S} . If $\{\Theta_\alpha \cup \mathcal{Z}\} \neq \emptyset$, then $F_0 = \mathbf{M}_0 \mathbf{B} \mathbf{I}_n \mathbf{D}_n^+$, $\hat{A}_0 = \text{diag}(\Theta_\alpha \cup \mathcal{Z})$ and \mathbf{M}_0^T that has left eigenvectors of Γ associated with $\text{diag}(\Theta_\alpha \cup \mathcal{Z})$ are solutions to the conditions (i)-(iii).*

Proof. Follows by direct substitution of the solution above into the conditions (i)-(iii) that verifies the result. □

Remark 5.2. *One may suggest to use the Jordan canonical form of Γ to obtain a solution to the conditions (i)-(iii), especially when the system \mathbf{S} has repeated MP transmission zeros. This may yield an \mathbf{M} having higher rank condition as compared to the solution provided by Lemma 5.1 under certain limited cases. However, in general this will not lead to a robust numerical procedure and in most cases the algorithm could fail numerically due to ill-conditioning.*

Lemma 5.1 implies that a solution for NMP systems exists unless the system \mathbf{S} has exactly n NMP transmission zeros (this is highly unusual in real applications).

Our proposed methodology for state estimation problem that will be subsequently discussed requires that $\text{rank}(\mathbf{M}) = n - \beta$. However, rank of \mathbf{M}_0 that is obtained from Lemma 5.1 is not necessarily equal to $n - \beta$, since Γ may have multiple eigenvectors due to repeated eigenvalues and the *generalized eigenvectors* are not a solution to the equation (5.11).

Specifically, the set \mathcal{Z} (as defined in Theorem 4.2) may have α_z elements sharing the same eigenvectors. We now consider the term $\mathbf{K}_n(\mathbf{I} - \mathbf{D}_n\mathbf{D}_n^+)\mathbf{C}_n$ in order to obtain linearly independent vectors associated with the elements of \mathcal{Z} . If the set \mathcal{Z} is not empty, then it implies that \mathbf{D}_n is rank deficient, and therefore $(\mathbf{I} - \mathbf{D}_n\mathbf{D}_n^+)$ is a nonzero matrix.

Let us now construct $\mathbf{M}_\#$ and $\hat{A}_\#$ such that they satisfy the following Sylvester equation,

$$\hat{A}_\#\mathbf{M}_\# = \mathbf{M}_\#(A - B\mathbf{I}_n\mathbf{D}_n^+\mathbf{C}_n) + \mathbf{K}_n(\mathbf{I} - \mathbf{D}_n\mathbf{D}_n^+)\mathbf{C}_n \quad (5.12)$$

Since $(\mathbf{I} - \mathbf{D}_n\mathbf{D}_n^+)\mathbf{C}_n$ is not identically zero, a non-trivial solution exists and $\hat{A}_\#$, $\mathbf{M}_\#$ and \mathbf{K}_n can be selected such that the condition (i) is satisfied. Therefore, we have the following theorem.

Theorem 5.1. *Let Assumption 1 hold and all the MP transmission zeros of \mathbf{S} have an algebraic multiplicity of 1. Then, the complete solution to the conditions (i)-(iii) is given by,*

$$\hat{A} = \begin{bmatrix} \hat{A}_0 & 0 \\ 0 & \hat{A}_\# \end{bmatrix}; \mathbf{M} = \begin{bmatrix} \mathbf{M}_0 \\ \mathbf{M}_\# \end{bmatrix} \quad (5.13)$$

where $\text{rank}(\mathbf{M}) = n - \beta$.

Proof. Since the system \mathbf{S} has α_1 transmission zeros having an algebraic multiplicity of 1, therefore Γ has α_1 linearly independent eigenvectors. Therefore, \mathbf{M}_0 has at least α_1 linearly independent rows. On the other hand, the set \mathcal{Z} (as defined in Theorem 4.2) has α_z zeros, where $\alpha_z = n - \beta - \alpha_1$. Therefore, $\mathbf{I} - \mathbf{D}_n\mathbf{D}_n^+$ has α_z independent

rows. This implies that $\mathbf{M}_\#$ has α_z linearly independent rows. Therefore, \mathbf{M} has $\alpha_z + \alpha_1 = n - \beta$ linearly independent rows.

□

Note that if the system \mathbf{S} has MP transmission zeros with an algebraic multiplicity that is higher than 1, then the rank of $\mathbf{M}_\#$ is reduced proportionally by the multiplicity of the MP transmission zeros. This is due to the fact that $(\mathbf{I} - \mathbf{D}_n \mathbf{D}_n^+)$ loses its rank. On the other hand, \mathbf{M}_0 also loses its rank by such MP transmission zeros. Therefore, our method fails, since the rank of \mathbf{M} will be less than $n - \beta$.

The solution given in equation (5.12) is closely related to equation (5.5). The matrix $\mathbf{I} - \mathbf{D}_n \mathbf{D}_n^+$ gives the null space of \mathbf{D}_n . Multiplication of both sides of equation (5.5) by this matrix yields,

$$(\mathbf{I} - \mathbf{D}_n \mathbf{D}_n^+) \mathbf{Y}(k - n) = (\mathbf{I} - \mathbf{D}_n \mathbf{D}_n^+) \mathbf{C}_n x(k - n) \quad (5.14)$$

Let us now define $\mathbf{P} = (\mathbf{I} - \mathbf{D}_n \mathbf{D}_n^+) \mathbf{C}_n$. It follows that the rank of \mathbf{P} depends on the rank of $\mathcal{N}(\mathbf{D}_n)$. If the system \mathbf{S} has exactly $p = n$ transmission zeros, then $\mathcal{N}(\mathbf{D}_n) = 0$, and consequently $\mathbf{P} \equiv 0$. On the other hand, \mathbf{M}_0 will be full row rank and will have $n - \beta$ linearly independent rows if the MP transmission zeros are simple. As p is reduced, then the rank of \mathbf{P} increases and the rank of \mathbf{M}_0 decreases. This relationship reveals several important characteristics of $\mathcal{N}(\mathbf{D}_n)$. A more detailed discussion of these properties is beyond the scope of this chapter.

5.2.2 Partitioning of the States

If the system \mathbf{S} has any NMP transmission zeros, then $\text{rank}(\mathbf{M}) = q < n$, and therefore the states cannot be fully estimated. Let us now perform an LQ decomposition of the matrix \mathbf{M} to decouple or partition the estimation of the q states from the estimation of the other $n - q$ states. Namely, let us set $\mathbf{M} = LQ$.

The unknown input observer (UIO) is described by equation (5.3), where \hat{A} and F are selected according to Theorem 5.1 and equation (5.9), and where $\eta(k-n) = \mathbf{M}\hat{x}(k-n)$. Equivalently, we have $\eta(k-n) = LQ\hat{x}(k-n)$. Let us now set the similarity transformation matrix $\mathbf{T}^{(1)} = Q$. Therefore, $\eta(k-n) = \begin{bmatrix} \mathbf{M}_q^{(1)} & 0 \end{bmatrix} \hat{x}^{(1)}(k-n)^1$, where $\begin{bmatrix} \mathbf{M}_q^{(1)} & 0 \end{bmatrix} = L$. The matrix $\mathbf{M}_q^{(1)} \in \mathbb{R}^{q \times q}$ is a non-singular matrix, hence the first q states can be independently reconstructed from $\eta(k-n)$ as follows,

$$\hat{x}^{(1)}(1:q)(k-n) = \mathbf{M}_q^{(1)-1} \eta(k-n) \quad (5.15)$$

where $x(1:q)$ denotes the first q elements of the vector x .

Definition 5.2. *The MP and NMP states correspond to the first q and the last $n-q$ states of the system $S^{(1)}$ and are denoted by $x_1^{(1)}(k)$ and $x_2^{(1)}(k)$, respectively. In other words, $x^{(1)}(k) = \begin{bmatrix} (x_1^{(1)}(k))^T & (x_2^{(1)}(k))^T \end{bmatrix}^T$, where*

$$\mathbf{S}^{(1)} : \begin{cases} x^{(1)}(k+1) = A^{(1)}x^{(1)}(k) + B^{(1)}u(k) \\ y(k) = C^{(1)}x^{(1)}(k) + Du(k) \end{cases} \quad (5.16)$$

Considering the Definition 5.2 and equation (5.15), we have,

$$\hat{x}_1^{(1)}(k-n) = \mathbf{M}_q^{(1)-1} \eta(k-n) \quad (5.17)$$

or in the state space representation,

$$\begin{cases} \eta(k-n+1) = \hat{A}\eta(k-n) + F\mathbf{Y}(k-n) \\ \hat{x}_1^{(1)}(k-n) = \mathbf{M}_q^{(1)-1} \eta(k-n) \end{cases} \quad (5.18)$$

Equation (5.18) shows that the MP states can be independently and accurately estimated from the system measurements. In other words, $\hat{x}_1^{(1)}(k-n) \rightarrow x_1^{(1)}(k-n)$ as $k \rightarrow \infty$. This is due to the fact that according to the error dynamics (5.8) and conditions (i)-(iii), $\eta(k-n) - \mathbf{M}x(k-n) \rightarrow 0$ as $k \rightarrow \infty$. Therefore, $L\hat{x}^{(1)}(k-n) - Lx^{(1)}(k-n) \rightarrow 0$ as $k \rightarrow \infty$, which yields the desired result. An important property of the MP states is now given by the following theorem.

¹Recall the notation that was defined in Section 5.1, namely, $x^{(1)}(k) = \mathbf{T}^{(1)}x(k)$, $x_1^{(1)}(k) = \mathbf{T}^{(1)}x^{(1)}(k)$, $A^{(1)} = \mathbf{T}^{(1)}A(\mathbf{T}^{(1)})^{-1}$, $B^{(1)} = \mathbf{T}^{(1)}B$, and $C^{(1)} = C(\mathbf{T}^{(1)})^{-1}$.

Theorem 5.2. *Let Assumption 1 hold. Then $x_1^{(1)}(k) \rightarrow 0$ as $k \rightarrow \infty$ if and only if $y(k) = 0$ for $k = k_0, k_0 + 1, \dots, \infty$, $k_0 > 0$.*

Proof. It is known from the state equation of the system (5.18) that $\eta(k) = 0$ if and only if $y(k) = 0$ ($\Rightarrow \mathbf{Y}(k) = 0$) for $k = k_0, k_0 + 1, \dots, \infty$, $k_0 > 0$. On the other hand, $\eta(k) = \mathbf{M}_q^{(1)} \hat{x}_1^{(1)}(k)$. Since $\mathbf{M}_q^{(1)}$ is a nonsingular matrix, it follows that $\hat{x}_1^{(1)}(k) \equiv 0$ if and only if $\eta(k) \equiv 0$. Moreover, $x_1^{(1)}(k) \rightarrow \hat{x}_1^{(1)}(k)$ as $k \rightarrow \infty$. Therefore, $x_1^{(1)}(k) \rightarrow 0$ as $k \rightarrow \infty$, if and only if $y(k) = 0$ for $k = k_0, k_0 + 1, \dots, \infty$, $k_0 > 0$. □

The above decoupling or partitioning is quite helpful in several ways. The most important one is that it renders an elegant expression for the NMP states reconstruction estimation error as discussed in the next section. Furthermore, in certain applications such as in fault detection and isolation problems, the considered faults may only affect the MP states of the system. Therefore, it will not be necessary to estimate the NMP system states that can be computationally costly as well as an error prone process.

5.2.3 Dynamics of the MP and NMP States

The unknown input estimation problem requires a successful reconstruction of both the MP and the NMP states. Towards this end, we partition the state space model of the system \mathbf{S} or $\mathbf{S}^{(1)}$ as follows $(x_1^{(1)}(k) \in \mathbb{R}^q$ and $x_2^{(1)}(k) \in \mathbb{R}^{n-q})$,

$$\mathbf{S}^{(1)} : \begin{cases} x_1^{(1)}(k-n+1) = A_{11}^{(1)} x_1^{(1)}(k-1) + A_{12}^{(1)} x_2^{(1)}(k-n) + B_1^{(1)} u(k-n) \\ x_2^{(1)}(k-n+1) = A_{21}^{(1)} x_1^{(1)}(k-n) + A_{22}^{(1)} x_2^{(1)}(k-n) + B_2^{(1)} u(k-n) \\ y(k-n) = C_1^{(1)} x_1^{(1)}(k-n) + \begin{bmatrix} C_2^{(1)} & D \end{bmatrix} \begin{bmatrix} x_2^{(1)}(k-n) \\ u(k-n) \end{bmatrix} \end{cases} \quad (5.19)$$

where,

$$A^{(1)} = \begin{bmatrix} A_{11}^{(1)} & A_{12}^{(1)} \\ A_{21}^{(1)} & A_{22}^{(1)} \end{bmatrix}; B^{(1)} = \begin{bmatrix} B_1^{(1)} \\ B_2^{(1)} \end{bmatrix}; C^{(1)} = \begin{bmatrix} C_1^{(1)} & C_2^{(1)} \end{bmatrix}. \quad (5.20)$$

It is now straightforward to conclude from Theorem 5.2 that the following lemmas imply that the NMP states cannot be algebraically estimated from the MP states and the system measurement outputs. Specifically, we have:

Lemma 5.2. *Let Assumption 1 hold and $0 < q < n$. Then the columns of $\begin{bmatrix} C_2^{(1)} & D \\ A_{12}^{(1)} & B_1^{(1)} \end{bmatrix}$ are linearly dependent.*

Proof. Since the system \mathbf{S} has at least one NMP zero ($q < n$), then by the definition of transmission zeros, there exists a nonzero $u(k)$ that yields a zero output ($y(k) = 0$ for all k). On the other hand, according to Theorem 5.2, $x_1^{(1)}(k)$ approaches to zero when $y(k) = 0$ for $k = k_0, k_0+1, \dots$. Therefore, from the first and the third equations of (5.19), we have for $k \rightarrow \infty$,

$$\begin{bmatrix} 0 \\ 0 \end{bmatrix} = \begin{bmatrix} C_2^{(1)} & D \\ A_{12}^{(1)} & B_1^{(1)} \end{bmatrix} \begin{bmatrix} x_2^{(1)}(k-n) \\ u(k-n) \end{bmatrix}. \quad (5.21)$$

Since $\begin{bmatrix} x_2^{(1)}(k-n) \\ u(k-n) \end{bmatrix}$ is nonzero, it implies that the columns of $\begin{bmatrix} C_2^{(1)} & D \\ A_{12}^{(1)} & B_1^{(1)} \end{bmatrix}$ are linearly dependent. \square

Lemma 5.3. *Let Assumption 1 hold and $0 < q < n$. Then the transmission zeros of $\begin{bmatrix} A_{22}^{(1)} & B_2^{(1)} \\ A_{12}^{(1)} & B_1^{(1)} \end{bmatrix}$ are a subset of the system \mathbf{S} transmission zeros.*

Proof. First note that $A_{11}^{(1)}$ in equation (5.19) is a Hurwitz matrix, otherwise $x_1^{(1)}(k) \rightarrow \infty$ as $k \rightarrow \infty$. Next, consider the following system,

$$S^{(z_1)} : \begin{cases} x_2^{(1)}(k-n+1) = A_{22}^{(1)}x_2^{(1)}(k-n) + B_2^{(1)}u(k-n) \\ \xi(k-n) = A_{12}^{(1)}x_2^{(1)}(k-n) + B_1^{(1)}u(k-n) \end{cases} \quad (5.22)$$

If there exists a nonzero $u(k)$ that yields $\xi(k) = 0$, then this implies that from the first equation of (5.19) we have, $x_1^{(1)}(k) \rightarrow 0$ as $k \rightarrow \infty$. Therefore, $y(k) \rightarrow 0$ as $k \rightarrow \infty$ according to Theorem 5.2. Therefore, the transmission zeros of $S^{(z1)}$ are also the transmission zeros of $S^{(1)}$. \square

Lemma 5.4. *Let Assumption 1 hold and $0 < q < n$. Then the transmission zeros*

of $\begin{bmatrix} A_{22}^{(1)} & B_2^{(1)} \\ C_2^{(1)} & D \end{bmatrix}$ are a subset of the system \mathbf{S} transmission zeros.

Proof. Consider the following system,

$$S^{(z2)} : \begin{cases} x_2^{(1)}(k-n+1) = A_{22}^{(1)}x_2^{(1)}(k-n) + B_2^{(1)}u(k-n) \\ \xi(k-n) = \begin{bmatrix} C_2^{(1)} & D \end{bmatrix} \begin{bmatrix} x_2^{(1)}(k-n) \\ u(k-n) \end{bmatrix} \end{cases} \quad (5.23)$$

If there exists a nonzero $u(k)$ that yields $\xi(k) = 0$, then since $\begin{bmatrix} \mathbf{I} & C_1 \end{bmatrix}$ is full row rank, it implies from the third equation of (5.19) that $x_1^{(1)}(k) = 0$, and $y(k) = 0$. Therefore, the transmission zeros of $S^{(z2)}$ are also the transmission zeros of $S^{(1)}$. \square

Let us now assume that $B_1^{(1)}$ is full column rank. Then, the unknown input $u(k)$ in terms of the system states is obtained by the first expression of equation (5.19), according to

$$u(k-n) = B_1^{(1)\dagger} \left(x_1^{(1)}(k-n+1) - A_{11}^{(1)}x_1^{(1)}(k-n) - A_{12}^{(1)}x_2^{(1)}(k-n) \right) \quad (5.24)$$

By substituting the above equation into the second and third equations of (5.19) yields,

$$\begin{cases} x_2^{(1)}(k-n+1) = A_z x_2^{(1)}(k-n) + B_z X_1^{(1)}(k-n) \\ y(k-n) = C_{z2} x_2^{(1)}(k-n) + C_{z1} X_1^{(1)}(k-n) \end{cases} \quad (5.25)$$

where,

$$A_z = A_{22}^{(1)} - B_2^{(1)} B_1^{(1)\dagger} A_{12}^{(1)} \quad (5.26)$$

$$B_z = \begin{bmatrix} B_2^{(1)} B_1^{(1)\dagger} & A_{21}^{(1)} - B_2^{(1)} B_1^{(1)\dagger} A_{11}^{(1)} \end{bmatrix} \quad (5.27)$$

$$X_1^{(1)}(k-n) = \begin{bmatrix} x_1^{(1)}(k-n+1) \\ x_1^{(1)}(k-n) \end{bmatrix} \quad (5.28)$$

and where $C_{z2} = C_2^{(1)} - DB_1^{(1)\dagger} A_{12}^{(1)}$ and $C_{z1} = \begin{bmatrix} DB_1^{(1)\dagger} & C_1^{(1)} - DB_1^{(1)\dagger} A_{11}^{(1)} \end{bmatrix}$. The quadruple $\Sigma_z := (A_z, B_z, C_{z1}, C_{z2})$ have interesting properties that are related to the transmission zeros of the system \mathbf{S} . We are now in a position to state our next result.

Theorem 5.3. *Let Assumption 1 hold, $0 < q < n$ and $B_1^{(1)}$ be a full column rank matrix. Then, the eigenvalues of A_z are the NMP zeros of the system \mathbf{S} . Moreover, $C_{z2} = 0$.*

Proof. Note that $C_{z2} = 0$ is an immediate result of the Schur identity and Lemma 5.2. The eigenvalues of A_z are a subset of the transmission zeros of $\begin{bmatrix} A_{22}^{(1)} & B_2^{(1)} \\ A_{12}^{(1)} & B_1^{(1)} \end{bmatrix}$, which are a subset of the system \mathbf{S} zeros according to Lemma 5.3. According to Theorem 5.2 and Theorem 5.3 ($C_{z2} = 0$), the output of the system (5.25) goes to zero as $k \rightarrow \infty$ if and only if $x_1^{(1)}(k)$, and consequently, $X_1^{(1)}(k)$ goes to zero as $k \rightarrow \infty$. The first equation of (5.25) implies that if A_z is a Hurwitz matrix, then $x_2^{(1)}(k)$ must approach to zero when $X_1^{(1)}(k)$ is zero. However, we know that there exists nonzero $x_2^{(1)}(k)$ and $u(k)$ that yield a zero $y(k)$ for all k . Therefore, since the response of an unforced linear system can approach to zero or infinity (recall we excluded systems with transmission zeros on the unit circle in Assumption 1), therefore $x_2^{(1)}(k)$ must approach to infinity. This implies that the eigenvalues of A_z are the NMP zeros of \mathbf{S} . \square

Remark 5.3. *According to Theorem 5.3 and the definition of C_{z2} , if D happens to be zero, then, $C_2^{(1)}$ must be zero which implies $y(k) = C_1^{(1)} x_1^{(1)}(k)$. This fact seems to be useful for design of a robust fault detection and isolation scheme, that is left as a topic of our future research.*

If on the other hand $B_1^{(1)}$ is *not* a full column rank matrix, then let us assume that D is full column rank. In this case, the unknown input in terms of the system states is given by the following expression,

$$u(k - n) = D^\dagger \left(y(k - n) - C_1^{(1)} x_1^{(1)}(k - n) - C_2^{(1)} x_2^{(1)}(k - n) \right) \quad (5.29)$$

By substituting equation (5.29) into the second equation of (5.19), it yields,

$$x_2^{(1)}(k - n + 1) = A_{zd} x_2^{(1)}(k - n) + B_{zd} X_{1d}^{(1)}(k - n) \quad (5.30)$$

where,

$$A_{zd} = A_{22}^{(1)} - B_2^{(1)} D^\dagger C_2^{(1)} \quad (5.31)$$

$$B_{zd} = \begin{bmatrix} A_{21}^{(1)} - B_2^{(1)} D^\dagger C_1^{(1)} & B_2^{(1)} D^\dagger \end{bmatrix} \quad (5.32)$$

$$X_{1d}^{(1)}(k - n) = \begin{bmatrix} x_1^{(1)}(k - n) \\ y(k - n) \end{bmatrix} \quad (5.33)$$

We can now state the next result of this chapter.

Theorem 5.4. *Let Assumption 1 hold, $0 < q < n$, and D be a full column rank matrix. Then, the eigenvalues of A_{zd} are the NMP zeros of the system \mathbf{S} .*

Proof. The eigenvalues of A_{zd} are a subset of the transmission zeros of $\begin{bmatrix} A_{22}^{(1)} & B_2^{(1)} \\ C_2^{(1)} & D \end{bmatrix}$, that are a subset of the system \mathbf{S} zeros according to Lemma 5.4. According to Theorem 5.2, $y(k) \rightarrow 0$ as $k \rightarrow \infty$ if and only if $x_1^{(1)}(k) \rightarrow 0$ as $k \rightarrow \infty$. The equation (5.30) implies that if A_{zd} is a Hurwitz matrix, then $x_2^{(1)}(k) \rightarrow 0$ when $X_{1d}^{(1)}(k)$ is zero. However, we know that there exists nonzero $x_2^{(1)}(k)$ and $u(k)$ that yield a zero $y(k)$ for all k . Therefore, since the response of an unforced linear system can approach to zero or infinity (recall we excluded systems with transmission zeros on the unit circle in Assumption 1), therefore $x_2^{(1)}(k)$ must approach to infinity. This implies that the eigenvalues of A_{zd} are the NMP zeros of \mathbf{S} . \square

It should be noted that if both $B_1^{(1)}$ and D are column rank deficient matrices, then the NMP states and the unknown input can no longer be estimated. This is a slightly stronger assumption than the *input observability* that requires the matrix $\begin{bmatrix} B^{(1)} \\ D \end{bmatrix}$ to be full column rank. In our proposed approach, the matrix $\begin{bmatrix} B_1^{(1)} \\ D \end{bmatrix}$ should now be full column rank.

5.2.4 Estimation of the NMP States

The state equation (5.25) (or similarly the equation (5.30) depending on the rank condition of $B_1^{(1)}$ or D) describes the dynamics of the NMP states. The eigenvalues of A_z (or A_{zd}) coincide with the NMP transmission zeros of the system \mathbf{S} . Therefore, the dynamics of equation (5.25) or equation (5.30) is unstable. This unstable dynamics should be treated in a manner that provides a stable estimation of the NMP states. Towards this end, let us now consider the following *non-casual* structure that is obtained by re-arranging the state representation (5.25) or (5.30) as follows

$$x_2^{(1)}(k-n) = \tilde{A}_z x_2^{(1)}(k-n+1) - \tilde{B}_z \Theta_1^{(1)}(k-n) \quad (5.34)$$

where,

$$\tilde{A}_z = (A_z)^{-1} \text{ (for (5.25)) or } (A_{zd})^{-1} \text{ (for (5.30))} \quad (5.35)$$

$$\tilde{B}_z = (A_z)^{-1} B_z \text{ (for (5.25)) or } (A_{zd})^{-1} B_{zd} \text{ (for (5.30))} \quad (5.36)$$

$$\Theta_1^{(1)}(k-n) = X_1^{(1)}(k-n) \text{ (for (5.25)) or } X_{1d}^{(1)}(k-n) \text{ (for (5.30))} \quad (5.37)$$

Iterating equation (5.34) for n_d time steps yields,

$$x_2^{(1)}(k-n-n_d) = \tilde{A}_z^{n_d} x_2^{(1)}(k-n) - \sum_{i=0}^{n_d-1} (\tilde{A}_z)^i \tilde{B}_z \Theta_1^{(1)}(k-n-i-1) \quad (5.38)$$

where $\tilde{A}_z^{n_d}$ denotes \tilde{A}_z raised to the power of n_d . The inverse of A_z (or A_{zd}) exists since A_z (or A_{zd}) does not have a zero eigenvalue. Also, \tilde{A}_z is Hurwitz due to the fact

that the eigenvalues of the inverse matrix is the inverse of the matrix eigenvalues. Equation (5.38) provides the key to estimation of the NMP states.

Let us now construct the following FIR filter,

$$\hat{x}_2^{(1)}(k - n - n_d) = \tilde{A}_z^{n_d} \bar{x}_{20}^{(1)}(k - n) - \sum_{i=0}^{n_d-1} (\tilde{A}_z)^i \tilde{B}_z \hat{\Theta}_1^{(1)}(k - n - i - 1) \quad (5.39)$$

where $\bar{x}_{20}^{(1)}(k - n)$ denotes the random initial condition of the FIR filter at each time step $k - n$ and $\hat{\Theta}_1^{(1)}(k - n) = \hat{X}_1^{(1)}(k - n)$ or $\hat{\Theta}_1^{(1)}(k - n) = \hat{X}_{1d}^{(1)}(k - n)$, depending on whether $B^{(1)}$ or D is full column rank, respectively. Moreover, $\hat{X}_1^{(1)}(k - n) = \begin{bmatrix} \hat{x}_1^{(1)}(k - n + 1) \\ \hat{x}_1^{(1)}(k - n) \end{bmatrix}$ and $\hat{X}_{1d}^{(1)}(k - n) = \begin{bmatrix} \hat{x}_1^{(1)}(k - n) \\ y(k - n) \end{bmatrix}$. The estimate of the MP states ($\hat{x}_1^{(1)}(k)$) as previously discussed is given by (5.18). The random initial condition $\bar{x}_{20}^{(1)}(k - n)$ at each time step introduces errors in the estimation process, but for sufficiently large n_d , the effects of the initial conditions will vanish and $\hat{x}_2^{(1)}(k - n - n_d) - x_2^{(1)}(k - n - n_d) \rightarrow 0$ as $k \rightarrow \infty$ (note that $\tilde{A}_z^{n_d} \rightarrow 0$ for $n_d \gg 1$), as shown subsequently. Practically, n_d must be as small as possible, however an accurate estimation requires a large n_d . Hence, selection of n_d requires a trade-off analysis by quantification of the estimation error versus n_d at each time step. Below, we provide an explicit expression for the reconstruction or estimation error as a function of the delay n_d and the initial condition.

Definition 5.3. *The NMP state estimation error is defined according to $e_{x_2}(k) = x_2^{(1)}(k) - \hat{x}_2^{(1)}(k)$.*

Theorem 5.5. *Let Assumption 1 hold, $0 < q < n$, and $\begin{bmatrix} B_1^{(1)} \\ D \end{bmatrix}$ be a full column rank matrix. Then the NMP state estimation error at the time step $k - n - n_d$ is given by $\tilde{A}_z^{n_d}(x_2^{(1)}(k - n) - \bar{x}_{20}^{(1)}(k - n))$.*

Proof. Note that we have,

$$\begin{aligned}
e_{x_2}(k - n - n_d) &= x_2^{(1)}(k - n - n_d) - \hat{x}_2^{(1)}(k - n - n_d) \\
&= \tilde{A}_z^{n_d}(x_2^{(1)}(k - n) - \bar{x}_{20}^{(1)}(k - n)) \\
&\quad - \sum_{i=0}^{n_d-1} (\tilde{A}_z)^i \tilde{B}_z(\Theta_1^{(1)}(k - n - i - 1)) \\
&\quad - \hat{\Theta}_1^{(1)}(k - n - i - 1)
\end{aligned}$$

Since $x_1^{(1)}(k) - \hat{x}_1^{(1)}(k) \rightarrow 0$ as $k \rightarrow \infty$, then $\Theta_1^{(1)}(k) - \hat{\Theta}_1^{(1)}(k) \rightarrow 0$ as $k \rightarrow \infty$.

Therefore, the NMP state estimation error is now given by $e_{x_2}(k - n - n_d) = \tilde{A}_z^{n_d}(x_2^{(1)}(k - n) - \bar{x}_{20}^{(1)}(k - n))$ as $k \rightarrow \infty$. \square

Theorem 5.5 highlights a number of important trade-off analysis considerations regarding the nature of the NMP state estimation error and the selection of the delay n_d . Specifically, the following observations can be made:

- The farther the NMP transmission zeros are from the unit circle, one can ensure a smaller NMP state estimation error given that the term $\tilde{A}_z^{n_d}$ decays faster to zero,
- The NMP state estimation error for the MP strictly stable system is zero since these systems have a NMP zero at infinity that results in $\tilde{A}_z^{n_d} \equiv 0$, and
- The closer the NMP transmission zeros are to the unit circle, one can ensure a larger NMP state estimation error to the point that if the system \mathbf{S} has any transmission zeros on the unit circle, then the NMP state estimation results will be certainly biased regardless of the choice of n_d .

It turns out that one can obtain a conservative upper bound on the NMP state estimation error by considering the 2-norm of $e_{x_2}(k)$. We are now in a position to state our next result.

Theorem 5.6. *Let Assumption 1 hold, $0 < q < n$, $\begin{bmatrix} B_1^{(1)} \\ D \end{bmatrix}$ be a full column rank matrix and $\bar{x}_{20}^{(1)}(k) = 0$ for all k . Then $\sup(\|e_{x2}(k)\|_2) = \sigma_{max}(\tilde{A}_z^{n_d})\|(z\mathbf{I} - A^{(1)})^{-1}B^{(1)}\|_\infty$, where $\sigma_{max}(\cdot)$ denotes the largest singular value operator.*

Proof. It follows from Theorem 5.5 that,

$$\begin{aligned} \|e_{x2}(k - n - n_d)\|_2 &= \|\tilde{A}_z^{n_d}x_2^{(1)}(k - n)\|_2 & (5.40) \\ &\leq \|\tilde{A}_z^{n_d}\|_2\|x_2^{(1)}(k - n)\|_2 \\ &\leq \sigma_{max}(\tilde{A}_z^{n_d})\|(z\mathbf{I} - A^{(1)})^{-1}B^{(1)}\|_\infty \end{aligned}$$

The last inequality holds since the L_2 input-output gain is bounded by the ∞ -norm of the system \mathbf{S} . \square

The above upper bound can be plotted as a function of n_d to perform a trade-off analysis. Note that $\sigma_{max}(\tilde{A}_z^{n_d})$ is determined by the smallest NMP transmission zero of the system \mathbf{S} due to the fact that the eigenvalues of \tilde{A}_z are inverse of the system \mathbf{S} NMP transmission zeros. This is in accordance with the results that are stated in [75]. Note that $\sigma_{max}(\tilde{A}_z^{n_d})$ asymptotically decays to zero as n_d is increased. Therefore, an almost perfect estimation can be achieved when n_d is equal to several times that of the system order.

Remark 5.4. *If the system \mathbf{S} is stimulated by an input such that $u(k+1) \neq u(k)$ at finite k 's (such as in a step function) or $\|u(k+1) - u(k)\|$ is sufficiently small (such as in a harmonic function), then one can choose $\bar{x}_{20}^{(1)}(k - n) = \hat{x}_2^{(1)}(k - n - n_d - 1)$ in the filter (5.39) which may yield an almost unbiased state estimate by selecting the smallest possible choice of $n_d = 2$. This is due to the fact that in these cases $\hat{x}_2^{(1)}(k - n - n_d - 1)$ is a close approximation to $x_2^{(1)}(k - n - n_d - 1)$ and $x_2^{(1)}(k - n)$ (for small n_d), and therefore it may yield a sufficiently small NMP state estimation error, i.e., $e_{x2}(k - n - n_d) = \tilde{A}_z^{n_d}(x_2^{(1)}(k - n) - \bar{x}_{20}^{(1)}(k - n)) = \tilde{A}_z^{n_d}(x_2^{(1)}(k - n) - \hat{x}_2^{(1)}(k - n - n_d - 1)) \approx 0$ even if n_d is selected to be sufficiently small.*

We will illustrate the above statement in our simulation case study section. Once both the MP and NMP states are estimated, the unknown input can now be easily estimated by using equation (5.24) (or (5.29)). Specifically, if $B_1^{(1)}$ is full column rank, then $\hat{u}(k)$ is given by,

$$\hat{u}(k - n) = B_1^{(1)\dagger} \left(\hat{x}_1^{(1)}(k - n + 1) - A_{11}^{(1)} \hat{x}_1^{(1)}(k - n) - A_{12}^{(1)} \hat{x}_2^{(1)}(k - n) \right) \quad (5.41)$$

and if D is full column rank, it is given by,

$$\hat{u}(k - n) = D^\dagger \left(y(k - n) - C_1^{(1)} \hat{x}_1^{(1)}(k - n) - C_2^{(1)} \hat{x}_2^{(1)}(k - n) \right) \quad (5.42)$$

Definition 5.4. *The unknown input estimation error is defined according to $e_u(k) = \hat{u}(k) - u(k)$.*

Proposition 5.1. *Let Assumption 1 hold, $0 < q < n$, and $B_1^{(1)}$ be a full column rank matrix. Then,*

$$e_u(k) \rightarrow -B_1^{(1)\dagger} A_{12}^{(1)} e_{x2}(k) \text{ as } k \rightarrow \infty. \quad (5.43)$$

Proof. The result follows readily from equations (5.24) and (5.41) by noting that $u(k) - \hat{u}(k) = B_1^{(1)\dagger} (x_1^{(1)}(k + 1) - A_{11}^{(1)} x_1^{(1)}(k) - A_{12}^{(1)} x_2^{(1)}(k)) - B_1^{(1)\dagger} (\hat{x}_1^{(1)}(k + 1) - A_{11}^{(1)} \hat{x}_1^{(1)}(k) - A_{12}^{(1)} \hat{x}_2^{(1)}(k)) \rightarrow -B_1^{(1)\dagger} A_{12}^{(1)} e_{x2}(k)$ as $k \rightarrow \infty$. This follows due to the fact that $\hat{x}_1^{(1)}(k) \rightarrow x_1^{(1)}(k)$ as $k \rightarrow \infty$ and $e_{x2}(k) = x_2^{(1)}(k) - \hat{x}_2^{(1)}(k)$ (Definition 5.3). \square

The Proposition 5.1 links the unknown input estimation error to the state estimation error. This may serve as a means for conducting a trade-off analysis. The above implies that the state estimation error is propagated through the gain $-B_1^{(1)\dagger} A_{12}^{(1)}$ to the unknown input estimation error. One can interestingly conclude that if $-B_1^{(1)\dagger} A_{12}^{(1)}$ happens to be zero, then the unknown input estimation process will be unbiased regardless of the NMP states estimation error. Therefore, it can immediately be concluded that $-B_1^{(1)\dagger} A_{12}^{(1)} = 0$ if and only if the NMP zero of the

system \mathbf{S} is at infinity. In other words, the system \mathbf{S} is strictly stable and MP. The proposition 5.1 provides an explicit unknown input estimation error expression if $B_1^{(1)}$ is full column rank. In case that D is a full column rank matrix, we arrive at the following result.

Proposition 5.2. *Let Assumption 1 hold, $0 < q < n$, and D be a full column rank matrix. Then,*

$$e_u(k) \rightarrow -D^\dagger C_2^{(1)} e_{x_2}(k) \text{ as } k \rightarrow \infty. \quad (5.44)$$

Proof. It follows readily from equations (5.29) and (5.42) that we have $u(k) - \hat{u}(k) = D^\dagger(y(k) - C_1^{(1)}x_1^{(1)}(k) - C_2^{(1)}x_2^{(1)}(k)) - D^\dagger(y(k) - C_1^{(1)}\hat{x}_1^{(1)}(k) - C_2^{(1)}\hat{x}_2^{(1)}(k)) \rightarrow -D^\dagger C_2^{(1)} e_{x_2}(k)$ as $k \rightarrow \infty$. This follows due to the fact that $\hat{x}_1^{(1)}(k) \rightarrow x_1^{(1)}(k)$ as $k \rightarrow \infty$ and $e_{x_2}(k) = x_2^{(1)}(k) - \hat{x}_2^{(1)}(k)$ (Definition 5.3). \square

An immediate conclusion from the Propositions 5.1 and 5.2 is that if the system \mathbf{S} is NMP and both $B_1^{(1)}$ and D are full column rank matrices, then $B_1^{(1)\dagger} A_{12}^{(1)} = D^\dagger C_2^{(1)}$, which we have already derived through a different method in Theorem 5.3 ($C_{z_2}^{(1)} = 0$). This completes our solution to the Problem 1. In the next section, we discuss a solution to the Problem 2.

5.3 Inversion-Based Output Tracking

We have shown earlier that in presence of NMP states, accurate estimation of the MP states as well as bounded error estimation of the NMP states are possible under certain conditions. In this section, by utilizing the previous results we will introduce and develop an inversion-based output tracking control methodology as a solution to Problem 2. Specifically, we will obtain relationship between the resulting tracking error performance and the unknown input and state estimation errors. We also demonstrate that almost perfect tracking of an arbitrary desired output trajectory can be achieved.

For the output tracking problem a delayed state and input estimation may not be useful or practical given that the controller should issue the command at a given present time. This challenge can be resolved if we assume that the desired output trajectory from $y_d(k)$ to $y_d(k + n + n_d)$ is known *a priori* at a given time step k , which is known as the *preview time* (window) in the literature [78]. This is actually a reasonable and acceptable assumption given that the desired trajectory is typically planned in advance and at least it can be assumed practically to be known for $n + n_d$ time steps ahead. Our proposed estimation scheme is now slightly modified to incorporate this conditional change. A summary of the procedure for implementation of our proposed scheme is presented in Table 5.1.

Let us now define $\mathbf{Y}_d(k)$ as $\left[y_d(k)^T \ \dots \ y_d(k + n)^T \right]^T$, where $\mathbf{Y}_d(k)$ is assumed to be a *known* signal. It is now utilized to derive the unknown input observer following equation (5.18) to yield $\hat{x}_1^{(1)}(k)$ as follows,

$$\begin{cases} \eta(k + 1) = \hat{A}\eta(k) + F\mathbf{Y}_d(k) \\ \hat{x}_1^{(1)}(k) = \mathbf{M}_q^{(1)-1}\eta(k) \end{cases} \quad (5.45)$$

An estimate of $x_2^{(1)}(k)$ is now given by,

$$\hat{x}_2^{(1)}(k) = \tilde{A}_z^{n_d}\tilde{x}_{20}^{(1)}(k + n_d) - \sum_{i=0}^{n_d-1} (-\tilde{A}_z)^i \tilde{B}_z \hat{\Theta}_1^{(1)}(k + n_d - i - 1) \quad (5.46)$$

where $\tilde{x}_{20}^{(1)}(k + n_d)$ is a random initial condition of the FIR filter at each time step $k + n_d$, and $\hat{\Theta}_1^{(1)}(k) = \hat{X}_1^{(1)}(k)$ or $\hat{\Theta}_1^{(1)}(k) = \hat{X}_{1d}^{(1)}(k)$, if $B^{(1)}$ or D is full column rank,

respectively. Moreover, $\hat{X}_1^{(1)}(k) = \begin{bmatrix} \hat{x}_1^{(1)}(k + 1) \\ \hat{x}_1^{(1)}(k) \end{bmatrix}$ and $\hat{X}_{1d}^{(1)}(k) = \begin{bmatrix} \hat{x}_1^{(1)}(k) \\ y(k) \end{bmatrix}$. If

$B_1^{(1)}$ is full column rank, then $\hat{u}(k)$ is given by,

$$\hat{u}(k) = B_1^{(1)\dagger} \left(\hat{x}_1^{(1)}(k + 1) - A_{11}^{(1)}\hat{x}_1^{(1)}(k) - A_{12}^{(1)}\hat{x}_2^{(1)}(k) \right) \quad (5.47)$$

and if D is full column rank, then $\hat{u}(k)$ is given by,

$$\hat{u}(k) = D^\dagger \left(y(k) - C_1^{(1)}\hat{x}_1^{(1)}(k) - C_2^{(1)}\hat{x}_2^{(1)}(k) \right) \quad (5.48)$$

Since the NMP state estimation scheme is subject to errors, if the computed $\hat{u}(k)$ is fed to the system, it will then generate $y(k)$ that is different from the desired $y_d(k)$. In other words, $y(k)$ is the real output of the system subjected to and stimulated by $\hat{u}(k)$, that is (in view of the state space representation (5.16))

$$\begin{cases} \tilde{x}^{(1)}(k+1) = A^{(1)}\tilde{x}^{(1)}(k) + B^{(1)}\hat{u}(k) \\ y(k) = C^{(1)}\tilde{x}^{(1)}(k) + D\hat{u}(k) \end{cases} \quad (5.49)$$

where $\tilde{x}^{(1)}(k)$ denotes the state response of the system to the input $\hat{u}(k)$. If the exact $u(k)$ is known, then we would have obtained,

$$\begin{cases} x^{(1)}(k+1) = A^{(1)}x^{(1)}(k) + B^{(1)}u(k) \\ y_d(k) = C^{(1)}x^{(1)}(k) + Du(k) \end{cases} \quad (5.50)$$

We are now in a position to define the output tracking error as follows.

Definition 5.5. *The output tracking error is defined as $e_y(k) = y(k) - y_d(k)$.*

It now follows from equations (5.49) and (5.50) that,

$$\begin{cases} \tilde{e}_x(k+1) = A^{(1)}\tilde{e}_x(k) + B^{(1)}e_u(k) \\ e_y(k) = C^{(1)}\tilde{e}_x^{(1)}(k) + De_u(k) \end{cases} \quad (5.51)$$

where $\tilde{e}_x(k) = \tilde{x}^{(1)}(k) - x^{(1)}(k)$. It is straightforward to conclude from equation (5.51) that $e_y(k) \rightarrow 0$ as $k \rightarrow \infty$ if $e_u(k) \rightarrow 0$ as $k \rightarrow \infty$. However, $e_u(k)$ is given by the NMP state estimation error ($e_{x_2}(k)$) that is multiplied by a gain as formally stated in Propositions 5.1 or 5.2. We have shown in Theorem 5.6 that the NMP state estimation error ($e_{x_2}(k)$) decays asymptotically as n_d increases. Hence, an almost perfect output tracking for any desired trajectory can be achieved by selecting n_d to be sufficiently large by as much as few times of the system order in most cases. The following theorem formally establishes the above statement and provide an upper bound on the output tracking error versus the delay parameter n_d .

Theorem 5.7. *Let Assumption 1 hold and $0 < q < n$. If $B_1^{(1)}$ is full column rank, then $\|e_y(k)\|_2 \leq \sigma_{\max}(\tilde{A}_z^{n_d}) \|C(zI - A)^{-1}B + D\|_\infty \|B_1^{(1)\dagger} A_{12}^{(1)}\|_2 \|(z\mathbf{I} - A^{(1)})^{-1}B^{(1)}\|_\infty$. On the other hand, if D is full column rank, then $\|e_y(k)\|_2 \leq \sigma_{\max}(\tilde{A}_z^{n_d}) \|C(zI - A)^{-1}B + D\|_\infty \|D^\dagger C_2^{(1)}\|_2 \|(z\mathbf{I} - A^{(1)})^{-1}B^{(1)}\|_\infty$.*

Proof. According to equation (5.51), $\|e_y(k)\|_2 = \|C(zI - A)^{-1}B + D\|_\infty \|e_u(k)\|_2$. If $B_1^{(1)}$ is full column rank, then from Proposition 5.1, $\|e_u(k)\|_2 = \|B_1^{(1)\dagger} A_{12}^{(1)} e_{x2}(k)\|_2 \leq \|B_1^{(1)\dagger} A_{12}^{(1)}\|_2 \|e_{x2}(k)\|_2$. Our desired result is now obtained if we substitute $\|e_{x2}(k)\|_2$, by using Theorem 5.6, into the above expression as $\sigma_{\max}(\tilde{A}_z^{n_d}) \|(z\mathbf{I} - A^{(1)})^{-1}B^{(1)}\|_\infty$. Following along the same procedure yields our other desired result for the case when D is full column rank. \square

As expected, Theorem 5.7 implies that the upper bound of the output tracking error has the same functionality in terms of the delay parameter n_d as that of the upper bound of the NMP states estimation error. Theorem 5.7 is quite useful for performing a trade-off analysis between the delay parameter n_d and the output tracking error. One may also suggest to reapply the proposed methodology in this chapter to estimate $e_u(k)$ from $e_y(k)$ of the system (5.51). However, this is not possible due to the fact that $e_y(k)$ is not available for at least n_d time steps ahead. This completes our proposed methodology for inversion-based output tracking and in the next section, we provide illustrative simulation case studies to substantiate the benefits and advantages of our proposed strategies.

5.4 Extension to Fault Estimation

An important application of unknown input reconstruction is fault estimation. Faults can be considered as unknown inputs to be reconstructed using the methodology proposed in the previous sections of this chapter. However, faults are accompanied by exogenous and known system inputs. Therefore, we slightly modify the proposed

Table 5.1: Inversion-based output tracking algorithm.

1. Calculate \hat{A} , F and \mathbf{M} from Theorem 5.1.
2. Calculate $\mathbf{T}^{(1)}$ and $\mathbf{M}_q^{(1)}$ from equations given in Section 5.2.2.
3. Calculate $A^{(1)}$, $B^{(1)}$ and $C^{(1)}$ by applying the similarity transformation to the system \mathbf{S} using the matrix $\mathbf{T}^{(1)}$ ($x^{(1)} = \mathbf{T}^{(1)}x$).
4. Partition $A^{(1)}$, $B^{(1)}$ and $C^{(1)}$ according to equation (5.20).
5. If $B_1^{(1)}$ is full column rank, then obtain A_z and B_z from equations (5.26) and (5.27). If $B_1^{(1)}$ is not full column rank and D is full column rank, then obtain A_{zd} and B_{zd} from equations (5.31) and (5.32).
6. Calculate \tilde{A}_z and \tilde{B}_z from equations (5.35) and (5.36).
7. Select n_d according to Theorem 5.7 to meet the desired estimation error specifications .
8. At each time step k ,
 - (a) Reconstruct $\hat{x}_1^{(1)}(k)$ from equation (5.45).
 - (b) Reconstruct $\hat{x}_2^{(1)}(k)$ using equation (5.46).
 - (c) If $B_1^{(1)}$ is full column rank, then reconstruct $\hat{u}(k)$ from equation (5.47). If $B_1^{(1)}$ is not full column rank and D is full column rank, then reconstruct $\hat{u}(k)$ from equation (5.48).

unknown input reconstruction scheme to incorporate the presence of known exogenous input. We only provide the final results since the derivation is repetitive and can be easily verified by the reader.

Consider the following system,

$$\mathbf{S}^{ex} : \begin{cases} x(k+1) = Ax(k) + Bu(k) + Gv(k) \\ y(k) = Cx(k) + Du(k) + Ev(k) \end{cases} \quad (5.52)$$

where $x \in \mathbb{R}^n$, $u \in \mathbb{R}^l$, $v \in \mathbb{R}^p$ and $y \in \mathbb{R}^l$ are system states, system unknown input, system known input and system measurement. In the above formulation, the signal $u(k)$ can represents the faults that are desired to be estimated.

The solution begins by calculating \hat{A} , F and \mathbf{M} from Theorem 5.1 and $\mathbf{T}^{(1)}$ and $\mathbf{M}_q^{(1)}$ from equations given in Section 5.2.2. Furthermore we define,

$$G^{(1)} = \mathbf{T}^{(1)}G; G^{(1)} = \begin{bmatrix} G_1^{(1)} \\ H_2^{(1)} \end{bmatrix}; G_1^{(1)} \in \mathbb{R}^{q \times p}$$

The counterpart dynamic filter to the filter (5.18) for estimation of the MP states in the presence of known input $v(k)$ is governed by,

$$\begin{cases} \eta(k-n+1) = \hat{A}\eta(k-n) + F\mathbf{Y}(k-n) + H\mathbf{V}(k-i) \\ \hat{x}_1^{(1)}(k-n) = \mathbf{M}_q^{(1)-1}\eta(k-n) \end{cases} \quad (5.53)$$

where G is given by $F\mathbf{E}_n - \mathbf{M}\mathbf{G}\mathbf{I}_n + H = 0$ and,

$$\mathbf{E}_n = \begin{pmatrix} E & 0 & \dots & 0 \\ CG & E & \dots & 0 \\ \vdots & \vdots & \vdots & \vdots \\ CA^{n-1}G & CA^{n-2}G & \dots & E \end{pmatrix} \quad (5.54)$$

Table 5.2: Definition of parameters that are used for NMP state reconstruction using FIR filter (5.55)

	$B^{(1)}$ is full column rank	D is full column rank
\tilde{A}_z	$(A_z)^{-1}$, A_z is given by equation (5.26)	$(A_{zd})^{-1}$, A_{zd} is given by equation (5.31)
\tilde{B}_z	$(A_z)^{-1} \begin{bmatrix} B_z & G_2^{(1)} - B_2^{(1)} B_1^{(1)\dagger} G_1^{(1)} \end{bmatrix}$ B_z is given by equation (5.27)	$(A_{zd})^{-1} \begin{bmatrix} B_{zd} & E - B_2^{(1)} D^\dagger E \end{bmatrix}$ B_{zd} is given by equation (5.32)
$\hat{\Theta}_1^{(1)}(k-n)$	$\begin{bmatrix} \hat{x}_1^{(1)}(k-n+1) \\ \hat{x}_1^{(1)}(k-n) \\ v(k-n) \end{bmatrix}$ $\hat{x}_1^{(1)}(k)$ is calculated using filter (5.53)	$\begin{bmatrix} \hat{x}_1^{(1)}(k-n) \\ y(k-n) \\ v(k-n) \end{bmatrix}$ $\hat{x}_1^{(1)}(k)$ is calculated using filter (5.53)

The NMP states are reconstructed using the following FIR filter,

$$\hat{x}_2^{(1)}(k-n-n_d) = \tilde{A}_z^{n_d} \bar{x}_{20}^{(1)}(k-n) - \sum_{i=0}^{n_d-1} (\tilde{A}_z)^i \tilde{B}_z \hat{\Theta}_1^{(1)}(k-n-i-1) \quad (5.55)$$

where $\bar{x}_{20}^{(1)}(k-n)$ denotes the random initial condition of the FIR filter at each time step $k-n$, and other parameters are defined in Table 5.2. Finally, if $B_1^{(1)}$ is full column rank, then $\hat{u}(k)$ is given by,

$$\hat{u}(k-n) = B_1^{(1)\dagger} \left(\hat{x}_1^{(1)}(k-n+1) - A_{11}^{(1)} \hat{x}_1^{(1)}(k-n) - A_{12}^{(1)} \hat{x}_2^{(1)}(k-n) - G_1^{(1)} v(k-n) \right) \quad (5.56)$$

and if D is full column rank, it is given by,

$$\hat{u}(k-n) = D^\dagger \left(y(k-n) - C_1^{(1)} \hat{x}_1^{(1)}(k-n) - C_2^{(1)} \hat{x}_2^{(1)}(k-n) - E v(k-n) \right) \quad (5.57)$$

This completes the extension of the work to the reconstruction of an unknown input in the presence of known inputs. If one consider faults as unknown inputs, then the above methodology in fact provides an estimation of faults. Note that in contrast to the results of the previous chapter, the proposed scheme in this chapter can reconstruct any general type of fault. Therefore, it completes our inversion-based approach for fault estimation.

5.5 Numerical Case Study Simulations

Consider the following discrete-time linear system,

$$G(z) = \frac{(z - 1.5)(z - 0.5)}{z^2} \quad (5.58)$$

or in its equivalent state space representation given by,

$$\begin{cases} x(k+1) = \begin{bmatrix} 0 & 0 \\ 1 & 0 \end{bmatrix} x(k) + \begin{bmatrix} 0 \\ 1 \end{bmatrix} u(k) \\ y(k) = \begin{bmatrix} -2 & 0.75 \end{bmatrix} x(k) + u(k) \end{cases} \quad (5.59)$$

Using Lemma 5.1, the solution to the conditions (i)-(iii) is given by $\hat{A} = 0.5$, $F = \begin{bmatrix} -0.5547 & 0 \end{bmatrix}$, and $\mathbf{M} = \begin{bmatrix} -0.5574 & 0.8321 \end{bmatrix}$. Therefore, the unknown input observer is now given by equation (5.18),

$$\begin{cases} \eta(k+1) = 0.5\eta(k) - 0.5574y(k) \\ \hat{x}_1^{(1)}(k) = \eta(k) \end{cases} \quad (5.60)$$

Moreover, we have from the LQ decomposition of \mathbf{M} and equations (5.31) and (5.32), the following

$$\mathbf{T}^{(1)} = \begin{bmatrix} -0.5547 & 0.8321 \\ 0.8321 & 0.5547 \end{bmatrix}; L = \begin{bmatrix} 1 & 0 \end{bmatrix}$$

$$A_{zd} = 1.5; B_{zd} = \begin{bmatrix} -1.5 & -1 \end{bmatrix}.$$

Therefore, by assuming $\bar{x}_{20}^{(1)}(k-n) = 0$ for $k = 0, \dots, \infty$, the FIR filter for estimation of NMP states is given by equation (5.39) as follows,

$$\hat{x}_2^{(1)}(k - n - n_d) = - \sum_{i=0}^{n_d-1} \left(\frac{1}{1.5}\right)^i \begin{bmatrix} -1 & -\frac{1}{1.5} \end{bmatrix} \begin{bmatrix} \hat{x}_1^{(1)}(k - n - i - 1) \\ y(k - n - i - 1) \end{bmatrix} \quad (5.61)$$

The upper bound for the state estimation error versus n_d is shown in Figure 5.1. We have applied a non-smooth random input to the system in order to illustrate and

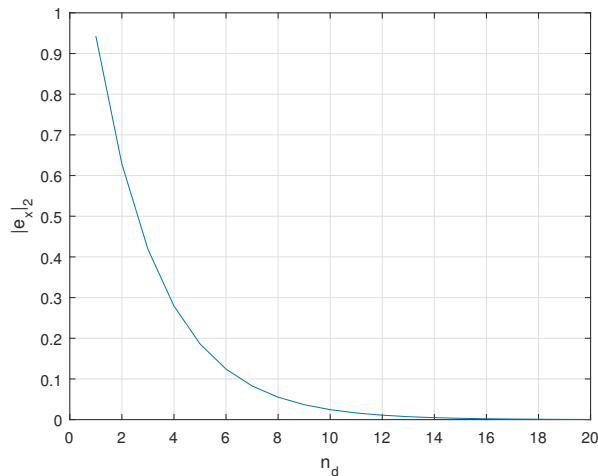


Figure 5.1: Upper bound of the NMP state estimation error versus n_d .

demonstrate the effects of n_d on the estimation error. A smooth input, as stated in Remark 5.4, will be estimated in an almost unbiased manner for any $n_d \geq 2$. Figure 5.2 depicts that $x_1^{(1)}(1)$ is perfectly estimated by using the unknown input observer (UIO) as expected. Figure 5.3 shows that a perfect reconstruction can be achieved for $x_2^{(1)}(1)$ by selecting $n_d = 15$, as expected from Figure 5.1. According to the Proposition 5.1, the unknown input should also be almost perfectly reconstructed with $n_d = 15$, which is also verified in Figure 5.4.

In another simulation case study, consider that a non-smooth $y_d(k)$ is required to be followed. The unknown input is reconstructed by using the Algorithm that is detailed in Table 5.1, and the results are depicted in Figure 5.5. This figure demonstrates that an almost perfect output tracking is achieved by selecting $n_d = 15$. Finally, consider a smooth $y_d(k)$ as given by $y_d(k) = k^2 \sin(5\pi k)$. The output tracking result for this smooth desired trajectory is shown in Figure 5.6, which confirms and is a demonstration of the statements that are made in Remark 5.4.

Finally, as a comparative study, consider a MIMO system that is taken from

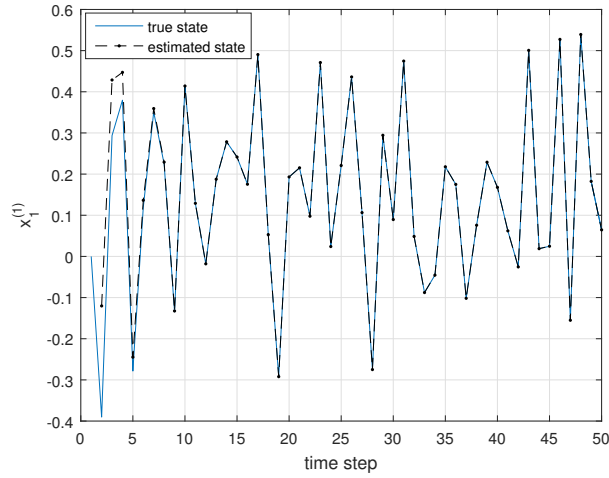


Figure 5.2: The estimation of the MP state by utilizing the filter (5.18).

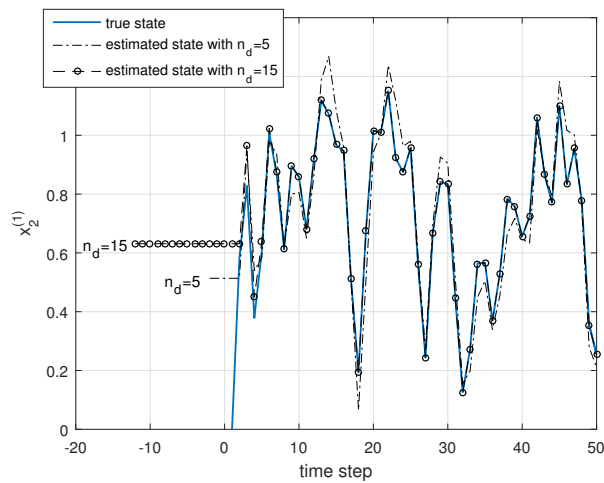


Figure 5.3: The estimation of the NMP state (the graphs are shifted by $n_d - n$ time steps to the left for the purpose of comparison) by utilizing the filter (5.39).

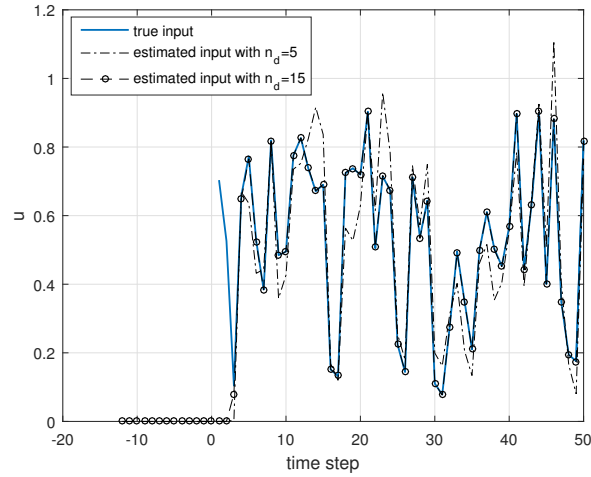


Figure 5.4: The estimation of the unknown input (the graphs are shifted by $n_d - n$ time steps to the left for the purpose of comparison) by utilizing equation (5.42).

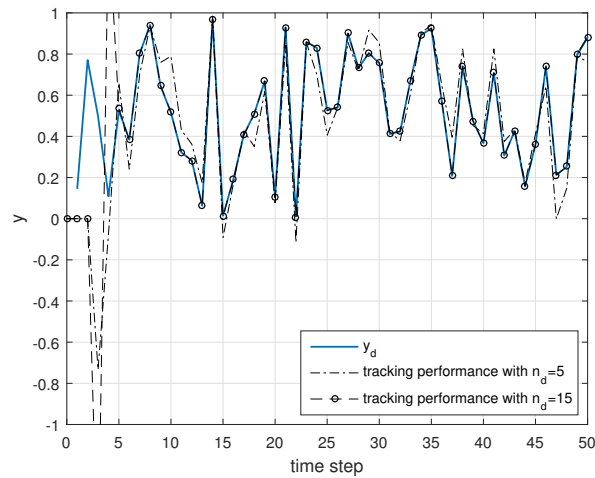


Figure 5.5: The output tracking performance corresponding to different values of n_d by utilizing equations (5.45), (5.46) and (5.48).

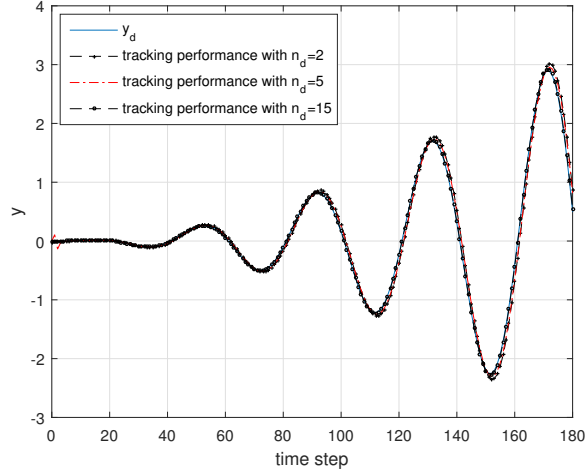


Figure 5.6: The output tracking performance by utilizing equations (5.45), (5.46) and (5.48) corresponding to a smooth trajectory.

the reference [75] with $A \in \mathbb{R}^{4 \times 4}$, $B \in \mathbb{R}^{4 \times 2}$ and $C \in \mathbb{R}^{2 \times 4}$ as follows,

$$\left\{ \begin{array}{l} x(k+1) = \begin{bmatrix} 0.6 & -0.3 & 0 & 0 \\ 0.1 & 1 & 0 & 0 \\ -0.4 & -1.5 & 0.4 & -0.3 \\ 0.3 & 1.1 & 0.2 & 0.9 \end{bmatrix} x(k) + \begin{bmatrix} 0 & 0.4 \\ 0 & 0 \\ 0 & -0.1 \\ 0.1 & 0.1 \end{bmatrix} u(k) \\ y(k) = \begin{bmatrix} 1 & 2 & 3 & 4 \\ 2 & 1 & 5 & 6 \end{bmatrix} x(k) \end{array} \right. \quad (5.62)$$

The system (5.62) has two zeros at $z_1 = 0.6072$ and $z_2 = 1.9928$. Therefore, it has three MP states and one NMP state. Authors of [75] proposed a geometric approach and applied it to the system (5.62) to achieve an *almost* perfect estimation of the states and unknown inputs with a delay of 20 time steps ($n_d = 20$). For comparison, our simulation results for the same example is shown in Figure 5.7. The numerical values of the estimation filters parameters for this example are as follows,

$$\hat{A} = \begin{bmatrix} 0.6072 & 0 & 0 \\ 0 & 0 & 0 \\ 0 & 0 & 0 \end{bmatrix}, \quad A_z = 1.9928$$

$$F = \begin{bmatrix} 0 & 0 & -0.662 & 0.0184 \\ 0 & 0 & -0.0206 & 0.1365 \\ 0 & 0 & 0.1337 & 0.0338 \end{bmatrix}; \mathbf{M} = \begin{bmatrix} 0.0488 & 0.9650 & 0.2063 & -0.1547 \\ 0.2523 & 0.0953 & 0.6205 & 0.7364 \\ 0.2013 & 0.3012 & 0.5700 & 0.7375 \end{bmatrix}$$

$$\mathbf{T}^{(1)} = \begin{bmatrix} -0.0488 & -0.9650 & -0.2063 & 0.1547 \\ 0.2483 & -0.0190 & 0.6003 & 0.7600 \\ -0.4645 & 0.2474 & -0.5833 & 0.6187 \\ -0.8487 & -0.0855 & 0.5067 & -0.1252 \end{bmatrix}; L = \begin{bmatrix} -1.0000 & 0 & 0 & 0 \\ -0.1183 & 0.9930 & 0 & 0 \\ -0.3039 & 0.9469 & 0.1048 & 0 \end{bmatrix}$$

$$B_z = \begin{bmatrix} -0.2463 & -2.0822 & 2.4171 & 5.3035 & -0.0678 & -2.3507 \end{bmatrix}$$

The results demonstrate that by using our proposed methodology the unknown states and inputs are almost perfectly reconstructed with only a delay of $n_d = 10$, which is half of the delay that was used in [75]. Moreover, as shown in Figure 5.7b, by using our approach the three MP states of the system are estimated without any delay when the transient response of the unknown initial condition dies off. This is in contrast to the delayed results that are shown in the work [75].

Our proposed methodology for partitioning and decoupling the system states does provide flexibility and versatility in its application to several important problems such as instantaneous estimation of MP states. Another important advantage of our approach is the fact that the developed machinery allows an almost perfect unknown input estimation and output tracking performance with a delay as small as 2 ($n_d = 2$) when the desired output trajectory is selected to be a smooth function of time.

5.6 Conclusion

In this chapter, we have shown that one can almost perfectly estimate and reconstruct the unknown state and inputs of a system if i) the system \mathbf{S} is square, and

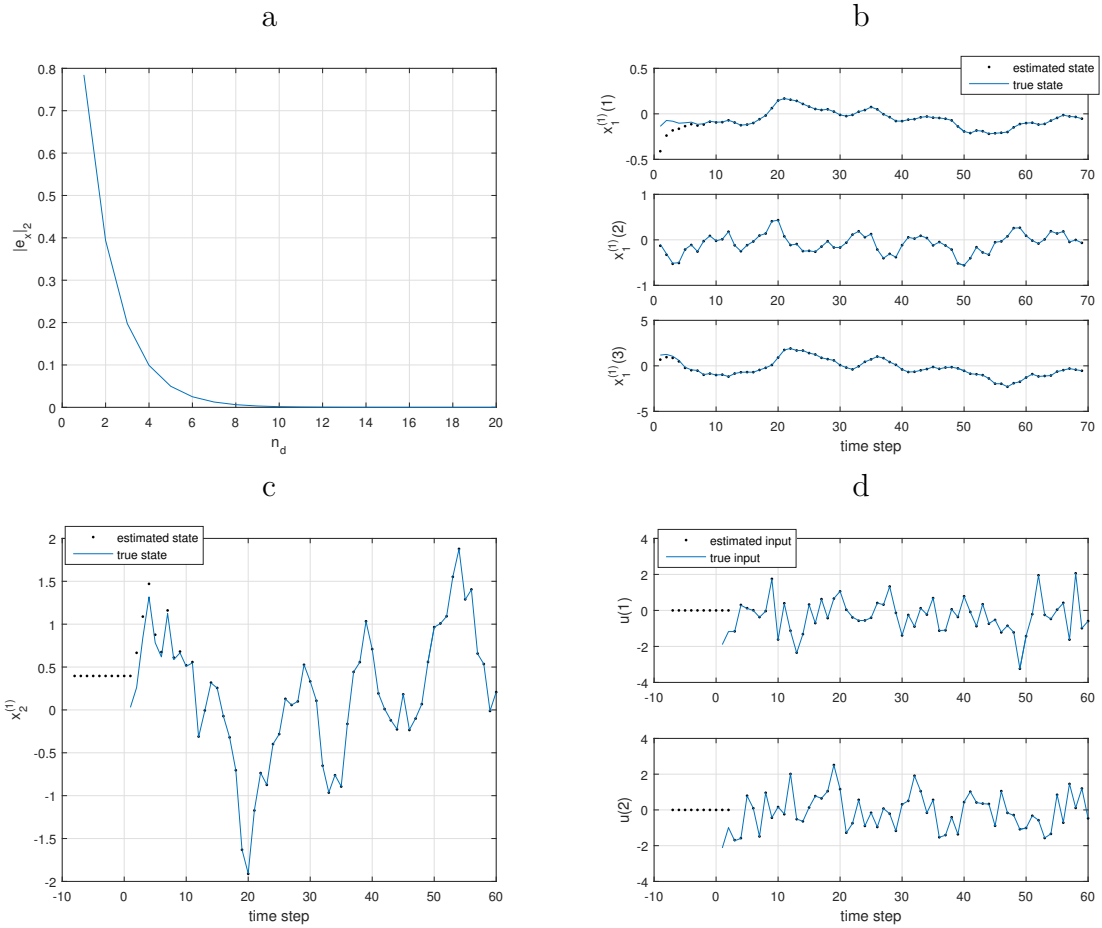


Figure 5.7: Simulation results for the MIMO system (5.62) taken from [75], (a) The NMP state estimation error versus n_d , (b) The MP state estimates, (c) The NMP state estimates, and (d) The unknown input estimates.

ii) $B_1^{(1)}$ or D is full column rank. Non-square systems rarely have transmission zeros [133], and therefore it is straightforward to design an unknown input observer (UIO) to estimate all the system states. We excluded non-square systems from our analysis since Theorem 4.2 is not guaranteed for this class of systems. In other words, the eigenvalues of $\Gamma = (A - B\mathbf{I}_n\mathbf{D}_n^+\mathbf{C}_n)$ may or may not coincide with the transmission zeros of the system. Also, it may or may not have the same characteristics, namely the MP transmission zero of \mathbf{S} remains the stable eigenvalue of Γ . However, if one determines the matrices \hat{A} , F and \mathbf{M} by using a different method for these systems, then the remainder of our procedure for unknown state and input reconstruction, as described in this chapter, will remain applicable and unchanged. We have also demonstrated that our proposed methods can provide an almost perfect tracking of any desired output trajectory by using data and information that correspond to a small preview time. Yet, further research is required to address issues of robustness and tracking error performance in presence of disturbances and modeling uncertainties. These issues are left as topics of future research.

Chapter 6

Data Driven Fault Detection, Isolation and Estimation

In this chapter, we propose explicit state-space based fault detection, isolation and estimation filters that are data-driven and are directly identified and constructed from only the system input-output (I/O) measurements and through estimating the system Markov parameters. The proposed methodology does not involve a reduction step and does not require identification of the system extended observability matrix or its left null space. The performance of our proposed filters is directly connected to and linearly dependent on the errors in the Markov parameters identification process. The estimation filters operate with a subset of the system I/O data that is selected by the designer. It is shown that the proposed filters provide asymptotically unbiased estimates by invoking low order filters as long as the selected subsystem has a stable inverse. We have derived the estimation error dynamics in terms of the Markov parameters identification errors and have shown that they can be directly synthesized from the healthy system I/O data. Consequently, the estimation errors can be effectively compensated for. Finally, we have provided several illustrative case study simulations that demonstrate and confirm the merits of our proposed

schemes as compared to methodologies that are available in the literature.

The outline of the remainder of the chapter is as follow. The preliminaries, problem definition and assumptions are provided in Section 6.1. In Section 6.2, we discuss the theoretical aspects of our proposed fault estimation scheme. We present the development and design of data-driven fault detection and isolation filters in Section 6.3. Next, we propose a data-driven fault estimation filter for both the actuators and sensors as well as a tuning procedure is introduced and developed in Section 6.4. Finally, we provide a number of illustrative simulation results in Section 6.5.

6.1 Preliminaries

Consider the following discrete-time linear system \mathbf{S} ,

$$\mathbf{S} : \begin{cases} x(k+1) = Ax(k) + Bu(k) + w(k) \\ y(k) = Cx(k) + v(k) \end{cases} \quad (6.1)$$

where $x \in \mathbb{R}^n$, $u \in \mathbb{R}^m$, and $y \in \mathbb{R}^l$. Moreover, $w(k) \in \mathbb{R}^n$ and $v(k) \in \mathbb{R}^l$ are white noise having zero mean and covariance matrices:

$$\mathbf{E} \left[\begin{bmatrix} w_i \\ v_i \end{bmatrix} \begin{bmatrix} w_j^T & v_j^T \end{bmatrix} \right] = \begin{bmatrix} Q & S \\ S^T & R \end{bmatrix} \delta_{i,j} \quad (6.2)$$

We model a given actuator or a sensor fault through additive terms that are injected in the system \mathbf{S} as follows,

$$\mathbf{S}_f : \begin{cases} x(k+1) = Ax(k) + Bu(k) + Bf^a(k) + w(k) \\ y(k) = Cx(k) + f^s(k) + v(k) \end{cases} \quad (6.3)$$

where $f^a(k) \in \mathbb{R}^m$ and $f^s(k) \in \mathbb{R}^l$ represent the actuator and sensor faults, respectively. These faults are commonly known as *additive faults*.

Remark 6.1. *The actuator and sensor faults are traditionally modeled in various manners in the literature. For instance, either as additive faults or multiplicative*

faults. The proper choice depends on the actual characteristics of the fault. Typically, sensor bias, actuator bias and actuator loss of effectiveness are considered as additive faults. Multiplicative fault models are more suitable for representing changes in the system dynamic parameters such as gains and time constants [77].

Problem Statement: The problem considered in this work deals with developing and designing fault detection, isolation and estimation schemes for *both* sensor and actuator faults under the following assumptions.

Assumption 1: The system \mathbf{S} is stable and observable.

Assumption 2: The system matrices and the system order are not known *a priori*.

Assumption 3: A sequence of healthy measured system I/O data, namely $u(k)$ and $y(k)$, for $k = 1, \dots, T$, are available and the input $u(k)$ satisfies the persistently exciting (PE) condition [93].

Assumption 4: The faults in the system \mathbf{S}_f are *detectable* and *isolable*, as comprehensively discussed in Chapter 4 of [134].

The above assumptions are required in all the lemmas and theorems provided in the chapter, however they are not explicitly stated in lemmas and theorems statements for sake of brevity.

Identification of the Markov Parameters: We define the set $\{H_0, H_1, H_2, \dots\}$, where $H_\beta = CA^\beta B$ is known as the Markov parameter. If $u(k)$ is persistently exciting, then several approaches are available in the literature to directly identify the Markov parameters from the I/O data $u(k)$ and $y(k)$ ([91, 93]). Specifically, we use *correlation analysis* [93] for accomplishing the Markov parameters estimation task. The estimated Markov parameters are denoted by \hat{H}_β in our subsequent derivations.

Notation: We will subsequently use an equivalent form of the system \mathbf{S} as

follows,

$$\mathbf{S} : \begin{cases} x(k-i+1) = Ax(k-i) + B\mathbf{I}_l^m \mathbf{U}_i(k-i) + w(k-i) \\ \mathbf{Y}(k-i) = \mathbf{C}x(k-i) + \mathbf{D}\mathbf{U}(k-i) \\ + \mathbf{E}\mathbf{W}(k-i) + \mathbf{V}(k-i) \end{cases} \quad (6.4)$$

where,

$$\mathbf{C} = \begin{pmatrix} C \\ CA \\ \vdots \\ CA^i \end{pmatrix}; \mathbf{D} = \begin{pmatrix} 0 & 0 & \dots & 0 & 0 \\ H_0 & 0 & \dots & 0 & 0 \\ \vdots & \vdots & \vdots & \vdots & \vdots \\ H_{i-1} & H_{i-2} & \dots & H_0 & 0 \end{pmatrix}; \mathcal{D} = \left[0 \quad H_1^T \quad \dots \quad H_{i-1}^T \right]^T$$

$$\mathbf{E} = \begin{pmatrix} 0 & 0 & \dots & 0 & 0 \\ C & 0 & \dots & 0 & 0 \\ \vdots & \vdots & \vdots & \vdots & \vdots \\ CA^{i-1} & CA^{i-2} & \dots & C & 0 \end{pmatrix} \quad (6.5)$$

For any given signal $g(k)$, the following matrices are defined,

$$\mathbf{G}(k-i) = \begin{bmatrix} g(k-i) \\ g(k-i+1) \\ \vdots \\ g(k) \end{bmatrix}; \mathbf{G}_+(k-i) = \begin{bmatrix} g(k-i) \\ g(k-i+1) \\ \vdots \\ g(k+1) \end{bmatrix} \quad (6.6)$$

We extensively use the notation \mathbf{I}_γ^α which is defined as,

$$\mathbf{I}_\gamma^\alpha = \left[\mathbf{I}_{\alpha \times \alpha} \quad \mathbf{0}_{\alpha \times (i\gamma - \alpha)} \right] \quad (6.7)$$

Moreover, we also define,

$$\mathbf{D}_+ = \begin{pmatrix} H_0 & 0 & \dots & 0 & 0 \\ \vdots & \vdots & \vdots & \vdots & \vdots \\ H_i & H_{i-1} & \dots & H_0 & 0 \end{pmatrix}; \mathcal{D}_+ = \begin{pmatrix} H_0 \\ \vdots \\ H_i \end{pmatrix}; \mathbf{C}_+ = \left[(CA)^T \quad \dots \quad (CA^{i+1})^T \right]^T \quad (6.8)$$

$$\mathbf{G}_{i,j}(k-i) = \begin{pmatrix} g(k-i) & g(k-i+1) & \dots & g(k-i+j) \\ g(k-i+1) & g(k-i+2) & \dots & g(k-i+j+1) \\ \vdots & \vdots & \vdots & \vdots \\ g(k) & g(k+1) & \dots & g(k+j) \end{pmatrix} \quad (6.9)$$

The matrices $\hat{\mathbf{D}}$, $\hat{\mathbf{D}}_+$, $\hat{\mathcal{D}}$ and $\hat{\mathcal{D}}_+$ are constructed similar to \mathbf{D} , \mathbf{D}_+ , \mathcal{D} and \mathcal{D}_+ where the actual Markov parameters H_β are replaced by their estimates \hat{H}_β .

We define two sets p and q that contain a selection of integer numbers from 1 to l and from 1 to m , respectively. The parameters n_p and n_q denote the number of elements in the sets p and q , respectively. Both p and q can be empty sets denoted by $p = \{\emptyset\}$ and $q = \{\emptyset\}$. We denote by kp (or kq), $k \in \mathbb{N}$, as a set that contains all the elements of p (or q) multiplied by k . The notation $\sim q$ (or $\sim p$) denotes the set that contains the integers from 1 to m (or 1 to l) that are not included in q (or p). For example, for a given Markov parameter matrix $H_0 \in \mathbb{R}^{5 \times 4}$, a typical p can be taken as $p = \{2, 4\}$. Moreover, $n_p = 2$, $3p = \{6, 12\}$ and $\sim p = \{1, 3, 5\}$. If $p = \{\emptyset\}$, then $\sim p = \{1, 2, 3, 4, 5\}$. The matrix \mathbf{O}_{p-}^{q-} is obtained by deleting the columns $q, 2q, \dots, iq$ and rows $p, 2p, \dots, ip$ of \mathbf{O} , respectively. The matrix \mathbf{O}^{q+} and \mathbf{O}_{p+} are defined as matrices that only contain the columns $q, 2q, \dots, iq$ and the rows $p, 2p, \dots, ip$ of \mathbf{O} , respectively. The vector \mathbf{P}^{p-} is obtained by deleting the rows $p, 2p, \dots, ip$ of \mathbf{P} . Finally, \mathbf{P}^{p+} only contains the rows $p, 2p, \dots, ip$ of \mathbf{P} . Similar notations are defined for \mathbf{P}^{q+} and \mathbf{P}^{q-} . The signs \dagger , \mathcal{N} and $\mathbb{E}\{\cdot\}$ denote the Moore-Penrose pseudo inverse, null space and the expectation operator. The matrix $\mathbf{O}(\alpha : \beta, \gamma : \theta)$ denotes a matrix that is constructed from an original matrix \mathbf{O} by only containing the rows α to β and the columns γ to θ . If α and β (or γ and θ) are not specified, then it implies that we are dealing with all the rows (or columns) of \mathbf{O} .

Remark 6.2. *The parameters p and q are defined in order to specify the set of I/O data that is to be fed to a fault isolation or estimation filter. For example, for a given*

Markov parameter matrix $H_0 \in \mathbb{R}^{5 \times 4}$, one may desire to design a filter that operates with information from input channels $\{3, 4\}$ and measurement channels $\{1, 2, 3\}$. Then, one should set $q = \{1, 2\}$ and $p = \{4, 5\}$. The above notation is critical for the task of fault isolation where one requires to construct a bank of filters each of which operates with a different set of inputs and outputs data.

6.2 Proposed Fault Estimation Scheme Using Exact Markov Parameters and Observability Matrix

In this section, we start by assuming availability of the exact Markov parameters and the extended observability matrix to introduce the basic concepts we utilize in this work. These assumptions will be relaxed and removed in the subsequent Sections 6.3, 6.4 and 6.5.

Let us consider a signal $\eta(k)$ that is governed by the following dynamics and stimulated by the information from the sensors $\sim p$ and actuators $\sim q$, that is

$$\eta(k+1) = A_r \eta(k) + B_r \mathbf{U}^{q^-}(k-i) + L_r \mathbf{Y}^{p^-}(k-i) \quad (6.10)$$

where $\eta(k) \in \mathbb{R}^{l'}$, $\mathbf{U}^{q^-}(k-i) \in \mathbb{R}^{im'}$ and $\mathbf{Y}^{p^-} \in \mathbb{R}^{il'}$, where $l' = (l - n_p)$ and $m' = (m - n_q)$. Our goal is to determine the *unknown* matrices A_r , B_r and L_r such that for the healthy system \mathbf{S} given by (6.4), we have

$$\mathbb{E}(e(k)) = \mathbb{E}(\eta(k) - \mathbf{T}x(k-i)) \rightarrow 0 \text{ as } k \rightarrow \infty \quad (6.11)$$

where $\mathbf{T} \in \mathbb{R}^{l' \times n}$ denotes a full column rank matrix. The error dynamics associated

with $e(k)$ is therefore given by,

$$\begin{aligned}
e(k+1) &= \eta(k+1) - \mathbf{T}x(k-i+1) \\
&= A_r e(k) + (A_r \mathbf{T} - \mathbf{T}A + L_r \mathbf{C}_{p-})x(k-i) \\
&+ (B_r + L_r \mathbf{D}_{p-}^{q-} - \mathbf{T}B^{q-} \mathbf{I}_{\nu'}^{m'}) \mathbf{U}^{q-}(k-i) \\
&+ (L_r \mathbf{D}_{p-}^{q+} - \mathbf{T}B^{q+} \mathbf{I}_{\nu'}^{n_q}) \mathbf{U}^{q+}(k-i) \\
&+ L_r \mathbf{E}_{p-}^{q-} \mathbf{W}^{q-}(k-i) + L_r \mathbf{V}^{p-}(k-i)
\end{aligned} \tag{6.12}$$

which is obtained by substituting $\eta(k+1)$ from equation (6.10) and $x(k-i+1)$ from equation (6.4). Condition (6.11) is now satisfied if and only if (a) A_r is a Hurwitz matrix, (b) $A_r \mathbf{T} - \mathbf{T}A + L_r \mathbf{C}_{p-} = 0$, (c) $B_r + L_r \mathbf{D}_{p-}^{q-} - \mathbf{T}B^{q-} \mathbf{I}_{\nu'}^{m'} = 0$, and (d) $L_r \mathbf{D}_{p-}^{q+} - \mathbf{T}B^{q+} \mathbf{I}_{\nu'}^{n_q} = 0$. The above conditions actually correspond to the Luenberger observer equations.

The key concept that is introduced in this chapter is that we specifically set,

$$\mathbf{T} = \mathbf{C}_{p-} \tag{6.13}$$

In other words, we select \mathbf{T} to be equal to the extended observability matrix. Let us now define the matrix \mathbf{M}_{p-} as follows,

$$\mathbf{M}_{p-} = A_r + L_r \tag{6.14}$$

Given (6.13) and (6.14) and in view of the fact that $\mathbf{C}_{p-} B^{q-} = \mathcal{D}_{+,p-}^{q-}$, $\mathbf{C}_{p-} B^{q+} = \mathcal{D}_{+,p-}^{q+}$, and $\mathbf{C}_{p-} A = \mathbf{C}_{+,p-}$, the conditions (a) to (d) can be rewritten as,

$$A_r \quad \text{is Hurwitz} \tag{6.15}$$

$$\mathbf{M}_{p-} \mathbf{C}_{p-} = \mathbf{C}_{+,p-} \tag{6.16}$$

$$L_r \mathbf{D}_{p-}^{q+} - \mathcal{D}_{+,p-}^{q+} \mathbf{I}_{\nu'}^{n_q} = 0 \tag{6.17}$$

$$B_r + L_r \mathbf{D}_{p-}^{q-} - \mathcal{D}_{+,p-}^{q-} \mathbf{I}_{\nu'}^{m'} = 0 \tag{6.18}$$

Remark 6.3. Recall that \mathbf{C}_{p-} should be full column rank according to the assignment (6.13). The matrix \mathbf{C}_{p-} will be full column rank if i is selected to be equal to or

greater than the observability index of the pair (C^{p-}, A) , which is denoted by ν_p . Given $i \geq \nu_p$, the matrix \mathbf{M}_{p-} is given by $\mathbf{C}_{+,p-}(\mathbf{C}_{p-})^\dagger + \Theta(\mathbf{I} - \mathbf{C}_{p-}(\mathbf{C}_{p-})^\dagger)$, where Θ is an arbitrary matrix introduced due to the Moore-Penrose pseudo inverse non-unique solution.

Definition 6.1. *The relative degree of the subsystem inputs to the outputs $\sim p$ is defined as the smallest non-negative τ_p such that $H_{i,p-} = 0$ for $i < \tau_p$ and \mathcal{D}_{p-} is full column rank for $i \geq \tau_p$ [73, 92].*

Remark 6.4. *It is well-known that the system of equations (6.14) and (6.15) to (6.18) has a solution if and only if i) $i \geq \tau_p$ and ii) the subsystem from the inputs q to the outputs $\sim p$ is minimum phase [126]. Particularly, the above equations always have a solution if $q = \{\emptyset\}$ since equation (6.17) vanishes. Consequently, one can arbitrarily select a Hurwitz A_r and then calculate L_r and B_r from equations (6.14) and (6.18). The restriction that is imposed is actually on the subsystems and not the entire system. Therefore, the designer has a freedom to select a different q if the minimum phase condition is not satisfied for the original selection.*

Let us assume that it is desired to estimate the faults in the actuators q by using the information from the sensors $\sim p$ and actuators $\sim q$. Then, the fault estimator filter is given by,

$$\begin{cases} \eta(k+1) = A_r \eta(k) + B_r \mathbf{U}^{q-}(k-i) + L_r \mathbf{Y}^{p-}(k-i) \\ \hat{f}^a(k-i) = -\mathbf{I}_m^m \mathbf{D}^\dagger (\eta(k) - \mathbf{Y}^{p-}(k-i) + \mathbf{D}_{p-} \mathbf{U}(k-i)) \end{cases} \quad (6.19)$$

where $\hat{f}^a(k)$ denotes an estimate of $f^a(k)$. The matrices A_r , B_r and L_r are obtained by solving the equations (6.14) and (6.15) to (6.18).

Theorem 6.1. *Assume that the subsystem from the inputs q to the outputs $\sim p$ is minimum phase, $i \geq \max\{\nu_p, \tau_p\}$ and the sensors $\sim p$ and actuators $\sim q$ are healthy, then the filter dynamics governed by (6.19) is asymptotically unbiased.*

Proof. The dynamics of the residuals in presence of actuator faults is given by,

$$\begin{cases} \eta(k+1) = A_r \eta(k) + B_r^{q-} (\mathbf{U}^{q-}(k-i) + \mathbf{F}^{a,q-}(k-i) + L_r^{p-} \mathbf{Y}^{p-}(k-i)) \\ r_q(k) = \eta(k) - \mathbf{Y}^{p-}(k-i) + \mathbf{D}_{p-} (\mathbf{U}(k-i) + \mathbf{F}^a(k-i)) \end{cases} \quad (6.20)$$

Since A_r , B_r and L_r satisfy equations (6.14) and (6.15) to (6.18) and the actuators $\sim q$ are healthy, therefore $\mathbb{E}\{\eta(k) - \mathbf{C}_{p-} x(k-i)\} \rightarrow 0$ as $k \rightarrow \infty$. The convergence is asymptotic since A_r is Hurwitz. Therefore, $\mathbb{E}\{r_q(k)\} \rightarrow -\mathbf{D}_{p-} \mathbf{F}^a(k-i)$ as $k \rightarrow \infty$. Therefore, $\hat{f}^a(k-i) = -\mathbf{I}_l^m \mathbf{D}_{p-}^\dagger \mathbb{E}\{r_q(k)\} - \mathbf{I}_m^m (\mathbf{I} - \mathbf{D}_{p-}^\dagger \mathbf{D}_{p-}) \Theta$, where Θ is an arbitrary matrix. However, since $i \geq \tau_p$, the subspace spanned by rows of \mathbf{I}_m^m are also spanned by the rows of \mathbf{D}_{p-} . Therefore, the projection of the row space of \mathbf{I}_m^m onto the null space of \mathbf{D}_{p-} given by $(\mathbf{I} - \mathbf{D}_{p-}^\dagger \mathbf{D}_{p-})$ is zero. In other words, $\mathbf{I}_m^m (\mathbf{I} - \mathbf{D}_{p-}^\dagger \mathbf{D}_{p-}) = 0$. This completes the proof of the theorem. \square

The above theorem guarantees that our proposed filter will generally have a lower order than the estimation filter that is proposed in [92] which requires $i \geq \nu_p + \tau_p$ or $i \rightarrow \infty$ depending on the transmission zeros of the quadruple $(A, B^{q-}, \mathbf{C}_{p-}, \mathcal{D}_{p-}^{q-})$.

The case of the sensor fault estimation is slightly different. One can estimate the faults in the sensors p if the sensors $\sim p$ and all the actuators are healthy. The fault estimator is now given by,

$$\begin{cases} \eta(k+1) = A_r \eta(k) + B_r \mathbf{U}(k-i) + L_r^{p\downarrow} \mathbf{Y}(k-i) \\ \hat{f}^s(k-i) = \mathbf{I}_l^l (\eta(k) - \mathbf{Y}^{p-}(k-i) + \mathbf{D}_{p-} \mathbf{U}(k-i)) \end{cases} \quad (6.21)$$

where $\hat{f}^s(k)$ denotes an estimate of $f^s(k)$, $L_r^{p\downarrow}$ denotes a matrix where its columns $p, 2p, \dots, ip$ are zero. The matrices A_r , B_r and $L_r^{p\downarrow}$ are obtained by solving the equations (6.14) and (6.15) to (6.18) by setting $p = q = \{\emptyset\}$ and by replacing L_r with $L_r^{p\downarrow}$.

The above proposed filter (6.21) is unbiased as established by the following theorem.

Theorem 6.2. *Assume that $i \geq \nu_p$ and the sensors $\sim p$ and all the actuators are healthy, then the filter dynamics that is governed by (6.21) is asymptotically unbiased.*

Proof. The dynamics of the residuals in presence of sensor faults is given by,

$$\begin{cases} \eta(k+1) = A_r \eta(k) + B_r \mathbf{U}(k-i) + L_r^{p\downarrow} (\mathbf{Y}(k-i) + \mathbf{F}^s(k-i)) \\ r_p(k) = \eta(k) - \mathbf{Y}(k-i) - \mathbf{F}^s(k-i) + \mathbf{D}_{p-} \mathbf{U}(k-i) \end{cases} \quad (6.22)$$

Since A_r , B_r and $L_r^{p\downarrow}$ satisfy equations (6.14) and (6.15) to (6.18) and the actuators and sensors p are healthy, therefore $\mathbb{E}\{\eta(k) - \mathbf{C}_{p-} x(k-i)\} \rightarrow 0$ as $k \rightarrow \infty$. The convergence is asymptotic since A_r is Hurwitz. Therefore, $\mathbb{E}\{r_p(k)\} \rightarrow \mathbf{F}^s(k-i)$ as $k \rightarrow \infty$. Therefore, $\hat{f}^s(k-i) = \mathbf{I}_l^m \mathbb{E}\{r_p(k)\}$. This completes the proof of the theorem. \square

Note that the subsystem from the inputs to the outputs $\sim p$ is *not* required to be minimum phase for solving the sensor fault estimation problem. Moreover, it can be theoretically shown that the filter (6.21) is unbiased by using information from the faulty actuators provided it is modified by the estimations that are provided by the filter (6.19). However, this coupling will cause significant biases in the data-driven solution since the actuator fault estimation scheme is itself biased.

6.3 Data-Driven Fault Detection and Isolation (FDI) Scheme

In this section, our proposed fault detection and isolation (FDI) filters are now directly constructed from the healthy system I/O data. First, we propose a data-driven estimation of the matrix \mathbf{M}_{p-} and then present the design procedure of the FDI filters.

Remark 6.5. *Theorems 6.1 and 6.2 provide the guidelines for selection of i . The parameter i is bounded by n which is not known a priori. The condition $i \geq \tau_p$ can be easily satisfied by checking the rank of \mathcal{D}_{p-} . However, the parameter ν_p is not known. Therefore, i should be selected sufficiently large that ensures $i \geq \max\{\nu_p, \tau_p\}$.*

6.3.1 Data-Driven Estimation of the Filter Parameters

In order to solve equations (6.14) and (6.15) to (6.18), one requires the Markov parameters and the extended observability matrix. The extended observability matrix is required to obtain \mathbf{M}_{p-} . However, in our subsequent data-driven derivations we will show that an estimate of the matrix \mathbf{M}_{p-} can be directly obtained from the system I/O data *without* applying the reduction step. Consequently, the matrix \mathbf{C}_{p-} or its equivalent forms are not actually required.

The objective of the equation (6.16) is in fact to enforce,

$$(A_r \mathbf{C}_{p-} - \mathbf{C}_{p-} A + L_r \mathbf{C}_{p-})x(k-i) \equiv 0 \quad (6.23)$$

On the other hand, from the measurement equation (6.4) it follows that,

$$\mathbf{C}_{p-}x(k-i) = \mathbf{Y}^{p-}(k-i) - \mathbf{D}_{p-}\mathbf{U}(k-i) - \mathbf{E}_{p-}\mathbf{W}(k-i) - \mathbf{V}^{p-}(k-i) \quad (6.24)$$

By substituting equation (6.24) into equation (6.23) one obtains,

$$\begin{aligned} & \mathbf{M}_{p-}(\mathbf{Y}^{p-}(k-i) - \mathbf{D}_{p-}\mathbf{U}(k-i) - \mathbf{E}_{p-}\mathbf{W}(k-i) \\ & - \mathbf{V}^{p-}(k-i)) - (\mathbf{Y}^{p-}(k-i+1) - \mathbf{D}_{+,p-}\mathbf{U}_+(k-i) \\ & - \mathbf{E}_{+,p-}\mathbf{W}_+(k-i) - \mathbf{V}^{p-}(k-i+1)) \\ & = 0 \end{aligned} \quad (6.25)$$

where,

$$\mathbf{M}_{p-} \triangleq A_r + L_r \quad (6.26)$$

Iterating the equation (6.25) from the time steps $k - i$ to $k - i + j$, where $j \gg i$, yields,

$$\mathbf{M}_{p-}(\Gamma_0^{p-} - \mathbf{E}_{p-} \mathbf{W}_{i,j}(k-i) - \mathbf{V}_{i,j}^{p-}(k-i)) - (\Gamma_1^{p-} - \mathbf{E}_{+,p-} \mathbf{W}_{(i+1),j}^{p-}(k-i) - \mathbf{V}_{(i+1),j}^{p-}(k-i+1)) = 0 \quad (6.27)$$

where $\Gamma_0^{p-} = \mathbf{Y}_{i,j}^{p-}(k-i) - \mathbf{D}_{p-} \mathbf{U}_{i,j}(k-i)$ and $\Gamma_1^{p-} = \mathbf{Y}_{(i+1),j}^{p-}(k-i+1) - \mathbf{D}_{+,p-} \mathbf{U}_{(i+1),j}(k-i)$. Equation (6.27) forms the basis for our proposed data-driven solution for estimating \mathbf{M}_{p-} . The matrix \mathbf{M}_{p-} minimizes the following cost function,

$$\|\Gamma_1^{p-} - \mathbf{M}_{p-} \Gamma_0^{p-}\|_2$$

We do not have access to the actual values of the Markov parameters. Instead, we construct the matrices $\hat{\Gamma}_0^{p-}$ and $\hat{\Gamma}_1^{p-}$ by using the estimated Markov parameters and the system I/O data (healthy data) as follows,

$$\hat{\Gamma}_0^{p-} = \mathbf{Y}_{i,j}^{p-}(k-i) - \hat{\mathbf{D}}_{p-} \mathbf{U}_{i,j}(k-i) \quad (6.28)$$

$$\hat{\Gamma}_1^{p-} = \mathbf{Y}_{(i+1),j}^{p-}(k-i+1) - \hat{\mathbf{D}}_{+,p-} \mathbf{U}_{(i+1),j}(k-i) \quad (6.29)$$

where $\hat{\mathbf{D}}_{p-}$ and $\hat{\mathbf{D}}_{+,p-}$ are constructed similar to \mathbf{D}_{p-} and $\mathbf{D}_{+,p-}$ but instead the estimated Markov parameters are utilized. Therefore, an estimate of \mathbf{M}_{p-} is given by $\hat{\Gamma}_1^{p-}(\hat{\Gamma}_0^{p-})^\dagger + \Theta(\mathbf{I} - \hat{\Gamma}_0^{p-}(\hat{\Gamma}_0^{p-})^\dagger)$, where Θ is an arbitrary matrix. However, the solution will be unique as $j \rightarrow \infty$ as stated in the following lemma.

Lemma 6.1. *If $j \rightarrow \infty$, then the matrix $\hat{\Gamma}_0^{p-}$ is full row rank and,*

$$\hat{\mathbf{M}}_{p-} = \hat{\Gamma}_1^{p-}(\hat{\Gamma}_0^{p-})^\dagger \quad (6.30)$$

Proof. According to equation (6.28) and the measurement equation (6.4), we have

$$\Gamma_0^{p-} = \mathbf{C}_{p-} X(k-i) + \mathbf{E}_{p-} \mathbf{W}_{i,j}(k-i) + \mathbf{V}_{i,j}^{p-}(k-i)$$

where,

$$X(k-i) = \begin{bmatrix} x(k-i) & \dots & x(k-i+j-1) \end{bmatrix}$$

Assume that two block rows γ and β of Γ_0^{p-} , where $\beta > \gamma$, are linearly dependent which implies,

$$\begin{aligned} & \mathbf{Y}_{1,j}^{p-}(k-i+\gamma) - (\mathbf{D}_{p-}((i+\gamma-1)l' : (i+\gamma)l', :))\mathbf{U}_{i,j}(k-i) \\ &= c(\mathbf{Y}_{1,j}^{p-}(k-i+\beta) - (\mathbf{D}_{p-}((i+\beta-1)l' : (i+\beta)l', :))\mathbf{U}_{i,j}(k-i)) \end{aligned} \quad (6.31)$$

where c is a constant. Equivalently, we have,

$$\begin{aligned} & CA^{\gamma-1}X(k-i) + (\mathbf{E}_{p-}((i+\gamma-1)l' : (i+\gamma)l', :))\mathbf{W}_{i,j}(k-i) + \mathbf{V}_{1,j}^{p-}(k-i+\gamma) \\ &= c(CA^{\beta-1}X(k-i) + (\mathbf{E}_{p-}((i+\beta-1)l' : (i+\beta)l', :))\mathbf{W}_{i,j}(k-i) + \mathbf{V}_{1,j}^{p-}(k-i+\beta)) \end{aligned} \quad (6.32)$$

If we multiply both sides of equation (6.32) by $(\mathbf{V}_{1,j}^{p-}(k-i+\beta))^T$ and take the limit as $j \rightarrow \infty$, all the terms will be zero except for the last one since all the terms except the last one are uncorrelated with $(\mathbf{V}_{1,j}^{p-}(k-i+\beta))$. Therefore, we obtain $0 = c$, which is a contradiction. Therefore, $\hat{\Gamma}_0^{p-}$ is full row rank. \square

The matrix $\hat{\mathbf{M}}_{p-}$ has a particular structure as shown in the following lemma.

Lemma 6.2. *The matrix $\hat{\mathbf{M}}_{p-}$ has the following structure,*

$$\hat{\mathbf{M}}_{p-} = \begin{bmatrix} 0_{(i-1)l' \times l'} & \mathbf{I}_{(i-1)l' \times (i-1)l'} \\ \mathbf{K}_1 & \mathbf{K}_2 \end{bmatrix} \quad (6.33)$$

where $\mathbf{K}_1 \in \mathbb{R}^{l' \times l'}$ and $\mathbf{K}_2 \in \mathbb{R}^{l' \times (i-1)l'}$ are nonzero matrices, where $l' = l - n_p$.

Proof. One can partition $\hat{\Gamma}_0^{p-}$ and $\hat{\Gamma}_1^{p-}$ as follows,

$$\hat{\Gamma}_0^{p-} = \begin{bmatrix} \hat{\Gamma}_{01} \\ \hat{\Gamma}_{02} \end{bmatrix}; \quad \hat{\Gamma}_1^{p-} = \begin{bmatrix} \hat{\Gamma}_{11} \\ \hat{\Gamma}_{12} \end{bmatrix} \quad (6.34)$$

where $\hat{\Gamma}_{01} \in \mathbb{R}^{l' \times il'}$, $\hat{\Gamma}_{02} \in \mathbb{R}^{(i-1)l' \times il'}$, $\hat{\Gamma}_{11} \in \mathbb{R}^{l' \times il'}$ and $\hat{\Gamma}_{12} \in \mathbb{R}^{(i-1)l' \times il'}$. It follows readily from definitions of $\hat{\Gamma}_0^{p-}$ and $\hat{\Gamma}_1^{p-}$ (equations (6.28) and (6.29)) that $\hat{\Gamma}_{11} = \hat{\Gamma}_{02}$. Since $\hat{\Gamma}_0^{p-}$ is full row rank, therefore we have

$$\hat{\Gamma}_{11} = \begin{bmatrix} 0 & \mathbf{I} \end{bmatrix} \begin{bmatrix} \hat{\Gamma}_{01} \\ \hat{\Gamma}_{02} \end{bmatrix} \quad (6.35)$$

Moreover, $\hat{\Gamma}_{12}$ can be written as a linear combination of the rows of $\hat{\Gamma}_{01}$ and $\hat{\Gamma}_{02}$ as follows,

$$\hat{\Gamma}_{12} = \begin{bmatrix} \mathbf{K}_1 & \mathbf{K}_2 \end{bmatrix} \begin{bmatrix} \hat{\Gamma}_{01} \\ \hat{\Gamma}_{02} \end{bmatrix} \quad (6.36)$$

Consequently, we obtain,

$$\hat{\Gamma}_1^{p-} = \begin{bmatrix} 0 & \mathbf{I} \\ \mathbf{K}_1 & \mathbf{K}_2 \end{bmatrix} \hat{\Gamma}_0^{p-} \quad (6.37)$$

which reveals the general structure of $\hat{\mathbf{M}}_{p-}$ as given by equation (6.33). \square

Lemma 6.3. *The matrix $\hat{\mathbf{M}}_{p-}$ is Hurwitz.*

Proof. Let us define $\psi(k-i) = \mathbf{Y}_{i,j}^{p-}(k-i) - \hat{\mathbf{D}}_{p-}\mathbf{U}_{i,j}(k-i)$. Therefore, $\psi(k-i+1)$ is governed by,

$$\begin{aligned} \psi(k-i+1) &= \mathbf{Y}_{i,j}^{p-}(k-i+1) - \hat{\mathbf{D}}_{p-}\mathbf{U}_{i,j}(k-i+1) \\ &= \mathbf{Y}_{(i+1),j}^{p-}(k-i+1) - \hat{\mathbf{D}}_{+,p-}\mathbf{U}_{(i+1),j}(k-i) - \hat{\mathcal{D}}_{+,p-}\mathbf{I}_{l'}^m\mathbf{U}_{i,j}(k-i) \\ &= \hat{\mathbf{M}}_{p-}\psi(k-i) - \hat{\mathcal{D}}_{+,p-}\mathbf{I}_{l'}^m\mathbf{U}_{i,j}(k-i) \end{aligned} \quad (6.38)$$

Due to the fact that $\psi(k-i)$ is bounded, therefore $\hat{\mathbf{M}}_{p-}$ is a Hurwitz matrix. This completes the proof of the lemma. \square

The above analysis shows that the estimation filter (6.10), which satisfies the condition (6.11), can be directly synthesized from the system I/O data *without* requiring any reduction step. The data-driven counterparts of equations (6.14) and (6.15) to (6.18) is now given by,

$$\hat{A}_r \quad \text{is Hurwitz} \quad (6.39)$$

$$\hat{A}_r + \hat{L}_r = \hat{\mathbf{M}}_{p-} \quad (6.40)$$

$$\hat{L}_r\hat{\mathbf{D}}_{p-}^{q+} - \hat{\mathcal{D}}_{+,p-}^{q+}\mathbf{I}_{l'}^{nq} = 0 \quad (6.41)$$

$$\hat{B}_r + \hat{L}_r\hat{\mathbf{D}}_{p-}^{q-} - \hat{\mathcal{D}}_+^{q-}\mathbf{I}_{l'}^{m'} = 0 \quad (6.42)$$

Theorem 6.3. Equations (6.39) to (6.42) have a solution if and only if $\hat{M}^{p-} - \hat{\mathcal{D}}_{+,p-}^{q+} \mathbf{I}_{l'}^{n_q} (\hat{\mathbf{D}}_{p-}^{q+})^\dagger - \Theta_1 (\mathbf{I} - \hat{\mathbf{D}}_{p-}^{q+} (\hat{\mathbf{D}}_{p-}^{q+})^\dagger)$ is Hurwitz for an arbitrary matrix $\Theta_1 \in \mathbb{R}^{il' \times il'}$.

Proof. Solving equation (6.41) for \hat{L}_r yields,

$$\hat{L}_r = \hat{\mathcal{D}}_{+,p-}^{q+} \mathbf{I}_{l'}^{n_q} (\hat{\mathbf{D}}_{p-}^{q+})^\dagger + \Theta_1 (\mathbf{I} - \hat{\mathbf{D}}_{p-}^{q+} (\hat{\mathbf{D}}_{p-}^{q+})^\dagger)$$

Substituting the above expression in equation (6.40) and comparing it with equation (6.39) concludes the result. \square

The arbitrary matrix Θ_1 in \hat{L}_r should be selected such that equation (6.39) is satisfied. Note that equation (6.41) and the free parameter Θ_1 vanish when $q = \{\emptyset\}$. Therefore, one can arbitrarily select a Hurwitz matrix \hat{A}_r and then obtain \hat{L}_r and \hat{B}_r from equations (6.41) and (6.42).

6.3.2 Fault Detection and Isolation Filters

Our proposed residual generator fault detection and isolation filter has the general structure that is as governed by,

$$\begin{cases} \eta(k+1) = \hat{A}_r \eta(k) + \hat{B}_r \mathbf{U}^{q-}(k-i) + \hat{L}_r \mathbf{Y}^{p-}(k-i) \\ \hat{r}(k) = \mathbf{I}_f (\eta(k) - \mathbf{Y}_i^{p-}(k-i) + \hat{\mathbf{D}}_{p-} \mathbf{U}(k-i)) \end{cases} \quad (6.43)$$

where $\hat{r}(k)$ denotes the residual signal, $\mathbf{I}_f = \mathbf{I}_m^m$ if $q \neq \{\emptyset\}$ and $\mathbf{I}_f = \mathbf{I}$, otherwise. The filter parameters are obtained from equations (6.39) to (6.42). The above general structure can be configured for both single or concurrent fault detection, isolation or estimation tasks by invoking different settings for p and q . Specifically, if both p and q are set to be empty sets, then the filter (6.43) will be in fact a fault detection filter.

Fault isolation is typically performed via *structured residuals*. In other words, a bank of residual observers is constructed where each filter in the bank is insensitive to a particular fault but sensitive to all the other faults. Therefore, in case

of occurrence of a fault, all the filters generate non-zero residuals that exceed their thresholds except for the one filter that can be used for determining the isolated fault. This can be achieved by invoking different settings for p and q for each filter in the bank.

For example, if a single actuator fault isolation scheme for a system with three inputs and four measurements is desired, then a bank that consists of three filters should be constructed. A possible configuration setting for the filters 1,2 and 3 in the bank is $q = \{1, 2\}$, $q = \{1, 3\}$ and $q = \{2, 3\}$, respectively, and $p = \{\emptyset\}$ for all. Alternatively, one may try the setting $q = \{1\}$, $p = \{3, 4\}$, $q = \{2\}$, $p = \{1, 2, 4\}$, and $q = \{1, 3\}$, $p = \{1, 3\}$ for the filters 1, 2 and 3, respectively. A particular configuration selection depends on the context of the problem and the requirements. Despite the above flexibility, our proposed scheme has a limitation that it cannot handle simultaneous concurrent actuator and sensor faults. This situation differs from the concurrent actuators or concurrent sensors faults which is well managed within our proposed framework.

The residuals that are generated by the filter (6.43) has an important property that is characterized in the next lemma.

Lemma 6.4. *Given $q = \{\emptyset\}$ and \hat{A}_r selected to be a diagonal Hurwitz matrix, then the first $(i-1)l'$ rows of $\hat{r}(k)$ converge to zero as $k \rightarrow \infty$ independent of the presence of the faults.*

Proof. We show that the first $(i-1)l$ rows of the residuals generated by the filter (6.43) approach to zero as $k \rightarrow \infty$ if $q = \{\emptyset\}$. We begin by noting that,

$$\hat{r}(k+1) = \eta(k+1) - \mathbf{Y}^{p^-}(k-i+1) + \hat{\mathbf{D}}_{p^-} \mathbf{U}(k-i+1) \quad (6.44)$$

Substituting $\eta(k+1)$ from the state equation of the filter (6.43) yields,

$$\hat{r}(k+1) = \hat{A}_r \eta(k) + \hat{B}_r \mathbf{U}(k-i) + \hat{L}_r \mathbf{Y}(k-i) - \mathbf{Y}^{p^-}(k-i+1) + \hat{\mathbf{D}}_{p^-} \mathbf{U}(k-i+1) \quad (6.45)$$

Next, we substitute \hat{B}_r and \hat{L}_r from equations (6.40), (6.41) and (6.42) and rearrange it to obtain,

$$\begin{aligned} \hat{r}(k+1) &= \hat{A}_r r(k) - \hat{\mathbf{M}}_{p-} \left(\mathbf{Y}^{p-}(k-i) - \hat{\mathbf{D}}_{p-} \mathbf{U}(k-i) \right) \\ &\quad - \mathbf{Y}^{p-}(k-i+1) + \hat{\mathbf{D}}_{p-} \mathbf{U}(k-i+1) + \hat{\mathcal{D}}_{+,p-} \mathbf{I}_l^m \mathbf{U}(k-i) \end{aligned} \quad (6.46)$$

Note that,

$$\hat{\mathbf{D}}_{p-} \mathbf{U}(k-i+1) + \hat{\mathcal{D}}_{+,p-} \mathbf{I}_l^m \mathbf{U}(k-i) = \hat{\mathbf{D}}_{+,p-} \mathbf{U}_+(k-i)$$

Therefore, by considering the structure of $\hat{\mathbf{M}}_{p-}$ in Lemma 6.2, one can verify that (E.3) becomes,

$$\hat{r}(k+1) = \hat{A}_r \hat{r}(k) + \begin{bmatrix} 0_{(i-1)l \times 1} \\ y^{p-}(k+1) - \bar{\mathbf{D}}_{+,p-} \mathbf{U}_+(k-i) \end{bmatrix} \quad (6.47)$$

which shows that if \hat{A}_r is a diagonal Hurwitz matrix, then the first $(i-1)l$ rows of $\hat{r}(k)$ approach to zero as $k \rightarrow \infty$. Note that we did not use the relation $\hat{\mathbf{M}}\hat{\Gamma}_0(:, 1) = \hat{\Gamma}_1(:, 1)$ that only holds for the healthy system. In that case, we would clearly obtain $\hat{r}(k+1) = \hat{A}_r \hat{r}(k) + 0$, which is a valid model. This completes the proof of the lemma. \square

Based on the above lemma, the first $(i-1)l'$ rows of $\hat{r}(k)$ do not contain any useful information that would allow a model reduction. The general structure of the residual generator filter for the actuator or sensor fault detection or the sensor fault isolation ($q = \{\emptyset\}$) is then given by,

$$\begin{cases} \eta_r(k+1) = \hat{A}_r \eta_r(k) + \hat{B}_r \mathbf{U}(k-i) + \hat{L}_r \mathbf{Y}^{p-}(k-i) \\ \hat{r}(k) = \eta_r(k) - y^{p-}(k) + \hat{\mathbf{D}}_{p-} \mathbf{U}(k-i) \end{cases} \quad (6.48)$$

where $\eta_r(k) \in \mathbb{R}^{l'}$, $\hat{A}_r = A_r((i-1)l' + 1 : il', il' + 1 : il')$, $\hat{B}_r = \hat{B}_r((i-1)l' + 1 : il', :)$, $\hat{L}_r = \hat{L}_r((i-1)l' + 1 : il', :)$ and $\hat{\mathbf{D}}_{i,p-} = \hat{\mathbf{D}}_{i,p-}((i-1)l' + 1 : il', :)$.

The same model reduction procedure cannot be applied to the actuator fault isolation filter (i.e. when $q \neq \{\emptyset\}$) since \hat{A}_r that is obtained from equations (6.39) to (6.42) is not necessarily diagonal.

6.3.3 Residual Dynamics In Presence of A Fault

Let us now investigate the corresponding residual dynamics in presence of faults. If $f^a(k)$ and/or $f^s(k)$ are nonzero, then the residual dynamics is given by,

$$\begin{cases} \eta(k+1) = \hat{A}_r \eta(k) + \hat{B}_r (\mathbf{U}^{q^-}(k-i) + \mathbf{F}^{a,q^-}(k-i)) + \hat{L}_r (\mathbf{Y}^{p^-}(k-i) + \mathbf{F}^{s,p^-}(k-i)) \\ \hat{r}(k) = \mathbf{I}_f \left(\eta(k) - \mathbf{Y}_i^{p^-}(k-i) - \mathbf{F}^{s,p^-}(k-i) + \hat{\mathbf{D}}_{p^-} (\mathbf{U}(k-i) + \mathbf{F}^a(k-i)) \right) \end{cases} \quad (6.49)$$

where $\mathbf{F}^a(k-i)$ and $\mathbf{F}^s(k-i)$ are construed similar to $\mathbf{G}(k-i)$ using the actuator fault and the sensor fault signals, respectively. The vectors $\mathbf{F}^{a,q^-}(k-i)$ and $\mathbf{F}^{s,p^-}(k-i)$ are then obtained by deleting the rows q, \dots, iq and p, \dots, ip of $\mathbf{F}^a(k-i)$ and $\mathbf{F}^s(k-i)$, respectively. The filter dynamics (6.49) shows that the residual $\hat{r}(k)$ is clearly affected by the faults except those in the sensors p or the actuators q .

Conventionally, the following decision logic is utilized for performing the fault detection task, namely

$$\begin{cases} \text{If } r_{min} \leq \mathbb{E}\{\|\hat{r}(k)\|\} \leq r_{max} \Rightarrow \text{System is healthy} \\ \text{If } \mathbb{E}\{\|\hat{r}(k)\|\} < r_{min} \text{ or } \mathbb{E}\{\|\hat{r}(k)\|\} > r_{max} \Rightarrow \text{System is faulty} \end{cases} \quad (6.50)$$

where r_{min} and r_{max} denote the lower and the upper bound thresholds, respectively. The thresholds are selected through conducting comprehensive Monte Carlo simulation runs so that the missed alarms and false alarms are minimized.

A similar structure can be utilized for selecting the fault isolation decision

logic. Specifically, a fault is detected and isolated in the actuator q_0 if,

$$\begin{cases} \mathbb{E}\{\|\hat{r}^a(k)\|\} < r_{min} \text{ or } \mathbb{E}\{\|\hat{r}^a(k)\|\} > r_{max} & ; a \neq q_0, a = 1, \dots, m, \text{ and} \\ r_{min} \leq \mathbb{E}\{\|\hat{r}^a(k)\|\} \leq r_{max} & ; a = q_0. \end{cases} \quad (6.51)$$

where $\hat{r}^a(k)$ denotes the residual that is obtained by setting $q = \{a\}$.

This completes our proposed solution to the problem of data-driven fault detection and isolation. In the next section, we consider the problem of data-driven fault estimation.

6.4 The Proposed Fault Estimation Scheme

In many practical control problems, it is crucial to estimate the faults once they are detected and isolated. In this section, we provide a data-driven based methodology for design of fault estimation filters. Our proposed fault estimation scheme can be integrated with the FDI scheme. In other words, the FDI scheme introduced in the previous section can be utilized to distinguish between the healthy actuators and sensors from those where their data are used for fault estimation of faulty actuators and sensors.

In this section, we first propose fault estimation filters. It turns out that these filters are biased due to presence of estimation errors in the Markov parameters and the matrix $\hat{\mathbf{M}}_p$. We then derive the dynamics corresponding to the fault estimation errors and show that it can be directly identified from the healthy system I/O data. Finally, we propose our so-called *tuned fault estimation filters* that are obtained for a reliable and actuator fault estimation by integrating the proposed estimation filters with the identified estimation error dynamics.

6.4.1 Sensor Fault Estimation Filters

The following filter is now proposed to estimate the faults in the sensors p by using data from the sensors $\sim p$ and all the actuators,

$$\begin{cases} \eta(k+1) = \hat{A}_r \eta(k) + \hat{B}_r \mathbf{U}(k-i) + \hat{L}_r^{p\downarrow} \mathbf{Y}(k-i) \\ \hat{f}^s(k-i) = \mathbf{I}_l^l \left(\eta(k) - \mathbf{Y}(k-i) + \hat{\mathbf{D}} \mathbf{U}(k-i) \right) \end{cases} \quad (6.52)$$

where $\hat{f}^s(k-i)$ denotes an estimate of $f^s(k-i)$ and the filter parameters are obtained from the equations (6.39) to (6.42) by setting $p = q = \{\emptyset\}$ and by replacing \hat{L}_r with $\hat{L}_r^{p\downarrow}$.

Clearly, the filter (6.52) is biased due to presence of estimation errors in the Markov parameters and the matrix $\hat{\mathbf{M}}$. The matrix $\hat{\mathbf{M}}$ is defined to be the same as $\hat{\mathbf{M}}_{p-}$ when $p = \{\emptyset\}$. Let us define the estimation error as $\Delta f^s(k) = f^s(k-i) - \hat{f}^s(k-i)$. Therefore, we have,

$$\Delta f^s(k-i) = \mathbf{I}_l^l (\xi(k) + \Delta \mathbf{D} \mathbf{U}(k-i) + \mathbf{E} \mathbf{W}(k-i) + \mathbf{V}(k-i)) \quad (6.53)$$

where $\xi(k) = \mathbf{C}x(k-i) - \eta(k)$ and $\Delta \mathbf{D} = \mathbf{D} - \hat{\mathbf{D}}$. The dynamics of $\xi(k)$ is now governed by,

$$\begin{aligned} \xi(k+1) &= \hat{A}_r \xi(k) + (\hat{A}_r - \mathbf{M} + \hat{L}_r^{p\downarrow}) \mathbf{C}x(k-i) \\ &+ (\hat{B}_r + \hat{L}_r^{p\downarrow} \mathbf{D} - \mathbf{C} \mathbf{B} \mathbf{I}_l^m) \mathbf{U}(k-i) \\ &+ \hat{L}_r^{p\downarrow} \mathbf{E} \mathbf{W}(k-i) + \hat{L}_r^{p\downarrow} \mathbf{V}(k-i) \end{aligned} \quad (6.54)$$

The matrix \mathbf{M} is equal to \mathbf{M}_{p-} when $p = \{\emptyset\}$. We substitute $\mathbf{C}x(k-i)$ by $\mathbf{Y}(k-i) - \mathbf{D} \mathbf{U}(k-i) - \mathbf{F}^s(k-i) - \mathbf{E} \mathbf{W}(k-i) - \mathbf{V}(k-i)$ in the above equation. Rearranging of the right hand side of the above equation after substitution yields the governing

dynamics of the fault estimation error as follows,

$$\begin{cases} \xi(k+1) = \hat{A}_r \xi(k) + \Delta_u \mathbf{U}(k-i) + \Delta_y \mathbf{Y}(k-i) - \Delta_y \mathbf{F}^s(k-i) \\ \quad + \mathcal{M}_1 \mathbf{W}(k-i) + \mathcal{M}_2 \mathbf{V}(k-i) \\ \Delta f^s(k-i) = \mathbf{I}_i^l (\xi(k) + \Delta \mathbf{D} \mathbf{U}(k-i) + \mathbf{E} \mathbf{W}(k-i) + \mathbf{V}(k-i)) \end{cases} \quad (6.55)$$

where $\delta A = \hat{A}_r - \mathbf{M} + \hat{L}_r^{p\downarrow}$, $\delta B = \hat{B}_r + \hat{L}_r^{p\downarrow} \mathbf{D} - \mathbf{C} \mathbf{B} \mathbf{I}_l^m$, $\Delta_u = \delta B - \delta A \mathbf{D}$, $\Delta_y = \delta A$, $\mathcal{M}_1 = \hat{L}_r^{p\downarrow} \mathbf{E} - \delta A \mathbf{E}$ and $\mathcal{M}_2 = \hat{L}_r^{p\downarrow} \delta A$.

Equation (6.55) clearly shows that the fault estimates are biased. All the parameters in the filter (6.55) are unknown since their computation requires the exact Markov parameters and the matrix \mathbf{M} . However, we will show that one can actually obtain an estimate of Δ_u , Δ_y and $\Delta \mathbf{D}$ by using the healthy I/O data.

Towards this end, we split the off-line available healthy I/O data into two segments. The first segment is utilized to estimate the system Markov parameters and the matrix $\hat{\mathbf{M}}$. Once the filter (6.52) is constructed, it is stimulated by the second segment of the I/O data to obtain $\hat{f}^s(k-i)$ using an arbitrary initial condition for $\eta(0)$ in (6.52). Theoretically, $\hat{f}^s(k-i)$ should be zero corresponding to the second segment of the healthy data, however, it will be biased due to presence of the estimation errors in the Markov parameters and the matrix $\hat{\mathbf{M}}$. The bias is governed and is given by $\Delta f^s(k) = f^s(k-i) - \hat{f}^s(k-i) \equiv -\hat{f}^s(k-i)$, and according to equation (6.55) is governed by,

$$\begin{cases} \xi(k+1) = \hat{A}_r \xi(k) + \Delta_u \mathbf{U}(k-i) + \Delta_y \mathbf{Y}(k-i) + \mathcal{M}_1 \mathbf{W}(k-i) + \mathcal{M}_2 \mathbf{V}(k-i) \\ \Delta f^s(k) = \mathbf{I}_i^l (\xi(k) + \Delta \mathbf{D} \mathbf{U}(k-i) + \mathbf{E} \mathbf{W}(k-i) + \mathbf{V}(k-i)) \end{cases} \quad (6.56)$$

One may consider the filter (6.56) as a stochastic LTI system that is described by the quadruple $(\mathcal{A}, \mathcal{B}, \mathcal{C}, \mathcal{G}) \equiv \left(\hat{A}_r, \begin{bmatrix} \Delta_u^T & \Delta_y^T \end{bmatrix}^T, \mathbf{I}_i^l, \begin{bmatrix} \Delta \mathbf{D}^T & 0 \end{bmatrix}^T \right)$. The process and measurement noise are given by $\mathcal{M}_1 \mathbf{W}(k-i) + \mathcal{M}_2 \mathbf{V}(k-i)$ and $\mathbf{E} \mathbf{W}(k-i) + \mathbf{V}(k-i)$, respectively. The matrices \mathcal{A} and \mathcal{C} and the order of this system are already known.

Given that $\Delta f^s(k) = -\hat{f}^s(k-i)$ corresponding to the second segment of the healthy data, and \mathcal{A} and \mathcal{C} , one can *estimate* \mathcal{B} and $\mathcal{G} = \begin{bmatrix} \mathcal{G}_1 & 0 \end{bmatrix}$ by invoking an optimization problem that is described in detail below.

Let us define the matrices $\mathcal{E}_{1,j}(k)$ and $\mathcal{Z}_{(\lambda-1),j}(k)$ similar to $\mathbf{G}_{i,j}(k)$ by replacing the signal $g(k)$ with the signals $-\hat{f}^s(k-i)$ and $\mathbf{Z}(k)$, respectively, where $\mathbf{Z}(k) = \begin{bmatrix} \mathbf{U}(k) \\ \mathbf{Y}(k) \end{bmatrix}$, and j is selected as large as the available data of the second segment allows. Therefore, for the system (6.56), we have,

$$\mathcal{E}_{1,j}(k) = \mathcal{C}\mathcal{A}^\lambda \xi(k-\lambda) + \mathcal{T}_{1,\lambda} \mathcal{Z}_{(\lambda-1),j}(k-\lambda) + ST \quad (6.57)$$

where the term ST denotes the stochastic terms which have zero mean and are neglected here for sake of brevity, and $\mathcal{T}_{1,\lambda}$ is defined as,

$$\mathcal{T}_{1,\lambda} = \begin{pmatrix} \mathcal{H}_{\lambda-1} & \mathcal{H}_{\lambda-2} & \dots & \mathcal{H}_0 & \mathcal{G} \end{pmatrix} \quad (6.58)$$

where $\mathcal{H}_\beta = \mathcal{C}\mathcal{A}^\beta \mathcal{B}$. The definition (6.58) shows dependence of $\mathcal{T}_{1,\lambda}$ on the matrices \mathcal{B} and \mathcal{G} . If λ is selected such that $\mathcal{A}^\lambda \approx 0$, then according to equation (6.57), one can obtain the estimates $\hat{\mathcal{B}}$ and $\hat{\mathcal{G}}$ by invoking the following minimization problem,

$$\begin{aligned} & \underset{\mathcal{B}, \mathcal{G}_1}{\text{minimize}} && \|\mathcal{E}_{1,j}(k) - \mathcal{T}_{1,\lambda} \mathcal{Z}_{(\lambda-1),j}(k-\lambda)\|_2 \\ & \text{subject to} && (\mathcal{B}(:, im+1 : im+il))^{p+} = 0. \end{aligned} \quad (6.59)$$

The constraint above does in fact enforce the columns p, \dots, ip of Δ_y to be equal to zero. For the case of sensor fault estimation problem, \hat{A}_r is selected to be an arbitrary Hurwitz matrix, therefore $\hat{A}_r = A_r$. On the other hand, $\Delta_y = \delta A = \hat{A}_r - \mathbf{M} + \hat{L}_r^{p\downarrow} = A_r - \mathbf{M} + \hat{L}_r^{p\downarrow} = -L_r^{p\downarrow} + \hat{L}_r^{p\downarrow}$. Therefore, the columns p, \dots, ip corresponding to Δ_y should be equal to zero.

A methodology for solving the minimization problem (6.59) is provided in Section 6.4.3. The solution will be consistent if the matrix $\mathcal{Z}_{(\lambda-1),j}(k)$ is full row rank

which is not generally guaranteed. This condition on the matrix $\mathcal{Z}_{(\lambda-1),j}(k)$ depends on the nature of the system feedback control, the excitation signal and the available data and the real model of the system ([92, 97, 135]).

If the above condition on $\mathcal{Z}_{(\lambda-1),j}(k)$ is not satisfied, then the solution that is obtained by invoking the pseudo-inverse of $\mathcal{Z}_{(\lambda-1),j}(k)$ still minimizes the cost function in (6.59), but it will be biased.

An estimate of the error dynamics in presence of the sensor faults is therefore given by,

$$\begin{cases} \hat{\xi}(k+1) = \hat{A}_r \hat{\xi}(k) + \hat{\mathcal{B}} \mathbf{Z}(k-i) - \hat{\Delta}_y \mathbf{F}^s(k-i) \\ \Delta \hat{f}^s(k) = \mathbf{I}_i^l \left(\hat{\xi}(k) + \hat{\mathcal{G}}_1 \mathbf{U}(k-i) \right) \end{cases} \quad (6.60)$$

where $\Delta \hat{f}^s(k)$ is an estimate of $\Delta f^s(k)$. We assumed that the sensors $\sim p$ are healthy for the purpose of fault estimation of the sensors p . Moreover, the columns p, \dots, ip of $\hat{\Delta}_y$ are enforced to be zero in the minimization problem (6.59). Therefore, $\hat{\Delta}_y \mathbf{F}^s(k-i)$ is practically zero.

Consequently, one can now construct a new and a so-called *tuned* sensor fault estimation filter that is governed by,

$$\begin{cases} \eta(k+1) = \hat{A}_r \eta(k) + \tilde{\mathcal{B}}_s \mathbf{Z}(k-i) \\ \hat{f}^s(k-i) = \mathbf{I}_i^l \left(\eta(k) - \mathbf{Y}(k-i) + \tilde{\mathcal{D}}_s \mathbf{U}(k-i) \right) \end{cases} \quad (6.61)$$

where $\hat{f}^s(k-i)$ denotes the tuned estimate of the sensor fault, $\tilde{\mathcal{B}}_s = \begin{bmatrix} \hat{B}_r & \hat{L}^{p\downarrow} \end{bmatrix} + \hat{\mathcal{B}}$ and $\tilde{\mathcal{D}}_s = \hat{\mathbf{D}} + \hat{\mathcal{G}}_1$, where $\hat{\mathcal{B}}$ and $\hat{\mathcal{G}}_1$ are obtained and given by the minimization problem (6.59).

6.4.2 Actuator Fault Estimation Filters

The same procedure can now be followed for the actuator fault estimation filter. First, the following fault filter estimation is considered for the actuators q by using the data from the sensors $\sim p$ and actuators $\sim q$, namely

$$\begin{cases} \eta(k+1) = \hat{A}_r \eta(k) + \hat{B}_r \mathbf{U}^{q^-}(k-i) + \hat{L}_r \mathbf{Y}^{p^-}(k-i) \\ \hat{f}^a(k-i) = -\mathbf{I}_m^m \hat{\mathbf{D}}_{p^-}^\dagger (\eta(k) - \mathbf{Y}^{p^-}(k-i) + \hat{\mathbf{D}}_{p^-} \mathbf{U}(k-i)) \end{cases} \quad (6.62)$$

where $\hat{f}^a(k-i)$ denotes an estimate of $f^a(k-i)$ and the filter parameters are obtained from the solution to the equations (6.39) to (6.42).

However, following along the same lines as those used in the Subsection 6.4.1, the so-called *tuned* actuator fault estimation filter is now proposed as follows,

$$\begin{cases} \eta(k+1) = \hat{A}_r \eta(k) + \tilde{\mathbf{B}}_a \mathbf{Z}^{q^-, p^-}(k-i) \\ \hat{f}^a(k-i) = -\mathbf{I}_m^m \tilde{\mathbf{D}}_a^\dagger (\eta(k) - \mathbf{Y}^{p^-}(k-i) + \tilde{\mathbf{D}}_a \mathbf{U}(k-i)) \end{cases} \quad (6.63)$$

where $\tilde{\mathbf{B}}_a = \begin{bmatrix} \hat{B}_r & \hat{L}_r \end{bmatrix} + \hat{\mathbf{B}}$ and $\tilde{\mathbf{D}}_a = \hat{\mathbf{D}}_{p^-} + \hat{\mathbf{G}}_1$. The parameters $\hat{\mathbf{B}}$ and $\hat{\mathbf{G}}_1$ are obtained by invoking the following minimization problem,

$$\underset{\tilde{\mathbf{B}}, \tilde{\mathbf{G}}_1}{\text{minimize}} \quad \|\mathcal{E}_{1,j}(k) - \mathcal{T}_{1,\lambda} \mathcal{Z}_{(\lambda-1),j}^{q^-, p^-}(k-\lambda)\|_2 \quad (6.64)$$

where the matrices $\mathcal{E}_{1,j}(k)$ and $\mathcal{Z}_{(\lambda-1),j}^{q^-, p^-}(k)$ are constructed similar to $\mathbf{G}_{i,j}(k)$ by replacing the signal $g(k)$ with the signals $-\hat{f}^a(k-i)$ and $\mathbf{Z}^{q^-, p^-}(k)$, respectively, and

where $\mathbf{Z}^{q^-, p^-}(k) = \begin{bmatrix} \mathbf{U}^{q^-}(k) \\ \mathbf{Y}^{p^-}(k) \end{bmatrix}$, and j is selected as large as the available data corresponding to the second segment allows. Note that the signal $-\hat{f}^a(k-i)$ for construction of the matrix $\mathcal{E}_{1,j}(k)$ is obtained by stimulating the filter (6.62) with the second segment of the healthy I/O data using an arbitrary initial condition for $\eta(0)$.

The above minimization problem is solved similar to the problem (6.59) as described in Section 6.4.3. We will demonstrate in the next section that the above tuning procedures will significantly improve the faults estimation accuracy performance. Similarly, the same tuning procedure can be applied to the fault detection and isolation filters in order to improve their performance when applied to a specific application. However, these details are left as topics of our future work.

Remark 6.6. *As stated earlier in this section, one should partition the available off-line I/O data before applying the above tuning procedure. The length of the data in the segment that is used for solving the minimization problem (6.59) or (6.64) must be at least greater than λ , where λ was selected such that $\mathcal{A}^\lambda \approx 0$.*

6.4.3 A Methodology for Solving the Minimization Problems

The constraint in the optimization problem (6.59) enforces that columns that multiplied by the rows p, \dots, ip of $\mathbf{Y}(k)$ should be zero. Therefore, they can be simply removed by using $\mathcal{Z}^{\{\emptyset\},p^-}(k)$ instead of $\mathcal{Z}(k)$ and by invoking now the following optimization problem,

$$\underset{\mathcal{B}^\phi, \mathcal{G}_1}{\text{minimize}} \quad \|\mathcal{E}_{1,j}(k) - \mathcal{T}_{1,\lambda}^\phi \mathcal{Z}_{(\lambda-1),j}^{\{\emptyset\},p^-}(k-\lambda)\|_2 \quad (6.65)$$

where

$$\mathcal{T}_{1,\lambda}^\phi = \begin{pmatrix} \mathcal{C}\mathcal{A}^{\lambda-1}\mathcal{B}^\phi & \mathcal{C}\mathcal{A}^{\lambda-2}\mathcal{B}^\phi & \dots & \mathcal{C}\mathcal{B}^\phi & \mathcal{G} \end{pmatrix} \quad (6.66)$$

Once $\hat{\mathcal{B}}^\phi$ is computed, $\hat{\mathcal{B}}$ is easily constructed by inserting back zero columns at the columns $im + p, im + 2p, \dots, im + ip$ of the matrix $\hat{\mathcal{B}}^\phi$. An estimate of $\hat{\mathcal{T}}_{1,\lambda}^\phi$ is now given by,

$$\begin{aligned} \hat{\mathcal{T}}_{1,\lambda}^\phi &= \mathcal{E}_{1,j}(k) \left(\mathcal{Z}_{(\lambda-1),j}^{\{\emptyset\},p^-}(k-s) \right)^\dagger \\ &= \begin{bmatrix} \hat{\mathcal{T}}_1 & \dots & \hat{\mathcal{T}}_\lambda \end{bmatrix} \end{aligned} \quad (6.67)$$

where $\hat{\mathcal{T}}_\alpha \in \mathbb{R}^{l \times (im+il-in_p)}$. We reformulate the definition (6.66) in the matrix form as follows,

$$\begin{bmatrix} \hat{\mathcal{T}}_1 \\ \vdots \\ \hat{\mathcal{T}}_\lambda \end{bmatrix} = \begin{bmatrix} \mathfrak{C} & 0 \\ 0 & I \end{bmatrix} \begin{bmatrix} \hat{\mathcal{B}}^\phi \\ \hat{\mathcal{G}}_1 \end{bmatrix} \quad (6.68)$$

where,

$$\mathfrak{C} = \begin{bmatrix} \mathcal{C} \\ \mathcal{C}\mathcal{A} \\ \vdots \\ \mathcal{C}\mathcal{A}^{\lambda-1} \end{bmatrix} \quad (6.69)$$

Note that we have enforced $\mathcal{G} = \begin{bmatrix} \mathcal{G}_1 & 0 \end{bmatrix}$ in the right hand side of (6.68). The solution to (6.68) is now given by,

$$\begin{bmatrix} \hat{\mathcal{B}}^\phi \\ \hat{\mathcal{G}}_1 \end{bmatrix} = \begin{bmatrix} \mathfrak{C} & 0 \\ 0 & I \end{bmatrix}^\dagger \begin{bmatrix} \hat{\mathcal{T}}_1 \\ \vdots \\ \hat{\mathcal{T}}_\lambda \end{bmatrix} \quad (6.70)$$

Note that the matrix $\begin{bmatrix} \mathfrak{C} & 0 \\ 0 & I \end{bmatrix}$ is full column rank. The above solution provides the least square solution to the minimization problem (6.65). However, if $\mathcal{Z}_{(s-1),j}^{\{\emptyset\},p^-(k-s)}$ is full row rank, then the minimum value of zero will be achieved. For the problem (6.64), it is only sufficient to replace $\mathcal{Z}_{(\lambda-1),j}^{\{\emptyset\},p^-(k-\lambda)}$, $\mathcal{T}_{1,\lambda}^\phi$ and $\hat{\mathcal{B}}^\phi$ in equations (6.67) and (6.65) by $\mathcal{Z}_{(\lambda-1),j}^{q^-,p^-(k)}$, $\mathcal{T}_{1,\lambda}$, and $\hat{\mathcal{B}}$, respectively. This provides the details on the methodology for solving the minimization problems (6.59) and (6.64).

6.5 Simulation Results

In this section, we provide two numerical examples and simulations to illustrate the merits and advantages of our proposed schemes. In both cases, the healthy

input is generated by a Pseudo Random Binary Signal (PRBS) generator. The system healthy output is generated by simulating it subject to healthy input in addition to state and measurement noise ($\mathcal{N}(0, 0.1)$) as governed by the dynamics **S**. The Markov parameters are estimated by using the MATLAB built-in function *impulseest*.

Fault Detection and Isolation Results: We consider the following non-minimum phase system which includes the fault model for the actuator bias (f_k^a) and sensor bias (f_k^s) as additive terms,

$$\begin{aligned} x_{k+1} &= \begin{bmatrix} 0 & 0 & 0 & -0.01 \\ 1 & 0 & 0 & 0.08 \\ 0 & 1 & 0 & -0.27 \\ 0 & 0 & 1 & -0.54 \end{bmatrix} x_k + \begin{bmatrix} 1 & -0.3 \\ 0 & 3.82 \\ 0 & 1.55 \\ 0 & -0.61 \end{bmatrix} (u_k + f_k^a) \\ y_k &= \begin{bmatrix} 1.58 & 0.725 & -0.60 & 0.31 \\ 2.4 & -0.08 & 0.42 & -0.05 \end{bmatrix} x_k + f_k^s \end{aligned} \quad (6.71)$$

The poles and zeros of the above system are located at $\{-0.39 \pm 53j, 0.11 \pm 0.09j\}$ and $\{0.17, 1.49\}$, respectively. Figure 6.1a shows the output of the residual generator filter (equation (6.43)) for performing the fault detection task by setting $p = q = \{\emptyset\}$ when a bias fault is injected in the actuator 1 at the time instant $k = 150$. We set $i = 2$. The identification data include 1000 samples. The numerical values for the detection filter are as follows.

$$\hat{\mathbf{M}} = \begin{bmatrix} 0.00 & 0.00 & 1.00 & 0.00 \\ 0.00 & 0.00 & 0.00 & 1.00 \\ -0.30 & 0.12 & -0.51 & 0.51 \\ 0.28 & -0.11 & 0.31 & -0.16 \end{bmatrix}$$

$$\hat{A}_r = \begin{bmatrix} 0.26 & 0 \\ 0 & 0.44 \end{bmatrix}; \hat{B}_r = \begin{bmatrix} 0.70 & -0.99 & 0 & 0 \\ 0.88 & 1.01 & 0 & 0 \end{bmatrix}$$

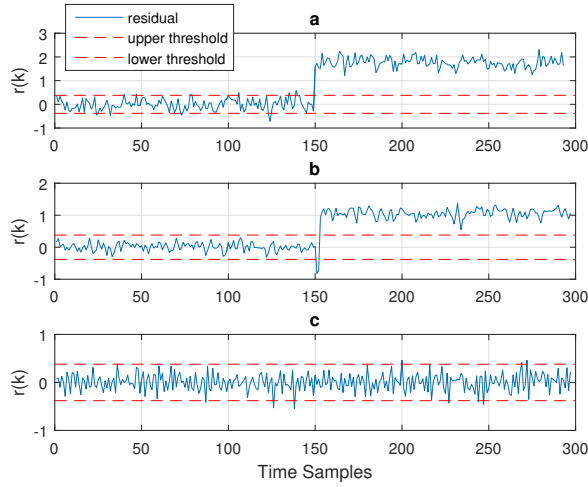


Figure 6.1: A fault is injected in the actuator 1 of the system (6.71) at $k = 150$. (a) The output of the residual generator filter for achieving the fault detection task, (b) The output of the residual generator filter insensitive to the fault in the actuator 2, and (c) The output of the residual generator filter that is insensitive to the fault in the actuator 1.

$$\hat{\hat{L}}_r = \begin{bmatrix} -0.30 & 0.12 & -0.78 & 0.5159 \\ 0.28 & -0.11 & 0.31 & -0.61 \end{bmatrix}$$

Figures 6.1b and 6.1c depict the outputs of the fault isolation filters 1 and 2 having the setting $q = \{1\}, p = \{\emptyset\}$ and $q = \{2\}, p = \{\emptyset\}$, respectively, and $i = 2$ for both. We have not yet applied the tuning process that was discussed in Section 6.4 to the above results, nevertheless these results demonstrate that actuator faults are successfully detected and isolated by application of our proposed data-driven methodology. In the next example, we will demonstrate the effects of the filter tuning process on the performance of the fault estimation accuracy.

Fault Estimation Results: Consider now the following minimum phase

system,

$$\begin{aligned}
 x_{k+1} &= \begin{bmatrix} -0.05 & -0.40 & 0 & -0.08 \\ -0.29 & -0.11 & 0.05 & -0.03 \\ -0.06 & 0.18 & -0.43 & 0.36 \\ 0.28 & 0.18 & -0.43 & 0.36 \end{bmatrix} x_k + \begin{bmatrix} -0.15 & -0.99 \\ 0 & 0 \\ -0.68 & 0.07 \\ -0.96 & -0.20 \end{bmatrix} (u_k + f_k^a) \\
 y_k &= \begin{bmatrix} -2.08 & 0 & -0.69 & 0 \\ 0 & -0.84 & 0.20 & 0.89 \end{bmatrix} x_k + f_k^s
 \end{aligned} \tag{6.72}$$

The poles and zeros of the system are located at $\{-0.37, 0.30, -0.51 \pm 0.52j\}$ and $\{0.08, -0.58\}$, respectively. We next present a typical simulation result for estimating a fault in the system (6.72), and then provide comprehensive Monte Carlo simulations. Assume that a fault having a severity of 2 is injected in the sensor 2 at the time step $k = 150$. We selected a relatively large amplitude input signal given below to magnify the presence of biases,

$$u(k) = \begin{bmatrix} 20 + 20 \sin(5k) \\ 30 + 30 \cos(7k) \end{bmatrix} \tag{6.73}$$

We set $i = 2$, $p = \{2\}$ and $q = \{\emptyset\}$. We used 700 data samples for estimation of the Markov parameters and $\hat{\mathbf{M}}$ (equation (6.30)) and 300 samples for the filter tuning process. First, we tested the performance of our proposed sensor fault estimator (6.52) that is shown in Figure 6.2(a). The results clearly indicate that the filter is biased with an estimation error of 24%. The numerical values of the filter matrices are as follows.

$$\hat{\mathbf{M}} = \begin{bmatrix} 0 & 0 & 1 & 0 \\ 0 & 0 & 0 & 1 \\ 0.06 & -0.18 & -0.19 & -0.17 \\ -0.17 & -0.43 & -0.48 & -0.81 \end{bmatrix}$$

$$\hat{B}_r = \begin{bmatrix} 0.61 & 1.61 & 0 & 0 \\ -1.06 & -0.34 & 0 & 0 \\ -0.28 & -0.51 & 0 & 0 \\ -0.15 & -1.71 & 0 & 0 \end{bmatrix}; \hat{L}_r^{p\downarrow} = \begin{bmatrix} 0.12 & 0 & 0.20 & 0 \\ 0.59 & 0 & 0.08 & 0 \\ 0.24 & 0 & 0.19 & 0 \\ 0.28 & 0 & 0.59 & 0 \end{bmatrix}$$

$$\hat{A}_r = \hat{M} - \hat{L}_r^{p\downarrow}; \hat{D} = \begin{bmatrix} 0 & 0 & 0 & 0 \\ 0 & 0 & 0 & 0 \\ 0.76 & 2.03 & 0 & 0 \\ -0.99 & -0.16 & 0 & 0 \end{bmatrix}$$

We then tune the filter by solving the minimization problem (6.59) and construct the estimation filter as described by equation (6.61). The numerical values for the matrices of the tuned filter are as follows.

$$\hat{\mathcal{B}}(:, 1 : 4) = \begin{bmatrix} -0.07 & -0.03 & 0.07 & 0.14 \\ 0.01 & -0.16 & 0.03 & 0.09 \\ 0 - 0.09 & 0.03 & 0.06 & 0 \\ -0.04 & -0.16 & 0 & 0 \end{bmatrix}$$

$$\hat{\mathcal{B}}(:, 5 : 8) = \begin{bmatrix} 0.02 & 0 & 0 & 0 \\ -0.01 & 0 & 0.02 & 0 \\ -0.01 & 0 & 0.08 & 0 \\ -0.02 & 0 & 0.17 & 0 \end{bmatrix}; \hat{\mathcal{G}} = \begin{bmatrix} 0 & 0 & 0 & 0 \\ 0 & 0 & 0 & 0 \\ -0.05 & -0.07 & 0 & 0 \\ 0 & 0 & 0 & 0 \end{bmatrix}$$

The resulting estimation error for the tuned filter is now 1% as shown in Figure 6.2(b) which illustrates a significantly improved and enhanced performance as compared to those depicted in Figure 6.2(a). A better illustration of the improved performance is now provided through Monte Carlo simulation runs as described below.

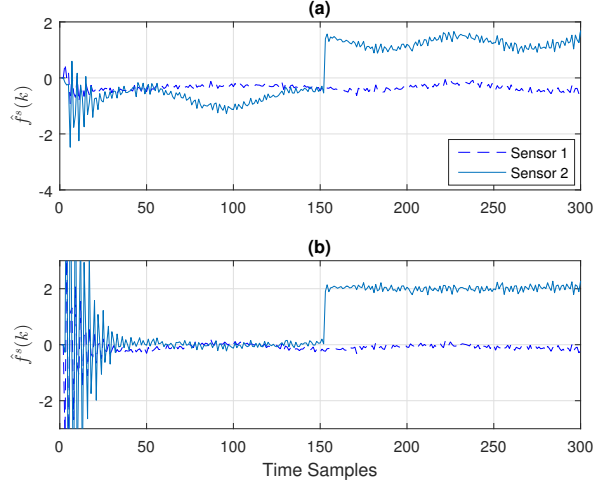


Figure 6.2: A fault having a severity of 2 is injected in the sensor 2 of the system (6.72) at $k = 150$. (a) The output of the original sensor fault estimation filter, and (b) The output of the tuned sensor fault estimation filter.

Table 6.1: The Monte Carlo simulation results for estimation of the faults in the system (6.72) using different filters and under two different system inputs, where μ and σ denote the mean and variance, respectively. The filters are specifically the sensor fault estimator (6.52), the tuned sensor fault estimator (6.61), the actuator fault estimator (6.62) and the tuned fault estimator (6.63) denoted by F(6.52), F(6.61), F(6.62) and F(6.63), respectively.

	$u_1(k)$		$u_2(k)$	
	$\mu(\Delta f)$	$\sigma(\Delta f)$	$\mu(\Delta f)$	$\sigma(\Delta f)$
F(6.52)	(-0.47, -0.06)	(0.30, 1.13)	(-0.03, 0)	(0.0, 0.02)
F(6.61)	(-0.02, 0)	(0.07, 0.18)	(-0.04, 0)	(0, 0.01)
F(6.62)	(1.31, -4.02)	(3.2, 11.3)	(0.14, -0.4)	(0.02, 0.09)
F(6.63)	(-0.01, 0.01)	(0.01, 0.02)	(0, 0)	(0, 0)

Monte Carlo Simulation Results: We have conducted Monte Carlo simulation runs for estimation of the faults in the system (6.72). We set $i = 2$, $p = \{1, 2\}$ and $q = \{\emptyset\}$ and $i = 2$, $p = \{\emptyset\}$ and $q = \{1, 2\}$ for the sensor and the actuator fault estimations, respectively. Sensors faults having severities of -1 and 1 are injected to the sensor 1 and the sensor 2 at the time step $k = 150$, respectively. The same fault scenario is considered for the actuator fault estimation problem. We performed 400 Monte Carlo simulation runs for two inputs that are selected as $u_1(k) = u(k)$ given by equation (6.73) and $u_2(k) = 0.1u(k)$. The results are shown in Figure 6.3 and numerically presented in Table 6.1. It can be concluded that the filters (6.52) and (6.62) have an acceptable performance for relatively small inputs (in terms of the norm of the signal). On the other hand, relatively large inputs clearly magnify the biases although they are well-managed by utilizing our proposed tuning process. An approximation to the biases for the filters (6.52) and (6.62) can be obtained by using equation (6.55). The L_2 gain of the error dynamics is then given by,

$$\|\Delta f^s(k)\|_2 \leq \|(zI - \hat{A}_r)\hat{\mathcal{B}} + \hat{\mathcal{G}}\|_\infty \|\mathbf{Z}(k)\|_2$$

The matrices $\hat{\mathcal{B}}$ and $\hat{\mathcal{G}}_1$ are obtained by solving the minimization problems (6.59) and (6.64). Therefore, one can obtain a prediction of the error margin corresponding to a certain input.

Comparative Study: Finally, in order to perform a comparative study to demonstrate the capability and advantage of our proposed methodology, we consider the example that was provided in [92] and evaluate our corresponding results with those in [92]. The system in [92] is a continuous-time system and represents a

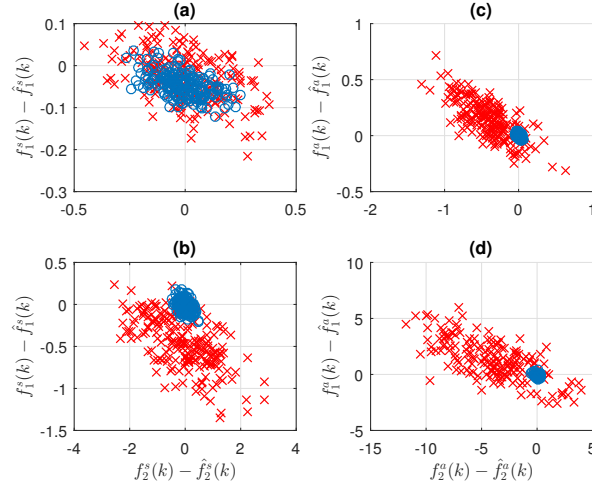


Figure 6.3: Faults having severities of 1 and -1 are injected in the actuators or sensors of the system (6.72). The red marks represent results for the filters (6.52) or (6.62) and the blue circles represent results for the tuned filters (6.61) or (6.63). (a) Sensors fault estimation error when the system is stimulated by $u_2(k)$, (b) Sensors fault estimation error when the system is stimulated by $u_1(k)$, (c) Actuator fault estimation errors when the system is stimulated by $u_2(k)$, and (d) Actuator fault estimation errors when the system is stimulated by $u_1(k)$.

linearized model of a vertical take-off and landing (VTOL) aircraft that is given by,

$$\begin{aligned}
 \dot{x}(t) &= \begin{bmatrix} -0.036 & 0.027 & 0.018 & -0.455 \\ 0.048 & -1.01 & 0.002 & -4.020 \\ 0.100 & 0.368 & -0.707 & 1.42 \\ 0 & 0 & 1 & 0 \end{bmatrix} x(t) + \begin{bmatrix} 0.44 & 0.17 \\ 3.54 & -7.59 \\ -5.52 & 4.49 \\ 0 & 0 \end{bmatrix} (u(t) + f^a(t)) \\
 y(t) &= \begin{bmatrix} 1 & 0 & 0 & 0 \\ 0 & 1 & 0 & 0 \\ 0 & 0 & 1 & 0 \\ 0 & 1 & 1 & 1 \end{bmatrix} x(t) + f_s(t)
 \end{aligned} \tag{6.74}$$

where $f^s(t) \in \mathbb{R}^4$ and $f^a(t) \in \mathbb{R}^2$ and $f^a(t)$ with $f^s(t)$ representing the actuator and sensor bias faults, respectively. The discrete-time model associated with the system (6.74) is obtained by using a sampling rate of 0.5 seconds. Furthermore, it is assumed that the system is stabilized by applying the following control law which

is experimentally obtained,

$$u(k) = - \begin{bmatrix} 0 & 0 & -0.5 & 0 \\ 0 & 0 & -0.1 & -0.1 \end{bmatrix} y(k) + \xi(k)$$

where $\xi(k)$ denotes the reference signal. The process and measurement noise are white having zero mean and covariances $Q = 0.16\mathbf{I}$ and $R = 0.64\mathbf{I}$, respectively. The reference signal is selected to be a PRBS signal for identification of the Markov parameters.

The identification data set includes 1000 samples. Note that the *correlation analysis* cannot be directly applied to unstable systems. Therefore, response of the stable closed-loop system is obtained by injecting the input that is computed at each time step using the above control law. Next, the input and closed-loop system responses are used as I/O data for identification of the closed-loop system Markov parameters through the *correlation analysis*. The injected fault signals to the actuators and sensors are given by,

$$f^a(k) = \begin{cases} \begin{bmatrix} 0 & 0 \end{bmatrix}^T & 0 \leq k \leq 50 \\ \begin{bmatrix} \sin(0.1\pi k) & 1 \end{bmatrix}^T & k > 50 \end{cases}$$

$$f^s(k) = \begin{cases} \begin{bmatrix} 0 & 0 & 0 & 0 \end{bmatrix}^T & 0 \leq k \leq 50 \\ \begin{bmatrix} \sin(0.1\pi k) & 1 & 0 & 0 \end{bmatrix}^T & k > 50 \end{cases}$$

We have set $i = 2$, $p = \{1, 2\}$ and $q = \{\emptyset\}$ and $i = 3$, $p = \{\emptyset\}$ and $q = \{1, 2\}$ for the sensor and actuator fault estimation filters, respectively. The reference signal is set to $\xi(k) = 15$ in order to duplicate the Monte Carlo simulation results that were reported in [92].

Figures 6.4a and 6.4b show 500 and 400 Monte Carlo simulation runs for estimation of the actuator and sensor faults, respectively. The average estimation errors are given by $\mu(\hat{f}_1^a - f_1^a, \hat{f}_2^a - f_2^a) = (0.018, 0.039)$ and $\mu(\hat{f}_1^s - f_1^s, \hat{f}_2^s - f_2^s) =$

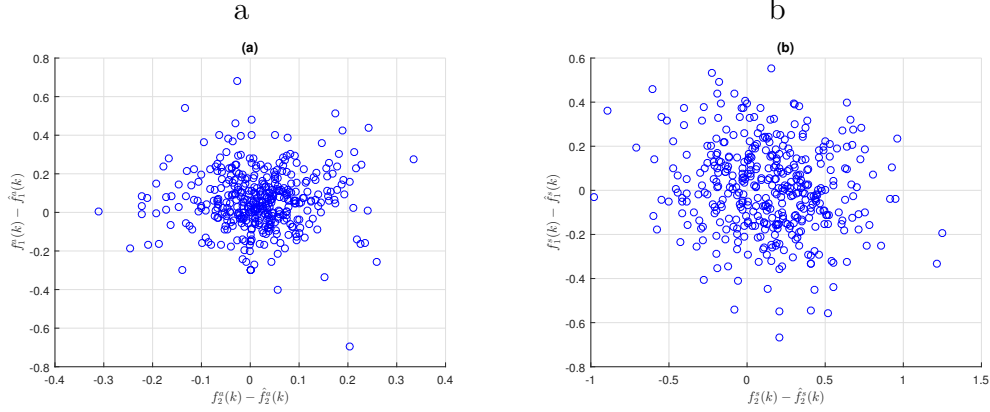


Figure 6.4: (a) The first actuator fault estimation error versus the second actuator fault estimation error for the system (6.74) using 500 Monte Carlo simulation runs, and (b) The first sensor fault estimation error versus the second sensor fault estimation error for the system (6.74) using 400 Monte Carlo simulation runs.

(0.005, 0.139). The variances are given by $\sigma(\hat{f}_1^a - f_1^a, \hat{f}_2^a - f_2^a) = (0.008, 0.0097)$ and $\sigma(\hat{f}_1^s - f_1^s, \hat{f}_2^s - f_2^s) = (0.0398, 0.1074)$.

The above results clearly show that our proposed scheme has significant advantages, benefits, and capabilities over the receding horizon fault estimator that was proposed in [92], although it uses the same set of assumptions. This is substantiated by the following observations. First, our proposed filter order is significantly lower than that in [92] as we have theoretically shown in Theorems 6.1 and 6.2. For this particular example, we have used $i = 2$ for the sensor and actuator fault estimation filters, respectively, whereas i is set to $i = 30$ in [92]. Moreover, we have achieved a better performance by invoking an offline tuning procedure as compared to the Algorithm 3 utilized in [92] that performs an online optimization solution. Consequently, the computational burden of [92] to the user increases to the point where the average computational time per sample takes 2.05 seconds on a 3.4 GHz computer having 8 GB of RAM. Whereas, the computational time associated with our proposed methodology per sample using the same computer takes only 8.2×10^{-7} seconds.

6.6 Conclusion

We have proposed fault detection, isolation and estimation schemes that are all directly constructed and designed in the state-space representation form by utilizing only the system I/O data. We have shown that to design and develop our schemes it is only sufficient to estimate the system Markov parameters. Consequently, the reduction step that is commonly used in the literature, and that also introduces nonlinear errors, and also requires an *a priori* knowledge of the system order is completely eliminated in our schemes. We have shown that the performance of the estimation scheme is linearly dependent on the Markov parameters estimation process errors. We also proposed an offline tuning procedure that effectively compensates for the estimation errors that are caused by errors in the estimation of the Markov parameters. Comparisons of our proposed schemes with those available in the literature have revealed that our methodology is mathematically simpler to develop and computationally more efficient, while it maintains the same level of performance and requires a lower set of assumptions. Further research is required to investigate the robustness of our scheme to estimation errors and presence of concurrent sensor and actuator faults.

Chapter 7

Implementation and Application of the FDI&E Methodologies to Gas Turbines

In this chapter, we applied and demonstrated our proposed data driven fault diagnosis and estimation scheme in Chapter 5 to the gas turbines. The healthy gas turbine engine is stimulated by a sinusoidal input containing a limited number of frequencies. First, the associated system Markov parameters are estimated by using the FFT of the input and output signals to obtain the frequency response of the engine. These data are then used for *direct* design and realization of the fault detection, isolation and estimation filters. Our proposed scheme therefore does not require any *a priori* knowledge of the system linear model or its number of poles and zeros at each operating point. We have investigated the effects of the size of the frequency response data on the performance of our proposed schemes. We have shown through comprehensive case studies simulations that desirable fault detection, isolation and estimation performance metrics defined in terms of the confusion matrix criterion can be achieved by having access to only frequency response of the system at only

a limited number of frequencies.

This chapter is organized as follows. The preliminaries are presented in Section 7.1. The Markov parameters estimation methodology accomplished by using the frequency response data is explained in Section 7.2. Finally, comprehensive case studies simulations are presented in Section 7.3. The chapter is concluded in Section 7.4.

7.1 Preliminaries

In this work, we have used the nonlinear model of a single spool gas turbine engine that was proposed in Chapter 2 for generating the I/O data. This model has fuel flow rate as an input signal and five measurements that are denoted by T_C , P_C , N , P_T and T_T (representing the gas temperature after the compressor, the gas pressure after the compressor, the shaft rotational speed, the pressure after the turbine, and the temperature after the turbine, respectively).

All the measurements are noise corrupted, where the noise levels are taken from [20]. For our analysis, we have considered *one* actuator fault and *five* sensor faults. All the faults are additive in nature which represent the loss of effectiveness in the actuator and biases in the sensors. Our proposed scheme is based on the results of chapter 6 which requires that the following assumptions to hold, specifically **(i)** the aircraft gas turbine engine is stable and observable (at any given operating point), **(ii)** the gas turbine engine linearized model matrices and the order of the system at an operating point are *unknown*, **(iii)** the Markov parameters are estimated by using only the I/O data that are associated with the healthy system, and **(iv)** the faults are detectable and isolable. Moreover, it is assumed that the feed-through matrix of the linearized model is zero.

For a given Power Lever Angle (PLA), the aircraft gas turbine engine reaches

a steady state condition which defines a corresponding operating point. Therefore, we specify an operating point by the level of the PLA, i.e. a PLA=75% indicates an operating point when the PLA is set to 75% of its maximum PLA. We have verified that the above assumptions all hold corresponding to all the considered operating points by using the nonlinear model that is described in the Chapter 2.

7.2 Identification of the Aircraft Gas Turbine Engine Markov Parameters

Our proposed data-driven FDI&E scheme requires estimation of the Markov parameters associated with the system I/O data. Clearly, the Markov parameters are not defined for a given nonlinear system. Let us assume that the nonlinear model of the gas turbine engine is linearized at a given operating point and is described by the triple $\Sigma(A, B, C)$. It is assumed that none of these matrices are known *a priori*. The Markov parameters of the system at a given operating point is defined as the set $\{H_0, H_1, H_2, \dots\}$, where $H_i = CA^iB$. The dimension of H_i is known since $H_i \in \mathbb{R}^{l \times m}$, where m and l denote the number of inputs and outputs, respectively. In our case for the considered gas turbine engine, $m = 1$ and $l = 5$. Moreover, we define the Markov parameters associated with the input channel to the measurement p , $p = 1, 2, \dots, l$ by $H_i^p = C(p, :)A^iB$, where $C(p, :)$ denotes the p^{th} row of C , and where $H_i^p \in \mathbb{R}$. In our proposed methodology, we directly identify H_i^p 's from the input and the measurement p data. In other words, the Markov parameters corresponding to each channel is independently estimated. Clearly, H_i is given by $\left[H_i^1 \quad \dots \quad H_i^l \right]^T$, where T denotes the matrix transpose.

The Markov parameters associated with a gas turbine engine at each operating point can be estimated by using various methods such as the *correlation analysis* ([93]), *provided* that the healthy system is stimulated by a *persistently exciting*

input such as a random noise or a pseudo-random binary (PRBS) signal. However, stimulation of an aircraft gas turbine engine with a random noise or the PRBS command is *not* common, advisable, and justifiable in practice. Therefore, in the literature frequency-domain techniques have been reported to provide a “great potential” for tackling the gas turbine engine parameters estimation problem [136]. Evans and his colleagues have comprehensively studied these methods for the gas turbine engine dynamic identification and have demonstrated them to a Rolls Royce engine ([118, 136–139]).

In the frequency-domain, the system is stimulated by harmonic signals of different frequencies. The frequency response of the system is then obtained by simply taking the FFT of the collected input and output data. Mathematically speaking, the stimulating harmonic input can be expressed as,

$$u(t) = \sum_{i=0}^Q a_i \cos(2\pi n_i f_0 t + \phi_i) \quad (7.1)$$

where a_i , n_i , f_0 , ϕ_i and Q denote the amplitude, the harmonic number, the signal fundamental frequency, the harmonic phase, and the number of frequencies in the signal, respectively. We will subsequently determine proper numerical values for these parameters. It is recommended to select odd harmonics that will reduce the effects of the second order nonlinearities [138]. This implies that n_i should be an odd number. Moreover, the harmonic phases should be selected in order to minimize the crest factor (CF) that is given by,

$$CF = \frac{\max\|u(t)\|}{r.m.s(u(t))} \quad (7.2)$$

where *r.m.s.* stands for the *root mean square*.

The above can be achieved through a minimization algorithm that is described in [140]. The minimization of CF improves the signal-to-noise ratio as discussed in [118]. The frequency response function of the system corresponding to an input

channel U to the p – th measurement channel Y^p at the given frequency ω can be expressed as,

$$G^p(j\omega) = \frac{Y^p(j\omega)}{U(j\omega)} \quad (7.3)$$

where $U(j\omega)$ and $Y^p(j\omega)$ denote complex Fourier transforms of the input and the output signals at the frequency ω , respectively.

The common practice in parametric frequency-domain identification methods is to consider a generic transfer function as given by,

$$G^p(s) = \frac{b'_0 + b'_1 s + \dots + b'_m s^m}{a'_0 + a'_1 s + \dots + a'_n s^n} e^{-sT_d} \quad (7.4)$$

where the parameters a'_i 's and b'_i 's should be estimated by using least-square methods and measured frequency responses. This procedure is actually equivalent to the *reduction step*, and is the one that we are trying to avoid through our proposed methodology. The most important disadvantage of the methods that involve the reduction step is the need for an *a priori* knowledge of the system order. In other words, one requires to forcefully fit a presumed model of a given order to the system that may not be a true representative model. We address this challenging issue by designing a data-driven FDI&E scheme that avoids the reduction step.

Although, our method requires estimation of the Markov parameters that could have been achieved through a standard non-parametric identification method (*correlation analysis*), however, our simulations have shown that this approach will not be robust for our application when the harmonic input contains a limited number of frequencies. Therefore, in this chapter, we have invoked and utilized a robust procedure that is provided in [117].

Our selected procedure requires the frequency response of the system at $Q + 1$

uniformly spaced frequencies between 0 and π . Therefore, we choose the fundamental frequency as $f_0 = \frac{f_s}{2(2Q-1)}$, where f_s is the sampling rate and $n_i = 0, 1, 3, \dots, 2Q - 1$ for $i = 0, 1, \dots, Q$. The phase ϕ_i is obtained from minimization of the CF factor. Our comprehensive simulations in [20] have shown that each linear model that is obtained at a given operating point is valid for a $\pm 10\%$ change in the PLA. Therefore, we choose a_i in equation (7.1) to be 10% of the maximum PLA.

The frequency response of the system for the given input channel to the measurement channel p at each frequency ω_i is given by,

$$\tilde{G}^p(e^{j\omega_i}) = \frac{\sum_{\alpha=1}^E \tilde{Y}_\alpha^p(e^{j\omega_i})}{\sum_{\alpha=1}^N \tilde{U}_\alpha(e^{j\omega_i})} \text{ for } i = 0, 1, \dots, Q \text{ and } p = 1, \dots, l \quad (7.5)$$

where $\tilde{U}_\alpha(e^{j\omega_i})$ and $\tilde{Y}_\alpha^p(e^{j\omega_i})$ are obtained by taking the FFT of the I/O data measured across E periods of the signal. The parameter E is a fixed number. For our multiple sinusoidal input, E is determined based on the period of the lowest frequency. We used the notation $\tilde{G}^p(e^{j\omega_i})$ to differentiate it from $G^p(e^{j\omega_i})$, which is the true value of the system frequency response at the frequency ω_i . Note that $\tilde{G}^p(e^{j\omega_i})$ is noise corrupted due to presence of measurement noise. Similarly, the “ideal” or “true” FFT of the I/O data are denoted by $U_\alpha(e^{j\omega_i})$ and $Y_\alpha^p(e^{j\omega_i})$, which are clearly assumed to be *unknown*.

The above procedure provides the frequency response of the system at $Q + 1$ uniformly spaced frequencies as the required input to be used for the methodology that is proposed in [117]. Let \tilde{G}_i^p denote $\tilde{G}^p(e^{j\omega_i})$, where $i = 0, 1, \dots, Q$. We expand the frequency response samples by defining $\tilde{G}_{Q+k}^p = \tilde{G}_{Q-k}^p$ for $k = 1, \dots, Q - 1$. Let β_i^p be defined by the following $2Q$ -point Inverse Discrete Fourier Transform (IDFT), that is

$$\beta_i^p = \frac{1}{2M} \sum_{z=0}^{2Q-1} \tilde{G}_i^p e^{j2\pi iz/2Q} \quad (7.6)$$

It is shown in [117] that,

$$\beta_i^p = C(p, :)A^{i-1}(I - A^{2Q})^{-1}B \quad (7.7)$$

If the system is strictly stable, then for sufficiently large Q , we have $A^{2Q} \approx 0$. Thus,

$$\beta_i^p \approx C(p, :)A^{i-1}B \quad (7.8)$$

which is an approximation to the Markov parameter H_i^p .

Our simulations have shown that the above method is more robust and accurate for application to the aircraft gas turbine engine as compared to the standard non-parametric methods. Its disadvantage is the fact that Q should be sufficiently large for an accurate estimation of the Markov parameters, which may be restrictive in practice. However, we will show in the simulation Section 7.3 that our entire proposed scheme yields reasonable performance with a Q as small as 25.

7.3 Simulation Case Studies

In this section, we provide comprehensive simulation case studies for evaluating the performance and capabilities of our proposed data-driven FDI&E schemes. The aircraft gas turbine engine system is nonlinear, therefore it cannot be represented by a single linear model. Comprehensive simulations in [20] have shown that each linear model is valid corresponding to a PLA within the range of $\pm 10\%$ about that operating point. It is also concluded in [118] that each linear model at a given operating point is valid for a 10% variation in the PLA. Consequently, we have demonstrated through a comprehensive study and through extensive simulation runs as well as by employing the notion of the *confusion matrix* [141] that the estimated Markov parameters are also valid within a $\pm 10\%$ variations about the corresponding operating point as discussed in the Appendix A.1.

Therefore, we select a_i in equation (7.1) for $i = 0, \dots, Q$ to be equal to $0.1U_{100}$, where U_{100} is equal to the fuel flow rate at the PLA=100%. The conducted simulations are performed for Q equal to 25, 50 and 100. Evans *et. al* [138] have used an input that is composed of 30 harmonics (i.e., $Q = 30$) for achieving a model identification of the Rolls-Royce Spey engine. We have considered $Q = 25$ to evaluate the performance of our proposed FDI&E scheme given the scarcity of the available data, and $Q = 100$ as a reference of the theoretical benchmark. The sampling rate in all the simulations are set to 20 *ms*, which is commonly used in the engine FADEC technology [142].

We have conducted our simulations for three PLAs that are equal to 50, 75 and 100%, as these are typical values of PLAs during the cruise, the maneuver, and the take off modes of the flight, respectively. For example, Figure 7.1 shows the measured frequency response of the input channel to the shaft rotational speed (N) corresponding to three PLAs and $Q = 50$. We have conducted comprehensive simulation studies for determining the suitable value of the parameter E in equation (7.5). A summary of these studies are included in the Appendix A.4 which confirms that the values of $E = 5$ and $E = 6$ both yield satisfactory results. However, we have decided to set $E = 6$ to follow the recommendation that was made in [118].

The Markov Parameters Estimation Errors: The procedure that was introduced in Section 7.2 is now applied to estimate the system Markov parameters corresponding to three operating points associated with PLA=50, 75, and 100% for three different values of Q . The gas turbine engine nonlinear model is linearized at the same operating points in order to obtain the “actual values” of the Markov parameters. Figure 7.2 shows the relative error between the first ten estimated Markov parameters (obtained by using the frequency response) and those of the actual Markov parameters (obtained by using the system linearization model) of the input channel to the shaft rotational speed output channel at the PLA=75%. The

same results for PLA=50 and 100% are obtained that are provided in the Appendix A.2, which show similar trends. As expected, the estimation errors decrease as Q increases. However, the errors for the first and second Markov parameters are quite large as compared to the same errors for the input channel to the compressor pressure (P_C) output channel as shown in Figure 7.3. This difference will have an impact on the resulting fault estimation scheme as discussed subsequently. Table 7.1 summarizes the average relative error results for the first ten Markov parameters corresponding to all the channels that are obtained over 100 Monte Carlo simulation runs at the PLA=75%.

Fault Detection Case Study Results: We have constructed the fault detection filters according to the guidelines and procedures that are provided in Chapter 6. Figures 7.4 and 7.5 show “typical” results corresponding to actuator and sensor fault detection scenarios, respectively. In both cases, we have used measurements from all the five sensors. In the first scenario, a 10% loss of effectiveness fault is injected to the actuator at the time step 150. Figure 7.5 shows the fault detection filters residuals when a 1% bias fault is injected in the shaft rotational speed sensor. Note that the detection filter parameters are obtained from the frequency response of the system at the PLA=75%. However, we have performed the simulations at the PLA=80% to test the robustness and validity of the model for a different range of PLAs. A comprehensive study corresponding to other PLAs is provided below by using the concept of the *confusion matrix* [141]. Tables 7.2 to 7.4 provide the results associated with the actuator fault severities of 1%, 5%, and 10%, respectively, and Table 7.5 provides the results associated with the sensor fault severity of 1%. Additional results are provided in the Appendix A.3 corresponding to another PLA of PLA=55% in Tables A.3 to A.6.

Confusion Matrix Analysis and Evaluation of Fault Detection Performance: The *confusion matrix* [141] is a table that is commonly used in the field

of artificial intelligence and pattern recognition to illustrate the performance of a given algorithm. Several useful performance metrics can be defined by using the entries from this matrix. The interested reader is referred to [141] for a detailed description. Tables 7.2 to 7.5 represent the confusion matrix corresponding to different values of Q and different values of fault severities. All the values in these tables are obtained corresponding to 100 Monte Carlo simulation runs for each row. The filters are designed by using the Markov parameters that are estimated at the PLA=75% but stimulated by a fault that is injected to the gas turbine engine at the PLA=80% (again to verify the scheme robustness to uncertainties).

Several conclusions can be drawn from the results that are obtained in these tables: **i)** The higher the Q is selected, the lower the false alarms will be as indicated by smaller off-diagonal entries in these tables, **ii)** The actuator fault detection performance is unreliable for faults with severities lower than 5%, **iii)** On the other hand, sensor faults with severities as low as 1% can be reliably detected. The confusion matrices for higher sensor fault severities are not shown for brevity as clearly the performance of the schemes improves by considering higher severity faults, and **iv)** Finally, the same patterns for the other PLAs are observed as shown and provided in the Appendix A.3.

Threshold Setting: It was stated earlier that r_{min} and r_{max} are to be selected through conducting simulations corresponding to the healthy operation of the gas turbine engine. The confusion matrix actually can be used to provide a systematic procedure for selecting the thresholds. Towards this end, the metric *accuracy* for a scheme, that is denoted by ACC, is defined as

$$ACC = \frac{TP + TN}{TP + TN + FP + FN} \quad (7.9)$$

where TP (True Positive), TN (True Negative), FP (False Positive) and FN (False Negative) are defined in Table 7.6. Higher values of $|r_{min}|$ and $|r_{max}|$ will increase

the missed alarm quantity FP. Conversely, lower values of these bounds will increase the false alarm quantity FN. Therefore, there should be a trade-off analysis and threshold setting that maximizes the ACC, and which is obtained through trial and error. For example, the thresholds that are shown in Figure 7.4 yield an accuracy of 83%, 92% and 97.5% for $Q = 25, 50$ and 100 , respectively, based on the results that are shown in Table 7.3. One may also define the notion of *precision* metric for conducting the trial and error studies for threshold setting. The *precision* metric is defined as,

$$PPV = \frac{TP}{TP + FP} \quad (7.10)$$

The resulting values for ACC and PPV are provided in Tables 7.2 to 7.5 as well as Tables A.3 to A.6 in the Appendix A.3 for a different PLA.

Fault Isolation Case Studies: The task of accomplishing fault isolation requires a bank of filters as discussed in Chapter 6. Since our gas turbine engine system has only one actuator, the actuator fault isolation and actuator fault estimation filters are effectively the same. More specifically, an actuator isolation filter in the filter bank is in fact an UIO which is insensitive to a particular input. On the other hand, the actuator fault estimation filter is also an UIO which is not fed by the input data. Consequently, the two filters for a system with one input will be identical. We only discuss the performance of the actuator fault estimation filter subsequently that also represents the performance of the actuator fault isolation filter. Below, we provide the results corresponding to the sensor isolation case studies.

A “typical” sensor fault isolation scenario is illustrated in Figure 7.6. In this figure, only the compressor temperature (T_C) and the shaft rotational speed (N) measurements are used. Therefore, the filter bank contains two filters where one works with the T_C measurement and the other one with the N measurement. A 1% fault is injected in the temperature sensor at the time step 150 which is successfully

isolated corresponding to all values of Q . Theoretically, a large number of possibilities are available for configuring the filter banks. A functional selection among these configurations depends on the requirements and practical issues associated with a particular gas turbine engine. For instance, certain measurements may be considered as critical (or redundant) for a certain gas turbine engine that can impose different requirements. Subsequently, we have demonstrated the performance of a filter bank that is composed of five filters, each of which operates with four measurements as a typical configuration.

Confusion Matrix Analysis and Evaluation of the Sensor Fault Isolation: A broader picture for the sensor fault isolation performance can be obtained by investigating the confusion matrix. In this analysis, all the measurements are used for achieving the isolation of a single sensor fault. Therefore, the bank contains five filters each of which is operating with four measurements. The definition of the faults are provided in Table 7.7. The results are summarized in Tables 7.8, 7.9 and 7.10. As expected, the higher the value of Q , the better the obtained results. Similar patterns are also observed corresponding to other PLAs and fault severities as shown in the Appendix A.3 and Tables A.7 to A.9.

Concurrent Sensor Fault Isolation Case Studies: A more complicated architecture can be considered if one requires to address the concurrent fault isolation problem. Figure 7.7 shows the residuals corresponding to a bank of three filters where the first, second and third filters operate with the measurements T_C , N and P_C , respectively. A 1% fault in the T_C and N is injected at the time steps 150 and 200, respectively. As shown in Figure 7.7, the residuals associated with the filters except one exceed their thresholds, which indicate that concurrent faults in the sensors T_C and N are detected and isolated. Again, this is a “typical” scenario of a hierarchy among many configurations for a particular concurrent fault isolation task. For example, one may perform a similar task by using a filter bank that consists

of six filters each of which operates with two measurements selected from a set of four measurements. The best configuration for a particular application depends on the context of the problem. One advantage of our proposed procedure is the fact that it does not impose a particular limit on the structure of the filters banks. Our methodology can be adapted to configure various scenarios for matching a given set of requirements.

Fault Estimation Results: The results provided above demonstrate that the FDI filters can be successfully constructed from the frequency response data that are measured at only a limited number of frequencies. This is an important advantage of our proposed methodology from a practical point of view. However, the same property cannot be extended to the case of fault estimation problem. In other words, the performance of the fault estimation filters are significantly more sensitive to the accuracy of the obtained Markov parameter estimates, and consequently to the number of selected frequencies.

Actuator Fault Estimation Case Studies: Figure 7.8 depicts the residuals that are generated by an actuator fault estimation filter that is fed by two measurements P_C and P_T corresponding to a scenario in which a 10% actuator fault is injected at the time step 150. The estimation errors for $Q = 25, 50$ and 100 are obtained as 3%, 1% and 1% respectively. If the measurements P_C and N are used instead, then the estimation errors are larger as shown in Figure 7.9. Namely, the estimation errors for $Q = 25, 50$ and 100 are obtained as 12%, 7% and 4%, respectively. Clearly, it can be observed that the estimation errors for the first and second Markov parameters of the input channel to the shaft rotational speed output channel as shown in Figure 7.2 are relatively large.

Sensor Fault Estimation Case Studies: Figure 7.10 shows the performance of the sensor fault estimation filter that is fed by two measurements P_C and P_T when a 1% fault is injected in the sensors measuring P_C and P_T at the time steps

100 and 200, respectively. The estimation error for the sensor P_C for $Q = 25, 50$ and 100 are obtained as 2%, 0.5% and 0.5%, respectively. It can be shown that an almost the same performance is obtained in the fault estimation error of the sensor P_T .

Finally, it can be concluded that in both actuator and sensor fault estimation scenarios the results that are obtained can also be verified by the FDI schemes in terms of the presence of the fault and its isolation as shown in Figures 7.4 and 7.5.

Fault Estimation Performance Evaluation Using Monte Carlo Simulations: Tables 7.11 and 7.12 summarize the performance of the fault estimation errors for the actuator and the sensor faults under various sets of measurement groupings. The information that are obtained from these tables demonstrate and confirm the fact that by increasing Q and/or inclusion of more measurements the fault estimation accuracy will be clearly improved. Moreover, additional simulation results are shown in Tables A.10 and A.11 in the Appendix A.3 corresponding to a different PLA setting.

Comparative Study Using PBRs and Noise Signals: Finally, as a comparative study, in a separate Monte Carlo simulation runs, we applied persistently exciting noise and PBRs inputs to the gas turbine engine system and estimated the Markov parameters by using *correlation analysis*. This method uses a time-series data instead of the frequency response data for estimation of the Markov parameters. Table 7.13 summarizes the results corresponding to the sensor fault estimation errors under various sets of measurement groupings that show that theoretically it would be significantly superior to the frequency domain approach. However, this approach, as we discussed earlier, is not practically plausible. The gas turbine engine manufacturers generally measure the frequency response of the system at different operating points for advanced dynamics and structural analysis, but they are less likely to stimulate and subject intentionally the gas turbine engine to noise or PRBS

signals. Consequently, the frequency response data are more likely to be available as compared to the test results of the gas turbine engine system that is stimulated by other types of either high frequency or wide band input signals.

7.4 Conclusion

This chapter addresses several important practical challenges for designing a data-driven FDI&E scheme for the aircraft gas turbine engines. These problems include the structure of the FDI schemes, the amount and nature of the data that are required, and the *a priori* knowledge about the system dynamics. Statistical and artificial intelligence-based methods have complex structures and require numerous learning and tuning parameters that necessitate extensive trade-off analysis and studies for determining the optimal selection of these schemes' structure and parameters. In addition, these methods require large amount of data for proper training of their available adjustable parameters. In contrast, in our proposed schemes, the dynamical filters are directly designed and constructed from only the estimated system Markov parameters. The Markov parameters are estimated by using only the frequency response data that are quite commonly and practically available. We have demonstrated that our proposed methodology provides a satisfactory performance by only utilizing the frequency response of the system at a limited number of frequencies. Our proposed schemes are well-suited for real applications due to the fact that they require availability of only frequency response data. Finally, our proposed approach eliminates the restrictive assumption on the availability of an accurate estimation of the number of system poles and zeros. Further research are required to address the robustness and improve the accuracy of the proposed fault estimation filters.

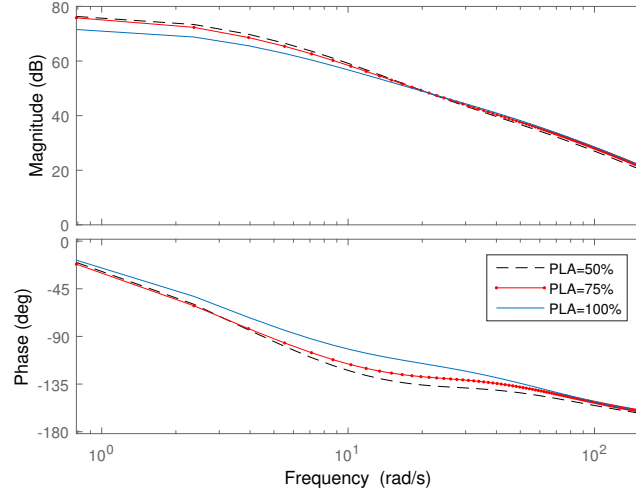


Figure 7.1: The frequency response \tilde{G}_i^p (from the input channel to the shaft rotational speed (N) output channel) ($i = 0, 1, \dots, 50$ and $p = 3$) computed at three PLAs equal to 50, 75 and 100%.

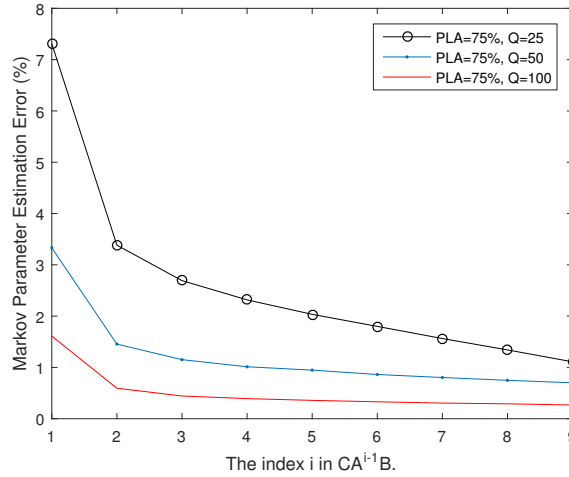


Figure 7.2: The relative errors between the estimated and the actual Markov parameters of the input channel to the shaft rotational speed output channel at the PLA=75% for three different values of Q .

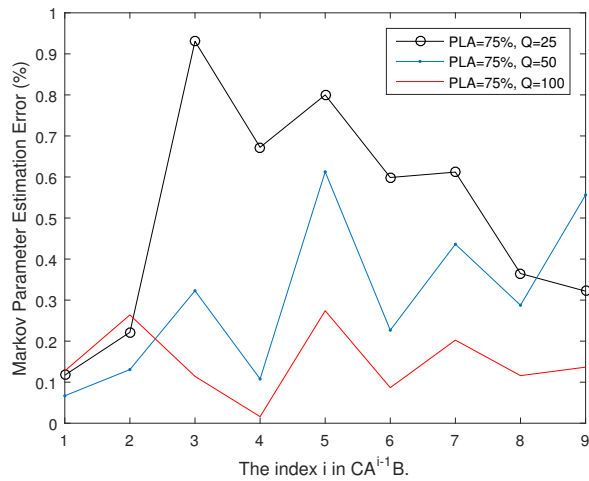


Figure 7.3: The relative errors between the estimated and the actual Markov parameters of the input channel to the compressor pressure output channel at the PLA=75% for three different values of Q .

Table 7.1: The average estimation relative errors for the first ten Markov parameters for all channels over 100 Monte Carlo simulation runs.

Channel	$Q = 25$	$Q = 50$	$Q = 100$
u to T_C	4.44	2.07	0.29
u to P_C	5.15	2.61	0.61
u to N	2.61	1.22	0.51
u to T_T	3.07	1.31	0.95
u to P_T	6.15	3.58	1.67

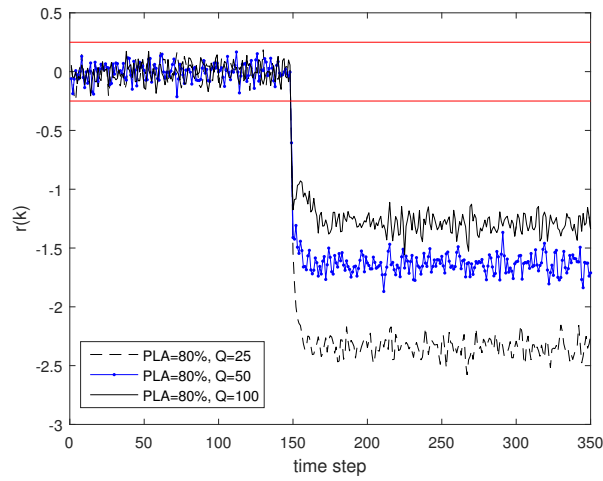


Figure 7.4: Fault detection filter residuals designed with the data obtained at PLA=75% but stimulated at PLA=80% while a 10% actuator fault is injected at the time step 150.

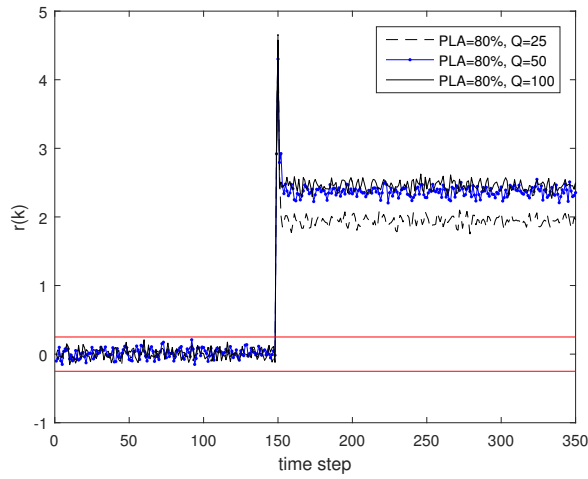


Figure 7.5: Fault detection filter residuals designed with the data obtained at PLA=75% but stimulated at PLA=80% while a 1% sensor fault in shaft rotational speed sensor is injected at the time step 150.

Table 7.2: Confusion matrix for the actuator fault detection performance. The fault severity and the PLA are 1% and 80%, respectively.

$Q = 25$		Healthy	Faulty	$Q = 50$		Healthy	Faulty	$Q = 100$		Healthy	Faulty
	Healthy	61	39		Healthy	72	28		Healthy	81	19
	Faulty	22	78		Faulty	17	83		Faulty	26	74
	ACC	69.5%			ACC	77.5			ACC	77.5	
	PPV	73.4			PPV	80.8			PPV	75.7	

Table 7.3: Confusion matrix for the actuator fault detection performance. The fault severity and the PLA are 5% and 80%, respectively.

$Q = 25$		Healthy	Faulty	$Q = 50$		Healthy	Faulty	$Q = 100$		Healthy	Faulty
	Healthy	82	18		Healthy	90	10		Healthy	99	1
	Faulty	16	84		Faulty	6	94		Faulty	4	96
	ACC	83%			ACC	90.4			ACC	97.5	
	PPV	83.6			PPV	93.7			PPV	96.1	

Table 7.4: Confusion matrix for the actuator fault detection performance. The fault severity and the PLA are 10% and 80%, respectively.

$Q = 25$		Healthy	Faulty	$Q = 50$		Healthy	Faulty	$Q = 100$		Healthy	Faulty
	Healthy	88	12		Healthy	96	4		Healthy	98	2
	Faulty	17	83		Faulty	9	91		Faulty	1	99
	ACC	85.5%			ACC	96.4			ACC	98.5	
	PPV	83.8			PPV	91.4			PPV	98.9	

Table 7.5: Confusion matrix for the sensor fault detection performance. The fault severity and the PLA are 1% and 80%, respectively.

$Q = 25$		Healthy	Faulty	$Q = 50$		Healthy	Faulty	$Q = 100$		Healthy	Faulty
	Healthy	85	15		Healthy	89	11		Healthy	94	6
	Faulty	11	89		Faulty	4	96		Faulty	6	94
	ACC	87%			ACC	92.5			ACC	94	
	PPV	88.5			PPV	95.6			PPV	94	

Table 7.6: The confusion matrix and definition of the parameters in equation (7.9). TP (true positive) denotes the number of healthy cases that are identified as healthy, FN (false negative) denotes the number of healthy cases that are identified as faulty, FP (false positive) denotes the number of faulty cases that are identified as healthy, and TN (true negative) denotes the number of cases that are faulty and identified as faulty.

		Predicted	
		Healthy	Faulty
Actual	Healthy	TP	FN
	Faulty	FP	TN

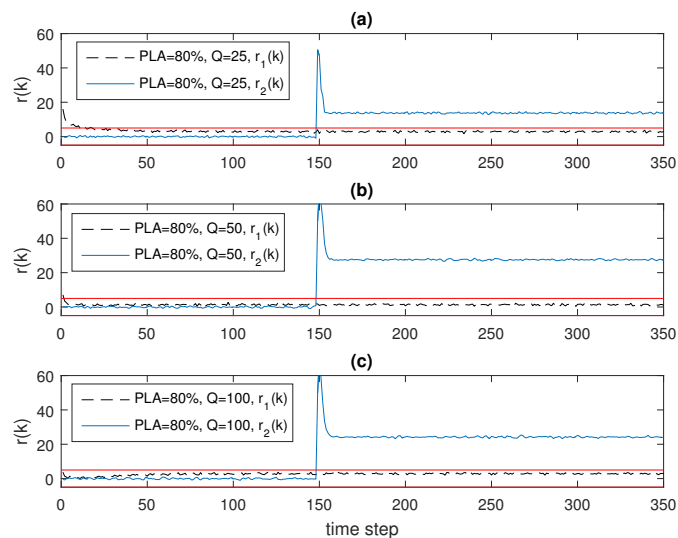


Figure 7.6: Residuals generated by a bank of two filters for the sensor fault isolation. The filters are designed with the data obtained at PLA=75% but stimulated at PLA=80% while a 1% fault is injected in the sensor measuring T_C at the time step 150.

Table 7.7: The fault definitions for the confusion matrix analysis.

Fault	Symbol
No fault	f_0
Actuator bias fault	f_1
T_C sensor bias fault	f_2
P_C sensor bias fault	f_3
N sensor bias fault	f_4
P_T sensor bias fault	f_5
T_T sensor bias fault	f_6

Table 7.8: Confusion matrix of the sensor fault isolation performance for $Q = 25$, PLA=80% and the fault severity of 1%. The filters are designed with the data obtained at PLA=75%.

		Predicted					
		f_0	f_2	f_3	f_4	f_5	f_6
Actual	f_0	83	8	0	3	4	2
	f_2	4	77	2	2	5	10
	f_3	9	2	75	2	7	6
	f_4	2	4	9	78	0	7
	f_5	8	3	6	3	78	2
	f_6	2	1	7	5	5	80

Table 7.9: Confusion matrix of the sensor fault isolation performance for $Q = 50$, PLA=80% and the fault severity of 1%. The filters are designed with the data obtained at PLA=75%.

		Predicted					
		f_0	f_2	f_3	f_4	f_5	f_6
Actual	f_0	94	0	0	1	3	2
	f_2	3	94	0	0	0	3
	f_3	3	0	90	3	4	0
	f_4	0	0	3	89	2	6
	f_5	1	3	0	2	91	3
	f_6	1	0	6	0	5	88

Table 7.10: Confusion matrix of the sensor fault isolation performance for $Q = 100$, PLA=80% and the fault severity of 1%. The filters are designed with the data obtained at PLA=75%.

		Predicted					
		f_0	f_2	f_3	f_4	f_5	f_6
Actual	f_0	97	0	0	0	0	3
	f_2	1	98	0	1	0	0
	f_3	0	0	98	0	2	0
	f_4	0	0	1	98	0	1
	f_5	1	1	0	0	98	0
	f_6	1	1	1	0	0	97

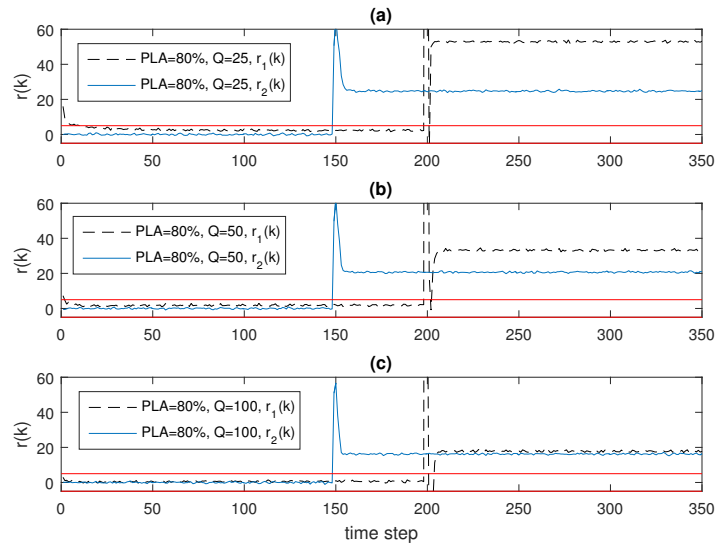


Figure 7.7: Residuals generated by a bank of three filters for the sensor fault isolation. The filters are designed with the data obtained at PLA=75% but stimulated at PLA=80% while a 1% fault is injected in the sensor measuring T_C and N at the time steps 150 and 200, respectively.

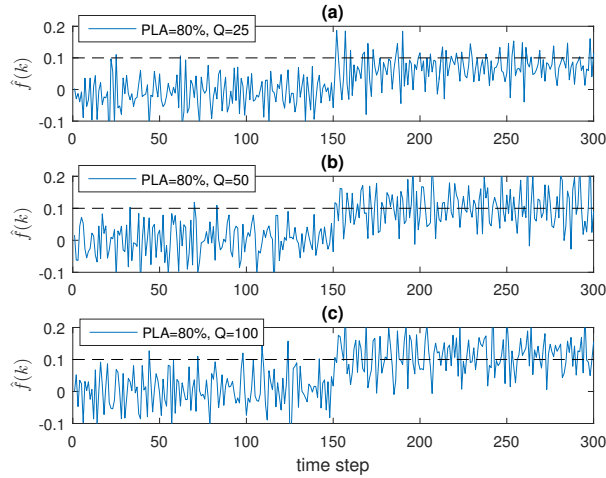


Figure 7.8: Actuator fault estimation filter residuals fed by measurements P_C and P_T for a 10% fault in the actuator. The filter is designed with the data obtained at PLA=75%. Note that the average of $\hat{f}(k)$ approach to 0.1 after the injection of the fault at the time step 150.

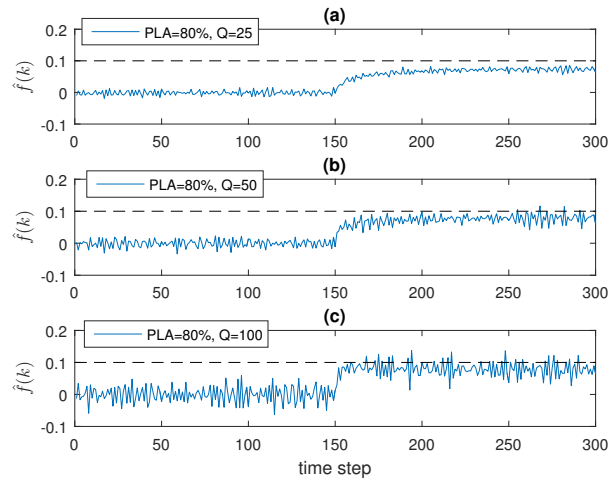


Figure 7.9: Actuator fault estimation filter residuals fed by the measurements P_C and N for a 10% fault in the actuator. The filter is designed with the data obtained at PLA=75%. Note that the average of $\hat{f}(k)$ approach to 0.1 after the injection of the fault at the time step 150.

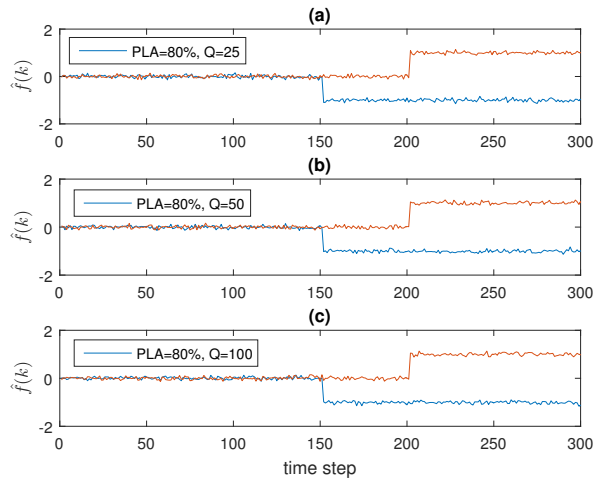


Figure 7.10: Sensor estimation filter residuals fed by the measurements P_C and P_T for 1% and -1% concurrent sensor faults in P_C and P_T injected at the time steps 100 and 200, respectively. The filter is designed with the data obtained at PLA=75%.

Table 7.11: Average actuator fault estimation errors for 100 Monte Carlo simulation runs at PLA=80%. The filters are designed with the data obtained at PLA=75%.

Set of measurements fed to the estimation filter	$Q = 25$	$Q = 50$	$Q = 100$
N, P_C	10.75%	8.49	7.25
N, P_C, P_T	10.11	7.25	7.81
N, P_C, P_T, T_T	9.51	9.60	6.98
N, P_C, P_T, T_T, T_C	9.73	8.50	6.14

Table 7.12: Average sensor fault estimation errors for 100 Monte Carlo simulation runs at PLA=80%. The filters are designed with the data obtained at PLA=75%.

Set of measurements fed to estimation filter	$Q = 25$	$Q = 50$	$Q = 100$
N, P_C	14.76%	12.83	13.75
N, P_C, P_T	13.02	11.86	9.22
N, P_C, P_T, T_T	11.64	8.76	9.64
N, P_C, P_T, T_T, T_C	12.07	10.29	7.93

Table 7.13: Average sensor fault estimation errors for different methods based on Markov parameter estimation and set of measurements (100 Monte Carlo simulation runs at PLA=80%). The filters are designed with the data obtained at PLA=75%.

Type of Input used for Markov parameter estimation	Noise	PBRS	Harmonic ($Q = 100$)
Set of measurements fed to the estimation filter			
N, P_C	6.54%	5.98	13.75
N, P_C, P_T	7.30	4.96	9.22
N, P_C, P_T, T_T	5.39	4.15	9.64
N, P_C, P_T, T_T, T_C	4.18	3.40	7.93

Chapter 8

Summary

In this theses, we targeted certain important practical issues in fault diagnosis of dynamical systems especially for the application of gas turbine. These practical issues are nonlinear dynamics of the system in certain phases of operation, the need for fault estimation and lack of mathematical model. Towards this end, we considered a sequence of interconnected problems as follows,

- Nonlinear FDI
- Estimation of certain categories of fault in MP and NMP linear systems
- Estimation of an arbitrary fault signal in MP and NMP linear systems
- Direct construction of FDI&E filters using time-domain data
- Direct construction of FDI&E filters using frequency-domain data

We provided a solution for each of these problems and illustrated their merits via comprehensive simulations.

We presented nonlinear MM-based FDI of gas turbines. The MM-based scheme is constructed using a bank of nonlinear Kalman filters and a conditional probability

evaluator. Each Kalman filter corresponds to a fault in the system. The probability associated with each fault mode is calculated using innovation vector and innovation covariance provided by each Kalman filter in the bank. The fault mode of the system is then determined based on the maximum probability criteria. We considered both EKF and UKF in construction of filter banks and comprehensively compared their performance. We found that UKF is superior to EKF in terms of robustness and detection time. Moreover, it does not require the calculation of Jacobian matrix. However, the computational costs significantly increase for UKF compared to EKF due to the fact that UKF requires multiple simulation of nonlinear model at each time-step.

Next, we proposed an inversion-based scheme that provides an unbiased estimation for certain categories of faults. We project the unknown input onto two subspaces. One projection is achieved through an algebraic operation, whereas the other is given by a dynamic filter whose poles coincide with the transmission zeros of the system. A feedback is then introduced to stabilize the above filter dynamics as well as provide an unbiased estimation of the unknown input. We comprehensively discussed the conditions under which the feedback control is feasible. An immediate result is that our approach can handle systems with transmission zeros on the unit circle. Moreover, the proposed scheme is significantly robust to the noise due to the feedback control. Further research is required to generalize this approach for reconstruction of arbitrary fault signals.

Our first inversion-based solution is only able to estimate certain categories of faults. We also considered the estimation of an arbitrary fault signal which is the subject of our next solution. Towards this end, we partitioned the system states

as MP and NMP states. The MP states are directly estimated from system measurements using an UIO filter. Later, we design an FIR filter that receives the MP states estimates and system measurements to reconstruct the NMP states with a delay. We derived the relation between the reconstruction error and the reconstruction delay. It is then straightforward to reconstruct the unknown input by having system measurements and reconstructed MP and NMP states. We invoked minor modifications to adjust the proposed solution for the problem of output tracking and estimation of faults in the presence of known inputs. Finally, we illustrated the merits of the proposed solution through simulation and comparative case studies.

So far, we assumed that a mathematical model of the system is available. However, it is not a practical assumption at least for the application of gas turbine. We developed two key ideas that renders direct construction of FDI&E filters in state-space form from system I/O data without involving reduction step or *a priori* knowledge of the system order. These key ideas are assignment (6.13) and data-driven estimation of $\hat{\mathbf{M}}$. We showed that our proposed solution is superior to available methods in the literature due to the fact that it is asymptotically unbiased if i is selected to be greater than the maximum of system relative degree and system observability index, whereas for other methods, i should go to infinity. We discussed that the estimation of Markov parameters are erroneous since system I/O data are noise corrupted. Consequently, the estimation will be biased especially for inputs with relatively large norm which magnifies these biases. In order to address this issue, we proposed an offline tuning procedure that compensates for errors caused by Markov parameters estimation errors. The parameters of the tuned dynamic filter is directly synthesized from system I/O data through invoking a least square optimization problem. Our simulation case studies show that the tuning process has been significantly effective in reducing the estimation errors.

An important practical concern led us to revise our proposed FDI&E scheme in Chapter 6 for the application of gas turbine. Our proposed data-driven FDI&E scheme requires that the identification input should be persistently exciting. In other words, it should be a wide band signal such as noise. However, it is less likely one stimulates a gas turbine by wide band signal. In order to resolve this issue, we proposed a solution that utilizes the frequency response data for robust and direct estimation of Markov parameters from I/O data. Furthermore, we showed through comprehensive simulations that our proposed methodology provides a satisfactory performance by only utilizing the frequency response of the system at a limited number of frequencies. Our proposed scheme is well-suited for real applications due to the fact that it requires availability of only frequency response data. More importantly, it does not require *a priori* knowledge about the mathematical model of the system such as numbers of poles and zeros.

Chapter 9

Conclusions and Future Work

9.1 Conclusion

Autonomous fault detection, isolation and estimation (FDI&E) is a promising approach for simultaneous promotion of safety and reduction of costs. However, numerous practical and theoretical issues have constantly challenged the delivery and implementation of a fully FDI&E scheme in real life applications. Among notable ones are nonlinear effects, lack of accurate mathematical data and customer requirement for strategic planning based on fault severities. In this thesis, we addressed the above important practical considerations as applied to gas turbine engines.

Gas turbines are nonlinear complex systems which in some cases, for instance on airplanes, have a wide range of operation. Certain phases of operation are short compared to the entire operation time, namely takeoff, however, those periods are perhaps the most critical phases of the operation. On the other hand, linear approaches may not be proper for fault detection and isolation during these phases due to the fact that operational condition rapidly varies. In order to address this issue, we proposed the nonlinear Multiple-Model based approach and demonstrated

its merits for our specific application.

Our proposed MM-based nonlinear FDI is composed of a bank of nonlinear Kalman filters and conditional probability evaluator. The innovation vector and innovation covariance generated by each Kalman filter is iteratively processed to calculate the conditional probability corresponding to each fault mode. A maximum probability condition determines the active fault mode. The nonlinear kalman filters can be both EKF and UKF, however, we showed that UKF is superior in terms of robustness and detection time.

Another important practical concern is fault estimation. In many cases including gas turbines, alarming a fault does not suffice for the purpose of strategic planning. Pilots and ground operators should know an estimation of the fault in order to decide on the continuation or abortion of the mission. We developed two closely interconnected fault estimation schemes. First, we proposed a stable dynamic filter that provides unbiased estimation for certain types of faults even if the system has unstable transmission zeros or transmission zeros on the unit circle. Second, we proposed a more general solution for reconstruction of a general unknown input. Moreover, we showed that the solution is applicable to the problem of output tracking.

The challenge of inversion-based unknown input reconstruction is the presence of unstable transmission zeros for non-minimum phase systems. We addressed this challenges in our solutions by invoking novel ideas. In our first solution, the unknown input is projected onto two subspaces. One projection is easily obtained through algebraic calculations. The other projection is given by a dynamical filter where its poles coincide with system transmission zeros. We introduced a feedback

that stabilizes this unstable dynamics for non-minimum phase system by arbitrary pole placement. Moreover, it provides unbiased estimation for certain categories of unknown inputs.

Our second inversion-based solution, in contrast to the first one, can provide an almost unbiased reconstruction of an unknown input of any type. The basic idea envisaged here is the reconstruction of the system states. We partitioned system states as MP and NMP states. The former is estimated using an UIO filter that operates with the system measurements and serves as input to an FIR filter for delayed reconstruction of the latter. The application of the first solution is limited to certain categories of the unknown inputs, yet it is superior to the second solution in terms of robustness since it has a feedback that counteracts disturbances. Moreover, it provides an exact unbiased estimation with significantly lower delay.

Perhaps lack of an accurate mathematical model is one of the most frequent issues that arises in real life. On the other hand, the experimental facilities and data recording equipment have significantly advanced during recent years. Naturally, one would suggest to shift from model-based design towards data-driven design. The field of fault diagnosis and estimation is also experiencing this shift due to its invaluable benefits. We proposed a data driven fault diagnosis and estimation scheme that is directly constructed in state-space form from the system I/O data. The proposed scheme does not involve reduction step, so it does not require *a priori* knowledge of the system order or its number of poles and zeros. More importantly, it is directly realized in state space form. We showed that our data-driven state-space based approach is significantly superior to the available FIR filter-based solutions in terms of FDI&E filter order.

Our data-driven FDI&E scheme requires that the identification input should be persistently exciting. In other words, it should be a wide band signal such as noise. However, it is not practically plausible to stimulate a gas turbine by a wide band signal. Instead, gas turbines are usually tested by harmonic inputs at several low frequencies for the purpose of identification. We extended our data-driven approach by robust and direct estimation of Markov parameters from frequency response data of the system. We showed through comprehensive simulations that our proposed scheme yields satisfactory performance by utilizing frequency response of the system at a limited number of frequencies.

9.2 Future Work

As mentioned before, numerous issues should be addressed and resolved for development and implementation of a fully operational and reliable FDI&E scheme for gas turbines. Towards this end, this research can be continued in various directions especially in the domain of inversion-based fault estimation and data-driven FDI&E.

Robust inversion-based fault estimation can be a research line to address the extension of our proposed solutions for stochastic systems. Also, inversion-based unknown input reconstruction decoupled from system disturbances needs to be investigated. Our first inversion-based solution is a promising approach for tackling the robustness issues since it has a feedback control that counteract noise and disturbances. However, it needs to be extended for reconstruction of a general unknown input. Our preliminary simulations show that it can reconstruct ‘low frequencies’ unknown inputs by an acceptable bias. The quantification of the bias and trade-off studies between reconstruction bias and robustness to noise and disturbances is an

interesting research topic.

Data-driven FDI&E is an active research field. Our proposed solution provides a ground for more advanced analysis to address the practical issues such as uncertainties and disturbances. One directions is to utilize H_∞ analysis for optimal selection of free parameters such that the estimation variance is minimized. It can also be used to remedy the effect of disturbances. A restrictive assumption in available data-driven approaches is the persistently exciting condition for identification input. This condition blocks using tremendous amount of data recorded during systems operation. Therefore, the data-driven approaches are not yet fully applicable to many real-life cases. A possible solution is to design FDI&E schemes that is decoupled from those responses of the system that has not been excited so far by inputs in operation.

References

- [1] R. Beard, “Failure accommodation in linear systems through self-reorganization,” *Ph.D dissertation, Dept. Aeronautics and Astronautics, MIT*, 1971.
- [2] Z. Gao, C. Cecati, and S. Ding, “A survey of fault diagnosis and fault-tolerant techniques;part i: Fault diagnosis with model-based and signal-based approaches,” *Industrial Electronics, IEEE Transactions on*, vol. 62, pp. 3757–3767, June 2015.
- [3] Z. Gao, C. Cecati, and S. X. Ding, “A survey of fault diagnosis and fault-tolerant techniques;part ii: Fault diagnosis with knowledge-based and hybrid/active approaches,” *IEEE Transactions on Industrial Electronics*, vol. 62, pp. 3768–3774, June 2015.
- [4] V. Venkatasubramanian, R. Rengaswamy, K. Yin, and S. N. Kavuri, “A review of process fault detection and diagnosis: Part i: Quantitative model-based methods,” *Computers and Chemical Engineering*, vol. 27, no. 3, pp. 293 – 311, 2003.
- [5] V. Venkatasubramanian, R. Rengaswamy, and S. N. Kavuri, “A review of process fault detection and diagnosis: Part ii: Qualitative models and search strategies,” *Computers & Chemical Engineering*, vol. 27, no. 3, pp. 313 – 326, 2003.

- [6] V. Venkatasubramanian, R. Rengaswamy, S. N. Kavuri, and K. Yin, “A review of process fault detection and diagnosis: Part iii: Process history based methods,” *Computers & Chemical Engineering*, vol. 27, no. 3, pp. 327 – 346, 2003.
- [7] I. Hwang, S. Kim, Y. Kim, and C. E. Seah, “A survey of fault detection, isolation, and reconfiguration methods,” *Control Systems Technology, IEEE Transactions on*, vol. 18, no. 3, pp. 636–653, 2010.
- [8] J. Marzat, H. Piet-Lahanier, F. Damongeot, and E. Walter, “Model-based fault diagnosis for aerospace systems: a survey,” *Proceedings of the Institution of Mechanical Engineers, Part G: Journal of Aerospace Engineering*, p. 0954410011421717, 2012.
- [9] P. Frank and X. Ding, “Survey of robust residual generation and evaluation methods in observer-based fault detection systems,” *Journal of process control*, vol. 7, no. 6, pp. 403–424, 1997.
- [10] R. Patton and J. Chen, “Observer-based fault detection and isolation: Robustness and applications,” *Control Engineering Practice*, vol. 5, no. 5, pp. 671 – 682, 1997.
- [11] K. Emami, T. Fernando, B. Nener, H. Trinh, and Y. Zhang, “A functional observer based fault detection technique for dynamical systems,” *Journal of the Franklin Institute*, vol. 352, no. 5, pp. 2113 – 2128, 2015.
- [12] Q. Jia, H. Li, Y. Zhang, and X. Chen, “Robust observer-based sensor fault reconstruction for discrete-time systems via a descriptor system approach,” *International Journal of Control, Automation and Systems*, vol. 13, no. 2, pp. 274–283, 2015.

- [13] T. G. Park and K. S. Lee, "Process fault isolation for linear systems with unknown inputs," *IEE Proceedings - Control Theory and Applications*, vol. 151, pp. 720–726, Nov 2004.
- [14] H. F. Wahab, R. Katebi, and M. A. Hannan, "Model based fault detection using unknown input observer- state dependent h_∞ filter," in *Control Conference (AUCC), 2015 5th Australian*, pp. 188–193, Nov 2015.
- [15] A. K. Prajapati and B. Roy, "Multi-fault diagnosis in three coupled tank system using unknown input observer," *IFAC-PapersOnLine*, vol. 49, no. 1, pp. 47 – 52, 2016.
- [16] Z. Gao, X. Liu, and M. Z. Q. Chen, "Unknown input observer-based robust fault estimation for systems corrupted by partially decoupled disturbances," *IEEE Transactions on Industrial Electronics*, vol. 63, pp. 2537–2547, April 2016.
- [17] H. Ye, G. Wang, and S. Ding, "A new parity space approach for fault detection based on stationary wavelet transform," *Automatic Control, IEEE Transactions on*, vol. 49, no. 2, pp. 281–287, 2004.
- [18] M. Zhong, Y. Song, and S. X. Ding, "Parity space-based fault detection for linear discrete time-varying systems with unknown input," *Automatica*, vol. 59, pp. 120 – 126, 2015.
- [19] Z. W. Huang, Y. Z. Yang, J. Wang, and Y. Li, "Parity space-based fault diagnosis of ccbii braking system," *Journal of Central South University*, vol. 20, no. 10, pp. 2922–2928, 2013.
- [20] E. Naderi, N. Meskin, and K. Khorasani, "Nonlinear fault diagnosis of jet engines by using a multiple model-based approach," *Journal of Engineering for Gas Turbines and Power*, vol. 134, no. 1, p. 011602, 2012.

- [21] P. S. Nag, G. kumar Silla, V. H. V. Gummadi, C. B. Harishankar, V. K. Ray, and C. S. Kumar, "Model based fault diagnosis of low earth orbiting (leo) satellite using spherical unscented kalman filter," *IFAC-PapersOnLine*, vol. 49, no. 1, pp. 635 – 638, 2016.
- [22] H. He, Z. Liu, and Y. Hua, "Adaptive extended kalman filter based fault detection and isolation for a lithium-ion battery pack," *Energy Procedia*, vol. 75, pp. 1950 – 1955, 2015.
- [23] L. Guo and H. Wang, "Fault detection and diagnosis for general stochastic systems using b-spline expansions and nonlinear filters," *Circuits and Systems I: Regular Papers, IEEE Transactions on*, vol. 52, no. 8, pp. 1644–1652, 2005.
- [24] R. H. Chen, D. L. Mingori, and J. L. Speyer, "Optimal stochastic fault detection filter," *Automatica*, vol. 39, no. 3, pp. 377–390, 2003.
- [25] S. Ding, "Data-driven design of monitoring and diagnosis systems for dynamic processes: A review of subspace technique based schemes and some recent results," *Journal of Process Control*, vol. 24, no. 2, pp. 431–449, 2014.
- [26] H. Li, Y. Gao, P. Shi, and H. K. Lam, "Observer-based fault detection for nonlinear systems with sensor fault and limited communication capacity," *IEEE Transactions on Automatic Control*, vol. 61, pp. 2745–2751, Sept 2016.
- [27] A. Sidhu, A. Izadian, and S. Anwar, "Adaptive nonlinear model-based fault diagnosis of li-ion batteries," *IEEE Transactions on Industrial Electronics*, vol. 62, pp. 1002–1011, Feb 2015.
- [28] C. Keliris, M. M. Polycarpou, and T. Parisini, "An integrated learning and filtering approach for fault diagnosis of a class of nonlinear dynamical systems," *IEEE Transactions on Neural Networks and Learning Systems*, vol. PP, no. 99, pp. 1–17, 2016.

- [29] S. Hashtrudi Zad, R. H. Kwong, and W. M. Wonham, “Fault diagnosis in discrete-event systems: framework and model reduction,” *Automatic Control, IEEE Transactions on*, vol. 48, no. 7, pp. 1199–1212, 2003.
- [30] J. Zaytoon and S. Lafortune, “Overview of fault diagnosis methods for discrete event systems,” *Annual Reviews in Control*, vol. 37, no. 2, pp. 308–320, 2013.
- [31] R. H. Kwong and D. L. Yonge-Mallo, “Fault diagnosis in discrete-event systems with incomplete models: Learnability and diagnosability,” *IEEE Transactions on Cybernetics*, vol. 45, pp. 1236–1249, July 2015.
- [32] Y. Pencle, R. Pichard, and P. Fernbach, “Modular fault diagnosis in discrete-event systems with a cpn diagnoser,” *IFAC-PapersOnLine*, vol. 48, no. 21, pp. 470 – 475, 2015.
- [33] S. J. Qin, “Survey on data-driven industrial process monitoring and diagnosis,” *Annual Reviews in Control*, vol. 36, no. 2, pp. 220–234, 2012.
- [34] S. Yin, S. X. Ding, X. Xie, and H. Luo, “A review on basic data-driven approaches for industrial process monitoring,” *IEEE Transactions on Industrial Electronics*, vol. 61, pp. 6418–6428, Nov 2014.
- [35] S. S. Tayarani-Bathaie and K. Khorasani, “Fault detection and isolation of gas turbine engines using a bank of neural networks,” *Journal of Process Control*, vol. 36, pp. 22 – 41, 2015.
- [36] S. S. Tayarani-Bathaie, Z. S. Vanini, and K. Khorasani, “Dynamic neural network-based fault diagnosis of gas turbine engines,” *Neurocomputing*, vol. 125, pp. 153 – 165, 2014. Advances in Neural Network Research and Applications Advances in Bio-Inspired Computing: Techniques and Applications Selected papers from the 9th International Symposium of Neural Networks, July 2012.

- [37] R. Mohammadi, E. Naderi, K. Khorasani, and S. Hashtrudi-Zad, “Fault diagnosis of gas turbine engines by using dynamic neural networks,” *ASME Conference Proceedings*, vol. 2010, no. 43987, pp. 365–376, 2010.
- [38] M. Witczak, M. Mrugalski, and J. Korbicz, “Towards robust neural-network-based sensor and actuator fault diagnosis: Application to a tunnel furnace,” *Neural Processing Letters*, vol. 42, no. 1, pp. 71–87, 2015.
- [39] R. T. Cabeza, E. B. Viciado, A. Prieto-Moreno, and V. M. Vega, *Fault Diagnosis with Missing Data Based on Hopfield Neural Networks*, pp. 37–46. Cham: Springer International Publishing, 2016.
- [40] J. Korbicz, *Fault diagnosis: models, artificial intelligence, applications*. Springer Science & Business Media, 2003.
- [41] A. Rodríguez Ramos, C. Domínguez Acosta, P. J. Rivera Torres, E. I. Serrano Mercado, G. Beauchamp Baez, L. A. Rifón, and O. Llanes-Santiago, “An approach to multiple fault diagnosis using fuzzy logic,” *Journal of Intelligent Manufacturing*, pp. 1–11, 2016.
- [42] L. J. de Miguel and L. F. Blzquez, “Fuzzy logic-based decision-making for fault diagnosis in a {DC} motor,” *Engineering Applications of Artificial Intelligence*, vol. 18, no. 4, pp. 423 – 450, 2005.
- [43] E. Sobhani-Tehrani, H. Talebi, and K. Khorasani, “Hybrid fault diagnosis of nonlinear systems using neural parameter estimators,” *Neural Networks*, vol. 50, pp. 12 – 32, 2014.
- [44] P. Baldi, M. Blanke, P. Castaldi, N. Mimmo, and S. Simani, “Combined geometric and neural network approach to generic fault diagnosis in satellite actuators and sensors,” *IFAC-PapersOnLine*, vol. 49, no. 17, pp. 432 – 437, 2016.

20th {IFAC} Symposium on Automatic Control in AerospaceACA 2016Sherbrooke, Quebec, Canada, 21-25 August 2016.

- [45] A. T. Jahromi, M. J. Er, X. Li, and B. S. Lim, “Sequential fuzzy clustering based dynamic fuzzy neural network for fault diagnosis and prognosis,” *Neurocomputing*, vol. 196, pp. 31 – 41, 2016.
- [46] Z. Gao, C. Cecati, and S. X. Ding, “A survey of fault diagnosis and fault-tolerant techniques ;part ii: Fault diagnosis with knowledge-based and hybrid/active approaches,” *IEEE Transactions on Industrial Electronics*, vol. 62, pp. 3768–3774, June 2015.
- [47] P. Maybeck, “Multiple model adaptive algorithms for detecting and compensating sensor and actuator/surface failures in aircraft flight control systems,” *International Journal of Robust and Nonlinear Control*, vol. 9, pp. 1051–1070, 1999.
- [48] T. Menke and P. Maybeck, “Sensor/actuator failure detection in the vista F-16 by multiple model adaptive estimation,” *IEEE Transactions on Aerospace and Electronic Systems*, vol. 31, no. 4, pp. 1218–1229, 1995.
- [49] Y. Zhan and J. Jiang, “An interacting multiple-model based fault detection, diagnosis and fault-tolerant control approach,” in *Proc. of the 38th IEEE Conference on Decision and Control*, pp. 3593 –3598, 1999.
- [50] G. G. Yen and L. Ho, “Online multiple-model-based fault diagnosis and accommodation,” *IEEE Transactions On Industrial Electronics*, vol. 50, no. 2, pp. 296–312, 2003.
- [51] R. Patton, C. Lopez Toribio, and S. Simani, “Robust fault diagnosis in a chemical process using multiple-model approach,” in *Proc. of 40th IEEE Conference on Decision and Control*, pp. 149 –154, 2001.

- [52] A. H. A. Sari, “Data-driven design of fault diagnosis systems: Nonlinear multimode processes,” 2014.
- [53] R. Yedavalli, “Robust estimation and fault diagnostics for aircraft engines with uncertain model data,” in *Proc. of American Control Conference, ACC '07*, pp. 2822–2827, 2007.
- [54] T. Kobayashi and D. L. Simon, “Application of a bank of kalman filters for aircraft engine fault diagnostics,” *ASME Conference Proceedings*, vol. 2003, no. 36843, pp. 461–470, 2003.
- [55] T. Kobayashi and D. L. Simon, “Hybrid kalman filter approach for aircraft engine in-flight diagnostics: Sensor fault detection case,” *Journal of Engineering for Gas Turbines and Power*, vol. 129, no. 3, pp. 746–754, 2007.
- [56] N. Meskin, E. Naderi, and K. Khorasani, “Fault diagnosis of jet engines by using a multiple model-based approach,” *ASME Conference Proceedings*, vol. 2010, no. 43987, pp. 319–329, 2010.
- [57] D. Simon, “A comparison of filtering approaches for aircraft engine health estimation,” *Aerospace Science and Technology*, vol. 12, no. 4, pp. 276–284, 2008.
- [58] J. Chen, R. Patton, and H. Zhang, “Design of unknown input observers and robust fault detection filters,” *International Journal of Control*, vol. 63, no. 1, pp. 85–105, 1996.
- [59] D. Tan, R. J. Patton, and X. Wang, “A relaxed solution to unknown input observers for state and fault estimation,” *IFAC-PapersOnLine*, vol. 48, no. 21, pp. 1048 – 1053, 2015. 9th {IFAC} Symposium on Fault Detection, Supervision and Safety for Technical Processes {SAFEPROCESS} 2015Paris, 24 September 2015.

- [60] H. Alwi and C. Edwards, “Robust sensor fault estimation for tolerant control of a civil aircraft using sliding modes,” in *American Control Conference, 2006*, pp. 6–pp, IEEE, 2006.
- [61] F. Szigeti, C. Vera, J. Bokor, and A. Edelmayer, “Inversion based fault detection and isolation,” in *Decision and Control, 2001. Proceedings of the 40th IEEE Conference on*, vol. 2, pp. 1005–1010, IEEE, 2001.
- [62] A. Edelmayer, J. Bokor, and Z. Szabó, “Inversion-based residual generation for robust detection and isolation of faults by means of estimation of the inverse dynamics in linear dynamical systems,” *International Journal of Control*, vol. 82, no. 8, pp. 1526–1538, 2009.
- [63] M. Figueroa, M. Bonilla, M. Malabre, and J. Martinez, “On failure detection by inversion techniques,” in *Decision and Control, 2004. CDC. 43rd IEEE Conference on*, vol. 5, pp. 4770 – 4775 Vol.5, dec. 2004.
- [64] B. Kulcsár and M. Verhaegen, “Robust inversion based fault estimation for discrete-time lpv systems,” *Automatic Control, IEEE Transactions on*, vol. 57, no. 6, pp. 1581–1586, 2012.
- [65] Z. Szabo, A. Edelmayer, and J. Bokor, “Inversion based fdi for sampled lpv systems,” in *Control and Fault-Tolerant Systems (SysTol), 2010 Conference on*, pp. 82 –87, oct. 2010.
- [66] R. Brockett and M. Mesarovic, “The reproducibility of multivariable systems,” *Journal of Mathematical Analysis and Applications*, vol. 11, pp. 548–563, 1965.
- [67] L. Silverman, “Inversion of multivariable linear systems,” *Automatic Control, IEEE Transactions on*, vol. 14, pp. 270 – 276, jun 1969.
- [68] J. Massey and M. Sain, “Inverses of linear sequential circuits,” *Computers, IEEE Transactions on*, vol. C-17, pp. 330 – 337, april 1968.

- [69] P. Moylan, “Stable inversion of linear systems,” *Automatic Control, IEEE Transactions on*, vol. 22, pp. 74 – 78, feb 1977.
- [70] S. Gilijns, *Kalman filtering techniques for system inversion and data assimilation*. PhD thesis, K.U.Leuven, Leuven, Belgium, 2007.
- [71] R. A. Chavan and H. J. Palanthandalam-Madapusi, “Delayed recursive state and input reconstruction,” *arXiv preprint arXiv:1509.06226*, 2015.
- [72] H. J. Palanthandalam-Madapusi and D. S. Bernstein, “Unbiased minimum-variance filtering for input reconstruction,” in *American Control Conference, 2007. ACC’07*, pp. 5712–5717, IEEE, 2007.
- [73] S. Kirtikar, H. Palanthandalam-Madapusi, E. Zattoni, and D. S. Bernstein, “l-delay input reconstruction for discrete-time linear systems,” in *Decision and Control, 2009 held jointly with the 2009 28th Chinese Control Conference. CDC/CCC 2009. Proceedings of the 48th IEEE Conference on*, pp. 1848–1853, IEEE, 2009.
- [74] T. Floquet and J.-P. Barbot, “A sliding mode approach of unknown input observers for linear systems,” in *Decision and Control, 2004. CDC. 43rd IEEE Conference on*, vol. 2, pp. 1724–1729, IEEE, 2004.
- [75] G. Marro and E. Zattoni, “Unknown-state, unknown-input reconstruction in discrete-time nonminimum-phase systems: Geometric methods,” *Automatica*, vol. 46, no. 5, pp. 815 – 822, 2010.
- [76] S. Wahls and H. Boche, “Novel system inversion algorithm with application to oversampled perfect reconstruction filter banks,” *IEEE Transactions on Signal Processing*, vol. 58, pp. 3008–3016, June 2010.
- [77] R. J. Patton, P. M. Frank, and R. N. Clark, *Issues of fault diagnosis for dynamic systems*. Springer Science & Business Media, 2013.

- [78] Q. Zou and S. Devasia, “Preview-based stable-inversion for output tracking of linear systems,” *Journal of dynamic systems, measurement, and control*, vol. 121, no. 4, pp. 625–630, 1999.
- [79] Q. Zou and S. Devasia, “Preview-based optimal inversion for output tracking: application to scanning tunneling microscopy,” *Control Systems Technology, IEEE Transactions on*, vol. 12, no. 3, pp. 375–386, 2004.
- [80] Q. Zou and S. Devasia, “Precision preview-based stable-inversion for nonlinear nonminimum-phase systems: The vtol example,” *Automatica*, vol. 43, no. 1, pp. 117–127, 2007.
- [81] Q. Zou, “Optimal preview-based stable-inversion for output tracking of nonminimum-phase linear systems,” *Automatica*, vol. 45, no. 1, pp. 230–237, 2009.
- [82] H. Wang, K. Kim, and Q. Zou, “B-spline-decomposition-based output tracking with preview for nonminimum-phase linear systems,” *Automatica*, vol. 49, no. 5, pp. 1295–1303, 2013.
- [83] B. Kiumarsi, F. L. Lewis, H. Modares, A. Karimpour, and M.-B. Naghibi-Sistani, “Reinforcement q-learning for optimal tracking control of linear discrete-time systems with unknown dynamics,” *Automatica*, vol. 50, no. 4, pp. 1167–1175, 2014.
- [84] M. Duan, K. S. Ramani, and C. E. Okwudire, “Tracking control of non-minimum phase systems using filtered basis functions: A nurbs-based approach,” in *ASME 2015 Dynamic Systems and Control Conference*, pp. V001T03A006–V001T03A006, American Society of Mechanical Engineers, 2015.

- [85] S. Ding, P. Zhang, A. Naik, E. Ding, and B. Huang, "Subspace method aided data-driven design of fault detection and isolation systems," *Journal of Process Control*, vol. 19, no. 9, pp. 1496–1510, 2009.
- [86] J. Dong, B. Kulcsr, and M. Verhaegen, "Subspace based fault detection and identification for LPV systems," vol. 42, pp. 336 – 341, 2009. 7th IFAC Symposium on Fault Detection, Supervision and Safety of Technical Processes.
- [87] Y. Wang, G. Ma, S. X. Ding, and C. Li, "Subspace aided data-driven design of robust fault detection and isolation systems," *Automatica*, vol. 47, no. 11, pp. 2474–2480, 2011.
- [88] J. Dong and M. Verhaegen, "Subspace based fault detection and identification for LTI systems," *IFAC Proceedings Volumes*, vol. 42, no. 8, pp. 330 – 335, 2009. 7th IFAC Symposium on Fault Detection, Supervision and Safety of Technical Processes.
- [89] J. Dong, M. Verhaegen, and F. Gustafsson, "Robust fault detection with statistical uncertainty in identified parameters," *IEEE Transactions on Signal Processing*, vol. 60, no. 10, pp. 5064–5076, 2012.
- [90] J. Dong, M. Verhaegen, and F. Gustafsson, "Robust fault isolation with statistical uncertainty in identified parameters," *IEEE Transactions on Signal Processing*, vol. 60, pp. 5556–5561, Oct 2012.
- [91] J. Dong and M. Verhaegen, "Identification of fault estimation filter from i/o data for systems with stable inversion," *IEEE Transactions on Automatic Control*, vol. 57, no. 6, pp. 1347–1361, 2012.
- [92] Y. Wan, T. Keviczky, M. Verhaegen, and F. Gustafsson, "Data-driven robust receding horizon fault estimation," *Automatica*, vol. 71, pp. 210 – 221, 2016.

- [93] L. Ljung, *System identification*. Springer, 1998.
- [94] P. Van Overschee and B. De Moor, “A unifying theorem for three subspace system identification algorithms,” *Automatica*, vol. 31, no. 12, pp. 1853–1864, 1995.
- [95] T. Katayama, *Subspace methods for system identification*. Springer Science & Business Media, 2006.
- [96] B. Huang and R. Kadali, *Dynamic modeling, predictive control and performance monitoring: A data-driven subspace approach*, vol. 374. Springer Science & Business Media, 2008.
- [97] A. Chiuso, “On the relation between cca and predictor-based subspace identification,” *IEEE Transactions on Automatic Control*, vol. 52, no. 10, pp. 1795–1812, 2007.
- [98] B. Pourbabaee, N. Meskin, and K. Khorasani, “Robust sensor fault detection and isolation of gas turbine engines subjected to time-varying parameter uncertainties,” *Mechanical Systems and Signal Processing*, vol. 76-77, pp. 136?–156, 2016.
- [99] S. Rahme and N. Meskin, “Adaptive sliding mode observer for sensor fault diagnosis of an industrial gas turbine,” *Control Engineering Practice*, vol. 38, pp. 57 – 74, 2015.
- [100] Z. S. Vanini, N. Meskin, and K. Khorasani, “Multiple-model sensor and components fault diagnosis in gas turbine engines using autoassociative neural networks,” *Journal of Engineering for Gas Turbines and Power*, vol. 136, no. 9, p. 091603, 2014.
- [101] J. S. Litt, D. L. Simon, and S. Garg, “A survey of intelligent control and health management technologies for aircraft propulsion systems,” *Journal of*

- Aerospace Computing, Information and Communication*, vol. 1, no. 12, pp. 543–563, 2004.
- [102] A. J. Volponi, “Gas turbine engine health management: Past, present, and future trends,” *Journal of Engineering for Gas Turbines and Power*, vol. 136, no. 5, p. 051201, 2014.
- [103] S. Gupta, A. Ray, S. Sarkar, and M. Yasar, “Fault detection and isolation in aircraft gas turbine engines. part 1: underlying concept,” *Proceedings of the Institution of Mechanical Engineers, Part G: Journal of Aerospace Engineering*, vol. 222, no. 3, pp. 307–318, 2008.
- [104] L. Marinai, D. Probert, and R. Singh, “Prospects for aero gas-turbine diagnostics: a review,” *Applied Energy*, vol. 79, no. 1, pp. 109 – 126, 2004.
- [105] L. A. Urban, “Modelling methods for improving robustness in fault diagnosis of jet engine system,” in *Proc. of the 8th ASME Joint Propulsion Specialist Conference*, p. 1972, 1972.
- [106] A. J. Volponi, “Foundations of gas path analysis,” in *Gas Turbine Condition Monitoring and Fault Diagnosis* (C. H. Sieverding and K. Mathioudakis, eds.), Belgium: von Karman Institute, 2003.
- [107] A. Volponi and B. Wood, “Engine health management for aircraft propulsion systems,” in *Proceedings of the Forum on Integrated System Health Engineering and Management (ISHEM) in Aerospace, Napa, CA, November*, pp. 7–10, 2005.
- [108] D. L. Simon and A. W. Rinehart, “A model-based anomaly detection approach for analyzing streaming aircraft engine measurement data,” in *ASME Turbo Expo 2014: Turbine Technical Conference and Exposition*, p. V006T06A032, American Society of Mechanical Engineers, 2014.

- [109] B. Pourbabae, N. Meskin, and K. Khorasani, "Multiple-model based sensor fault diagnosis using hybrid kalman filter approach for nonlinear gas turbine engines," in *2013 American Control Conference*, pp. 4717–4723, June 2013.
- [110] C. Svard, M. Nyberg, E. Frisk, and M. Krysander, "Data-driven and adaptive statistical residual evaluation for fault detection with an automotive application," *Mechanical Systems and Signal Processing*, vol. 45, no. 1, pp. 170–192, 2014.
- [111] J. Fan, Z. Zhang, and H. Hua, "Data processing in subspace identification and modal parameter identification of an arch bridge," *Mechanical Systems and Signal Processing*, vol. 21, no. 4, pp. 1674–1689, 2007.
- [112] J. Pan, J. Chen, Y. Zi, J. Yuan, B. Chen, and Z. He, "Data-driven mono-component feature identification via modified nonlocal means and mewt for mechanical drivetrain fault diagnosis," *Mechanical Systems and Signal Processing*, vol. 80, no. 1, pp. 533–552, 2016.
- [113] Z. S. Vanini, K. Khorasani, and N. Meskin, "Fault detection and isolation of a dual spool gas turbine engine using dynamic neural networks and multiple model approach," *Information Sciences*, vol. 259, pp. 234 – 251, 2014.
- [114] R. Joly, S. Ogaji, R. Singh, and S. Probert, "Gas-turbine diagnostics using artificial neural-networks for a high bypass ratio military turbofan engine," *Applied Energy*, vol. 78, no. 4, pp. 397 – 418, 2004.
- [115] S. Sarkar, X. Jin, and A. Ray, "Data-driven fault detection in aircraft engines with noisy sensor measurements," *Journal of Engineering for Gas Turbines and Power*, vol. 133, no. 8, p. 081602, 2011.

- [116] S. Ogaji, L. Marinai, S. Sampath, R. Singh, and S. Prober, “Gas-turbine fault diagnostics: a fuzzy-logic approach,” *Applied Energy*, vol. 82, no. 1, pp. 81 – 89, 2005.
- [117] T. McKelvey, H. Akcay, and L. Ljung, “Subspace-based multivariable system identification from frequency response data,” *IEEE Transactions on Automatic Control*, vol. 41, pp. 960–979, Jul 1996.
- [118] C. Evans, P. Fleming, D. Hill, J. Norton, I. Pratt, D. Rees, and K. Rodriguez-Vazquez, “Application of system identification techniques to aircraft gas turbine engines,” *Control Engineering Practice*, vol. 9, no. 2, pp. 135 – 148, 2001.
- [119] Wikipedia. https://en.wikipedia.org/wiki/Jet_engine.
- [120] S. M. Camporeale, B. Fortunato, and M. Mastrovito, “A modular code for real time dynamic simulation of gas turbines in SIMULINK,” *Journal of Engineering for Gas Turbines and Power*, vol. 128, pp. 506–517, 2006.
- [121] V. Panov, “Gasturbolib: Simulink library for gas turbine engine modelling,” *ASME Conference Proceedings*, vol. 2009, no. 48821, pp. 555–565, 2009.
- [122] G. L. Merrington, “Fault diagnosis in gas turbines using a model-based technique,” *Journal of Engineering for Gas Turbines and Power*, vol. 116, no. 2, pp. 374–380, 1994.
- [123] W. P. J. Visser, O. Kogenhop, and M. Oostveen, “A generic approach for gas turbine adaptive modeling,” *Journal of Engineering for Gas Turbines and Power*, vol. 128, no. 1, pp. 13–19, 2006.
- [124] D. Bernstein, *Matrix Mathematics: Theory, Facts, and Formulas (Second Edition)*. Princeton reference, Princeton University Press, 2009.

- [125] A. Willsky, “On the invertibility of linear systems,” *Automatic Control, IEEE Transactions on*, vol. 19, pp. 272 – 274, jun 1974.
- [126] S. Sundaram and C. N. Hadjicostis, “Delayed observers for linear systems with unknown inputs,” *IEEE Transactions on Automatic Control*, vol. 52, pp. 334–339, Feb 2007.
- [127] K. Mathioudakis, C. Romessis, and A. Stamatis, “Probabilistic methods for gas turbine fault diagnostics,” in *Gas Turbine Condition Monitoring and Fault Diagnosis* (C. H. Sieverding and K. Mathioudakis, eds.), Belgium: von Karman Institute, 2003.
- [128] E. A. Wan and R. V. D. Merwe, “The unscented kalman filter for nonlinear estimation,” in *Proc. of Adaptive Systems for Signal Processing, Communications, and Control Symposium*, pp. 153 –158, 2000.
- [129] P. Eide and P. Maybeck, “An MMAE failure detection system for the F-16,” *IEEE Transactions on Aerospace and Electronic Systems*, vol. 32, no. 3, pp. 1125–1136, 1996.
- [130] A. J. Volponi, “Extending gas path analysis coverage for other fault conditions,” in *Gas Turbine Condition Monitoring and Fault Diagnosis* (C. H. Sieverding and K. Mathioudakis, eds.), Belgium: von Karman Institute, 2003.
- [131] R. Kandepu, B. Foss, and L. Imsland, “Applying the unscented kalman filter for nonlinear state estimation,” *Journal of Process Control*, vol. 18, no. 7-8, pp. 753 – 768, 2008.
- [132] E. D. Sontag, *Mathematical control theory: deterministic finite dimensional systems*, vol. 6. Springer Science & Business Media, 2013.
- [133] E. Davison and S. Wang, “Properties and calculation of transmission zeros of linear multivariable systems,” *Automatica*, vol. 10, no. 6, pp. 643 – 658, 1974.

- [134] S. Ding, *Model-based fault diagnosis techniques: design schemes, algorithms, and tools*. Springer Science & Business Media, 2008.
- [135] G. van der Veen, J.-W. Van Wingerden, M. Bergamasco, M. Lovera, and M. Verhaegen, “Closed-loop subspace identification methods: an overview,” *Control Theory & Applications, IET*, vol. 7, no. 10, pp. 1339–1358, 2013.
- [136] C. Evans, D. Rees, and A. Borrell, “Identification of aircraft gas turbine dynamics using frequency-domain techniques,” *Control Engineering Practice*, vol. 8, no. 4, pp. 457 – 467, 2000.
- [137] C. Evans, D. Rees, and D. Hill, “Frequency-domain identification of gas turbine dynamics,” *IEEE Transactions on Control Systems Technology*, vol. 6, pp. 651–662, Sep 1998.
- [138] D. C. Evans, D. Rees, and D. L. Jones, “Identifying linear models of systems suffering nonlinear distortions, with a gas turbine application,” *IEE Proceedings - Control Theory and Applications*, vol. 142, pp. 229–240, May 1995.
- [139] V. Arkov, C. Evans, P. Fleming, D. Hill, J. Norton, I. Pratt, D. Rees, and K. Rodriguez-Vazquez, “System identification strategies applied to aircraft gas turbine engines,” *Annual Reviews in Control*, vol. 24, pp. 67 – 81, 2000.
- [140] P. Guillaume, J. Schoukens, R. Pintelon, and I. Kollar, “Crest-factor minimization using nonlinear chebyshev approximation methods,” *IEEE Transactions on Instrumentation and Measurement*, vol. 40, pp. 982–989, Dec 1991.
- [141] K. M. Ting, “Confusion matrix,” in *Encyclopedia of Machine Learning* (C. Sammut and G. I. Webb, eds.), pp. 209–209, Boston, MA: Springer US, 2010.
- [142] B. MacIsaac and R. Langton, *Gas Turbine Propulsion Systems*. Aerospace Series, Wiley, 2011.

Appendix A

A.1 Validity of the Estimated Markov Parameters

We have used the confusion matrix [141] to determine the validity of range of the Markov parameters. The obtained results are shown in Tables A.1 and A.2. In these tables, Q is set equal to 100. The estimated Markov parameters are obtained at the PLA=75%. Next, the fault detection filters are constructed corresponding to the confusion matrix analysis at six different PLAs, namely 60, 65, 70, 80, 85 and 90%. The resulting ACC for these PLAs are obtained as 78.5, 96, 97, 97.5, 92.5 and 82%, which show that one can consider a $\pm 10\%$ variation in the PLA about an operating point as a valid range where the resulting estimated Markov parameters are acceptable. Similar results are obtained at other operating points but are not included and omitted here for brevity.

Table A.1: Confusion matrix of the actuator fault detection performance. The fault severity and Q are 5% and 100, respectively.

PLA=80%	Healthy	99	1	85%	Healthy	92	8	90%	Healthy	81	19
	Faulty	4	96		Faulty	7	93		Faulty	17	83
	ACC	99.48%			ACC	92.46			ACC	82	
	PPV	96.11			PPV	92.9			PPV	82.6	

Table A.2: Confusion matrix of the actuator fault detection performance. The fault severity and Q are 5% and 100, respectively.

PLA=60%		Healthy	Faulty	PLA=65%		Healthy	Faulty	PLA=70%		Healthy	Faulty
		Healthy	77		13		Healthy		95	5	
	Faulty	20	80		Faulty	3	97		Faulty	4	96
	ACC	78.5%			ACC	96			ACC	97	
	PPV	79.3			PPV	96.9			PPV	96.07	

A.2 Markov Parameter Estimation Error for Different PLA

Figures 7.2 and 7.3 show the Markov parameters estimation errors for the PLA=75%. We provide similar results for the PLA=50% in Figures A.1 and A.2 and the PLA=100% in Figures A.3 and A.4. These figures confirm that the Markov parameters estimation errors follow almost the same pattern for all the PLAs. Therefore, one can expect that the performance that have been demonstrated for the PLA=75% will also be observed for the other PLAs. In another words, the nonlinearities of the gas turbine engine are not that severe so that a fundamental change in the system behavior is observed as the PLA varies [57].

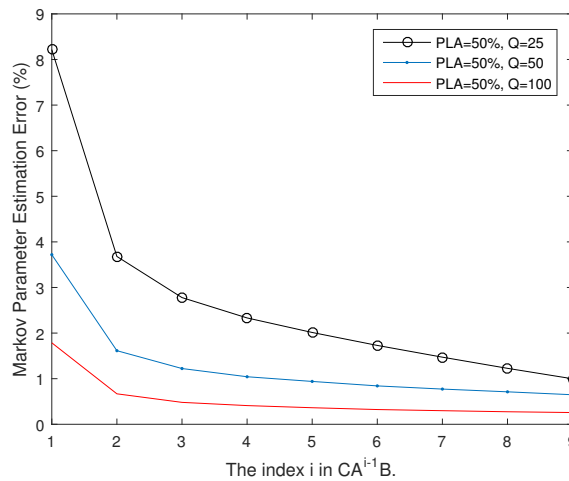


Figure A.1: The relative errors between the estimated and the actual Markov parameters of the input channel to the shaft rotational speed output channel at the PLA=50% for three different values of Q .

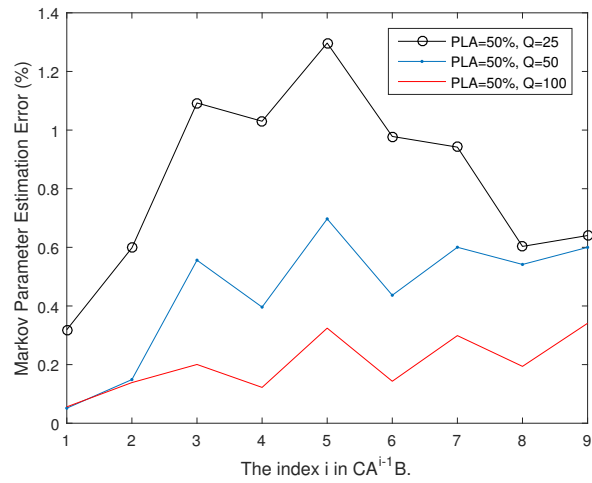


Figure A.2: The relative errors between the estimated and the actual Markov parameters of the input channel to the compressor pressure output channel at the PLA=50% for three different values of Q .

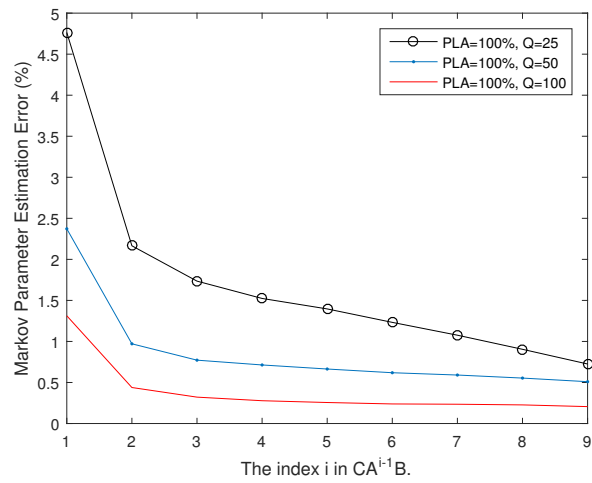


Figure A.3: The relative errors between the estimated and the actual Markov parameters of the input channel to the shaft rotational speed output channel at the PLA=100% for three different values of Q .

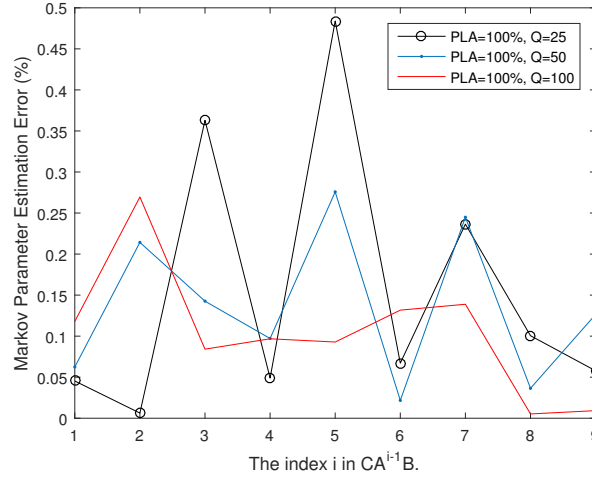


Figure A.4: The relative errors between the estimated and the actual Markov parameters of the input channel to the compressor pressure output channel at the PLA=100% for three different values of Q .

A.3 Confusion Matrix Analysis for PLA= 55%

In Section 7.3, we have provided several confusion matrix analyses for the PLA=80% using the FDI&E filters that are constructed from the data that are obtained at the PLA=75%. In this appendix, we provide similar analysis for the PLA=55% in order to demonstrate the performance of our proposed schemes at another PLA. The corresponding FDI&E filters are constructed from the data that are obtained at the PLA=50%.

Table A.3: Confusion matrix for the actuator fault detection performance. The fault severity and PLA are 1% and 55%, respectively.

		Healthy	Faulty			Healthy	Faulty			Healthy	Faulty
		Healthy	70			30	Healthy			80	20
$Q = 25$	Faulty	35	65	$Q = 50$	Faulty	19	81	$Q = 100$	Faulty	16	84
	ACC	67.5%			ACC	80.5			ACC	81.5	
	PPV	66.6			PPV	80.8			PPV	83.1	

Table A.4: Confusion matrix for the actuator fault detection performance. The fault severity and PLA are 5% and 55%, respectively.

$Q = 25$		Healthy	Faulty	$Q = 50$		Healthy	Faulty	$Q = 100$		Healthy	Faulty
	Healthy	76	24		Healthy	93	7		Healthy	93	7
Faulty	29	71	Faulty	5	95	Faulty	2	98			
ACC	73.5%		ACC	94.0		ACC	95.5				
PPV	72.3		PPV	94.8		PPV	97.8				

Table A.5: Confusion matrix for the actuator fault detection performance. The fault severity and PLA are 10% and 55%, respectively.

$Q = 25$		Healthy	Faulty	$Q = 50$		Healthy	Faulty	$Q = 100$		Healthy	Faulty
	Healthy	93	7		Healthy	98	2		Healthy	96	4
Faulty	11	89	Faulty	5	95	Faulty	3	97			
ACC	91%		ACC	96.5		ACC	96.5				
PPV	89.4		PPV	95.1		PPV	96.9				

Table A.6: Confusion matrix for the sensor fault detection performance. The fault severity and PLA are 1% and 55%, respectively.

$Q = 25$		Healthy	Faulty	$Q = 50$		Healthy	Faulty	$Q = 100$		Healthy	Faulty
	Healthy	71	29		Healthy	89	11		Healthy	90	10
Faulty	24	76	Faulty	7	93	Faulty	8	92			
ACC	73.5%		ACC	91.0		ACC	91.0				
PPV	74.7		PPV	92.7		PPV	91.8				

Table A.7: Confusion matrix of the sensor fault isolation performance for $Q = 25$, PLA=55% and the fault severity of 1%. The filters are designed with the data obtained at PLA=50%.

		Predicted					
		f_0	f_2	f_3	f_4	f_5	f_6
Actual	f_0	81	1	1	9	4	4
	f_2	2	79	6	2	6	5
	f_3	8	1	74	1	12	4
	f_4	4	7	3	86	1	1
	f_5	9	3	3	6	75	4
	f_5	4	1	1	3	10	81

Table A.8: Confusion matrix of the sensor fault isolation performance for $Q = 50$, PLA=80% and the fault severity of 1%. The filters are designed with the data obtained at PLA=75%.

		Predicted					
		f_0	f_2	f_3	f_4	f_5	f_6
Actual	f_0	87	5	1	3	2	2
	f_2	1	86	5	2	5	1
	f_3	0	1	93	0	0	6
	f_4	0	3	3	92	1	1
	f_5	5	0	2	4	89	0
	f_6	2	0	1	7	5	85

Table A.9: Confusion matrix of the sensor fault isolation performance for $Q = 100$, PLA=55% and the fault severity of 1%. The filters are designed with the data obtained at PLA=50%.

		Predicted					
		f_0	f_2	f_3	f_4	f_5	f_6
Actual	f_0	93	1	3	0	3	0
	f_2	0	96	0	1	2	1
	f_3	2	1	95	1	0	1
	f_4	0	2	0	95	2	1
	f_5	0	1	1	1	97	0
	f_6	0	0	0	1	1	98

Table A.10: Average actuator fault estimation error for 100 Monte Carlo simulations at PLA=55%. The filters are designed with the data obtained at PLA=50%.

Set of measurements fed to the estimation filter	$Q = 25$	$Q = 50$	$Q = 100$
N, P_C	19.14%	14.21	9.91
N, P_C, P_T	17.00	11.70	9.82
N, P_C, P_T, T_T	12.15	12.80	7.35
N, P_C, P_T, T_T, T_C	12.06	10.39	7.50

Table A.11: Average sensor fault estimation error for 100 Monte Carlo simulations at PLA=55%. The filters are designed with the data obtained at PLA=50%.

Set of measurements fed to estimation filter	$Q = 25$	$Q = 50$	$Q = 100$
N, P_C	17.12%	13.78	8.11
N, P_C, P_T	15.30	11.32	9.43
N, P_C, P_T, T_T	12.50	12.10	7.40
N, P_C, P_T, T_T, T_C	12.45	9.61	7.57

A.4 Analysis On the Selection of the Parameter

E

It was stated earlier in Section 7.2 that the I/O data are measured across E periods of the time-series signal. Moreover, in simulations conducted, we have selected and set $E = 6$ in Section 7.3 according to [118]. It is straightforward to obtain the response of the system at a given frequency by using a single period of data if both input and output are purely harmonic. However, the measurements are always noise-corrupted in practice. Therefore, one needs to process more data to obtain a reliable estimation of the frequency response. On the other hand, the amount of available data is constrained by practical issues such as time and costs of conducting experiments. Consequently, trade-off studies is required in order to determine the parameter E . Tables A.12 and A.13 show the confusion matrix analysis corresponding to different values of E . The results obtained confirm that an E equal to 5 will yield a satisfactory ! result. We have, nevertheless followed the recommendation of [118] that was verified by experimental results and set $E = 6$. Similar results for $E = 6$ have already been shown and can be found in Tables 7.3 and 7.5.

Table A.12: Confusion matrix for the sensor fault detection performance with different values of E . The fault severity, PLA and Q are 1%, 80% and 100, respectively.

$E = 2$		Healthy	Faulty	$E = 5$		Healthy	Faulty	$E = 10$		Healthy	Faulty
	Healthy	53	47		Healthy	91	9		Healthy	97	3
Faulty	34	66	Faulty	2	98	Faulty	4	96			
ACC	59.5%		ACC	94.5		ACC	96.5				
PPV	60.9		PPV	97.8		PPV	96.03				

Table A.13: Confusion matrix for the actuator fault detection performance with different values of E . The fault severity, PLA and Q are 5%, 80% and 100, respectively.

$E = 2$		Healthy	Faulty	$E = 5$		Healthy	Faulty	$E = 10$		Healthy	Faulty
	Healthy	65	35		Healthy	97	3		Healthy	98	2
Faulty	40	60	Faulty	6	94	Faulty	1	99			
ACC	62.5%		ACC	95.5		ACC	98.5				
PPV	61.9		PPV	94.1		PPV	98.9				